AN INVESTIGATION OF SOME MECHANICAL AND PHYSICAL PROPERTIES OF THIN LAMINATES OF POLYMER-CEMENT REINFORCED BY AN APPROXIMATELY RANDOM DISTRIBUTION OF GLASS FIBRES.

By

R. S. CHANNER

A Thesis Submitted For The Degree Of

MASTER OF PHILOSOPHY

Of The

UNIVERSITY OF SOUTHAMPTON

In The Faculty Of Engineering & Applied Science

Department Of Civil Engineering

February 1971

ABSTRACT

FACULTY OF ENGINEERING AND APPLIED SCIENCE
CIVIL ENGINEERING

Master of Philosophy

AN INVESTIGATION OF SOME MECHANICAL AND PHYSICAL PROPERTIES OF THIN LAMINATES OF POLYMER-CEMENT REINFORCED BY AN APPROXIMATELY RANDOM DISTRIBUTION OF GLASS FIBRES

by Reginald S. Channer

The study is presented in four sections.

1) A preliminary investigation into the production techniques and mechanical properties of High Alumina cement reinforced by E-glass fibres (Appendix).

2) A survey of admixtures for use with Portland and High Alumina cement systems. Attention is concentrated on those admixtures which will affect the mechanical properties and, in particular, the tensile fracture strain of inorganic cements. Five admixtures are selected and their mechanical and physical properties compared.

3) An investigation of a particular acrylic polymer - Portland cement system. A study is made of the tensile stress-strain diagram and the effect upon it of variations of environment, age and rate of strain. Empirical formulae are derived for relationships between stress, strain and strain rate.

Compression and flexural characteristics of the material are discussed. A long term creep study up to 33×10^6 s. is reported for various stress levels. Empirical creep laws are derived. Exploratory X-ray diffraction and micro examination by thin slide techniques are described in an attempt to establish the structure of this material.

4) An investigation of the mechanical properties of a thin composite based on the matrix of section 3), reinforced by a random array of discontinuous fibres. The material is tested in tension at various rates of strain and in compression and bending at one strain rate (one age, one environment). A long term creep investigation at various stress levels is described and empirical creep laws given.

For comparison tensile tests on a number of laminates of polymer-cement with various reinforcements are reported.

The principle of superposition of the stress-strain diagram is examined. Structural models to simulate the structure and elastic properties of the composite are given.

Computer programmes are provided.

ACKNOWLEDGEMENT

I wish to record my appreciation of my supervisor, Dr. H. G. Allen, for the time and assistance which he has given me over the whole period of this work and for his guidance and detailed criticism during the preparation of this manuscript.

I am indebted to the Construction Industries Research and Information Association who initiated and sponsored this project, also to the Department of Civil Engineering, University of Southampton. The staff of the Geology Department kindly allowed the use of their experimental equipment and were most co-operative.

My gratitude is extended to the Principal, Governors of Southampton Technical College and the local Education Authority who granted me leave of absence.

Finally, my wife has given me every encouragement throughout and placed my endeavours foremost. My wife also carefully typed and greatly helped in the preparation of this thesis.

CONTENTS

NOTATION

1, 2, 3	Rectangular coordinates
σ_{11} , σ_{22} , σ_{33}	Normal components of stress parallel to the 1, 2 and 3 axes
ε	General strain
$\dot{\varepsilon}$	Rate of crosshead speed
ε_{11} , ε_{22} , ε_{33}	Unit elongations in the 1, 2 & 3 directions
E_1, E_o	Initial elastic modulus determined by uniaxial tension along the 1 axis
E_2	Elastic modulus determined by uniaxial tension along the 2 axis
ϕ	% glass content by volume
ν	Degrees of freedom
ν_{11}	Poisson's ratio determined by uniaxial tension along the 1 axis
ν_{22}	Poisson's ratio determined by uniaxial tension along the 2 axis
G	Shear modulus determined by shear deformation with shear forces along the 1 and 2 axes
σ	Stress, universal standard deviation
$[C]$	Compliance or flexibility matrix
$[K]$	Stiffness matrix
$[T]$	Transformation matrix
t	Time, thickness
$\hat{s}$	Unbiased estimate
μ	Mean population
μ_1	First moment about the mean
$\bar{x}$	Mean of a sample

LIST OF PLATES

LIST OF FIGURES

LIST OF TABLES

CHAPTER 1

INTRODUCTION

1.1 Definition

The basic concept of a fibre reinforced material is to provide a dual phase composite structure in which the deformation of the matrix (usually of isotropic nature) is used to transfer stress to the fibres by means of shear stresses at the fibre-matrix interface.

For optimum strength in tension the fibres should be aligned parallel to the applied load in such a way that they do not touch each other. All fibres must be of the same strength, of uniform shape and be fully bonded to the matrix. When the fibres are of sufficient length they will be constrained to suffer the same deformation as the matrix. This is called 'combined action'.

Should some of the fibres be misaligned to the applied load then the effective efficiency of the composite will be reduced [7, 10, 27] and theoretically, if the fibres are distributed in a random manner, the effective stiffness of the

reinforcement will be one third of the stiffness of fibres parallel to the applied load.

Strength, elastic modulus and elongation of the fibres are usually much greater than that of the matrix. The ratio of volume of fibres to volume of matrix as well as fibre orientation plays an important role in the elastic properties and strength of the composite[7, 10, 43]. Further effects are brought about by variation of environment, mix ratio and void content of the composite, especially if an inorganic cement is employed for the matrix.

1.2 Discussion of Other Studies

Analytical and practical studies in the field of fibre reinforced plastics is extensive and has been pursued for some years, but the use of inorganic materials as a matrix is relatively recent. Russian workers [11] published a book in 1964. This lengthy work deals with fabrication problems and mechanical properties of various types of inorganic cements reinforced by glass fibres. Structures constructed in Russia with these materials are also discussed. The authors of this book report that work in the Chinese Peoples' Republic has been in progress since 1958 where very high values for tensile strengths and modulus of elasticity have been claimed.

Considerable work has been carried out at the Building Research Station (Watford) to produce a glass which can withstand chemical attack of Portland cement. They have also been working upon the reinforcement of Portland cement by glass fibres as reported by Majumdar and Ryder [32]. More detailed investigations by B.R.S. of the mechanical properties of glass reinforced ordinary Portland cement and Gypsum plaster are given by Grimer and Ali [1, 21].

Investigations have been carried out at Southampton by ALLEN and CHANNER[2, 4, 5, 6] to obtain an understanding of the mechanics of glass fibre reinforced inorganic cementous materials. Work has also been undertaken by BARTOS[9] on the bond between glass fibres and various inorganic cements.

1.3 Objectives of the Study

In 1967 a research project was initiated with the financial support of the Construction Industries Research and Information Association (C.I.R.I.A.), together with the co-operation of the Building Research Station. The research programme required the evaluation of the mechanical properties of inorganic cementitious materials reinforced by glass fibres.

Initial work carried out at Southampton using ordinary Portland cement and High Alumina cement as the matrix led to the conclusion that certain aspects of the Russian report [11] required further investigation.

The project was therefore subdivided to produce a wide range of relevant information as follows:

a) A study of a brittle matrix reinforced by glass fibres (Allen [2, 4, 5]).

b) A study of a comparatively ductile matrix reinforced by glass fibres (Channer).

c) A study of the bond between glass fibres and various inorganic cements (Bartos [9]).

Part b) is reported in this thesis and the objectives may be summarised as follows:

1) To conduct an exploratory study to establish manufacturing techniques and a suitable matrix for the investigation.

2) To investigate the short and long term mechanical properties of the matrix as a two phase material consisting of an organic material (Acrylic Polymer, Primal E330) and an inorganic material (hydrated ordinary Portland cement). To establish the effects of environment, rate of applied strain and level of stress upon the mechanical properties of the matrix. To obtain some understanding of the physical nature of the matrix.

3) To investigate the short term and time dependent properties of a composite consisting of the above matrix reinforced by an approximately random distribution of glass fibres. Also to compare this composite with composites using the same matrix but different types of glass reinforcement.

CHAPTER 2

THE PRELIMINARY INVESTIGATIONS

2.1 Introduction

The work described in Appendix D shows the tensile strength of glass reinforced cement to be in the range 2000 to 3000 lbf/in^2. This strength is regulated to some extent by the tendency of the high alumina cement matrix to crack at fairly low strains (about 0.4×10^{-3}), which is considerably lower than the quoted values for the fracture strain of the glass fibres (about 50×10^{-3}). At elevated tensile stresses the contribution of the cement to the tensile strength is greatly reduced. If the cracking strain of the matrix could be increased it would seem natural to expect improved tensile strengths.

A survey of high alumina and Portland cement admixtures was undertaken and is summarised in Table 2.1 and Tables F1 to F6. Each admixture was in turn combined with the cement to modify its mechanical and physical properties. It is obvious from the tables that only a few admixtures are compatible with high alumina cement and in general

only Portland cement can have its mechanical properties modified.

The ductility of Portland cement may be increased by the introduction of organic materials such as latex or resin. The admixtures A1 to A8 from Table 2.1 were considered by the author but A6, 7, and 8 were examined later in the programme and with hindsight, further work here was not considered necessary. Admixtures A9 to A12 were investigated by SASMAL[41].

It was necessary to obtain as quickly as possible a comparison between the admixture-cements with regard to the fracture strain of the resulting material. Simultaneously, effects due to variation of water to cement ratio, w/c, (by weight), solid to cement ratio*, s/c, (by weight) and effects caused by different curing conditions, were taken into account. Since only comparative tests were required the use of sophisticated testing equipment was not thought to be expedient, which explains the use of the adhoc bending tests described in Sec. 2.3.2.

Table 2.2 simply describes admixtures A1 to A5 in greater detail.

---

* Solid to cement ratio: this is the ratio of weight of solid polymer present in the admixture emulsion to the weight of dry cement powder.

TABLE 2.1

ADMIXTURES TO MODIFY THE MECHANICAL PROPERTIES OF CEMENT

NAME OF ADDITIVE		NAME OF COMPANY	TYPE OF CEMENT
A. 1	P.V.A. (Texicote VE 455)	Scott Bader and Company	Portland Cement
2	Acrylic/methacrylic Copolymers (Texicryl AM 655)	Scott Bader and Company	Portland Cement
3	Vinylidene Chloride Copolymer Emulsion (Polidene 904 DP)	Scott Bader and Company	Portland Cement
4	Copolymer Latex AL 911 (Viclan XVL 370/C)	I.C.I.	Portland Cement
5	Acrylic Polymer (Primal E-330 and Rhoplex MC-4530)	Lennig Chemicals Limited	Portland Cement
6	Sika-Latex	Sika Limited	Portland Cement
7	Vinamul 4001/B and 9810	Vinyl Products Limited	Portland Cement
8	Polimul 1188/1261 (PVA)	Dunlop Polymers	Portland Cement
9	Epoxy Resin	Borden Chemicals	Portland/H.A. Cement
10	Polyester Resin	Scott Bader and Company	Portland/H.A. Cement
11	Estercrete	Cement Marketing Company	Portland Cement
12	Acrylic Resin Emulsion	Rohm and Haas	Portland Cement

TABLE 2.2

DETAILS OF ADMIXTURES A1 to A5

A1.	TEXICOTE VE 455	
	(P.V.A. homopolymer emulsion)	
	Solid content	54 to 56%
	Plasticiser content	10%
	pH value	4.0 to 4.5
	Particle size	1 to 2 micron
	Specific gravity	1.08
	Freeze/Thaw stability	Unstable
	Colour	White
A2.	TEXICRYL AM 655	
	(Acrylic copolymer emulsion)	
	Solid content	55%
	pH value	9.0 to 9.5
	Particle size	0.25 micron
	Specific gravity	1.09
	Colour	White
A3.	POLIDENE 904 DP	
	(Vinylidene chloride copolymer)	
	Solid content	50 $\pm$ 1%
	pH value	4.0 to 4.5
	Particle size	0.22 to 0.28 micron
	Specific gravity	1.22
	Freeze/Thaw stability	Unstable
	Colour	White
A4.	VICLAN XVL 370/C	
	Solid content	47%
	pH value	2.3
	Colour	White
A5.	PRIMAL E330	
	(100% Acrylic dispersion)	
	Solid content	47 $\pm$ 1%
	pH value	9.5 to 10.0
	Particle size	Approx. 0.1 micron
	Specific gravity	1.059
	Freeze/Thaw stability	5 cycles
	Colour	White

2.2 The Physical Properties of Cement-Admixture Pastes

The physical characteristics of the matrix in its fresh state are important criteria in the manufacturing process of glass reinforced laminates. To obtain these characteristics a number of mixes were tried and then poured into perspex moulds (140 x 25 x 25 mm) to produce HAND samples. From these trials a subjective assessment was made to establish the suitability of particular admixture-cements for the production of glass reinforced laminates. This assessment is shown in Table 2.3 (column **5**), together with the corresponding admixture (column **1**), specimen identity number (column **2**), water/cement ratio (column **4**) and solid/cement ratio (column **3**). These details are also shown graphically in Figures 2.1 to 2.5. Each graph is a plot of solid/cement ratio against water/cement ratio on which is shown one continuous line (called the no-water-line) and one chain-dotted-line (called the good-mix-line). The former represents an extreme condition where only admixture and cement have been combined, i.e. no additional water has been used which would increase the value of water/cement ratio obtained by the presence of water in the polymer emulsion alone. The latter represents the various solid/cement and water/cement ratio which the author believes to be

suitable mixes when the paste is anticipated for use with glass fibres (this is the combination of dry cement powder, polymer emulsion and additional water). The numbered plots on these graphs correspond to the specimen numbers shown in Table 2.3.

Each cement-admixture will now be discussed.

CEMENT-TEXICOTE (Fig. 2.1)

This is a high viscosity latex compared with the other admixtures. Due to its high viscosity it is almost impossible to mix it with the cement powder without adding further water to the emulsion. This is illustrated in Fig. 2.1 where it can be seen that the 'good-mix-line' is parallel with the 'no-water-line'. It follows that the lowest possible water/cement ratio when contemplating subsequent use with glass fibres must be greater than 0.35 resulting in bleeding, reduced stiffness and strength. Any vertical upward displacement of the 'good-mix-line' results in a thicker mix and is therefore of limited use for the required purpose of this investigation. During mixing the emulsion foamed which promoted increased air entrainment, leading to reduced tensile strengths. The use of Texicote in conjunction with cement powder and water did not appear to produce a plasticising effect and it was necessary to mix

water with Texicote before mixing with the cement powder.

The hand samples appeared to be weak and soft although hardness may increase with age and the correct curing conditions. The hardened paste showed signs of shrinkage cracks and distortion.

CEMENT-TEXICRYL (Fig. 2.2)

The addition of Texicryl to cement paste had a plasticising effect. It was possible to use Texicryl directly with dry cement powder to obtain a high solid/cement ratio and low water/cement ratio. No coagulation was noticed when mixing without additional water so the mix appeared to be tacky rather than rubbery. The order of mixing did not seem to be of importance.

All the hardened specimens were weak when tested by hand and their hardness increased at decreased solid/cement ratios.

CEMENT-POLIDENE (Fig. 2.3)

Polidene displayed the same characteristics as Texicryl during mixing. The effects of moving the 'good-mix-line' horizontally to the right gives separation of the cement, water and admixture, indicating limits of saturation. Vertical downward

movement of the 'good-mix-line' results in a thicker mix and increased hardness in the hardened paste.

The solid specimens were free from visible cracks and considered brittle but a little stronger than A1 and A2. (Cement-Texicote and Cement-Texicryl).

CEMENT-VICLAN (Fig. 2.4)

The addition of Viclan to the fresh cement paste does not have a plasticising effect. At lower water/cement ratio (0.25) and the same solid/cement ratio it was found difficult to make the paste flow even under vibration. This means that high water/cement ratios and solid/cement ratios would be required if mixing with glass fibres is intended.

The hardened paste was hard, brittle and weak.

CEMENT-PRIMAL (Fig. 2.5)

This has a good plasticising effect but tends to foam at high solid/cement ratios. It would therefore be necessary to use some antifoaming agent to reduce porosity due to air bubbles. It is possible to add Primal direct to the cement powder although high speed mixing is required to obtain a creamy mix. It was preferable to mix the anti-foaming agent to the water, add to the admixture and then pour into the dry cement powder and mix

vigorously. If the good-mix-line is moved horizontally to the right, separation of water occurred. The same conditions apply if the good-mix-line is moved vertically upwards giving separation of the Primal, which was clearly visible in the hardened paste.

The hardened paste did not show any signs of distortion. The samples were fairly hard and ductility appeared to improve with increased solid/cement content.

OBJECTIVE ASSESSMENT OF ADMIXTURE-CEMENT PRISMS

TABLE 2.3

1	2	3	4	5
Admixture	Spec No.	s/c Ratio	w/c Ratio	Nature of Fresh Paste
Texicote	1	0.10	0.30	Very stiff - shrinkage cracks
"	2	0.15	0.30	- do -
"	3	0.20	0.35	- do -
"	4	0.10	0.40	Good
"	5	0.15	0.40	Good
"	6	0.20	0.40	Good
"	7	0.005	0.38	Good
"	8	0.10	0.45	Good
"	9	0.15	0.54	Good
"	10	0.20	0.60	Good
Texicryl	11	0.20	0.164	Good
"	12	0.10	0.282	Good
"	13	0.15	0.218	Good
"	14	0.242	0.198	Good (little wet)
"	15	0.15	0.25	Good
"	16	0.10	0.30	Good
"	17	0.05	0.32	Good
"	18	0.05	0.26	Good
"	19	0.05	0.40	Good
Polidene	20	0.121	0.212	Good
"	21	0.20	0.2	Little wet
"	22	0.20	0.35	Very wet
"	23	0.25	0.25	On wet side
"	24	0.156	0.156	Very stiff
"	25	0.175	0.175	Good, dry side
"	26	0.10	0.25	Good
"	27	0.05	0.30	Good
"	28	0.05	0.20	Stiff
"	29	0.05	0.40	Very wet

(No Shrinkage Cracks)

TABLE 2.3 (Continued)

1	2	3	4	5
Admixture	Spec No.	s/c Ratio	w/c Ratio	Nature of Fresh Paste
Viclan	30	0.216	0.244	Does not plasticise
"	31	0.226	0.256	Poor flow when vibrated
"	32	0.1	0.38	Good mix, just flows
"	33	0.1	0.40	Wet mix, flows readily
"	34	0.1	0.42	Wet, little vibration reqd.
"	35	0.15	0.3	Good, difficult to vibrate
"	36	0.15	0.32	Good
"	37	0.15	0.34	Good
"	38	0.20	0.26	Good, but doughy
"	39	0.20	0.30	- do -
"	40	0.20	0.338	- do -
Primal E330	41	0.2	0.3	Good
"	42	0.25	0.3	Good
"	43	0.12	0.2	Good, little stiff
"	44	0.2	0.25	Good
"	45	0.15	0.35	Good, little wet
"	46	0.15	0.25	Good
Sika-Latex	47	0.2	0.19	No foaming, quite tacky
"	48	0.163	0.238	Good
"	49	0.122	0.198	Slightly drier than 48
"	50	0.082	0.157	
"	52	0.147	0.141	Just mixes
"	53	0.104	0.178	Very dry, but will vibrate
"	54	0.104	0.218	Good mix, on dry side
"	55	0.104	0.258	Good mix, on wet side
"	56	0.104	0.298	Little too wet
"	57	0.104	0.338	Quite wet

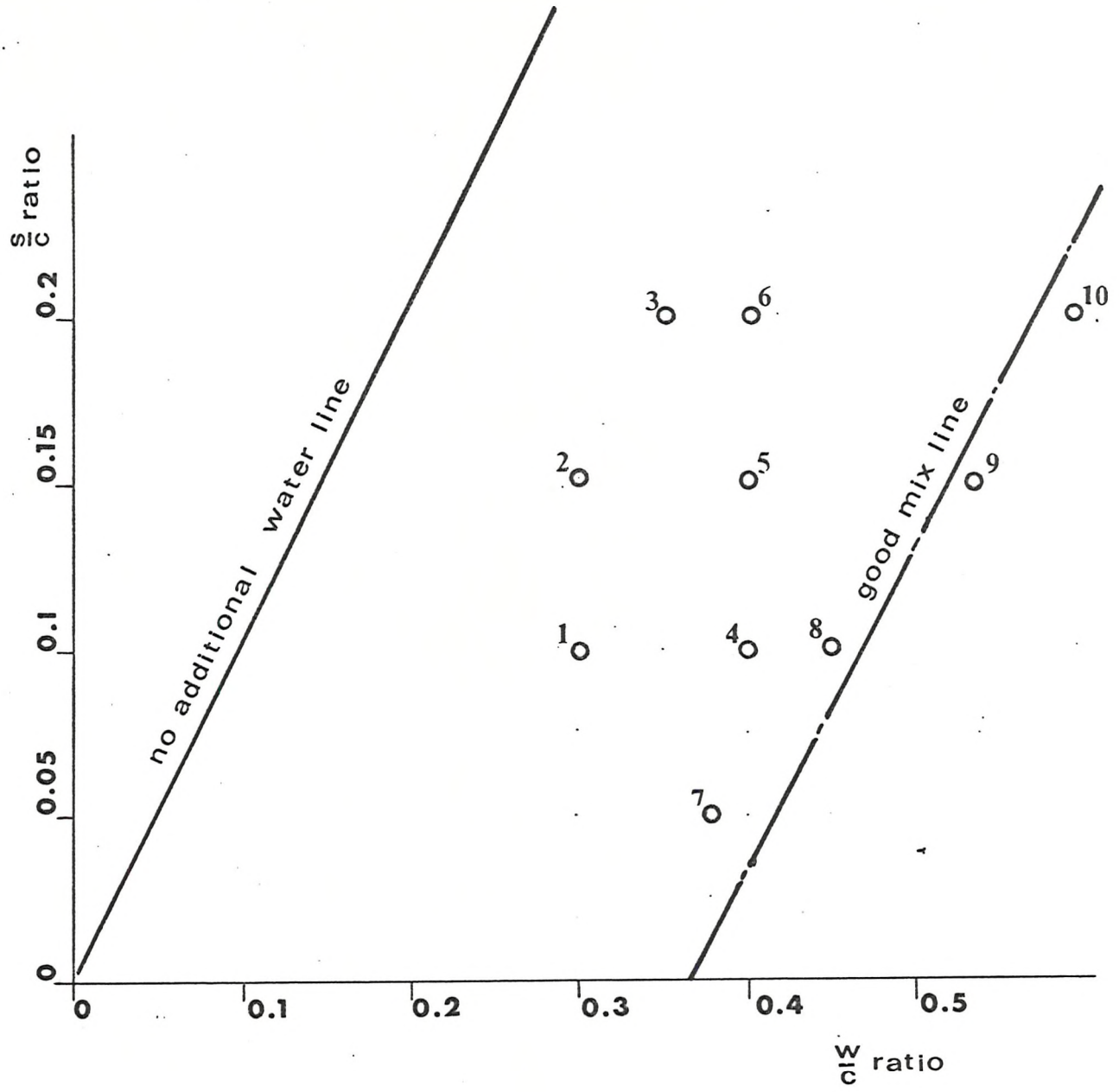

Physical Relationship Between S/C & W/C Ratio

(Texicote VE 455 + P. Cement)

Fig. 2.1

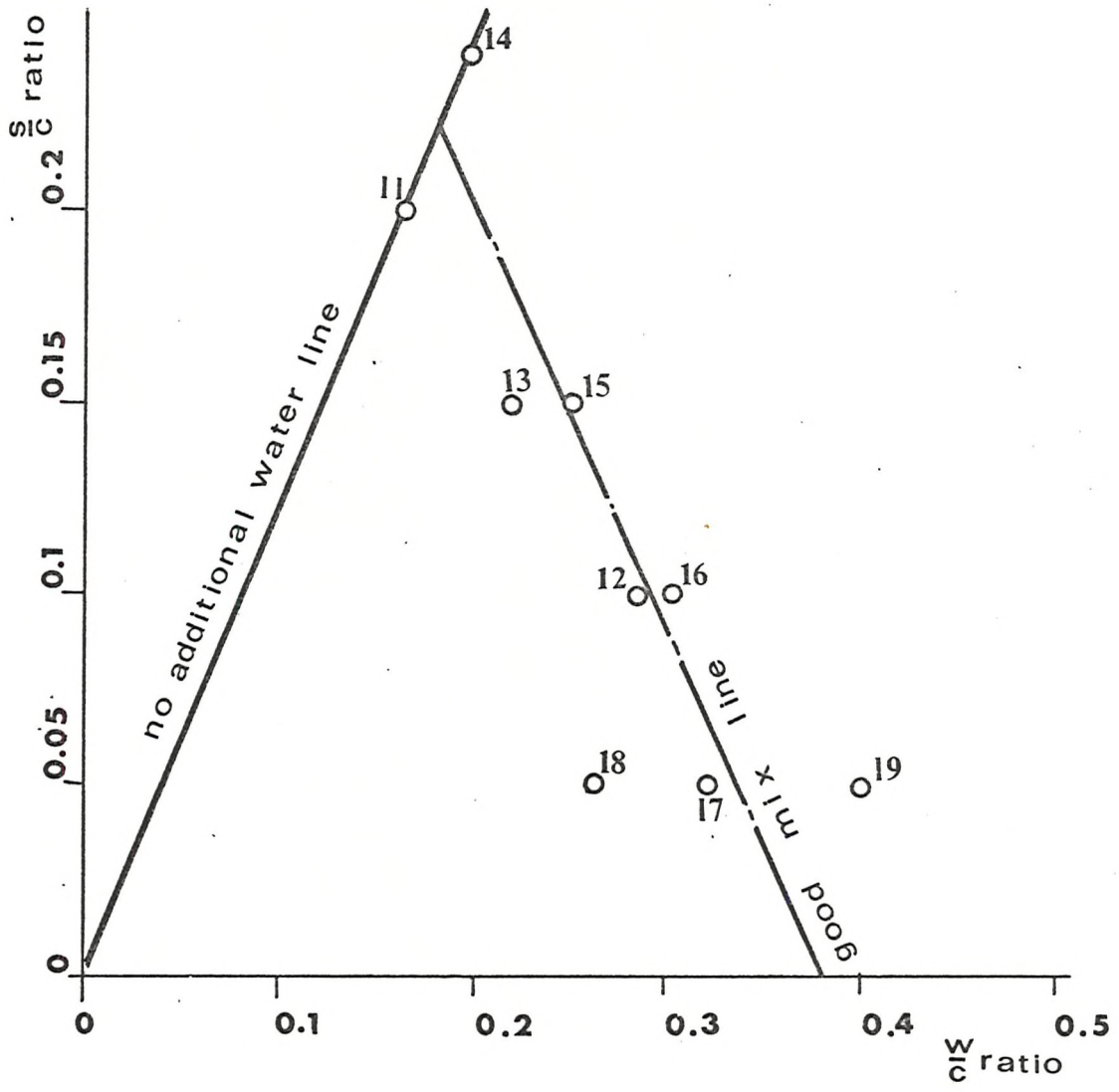

Physical Relationship Between S/C & W/C Ratio

(Texicryl AM 655+ P. Cement)

Fig. 2.2

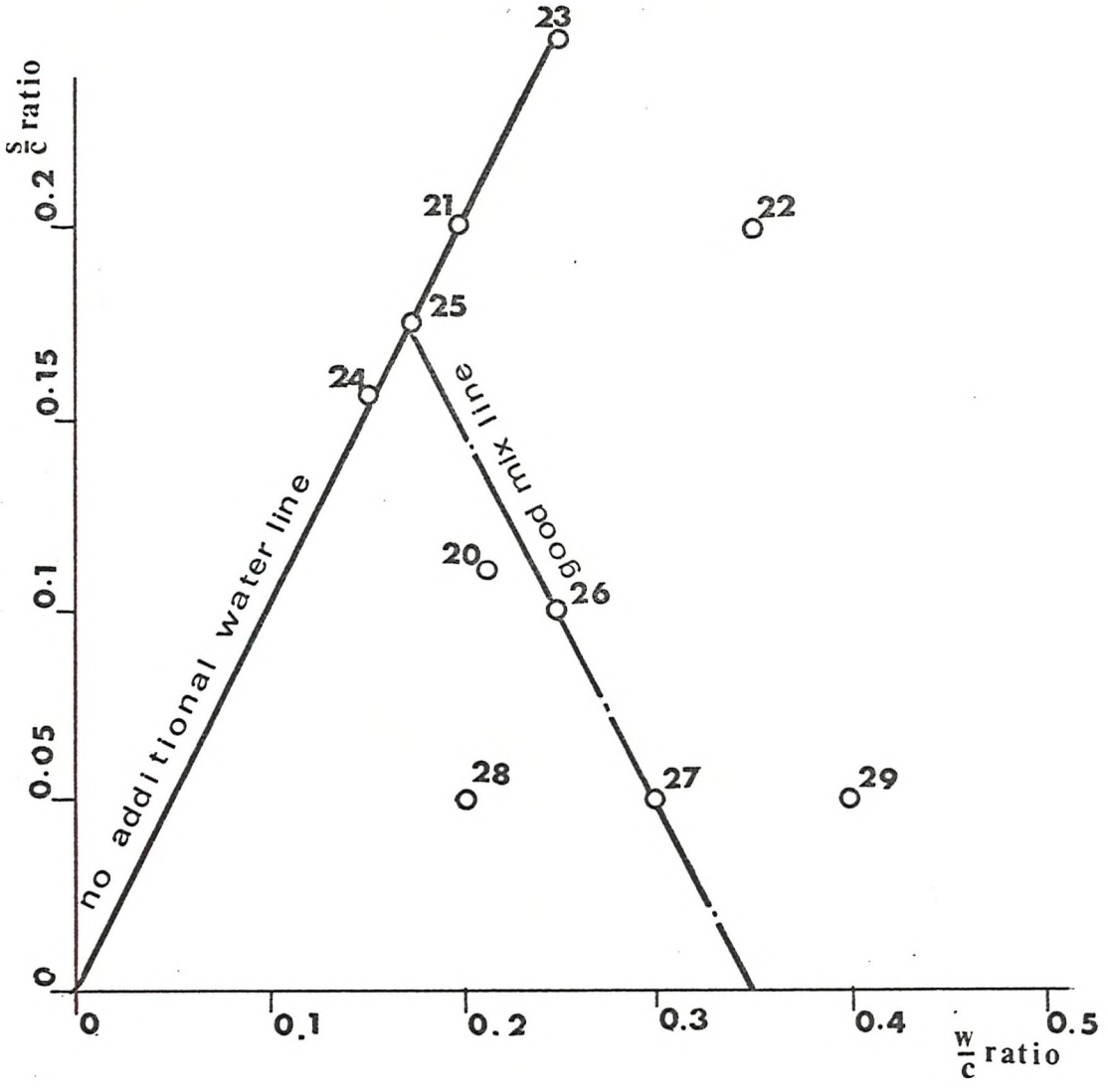

Physical Relationship Between S/C & W/C Ratio

(Polidene 904 DP+ P. Cement)

Fig. 2.3

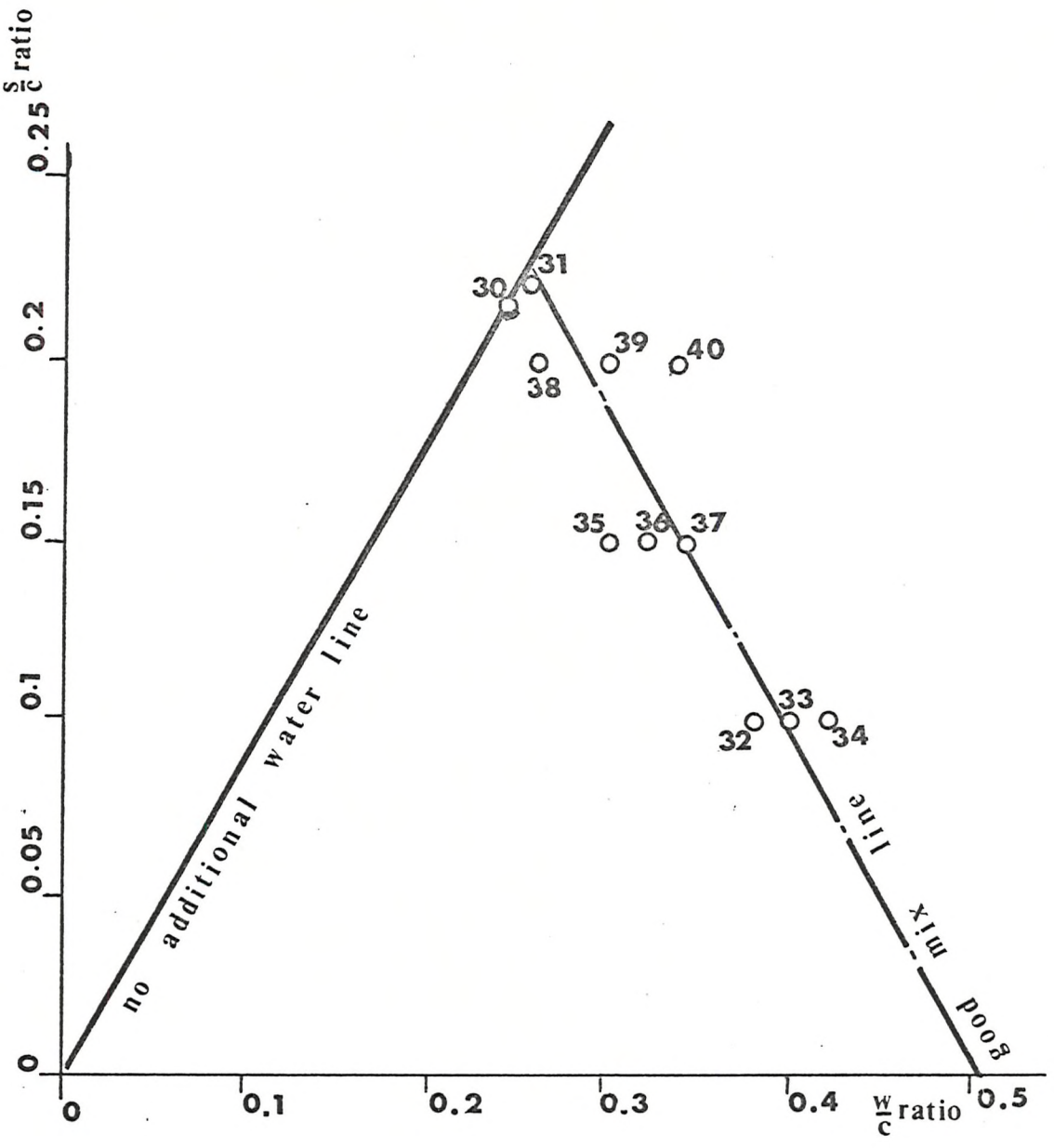

Physical Relationship Between S/C & W/C Ratio

(Viclan + P. Cement)

Fig. 2.4

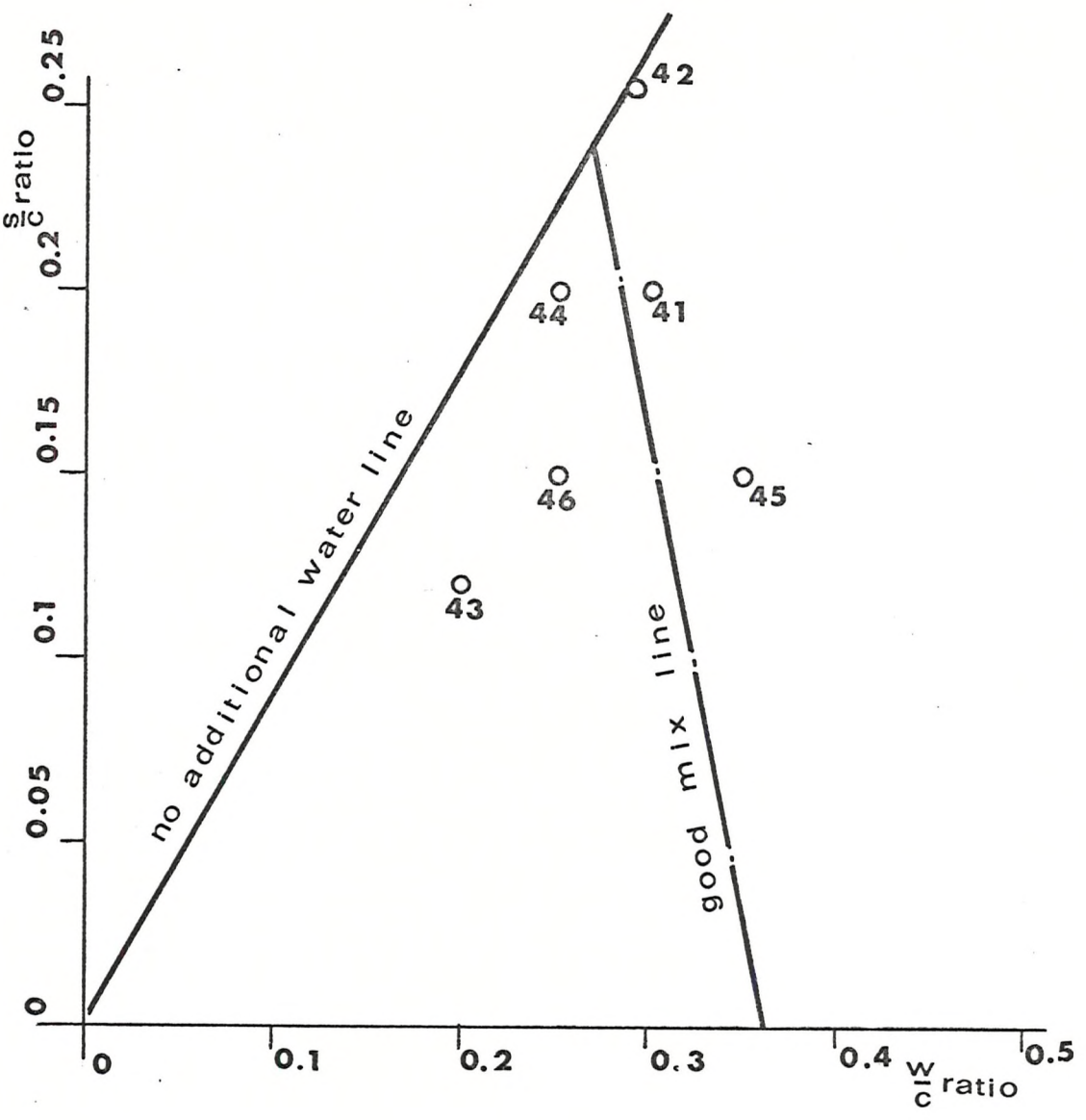

Physical Relationship Between S/C & W/C Ratio

(Primal E330 + P. Cement)

Fig. 2.5

2.3 Comparative Mechanical Properties of Cement-Admixture Pastes

2.3.1 Preparation and Composition of Test Pieces

In order to obtain an objective method of comparing the mechanical properties of hardened cement-admixture pastes, single test pieces were manufactured to form beams which could be subjected to bending stresses.

These beams were made in open rectangular perspex moulds (9 in. long) so that the depth of each specimen was the width of the individual moulds. In each mould a total of six specimens were cast and these were stored at ambient conditions for 24 hours. Pastes using Primal as an admixture remained in the mould for 48 hours to allow the specimens to become sufficiently hard so that they could be removed without damage. At the end of this time the specimens were demoulded and cured for a further period under various curing conditions. The curing conditions and composition of the specimens are detailed in Table 2.4.

Generally at the end of the first 24 hours the exposed face of the specimen whilst in the mould was concave. Therefore, just prior to testing, this face was ground to give a flat surface.

Since the moulds were not accurately machined the final widths of the test pieces also varied. The width and depth of every beam was measured at the centre of the beam length, also at one inch either side of this position. The arithmetic means of these observations is shown in Appendix F. (Table F7).

TABLE 2.4

COMPOSITION AND CURE OF BEAM SPECIMENS

Specimen Number	s/c Ratio	w/c Ratio	T. Age (Days)	Cure (Days) Air	Wet	Air	
60-65	0.10	0.4	22	21	-	-	Texicote
66-71	0.15	0.4	22	21	-	-	
72-77	0.20	0.4	22	21	-	-	
78-82	0.10	0.5	22	21	-	-	
83-87	0.10	0.3	22	21	-	-	
88-93	0.10	0.4	29	21	7	-	
94-97	0.1	0.36	22	21	-	-	Texicryl
98-103	0.15	0.22	22	21	-	-	
104-107	0.2	0.177	22	21	-	-	
108-112	0.227	0.185	22	21	-	-	
113-117	0.15	0.30	22	21	-	-	
118-123	0.10	0.25	22	21	-	-	
124-129	0.10	0.25	29	21	7	-	
130-135	0.147	0.28	22	21	-	-	Polidene
136-139	0.15	0.30	22	21	-	-	
140-144	0.15	0.20	22	21	-	-	
145-149	0.10	0.30	22	21	-	-	
150-155	0.15	0.20	22	21	7	-	
156-158	0.1	0.20	22	21	-	-	
159-163	0.1	0.35	22	21	-	-	Viclan
164-167	0.125	0.35	22	21	-	-	
168-172	0.15	0.35	22	21	-	-	
173-177	0.15	0.30	22	21	-	-	
178-182	0.12	0.2	22	20	-	-	Primal
183-187	0.25	0.3	9	7	-	-	
188-193	0.2	0.25	9	7	-	-	
194-198	0.15	0.35	9	7	-	-	
199-204	0.15	0.25	9	7	-	-	
205-210	0.25	0.3	14	-	7	5	
211-216	0.25	0.3	14	-	12	-	
217-222	0.25	0.3	14	7	5	-	
223-227	0.20	0.3	14	-	7	5	
228-233	0.20	0.3	14	-	12	-	
234-239	0.20	0.3	14	7	5	-	
240-244	0.20	0.3	14	12	-	-	

2.3.2 The Flexural Tests and Their Results

A three point bending rig (Plate 2.1) was incorporated with the compression cell of the Instron testing machine (Appendix C, Sec. C1). The test piece was then positioned and a dial gauge placed at midspan directly under the specimen. The load was applied at this point at a constant speed (0.01 in/min) until fracture of the specimen occurred. Having chosen a convenient chart drive speed this load was automatically reproduced on the X-Y chart as a continuous curve. An attachment to the Instron testing machine allows this continuous plot to be momentarily interrupted and is shown as a horizontal line (called blipping). This was done at particular dial gauge readings so the load was recorded on the X-Y chart. The graphs were then re-plotted and are shown as scatter diagrams in Appendix F, Figs. F1 to F12.

From this information NOMINAL values were obtained and are defined as follows:

Nominal Ultimate Strength (σ_u): the quotient of the maximum bending moment and the section modulus.

Nominal Cracking Strain (e_u): the maximum strain due to the deflection at the load (corresponding to the last recordable blip), assuming the beam behaved

in an elastic manner throughout the test.

Initial Elastic Modulus (E_o): if it is assumed that the tensile and compressive modulii are equal, then the initial slope of the load/deflection graph may be considered to be proportional to the initial elastic modulus.

A number of gross assumptions have been made here but this investigation is only intended to give comparative values and it is not expected that the data presented should be interpreted as absolute values. The simple theory of bending has been assumed to apply and obviously, in most cases, plastic flow occurs at high loads so the true stress would be lower than the values quoted and the true strain would be greater than nominal cracking strain. Also it is not general that the elastic modulii in tension and compression are equal.

These values are summarised in Tables 2.5, 2.6 and 2.7 which show the mean value of nominal ultimate strength (σ_u), nominal cracking strain (e_u), and initial elastic modulus (E_o). Also shown in these tables are the upper and lower confidence levels of the values which would be expected for probability 0.1 according to equation A15. Results for each specimen are recorded in Appendix F, Table F8.

Figures 2.6 to 2.8 compare and illustrate the variation of the ultimate tensile strength (σ_u), tensile cracking strain (e_u) and initial elastic modulus (E_o) of all beam specimens. Although Cement-Texicote is included in these figures it is excluded from further discussion in view of the difficulties explained on page 12.

Fig. 2.6 clearly shows that additions of Polidene and Primal to the cement paste increases the tensile strength of hardened Portland cement paste. When Primal is used as an admixture the hardened paste has a wide variation of tensile strengths, especially if the paste is exposed to various curing conditions. The minimum strengths of this paste appear to be in the region of the normal dry strengths of the other pastes where Texicote, Texicryl and Viclan are used. When comparing specimens 217-222, 223-227 and 240-244 (Tables 2.4 and 2.5) it can be seen that, although wet curing conditions reduce the tensile strengths of this material, they are regained after a period of air curing.

It is interesting to note in Fig. 2.7 that Cement-Viclan displays very low fracture strains so it may also be excluded as a possible matrix material since the required improvement of tensile strength and fracture strains are not obvious.

Although Cement-Polidene has fairly high tensile strengths a weakness with regards to fracture strain is indicated on Fig. 2.7 and is only of the order 2-3 times greater than that of Portland Cement paste. Thus only the admixtures Primal and Texicryl need be considered.

Fig. 2.8 shows the stiffness of pastes using the admixtures Texicryl and Primal to be approximately the same, whilst the pastes using Polidene and Viclan as admixtures, are greater.

In view of the greater tensile properties of Cement-Primal over Cement-Texicryl the former was selected as the matrix material for the investigation.

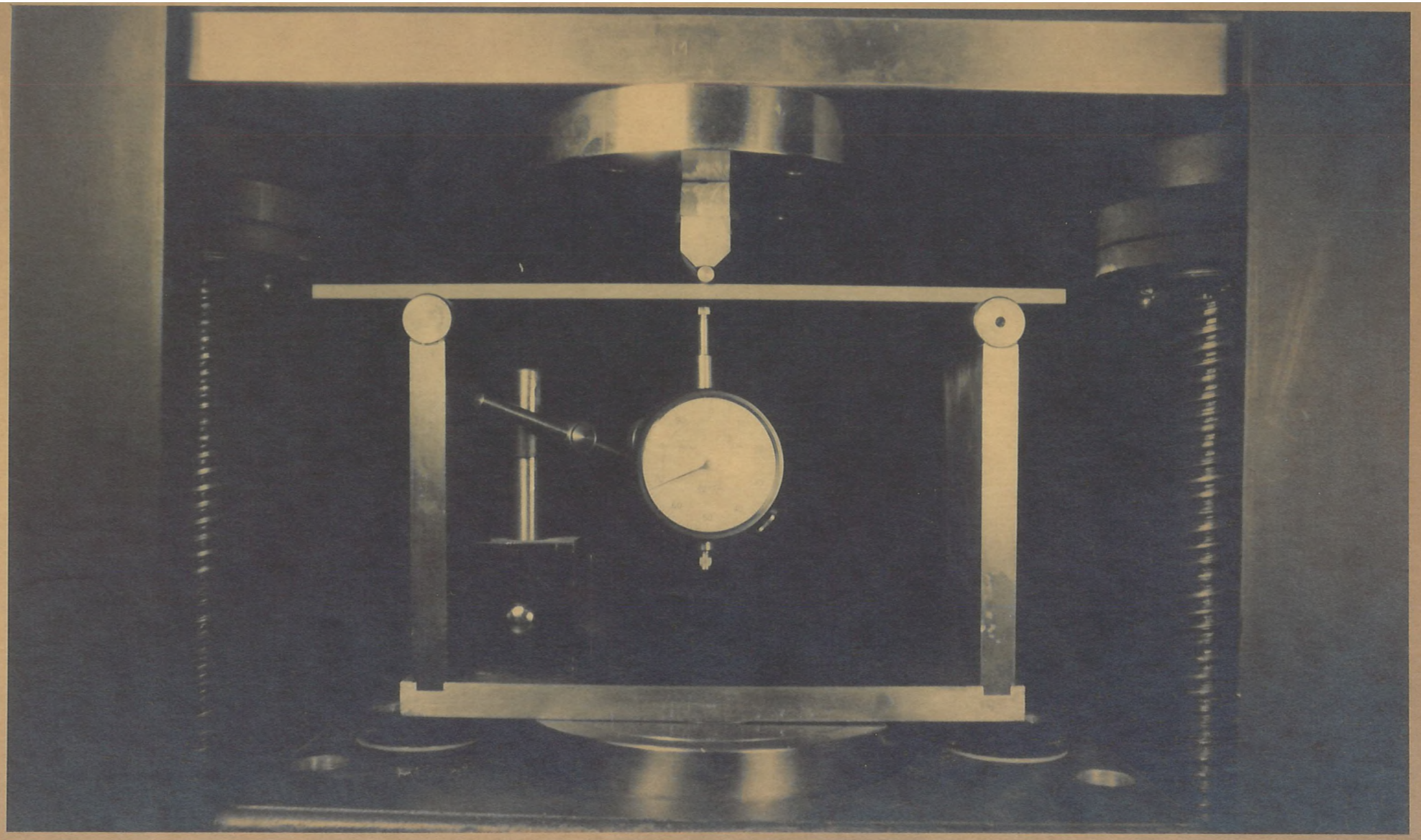

ASSEMBLED BENDING RIG

Plate 2.1

TABLE 2.5

MAXIMUM BENDING STRESSES

Specimen Number	Mean Value lbf/in^2	Standard Deviation lbf/in^2	Coeff. of Variance %	LIMIT p = 0.1 UPPER lbf/in^2	LIMIT p = 0.1 LOWER lbf/in^2
60-65	357.07	71.306	19.970	415.87	298.27
66-71	320.44	75.803	23.656	392.65	248.24
72-77	309.29	21.809	7.051	327.28	291.31
78-82	360.39	101.480	28.160	457.06	263.72
83-87	614.06	66.939	10.901	677.83	550.30
88-93	1216.30	34.123	2.805	1244.30	1188.10
94-97	690.25	36.569	5.297	733.22	647.28
98-103	918.27	110.580	12.042	1009.50	827.03
104-107	731.34	42.427	5.801	781.19	681.48
108-112	633.66	28.637	4.519	660.94	606.38
113-117	677.40	75.109	11.088	748.95	605.85
118-123	752.25	76.849	10.216	815.62	688.87
124-129	644.19	103.370	16.047	729.44	558.94
130-135	1232.20	147.510	11.972	1353.80	1110.50
136-139	1339.90	173.410	12.942	1543.70	1136.10
140-144	1376.20	276.720	20.108	1639.70	1112.60
145-149	1012.40	71.541	7.066	1080.50	944.25
150-155	1354.60	119.160	8.797	1452.80	1256.30
156-158					

TABLE 2.5 (Continued)

MAXIMUM BENDING STRESSES

Specimen Number	Mean Value lbf/in^2	Standard Deviation lbf/in^2	Coeff. of Variance %	LIMIT p = 0.1 UPPER lbf/in^2	LIMIT p = 0.1 LOWER lbf/in^2
159-163	682.37	67.696	9.920	796.50	568.25
164-167	709.94	126.520	17.821	858.60	561.28
168-172	595.36	103.210	17.336	693.68	497.04
173-177	619.10	49.729	8.032	677.53	560.66
178-182	1278.80	84.199	6.584	1359.00	1198.60
183-187					
188-193	1420.80	151.280	10.647	1545.50	1296.00
194-198	720.83	105.340	14.613	821.18	620.49
199-204	1278.80	107.610	8.414	1367.50	1190.00
205-210	966.03	78.231	8.098	1030.50	901.51
211-216	413.27	36.796	8.903	443.62	382.93
217-222	510.34	57.020	11.173	564.66	456.03
223-227	1293.30	75.677	5.851	1365.40	1221.20
228-233	578.43	42.361	7.322	618.84	538.13
234-239	603.93	58.370	9.665	652.06	555.79
240-244	1356.00	178.090	13.134	1565.30	1146.70

TABLE 2.6

TENSILE FRACTURE STRAIN x 10^3

Specimen Number	Mean Value	Standard Deviation	Coeff. of Variance %	LIMIT p = 0.1	
				UPPER	LOWER
60-65	1.565	0.3918	25.028	1.888	1.242
66-71	2.177	0.1840	8.456	2.352	2.001
72-77	4.568	0.6703	14.676	5.120	4.014
78-82	1.432	0.3154	22.032	1.732	1.131
83-87	1.747	0.2000	11.454	1.937	1.556
88-93	0.779	0.0282	3.619	0.802	0.756
94-97	1.299	0.0845	6.510	1.398	1.199
98-103	1.791	0.3553	19.837	2.084	1.498
104-107	2.766	0.1717	6.209	2.968	2.564
108-112	3.207	0.3256	10.153	3.518	2.897
113-117	2.657	0.4707	17.711	3.106	2.209
118-123	1.198	0.1661	13.863	1.335	1.061
124-129	1.436	0.2346	16.334	1.629	1.242
130-135	0.918	0.1377	15.004	1.031	0.804
136-139	1.267	0.1118	8.826	1.398	1.136
140-144	0.939	0.1903	20.250	1.121	0.758
145-149	0.637	0.0345	5.421	0.670	0.604
150-155	1.196	0.1091	9.125	1.286	1.106
156-158					

TABLE 2.6 (Continued)

TENSILE FRACTURE STRAIN x 10^3

Specimen Number	Mean Value	Standard Deviation	Coeff. of Variance %	LIMIT p = 0.1 UPPER	LOWER
159-163	0.427	0.0501	11.736	0.511	0.342
164-167	0.401	0.0847	21.118	0.501	0.301
168-172	0.363	0.0627	17.274	0.422	0.303
173-177	0.292	0.0447	15.294	0.345	0.239
178-182	1.573	0.1300	8.267	1.696	1.448
183-187					
188-193	2.703	0.5254	19.437	3.136	2.270
194-198	2.153	0.3594	16.694	2.495	1.810
199-204	1.383	0.2760	19.954	1.611	1.155
205-210	3.374	0.4551	13.487	3.749	2.999
211-216	1.262	0.1458	11.552	1.382	1.141
217-222	2.418	0.2618	10.829	2.667	2.168
223-227	2.936	0.3171	10.798	3.238	2.634
228-233	1.164	0.1360	11.731	1.294	1.034
234-239	1.553	0.1626	10.469	1.687	1.419
240-244	3.787	0.7263	19.180	4.640	2.933

TABLE 2.7

INITIAL ELASTIC MODULUS x 10^{-6} (LBF/IN^2)

Specimen Number	Mean Value	Standard Deviation	Coeff. of Variance %	LIMIT p = 0.1	
				UPPER	LOWER
60-65	0.273	0.0816	29.807	0.341	0.206
66-71	0.240	0.0789	32.910	0.315	0.164
72-77	0.134	0.0240	17.845	0.154	0.114
78-82	0.348	0.0542	15.576	0.400	0.296
83-87	0.464	0.0822	17.715	0.542	0.385
88-93	1.543	0.1029	6.670	1.627	1.458
94-97	0.610	0.0445	7.298	0.662	0.557
98-103	0.691	0.0269	3.892	0.713	0.669
104-107	0.495	0.0265	5.353	0.526	0.463
108-112	0.422	0.0236	5.593	0.445	0.400
113-117	0.430	0.0191	4.456	0.448	0.412
118-123	0.737	0.0415	5.634	0.771	0.702
124-129	0.575	0.1199	20.851	0.674	0.476
130-135	1.385	0.0617	4.454	1.436	1.335
136-139	1.092	0.1032	9.453	1.213	0.971
140-144	1.506	0.0584	3.881	1.561	1.450
145-149	1.578	0.0516	3.271	1.627	1.529
150-155	1.249	0.1203	9.634	1.348	1.149
156-158					

TABLE 2.7 (Continued)

INITIAL ELASTIC MODULUS x 10^{-6} (LBF/IN^2)

Specimen Number	Mean Value	Standard Deviation	Coeff. of Variance %	LIMIT p = 0.1	
				UPPER	LOWER
159-163	1.600	0.0318	1.988	1.654	1.547
164-167	1.783	0.1705	9.562	1.984	1.583
168-172	1.641	0.0788	4.801	1.716	1.566
173-177	2.447	0.4513	18.442	2.977	1.917
178-182	0.973	0.1019	10.478	1.070	0.876
183-187					
188-193	0.675	0.0338	5.015	0.703	0.647
194-198	0.531	0.0764	14.381	0.604	0.458
199-204	0.999	0.0729	7.302	1.059	0.939
205-210	0.438	0.0378	8.634	0.469	0.407
211-216	0.434	0.0386	8.887	0.466	0.402
217-222	0.309	0.0090	2.920	0.318	0.301
223-227	0.588	0.0831	14.140	0.667	0.509
228-233	0.586	0.0596	10.166	0.643	0.530
234-239	0.586	0.0785	13.385	0.651	0.522
240-244	0.998	0.0741	7.431	1.059	0.937

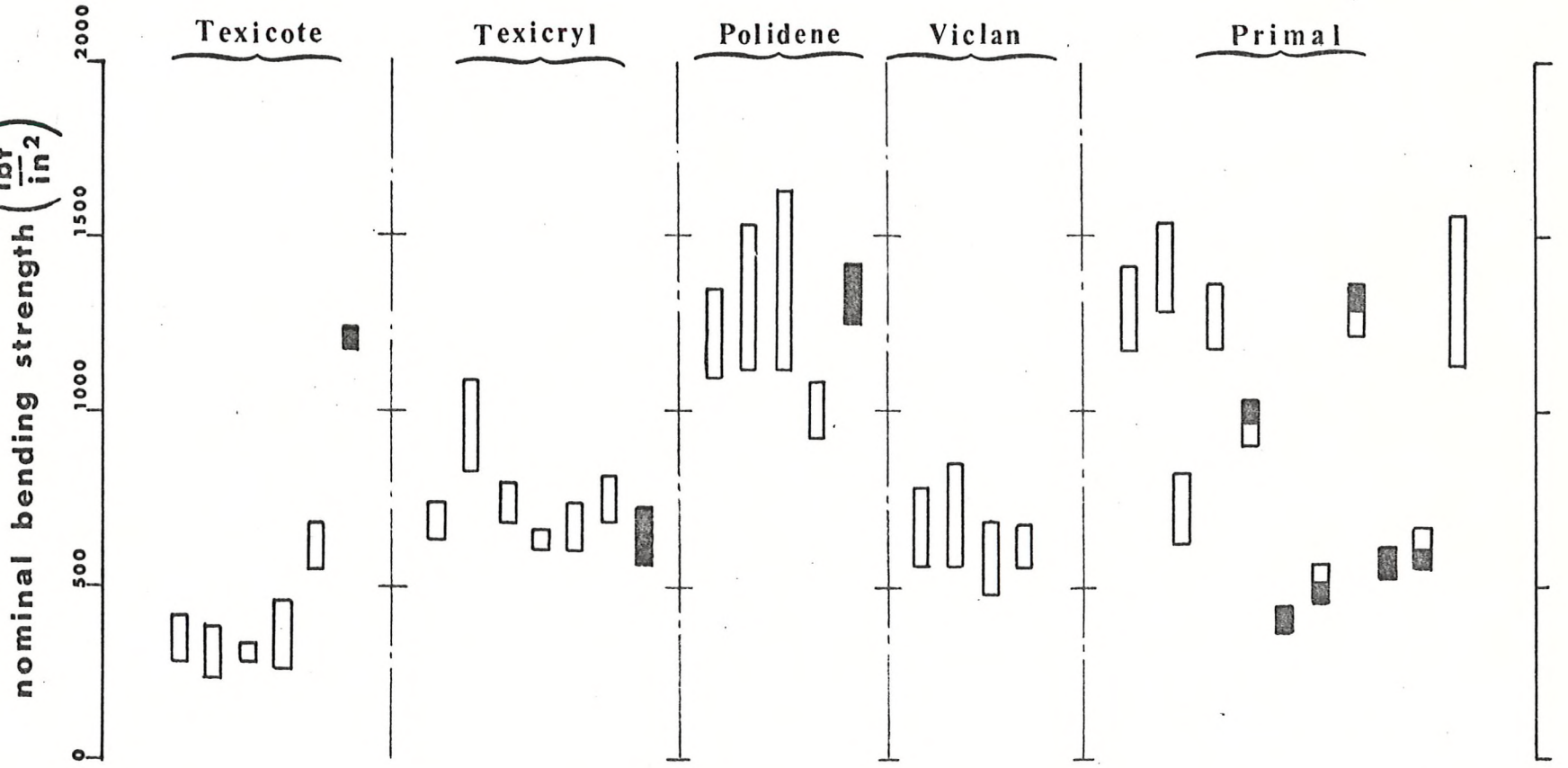

Comparative Chart for Bending Strengths

Fig 2.6

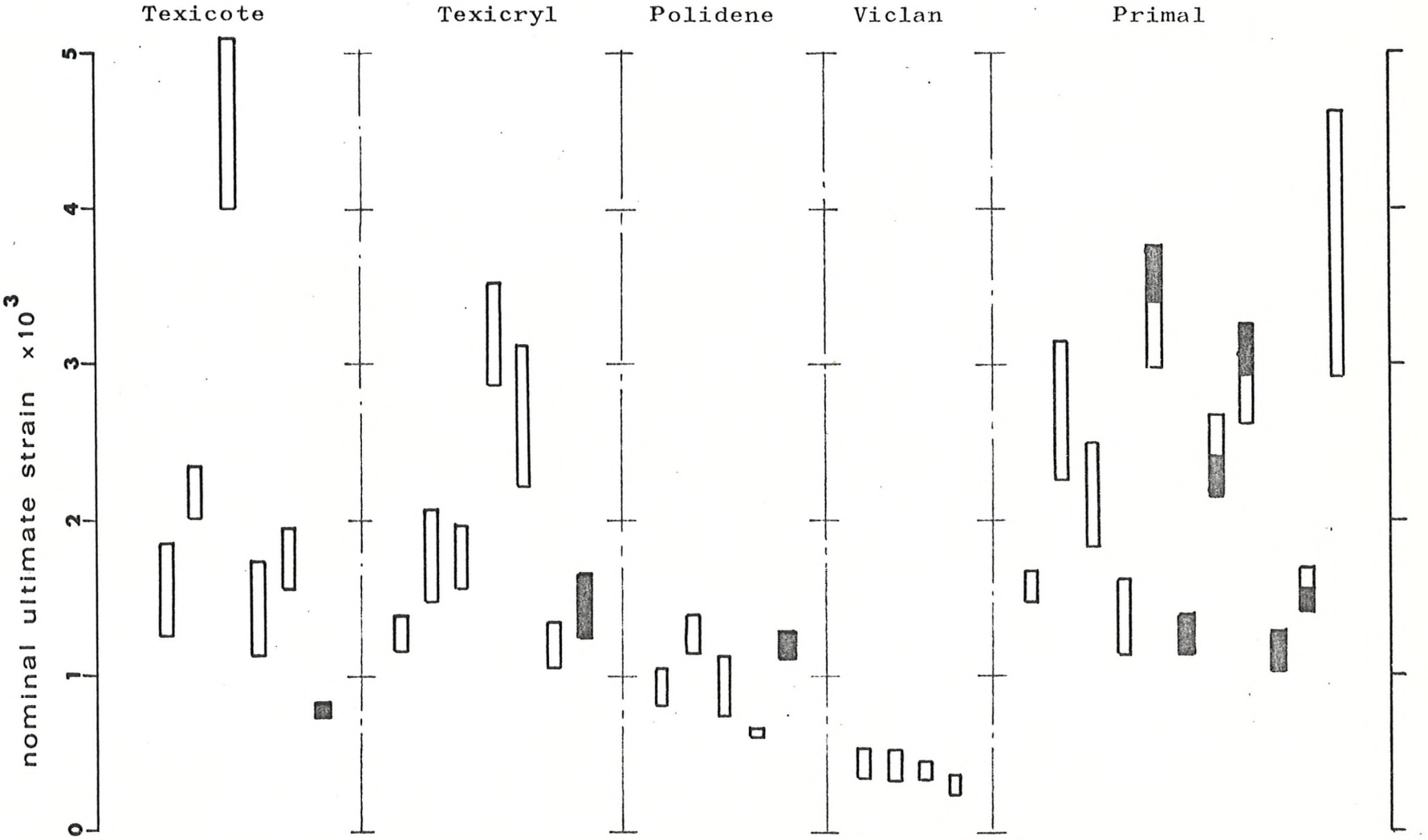

Comparative Chart for Bending Strains

Fig 2.7

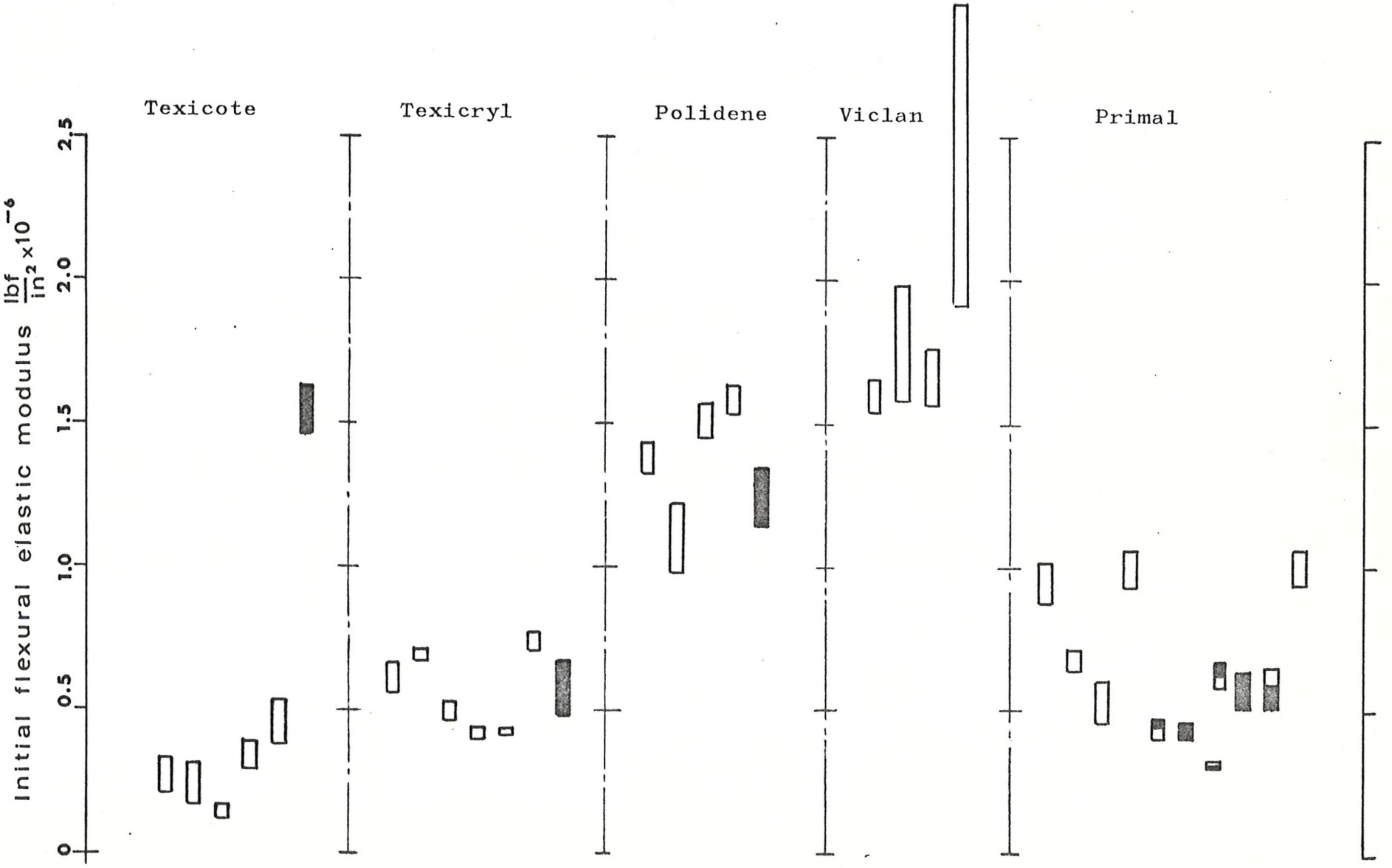

Comparative Chart for Elastic Modulii

Fig 2.8

2.3.3 Comparative Tensile Tests on Thin Glass-Reinforced Laminates

To obtain some preliminary information about the mechanical properties of glass-reinforced/cement-Primal laminates, a few tests were carried out to compare these properties with those of other similar materials. The comparative materials were polyester or epoxy resin with Portland cement systems reinforced by glass fibres together with the materials of Appendix F, Table F9.

Each laminate was manufactured using three layers of chopped strand mat (FGE 2000), having a nominal weight of 1.5 ozf/ft^2. These laminates were prepared by laying alternately the matrix material, in its fresh condition, and the glass mat and finally sandwiched between two smooth sheets of thin plastic. In order to improve the impregnation, surface finish and remove surplus air, the sandwich was subjected to pressure from rollers. The laminates remained between the two plastic sheets for the initial cure period of 24 hours, then left to cure in air at room temperature and humidity. (The laminated sheets were lettered A to H). Laminates A, B and C used an epoxy resin (supplied by Borden Chemicals Limited), specially selected for use with Portland

cement but not normally used in glass reinforced systems. This resin EL5 (100 parts) with hardener EHR1 (80 parts) was combined with glass fibres (laminate A), or with cement powder and glass fibres (laminate B) or with fresh cement paste with a water/cement ratio of 0.3 and glass fibres (laminate C).

Sheets D, E and F used cement-Primal as the matrix material with a constant water/cement ratio of 0.3 with various solid/cement ratios of 0.2, 0.25 and 0.15 respectively.

Laminates G and H incorporated a polyester resin, Crystic 189 supplied by Scott-Bader Company Limited, in the proportions shown in Table 2.8. Due to excessive bleeding of the water it was not found satisfactory to mix polyester resin with fresh cement paste.

All the hardened sheets were cut and prepared as described in Appendix C (Sec. C2) to produce six tensile specimens having a nominal width of 1 inch, from each sheet. The specimens were tested in tension to failure using the Instron testing machine. Extensions of the test piece were measured by a displacement transducer mounted in an extensometer (Plate 3.1).The transducer was linked to a transducer meter giving a reading of the specimen

extension. It was therefore possible to obtain an automatic plot of load against extension by using the Instron X-Y recorder, set at a constant drive speed, and the blipping device. For specimens cut from sheets G and H the microformer, which drives the X-Y recorder, was used also giving an automatic load/extension graph. These graphs can all be seen in Appendix F in the form of scatter diagrams. (Figs. F13, F14). If ultimate load (P_u) and stiffness per unit width ($E_o t$) are to be regarded as a criterion of efficient utilisation of the glass, then Table 2.8 shows polyester to be a superior laminating resin producing a strong stiff ductile material.

The epoxy resin (laminate B) shows a slight increase of stiffness, if cement is used as an inert filler, together with reduced strength and ductility. When cement paste is combined with the epoxy resin (laminate C) the strength, ductility and stiffness are all reduced.

Cement-Primal-glass laminates show the possible effect of solid/cement ratio upon their mechanical properties. Table 2.8 indicates that maximum values may be attained for strength, stiffness and ductility at water/cement ratio = 0.3 and solid/cement ratio = 0.2 (laminate D).

TABLE 2.8

RESULTS OF TENSILE TEST ON LAMINATES REINFORCED BY CHOPPED STRAND MAT

Spec. No.	Matrix Material	Ratios			Total Age (Days)	Thickness (t) in.	Ultimate Load (Pu) lbf.	Ultimate Stress (σ_u) lbf/in^2	Ultimate Strain x 10^3 (ε_u)	Initial Elastic Modulus x 10^{-6} (E_o) lbf/in^2	$E_o t \times 10^{-3}$ lbf/in^2	Approx. ϕ
		s/c	w/c	r/c								
A(1-6)	Epoxy Resin	-	-	-	8	0.103	1136.0	11090	24.12	0.655	67.5	0.206
B(1-6)	Epoxy Resin/ Cement Powder	-	-	1.0	8	0.116	1010.0	8990	17.07	0.672	77.9	0.183
C(1-6)	Epoxy Resin/ Cement Paste	-	0.3	1.0	8	0.103	757.0	7350	19.85	0.623	64.2	0.206
D(1-6)	Primal/ Cement Paste	0.2	0.3	-	8	0.114	815.0	7160	15.26	0.551	62.8	0.186
E(1-6)	- " -	0.25	0.3	-	8	0.114	742.0	6500	15.7	0.520	59.3	0.186
F(1-6)	- " -	0.15	0.3	-	8	0.121	525.0	4340	8.84	0.553	66.9	0.175
G(1-6)	Polyester Resin	-	-	-	10	0.071	1682.0	23750	19.51	1.473	104.6	0.299
H(1-6)	Polyester Resin/ Cement Powder	-	-	1.0	7	0.090	1247.0	14040	16.13	1.214	109.3	0.236

CHAPTER 3

PROPERTIES OF THE MATRIX

3.1 Outline

As a result of Chapter 2 it was decided to use for the investigation a particular matrix material with constant composition and curing conditions. There was insufficient time to investigate the effect of varying the composition and the cure, although the effect of varying the water/cement ratio and solid/cement ratio of admixture-cements was considered by ALLEN and CHANNER [6].

The matrix material chosen was composed of the combination of ordinary Portland cement, water and an acrylic emulsion (Primal E330 described by the manufacturers as a 100% acrylic dispersion), together with a liquid defoamer (Nopco NXZ) supplied by Nopco Hess Limited. The proportions of these constituents were:

w/c ratio	0.3
s/c ratio	0.2
a/c ratio	0.002

where w - total weight of water (to include weight of water in the polymer emulsion, E330).

c - weight of the dry Portland cement powder.

s - weight of solid polymer in the emulsion, E330.

a - weight of antifoaming agent (Nopco NXZ)

Chapter 2 shows that there are considerable effects due to various curing conditions and these were investigated in detail (Sec. 3.3.4). To reduce such effects to a minimum and for simplicity all moulded sheets of material were stored vertically in a rack at a constant temperature of 22°C and 40-60% relative humidity. This is the definition of an air cure.

Fig. 3.1 shows the flow-diagram of the experimental plan used for the investigation of the matrix. It can be seen from this diagram that the Portland cement, which was supplied in sealed drums, was subdivided into smaller quantities. The samples of cement powder to be used for the manufacture of the test material were stored in polythene bags to prevent premature hydration of the cement particles. As an additional precaution the bags were placed in a large polythene container, replaced in the original cement drums and resealed.

Fig. 3.1 also illustrates the mechanical tests performed upon the matrix material designed to elucidate in detail the effect of cure, strain rate, age and thus yield the short and long term properties of the material. These tests would produce the general characteristics of the material in tension, compression and bending.

Some exploratory non-destructive tests were conducted in an attempt to establish the structural nature of the material. This was done by the use of X-ray diffraction and thin slide micro examination techniques.

All tests were performed at a temperature of 22°C and a relative humidity in the range 40-60%. These parameters were regulated by a through the wall air conditioning unit (Carlyle model 360) and a Defensor A G humidifier. The system embodied a Honeywell electronic control system which produced a continuous record of temperature and humidity.

Preliminary tensile tests were run to obtain some understanding of the variation in properties within a cement board. These tests showed a coefficient of variation of approximately 15%. In order to reduce the effect of this and the variation from one sheet to another, a randomised plan was drawn up and is indicated in Fig. 3.2.

Sheets 1 and 2 were used for the long term creep studies. They also provided a number of control tensile specimen.

Sheets 4, 5, 6, 8 and 9 provided the tensile and compressive specimens for the study of the basic stress-strain curves and the effect of age upon these curves (for ages refer to Table 3.1).

Sheets 3 and 7 gave the required specimens to investigate the effect of rate of strain upon the stress-strain curves. These tests were run at an age of 30 days. The length of all specimens was kept constant and therefore the rate of crosshead movement of the Instron testing machine was directly proportional to the rate of strain.

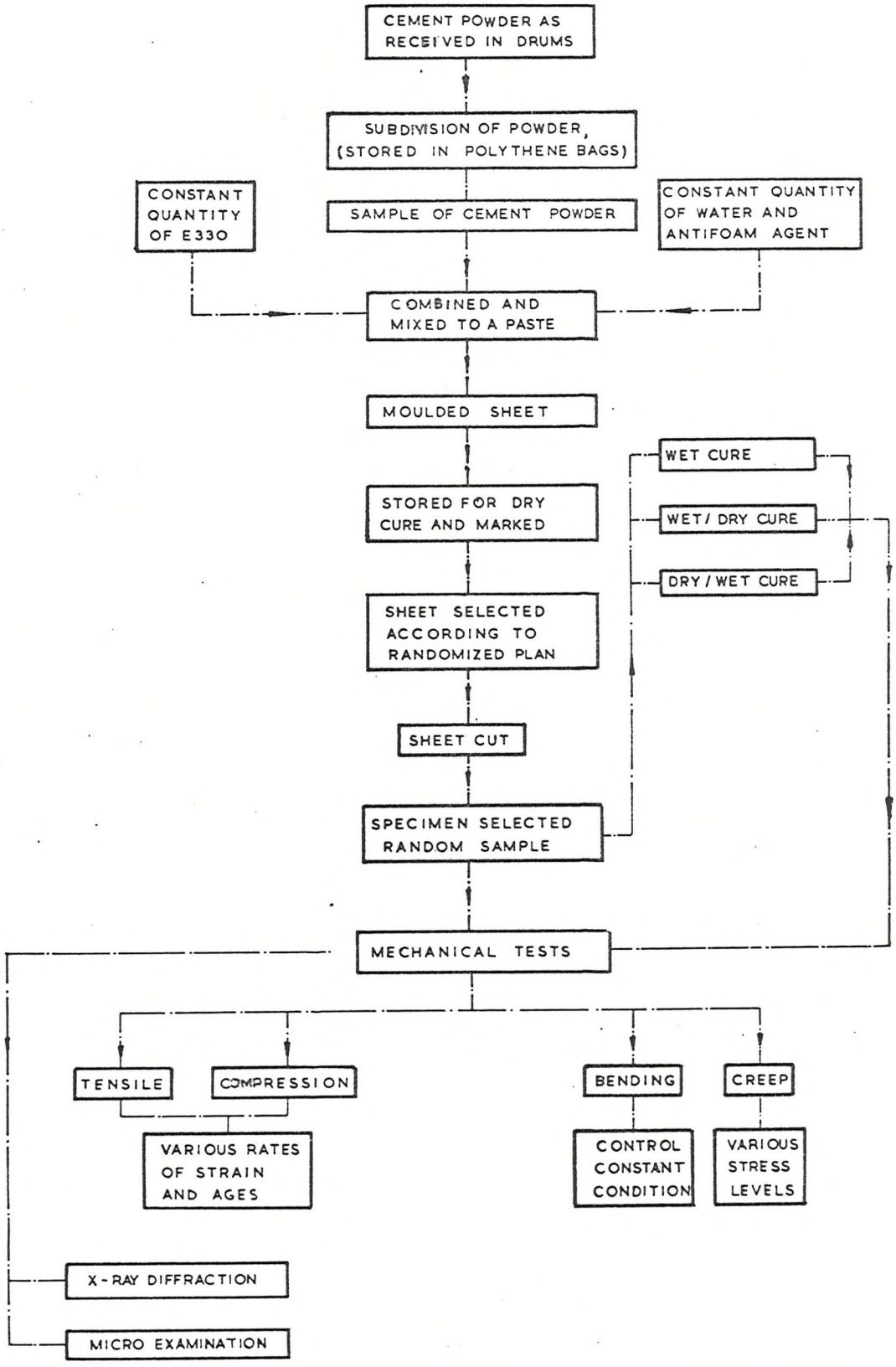

FLOW DIAGRAM ILLUSTRATING EXPERIMENTAL PROGRAMME

FIGURE 3.1

sheet 6

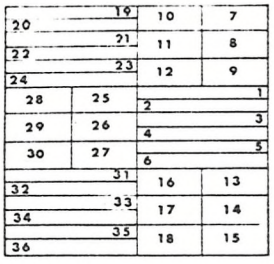

sheet 1

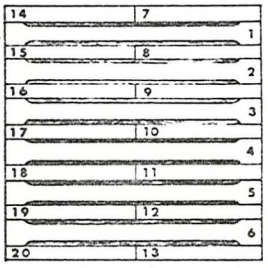

sheet 7

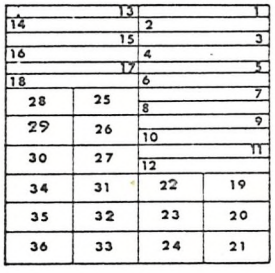

sheet 2

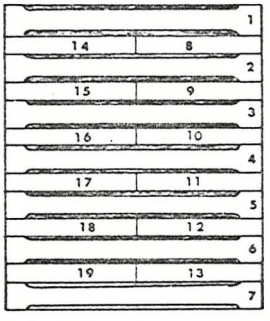

sheet 8

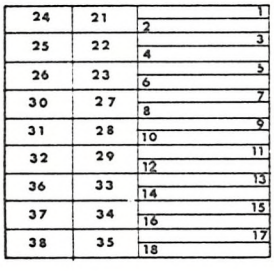

sheet 3

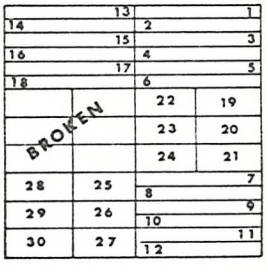

sheet 9

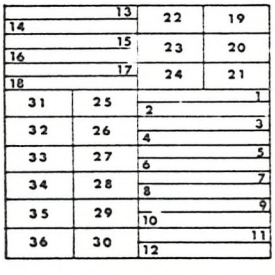

sheet 4

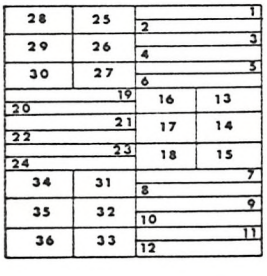

shrinkage specimens

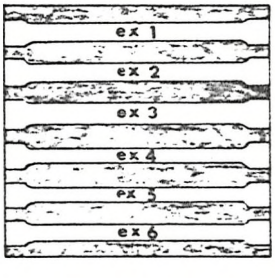

sheet 5

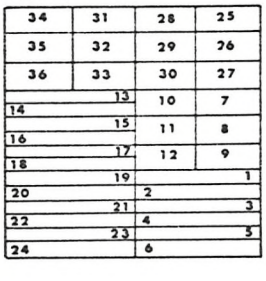

Randomised Plan for Specimen Selection

Fig 3.2

3.2 Preparation of Polymer-Cement Boards

It is well known that, when preparing a cement slurry, the angular velocity of the mixing paddle and the duration of mixing, prior to moulding, can affect the mechanical properties of the hardened paste. To reduce the effects of unwanted variables the paste was prepared in the following standardised manner.

1) Samples of cement powder, polymer emulsion and water were weighed and placed in separate containers.
2) Antifoaming agent was added to the water and stirred to give an opaque solution.
3) The emulsion of water and antifoaming agent was mixed into the polymer emulsion.
4) The complete content of 3 was poured into the cement powder.
5) This was then stirred at an angular velocity of 2400 rev/min for a period of 5 minutes. At the end of each minute the mixing bowl was rotated through approximately half a revolution. On completion of mixing, the bowl and contents were vibrated for one minute to expel some of the trapped air.

After the aforementioned procedure the polymer-cement was poured gently into the mould (Fig. 3.3) where it was allowed to stand for 10 minutes. During this time the mix tended to distribute itself and small air bubbles were seen to form at the surface. A very low pressure air jet was applied to free the trapped air caused by surface tension.

One edge of the plate glass sheet, whose dimensions were slightly smaller than those of the mould, was placed on two of the perspex spacers and slowly lowered until the glass sheet made contact with all four spacers. The excess cement was squeezed around the sides of the glass sheet and onto its surface.

After a period of 4 hours the cement was sufficiently set to allow removal of the wooden mould without damage to the cement board. If the wooden mould remained for times greater than 4 hours then its removal was difficult and the cement board suffered damage. When 24 hours had elapsed the moulded sheet was turned over and the p.v.c. sheeting peeled off, thus exposing one face of the cement board to the air. The sheet at this stage was not hard enough to remove from the plate glass sheet, therefore a further 24 hours elapsed before the demoulding of the cement board was completed.

All the cement boards were of even thickness and the surface finish excellent showing some signs of very small air bubbles at the surface adjacent to the plate glass sheet. To maintain the boards in a vertical plane they were placed in a rack and clamped at their edges.

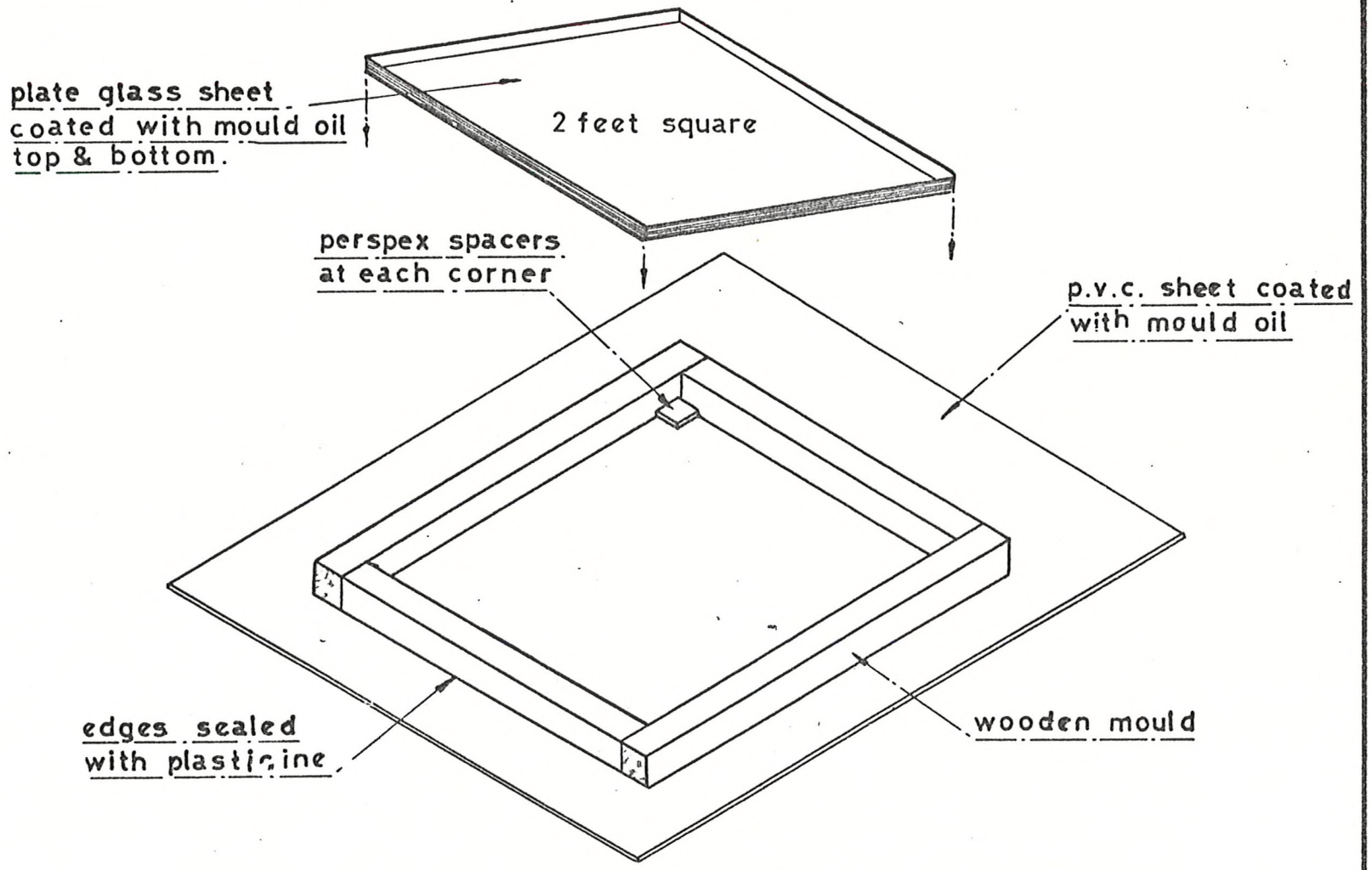

POLYMER-CEMENT MOULD

FIGURE 3.3

3.3 Tensile Stress-Strain Properties

3.3.1 The Experimental Method

The purpose of the experiment was to study the effect on the stress-strain diagram of varying the age and cure of the material and the rate of applied strain.

Tensile specimens were selected from cement boards 4, 5, 6, 8, 9 as shown in Fig. 3.2 when read in conjunction with Table 3.1. They were cut and prepared as described in Appendix C (Sec. C2).

The experiment was performed in two stages using the Instron Testing Machine:

STAGE 1) to obtain accurately the initial elastic modulus.

The specimen was placed between the upper and lower tensile jaws of the Instron machine. An extensometer in which was mounted an L.V.D., was then attached to the specimen. A signal from the transducer was relayed to a Boulton Paul transducer meter, thus indicating the specimen extension on a gauge length of 2.93 inches. By using the blipping attachment and setting the X-Y chart running mechanically at constant speed an automatic load-extension plot was obtained (Plate 3.1). The specimen was loaded to 20 lbf then unloaded and

this process was repeated. The information was re-plotted and the mean of the four slopes produced the initial elastic modulus.

STAGE 2) to obtain a full stress-strain diagram together with the load and extension at failure:

After removal of the mechanical extensometer, the strain gauge extensometer which detected specimen extension over a gauge length of 2 inches, was mounted on the specimen (Appendix C, Sec. C1.2). The X-Y chart was then driven by the electrical signal from the extensometer, thus producing the full stress-strain diagram.

Samples at various ages were tested in the manner just described and in addition specimens were taken from sheets 3 and 7 and tested at different crosshead speeds (0.002 - 0.2 in/min). Due to the wide variation of strain rates it was only possible to obtain stress-strain diagrams using the strain gauge extensometer. Thus the initial elastic modulus values quoted in Table 3.2 are obtained from the single initial slope of this diagram

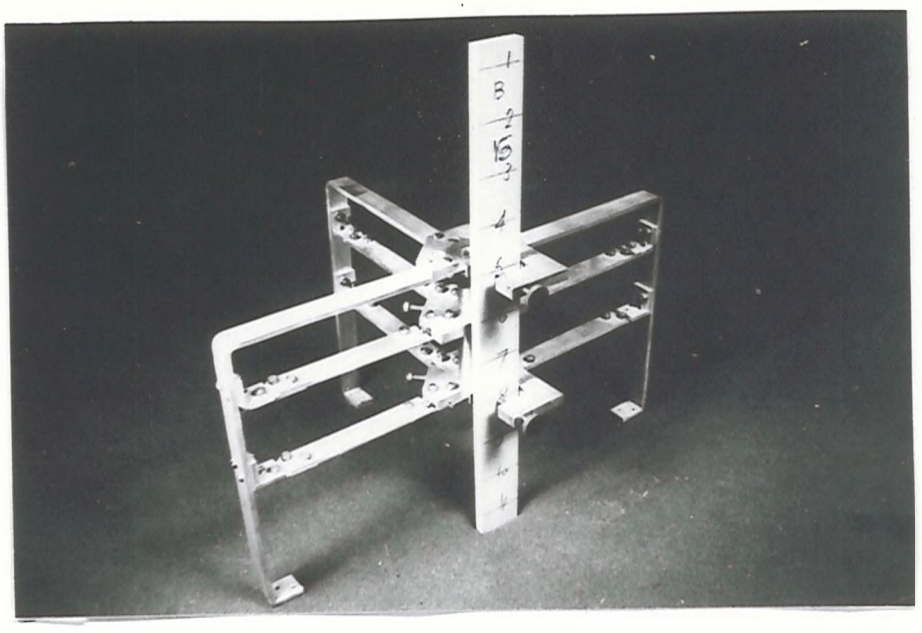

TENSILE EXTENSOMETER & SPECIMEN

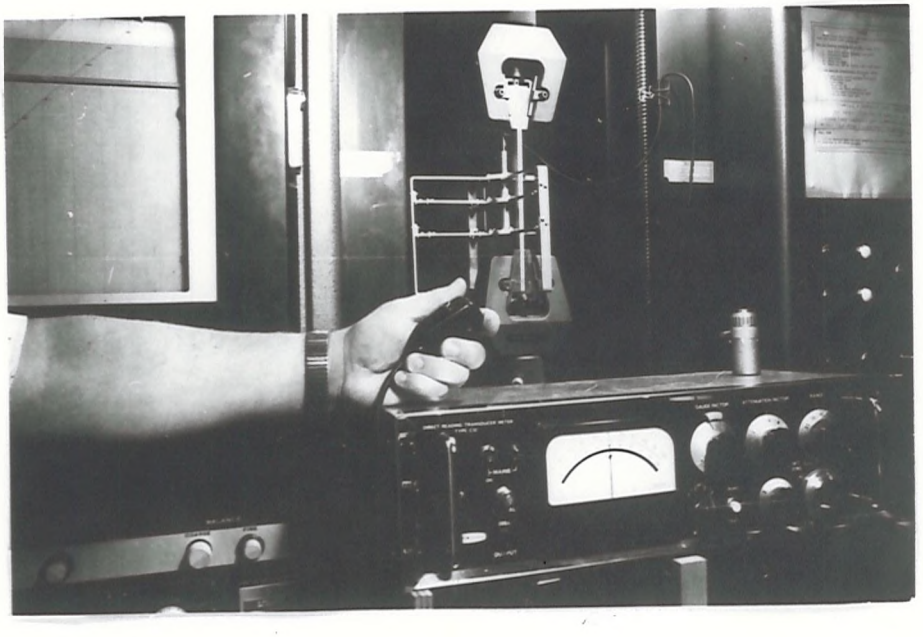

RECORDING INITIAL ELASTIC MODULUS

PLATE 3.1

3.3.2 Experimental Results: Effect of Age

The summary of results of the stress-strain experiments to show effect of age upon the material is shown in Tables 3.1, 3.2 and 3.3. Results of each specimen are shown in Appendix G (Table G1).

Figs. 3.4 to 3.12 give the scatter stress-strain diagrams for the specimens of Tables 3.1 to 3.3. These diagrams illustrate the variation in properties at various ages and were plotted by the computer as a result of programme G44A (Appendix E).

The development of ultimate strength as a function of time is illustrated in Fig. 3.13. It is clearly seen that the full strength is almost reached by 30 days. The maximum ultimate strength obtained in this series of tests was 530.6 lbf/in^2 (Specimen 9.16). When plotting the log (ultimate strength) against the log of time a linear relationship may exist. This graph was used to give the curve shown in Fig. 3.13.

The effect of age upon the initial elastic modulus was not marked (Fig. 3.14). The maximum value of the elastic modulus was 0.61×10^6 lbf/in^2 (Specimen 9.18).

TABLE 3.1

SUMMARY OF TENSILE ULTIMATE STRENGTH RESULTS AT VARIOUS AGES

(Crosshead Speed 0.005 in/min)

Specimen Number	Age (Days)	Mean Ultimate Strength (σ_u) lbf/in^2	Standard Deviation lbf/in^2	% Coeff. of Variation	Confidence Limits p = 0.1, lbf/in^2		Estimated Specific Gravity
					Upper	Lower	
8.1 - 8.10	3	354.4	21.43	6.04	366.9	342.1	1.671
6.1 - 6.6	7	400.7	46.41	11.63	439.1	362.2	1.615
5.1 - 5.6	9	419.0	9.69	2.31	427.0	411.0	1.628
8.11 - 8.20	15	446.8	25.41	5.69	461.5	432.1	1.668
4.19 - 4.23	19	438.0	15.87	3.62	453.4	423.2	1.662
3.10 - 3.18	29	459.0	15.17	3.30	472.3	447.3	1.585
9.1 - 9.6	66	444.9	4.82	1.98	452.2	437.6	1.654
9.7 - 9.12	88	452.0	11.31	2.50	461.4	442.7	1.650
9.13 - 9.18	98	513.0	15.83	3.09	526.1	500.0	1.645
4.1 - 4.6	119	499.8	14.61	2.92	511.8	487.8	1.637

TABLE 3.2

SUMMARY OF TENSILE INITIAL ELASTIC MODULUS VALUES AT VARIOUS AGES

Specimen Number	Age (Days)	Initial (E_o) Elastic Modulus lbf/in^2 x 10^{-6}	Standard Deviation lbf/in^2 x 10^{-6}	% Coeff. of Variation	Confidence Limits p = 0.1 lbf/in^2 x 10^{-6}	
					Upper	Lower
8.1 - 8.10	3	0.450	0.0228	5.01	0.468	0.442
6.1 - 6.6	7	0.514	0.0231	4.50	0.534	0.495
5.1 - 5.6	9	0.507	0.0462	9.11	0.545	0.469
8.11 - 8.20	15	0.526	0.0136	2.58	0.533	0.518
4.19 - 4.23	19	0.550	0.0406	7.37	0.588	0.511
9.1 - 9.6	66	0.538	0.0231	4.30	0.557	0.519
9.7 - 9.12	88	0.562	0.0297	5.28	0.586	0.537
9.13 - 9.18	98	0.570	0.0257	4.52	0.591	0.549
4.1 - 4.6	119	0.577	0.0207	3.59	0.595	0.561

TABLE 3.3

SUMMARY OF ULTIMATE TENSILE STRAINS AT VARIOUS AGES

Specimen Number	Age (Days)	Mean Ultimate Strain (ε_u) x 10^3	Standard Deviation x 10^3	% Coeff. of Variation	Confidence Limits p = 0.1, x 10^3	
					Upper	Lower
8.1 - 8.10	3	1.787	0.1979	11.08	1.901	1.693
6.1 - 6.6	7	2.505	0.2494	9.95	2.711	2.299
5.1 - 5.6	9	2.07	0.809	39.08	2.737	1.403
8.11 - 8.20	15	2.83	0.346	12.23	3.03	3.63
4.19 - 4.23	19	3.23	0.695	21.52	3.892	2.568
9.1 - 9.6	66	3.297	0.2802	8.5	3.528	3.066
9.7 - 9.12	88	2.99	0.192	6.43	3.143	2.827
9.13 - 9.18	98	3.69	0.725	19.63	4.293	3.097
4.1 - 4.6	119	4.788	0.5183	10.82	5.22	4.36

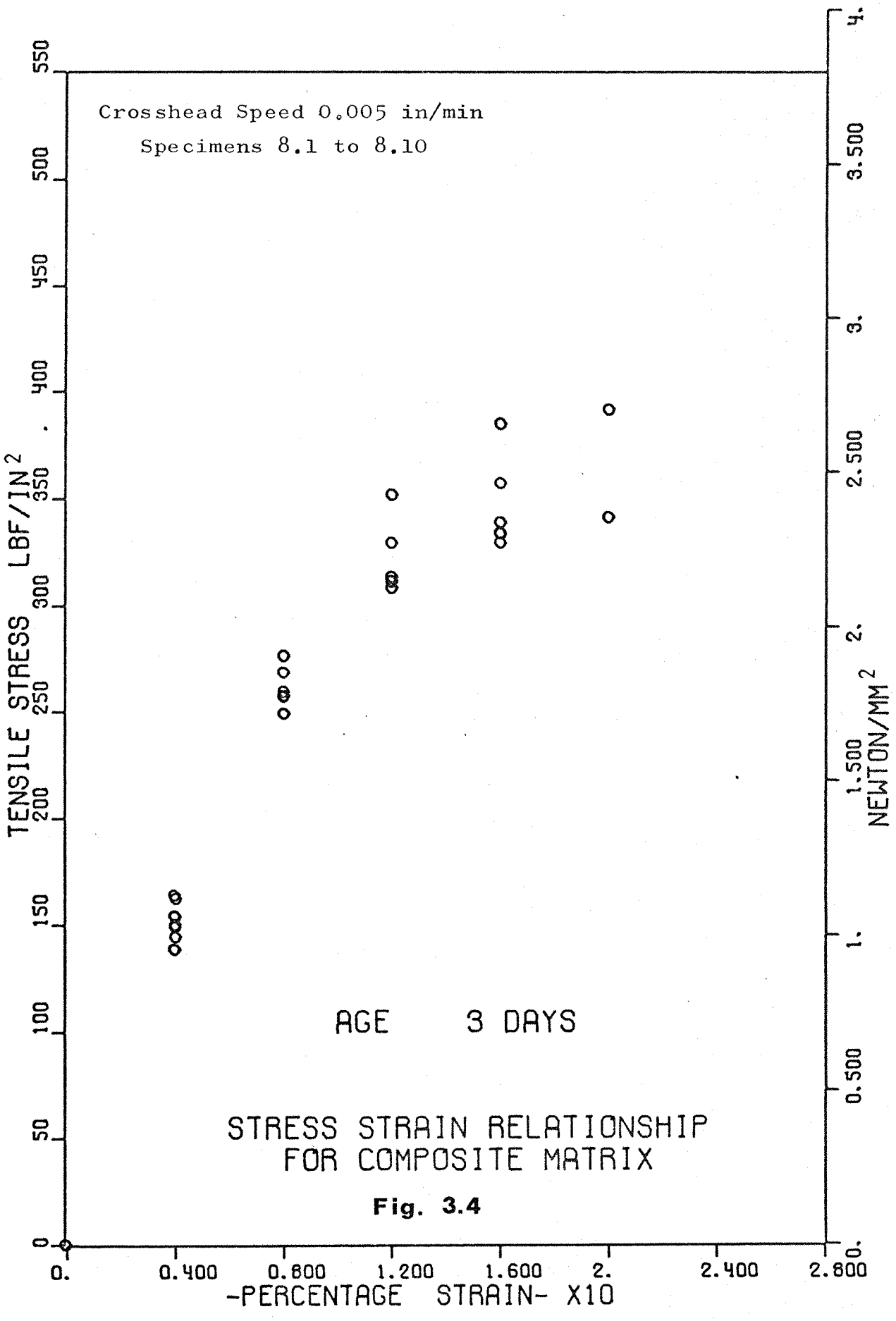
Crosshead Speed 0.005 in/min
Specimens 8.1 to 8.10
TENSILE STRESS LBF/IN2
NEWTON/MM2
AGE 3 DAYS
STRESS STRAIN RELATIONSHIP
FOR COMPOSITE MATRIX
-PERCENTAGE STRAIN- X10
0
50
100
150
200
250
300
350
400
450
500
550
0.500
1.
1.500
2.
2.500
3.
3.500
4.
0.
0.400
0.800
1.200
1.600
2.
2.400
2.800

Fig. 3.4

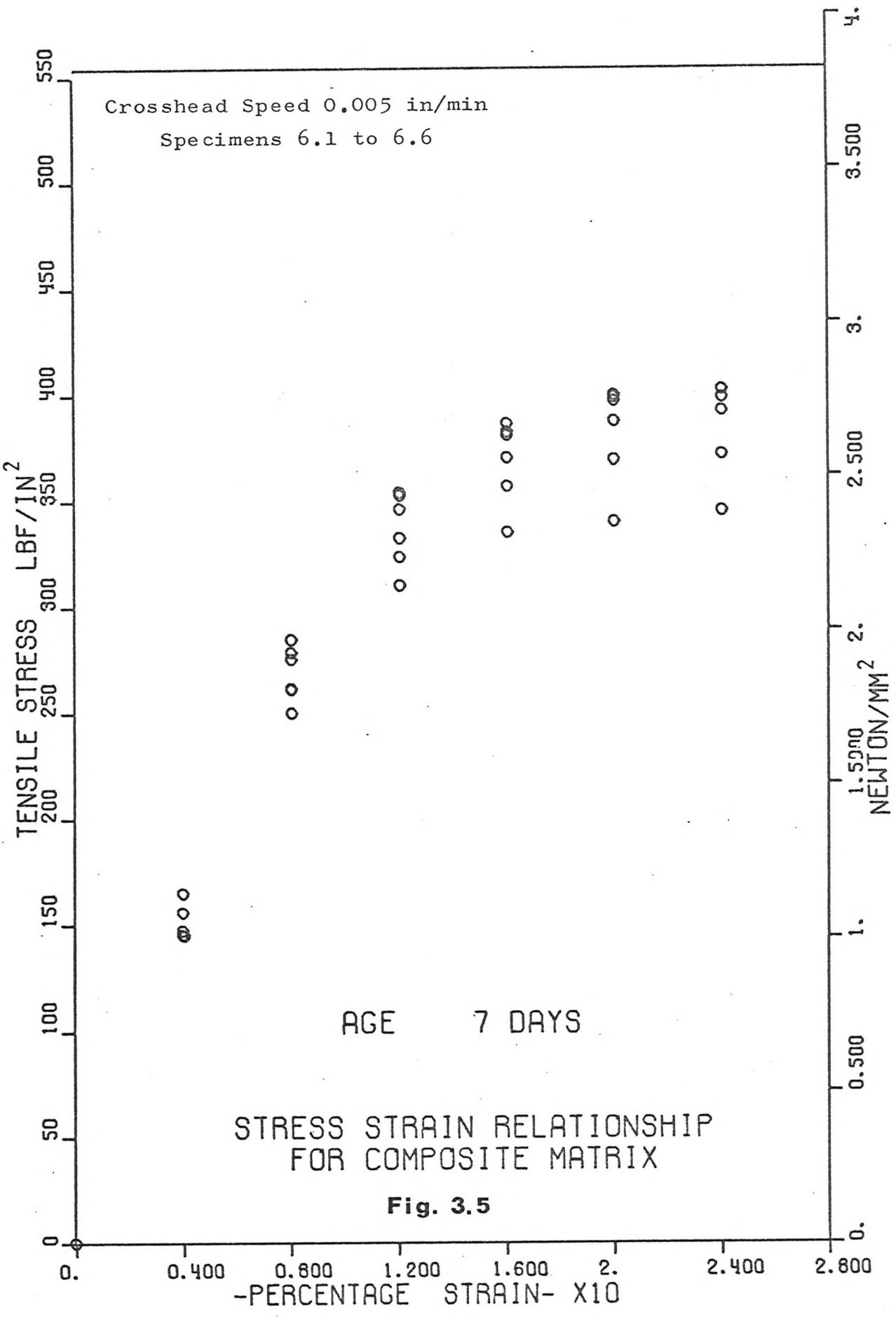
Crosshead Speed 0.005 in/min
Specimens 6.1 to 6.6
TENSILE STRESS LBF/IN^2
NEWTON/MM^2
AGE 7 DAYS
STRESS STRAIN RELATIONSHIP
FOR COMPOSITE MATRIX
-PERCENTAGE STRAIN- X10
0
50
100
150
200
250
300
350
400
450
500
550
0.500
1.
1.5000
2.
2.500
3.
3.500
4.
0.
0.400
0.800
1.200
1.600
2.
2.400
2.800

Fig. 3.5

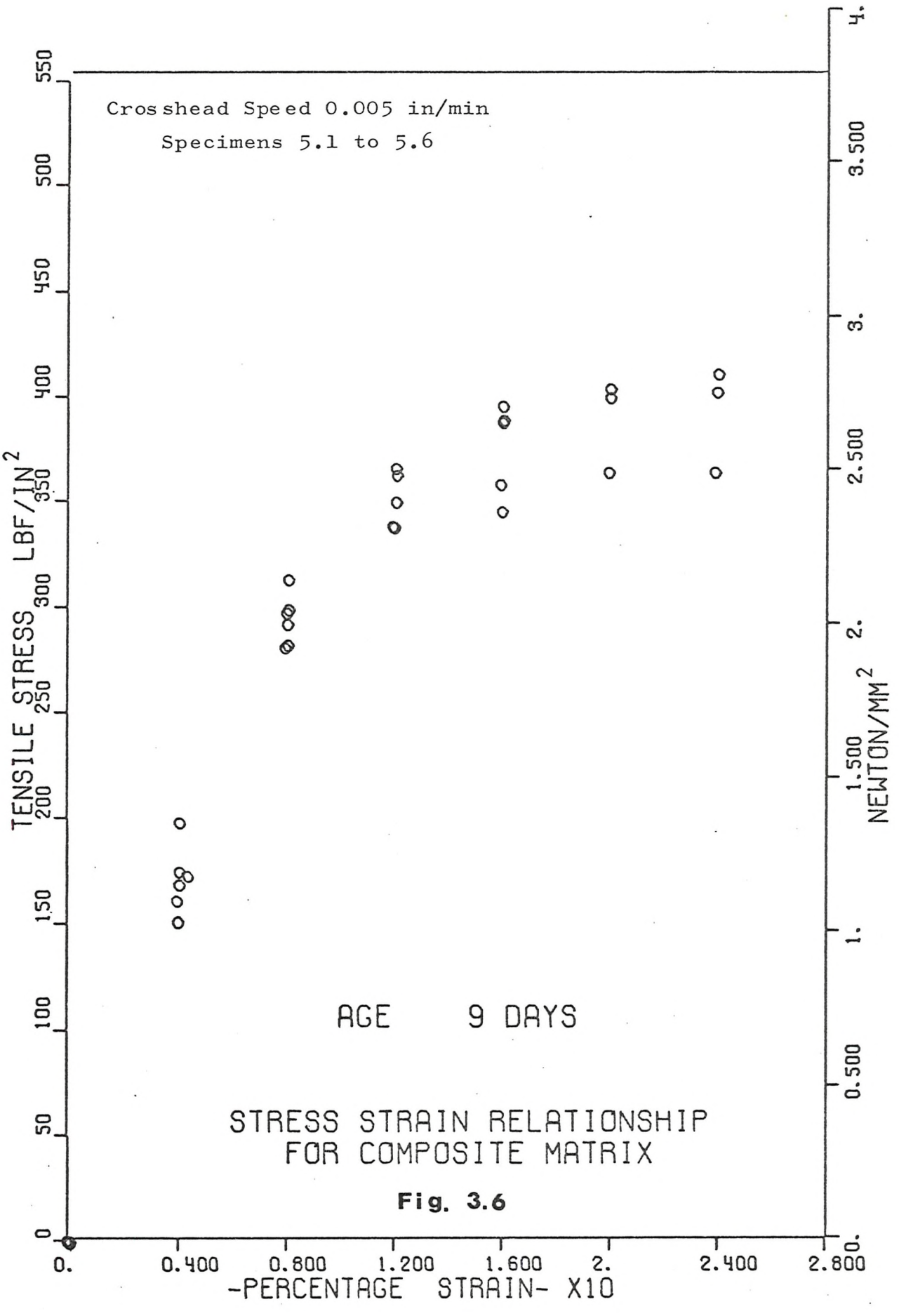
Crosshead Speed 0.005 in/min
Specimens 5.1 to 5.6
TENSILE STRESS LBF/IN^2
NEWTON/MM^2
AGE 9 DAYS
STRESS STRAIN RELATIONSHIP
FOR COMPOSITE MATRIX
-PERCENTAGE STRAIN- X10
0
50
100
150
200
250
300
350
400
450
500
550
0.500
1.
1.500
2.
2.500
3.
3.500
4.
0.
0.400
0.800
1.200
1.600
2.
2.400
2.800

Fig. 3.6

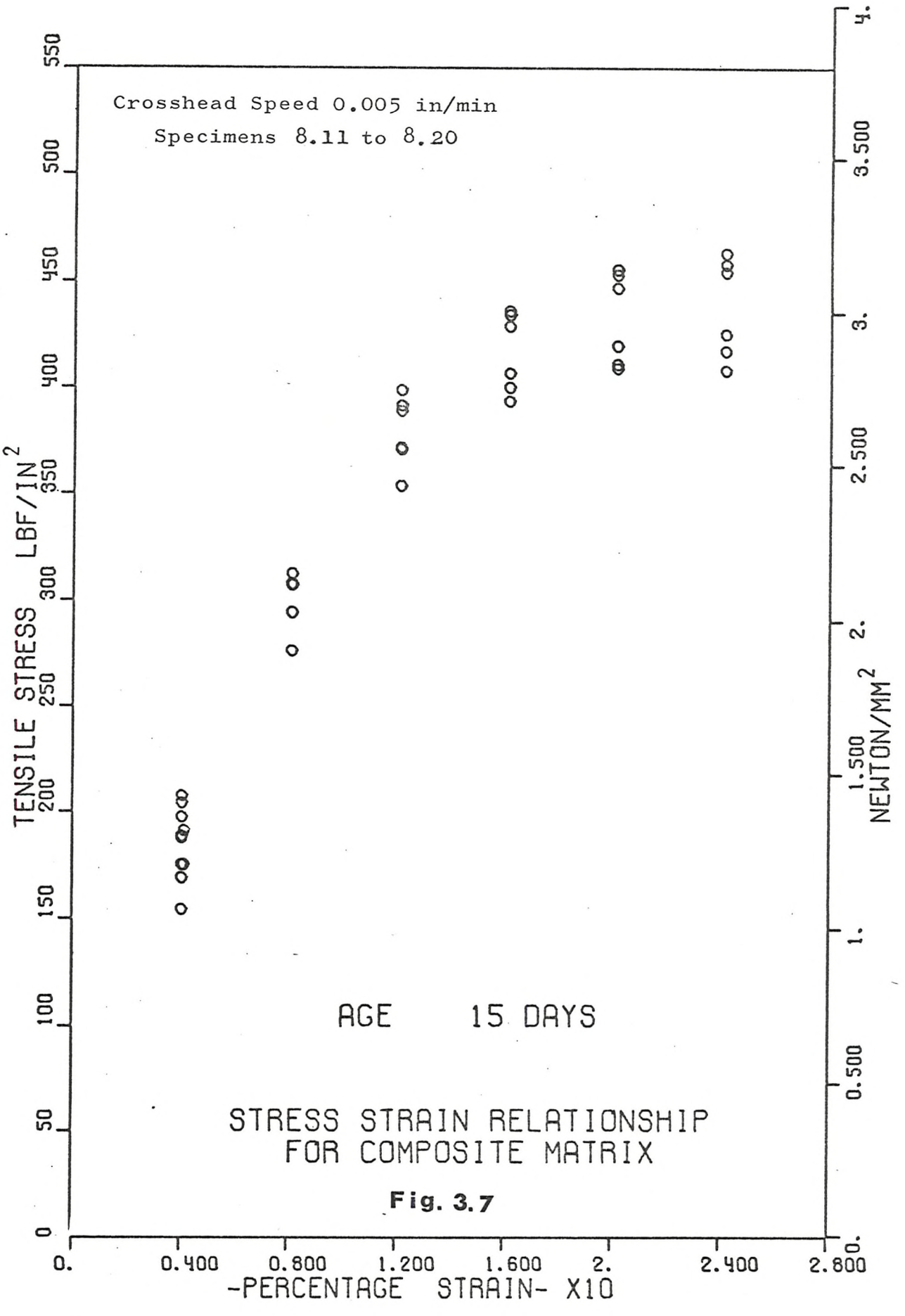
Crosshead Speed 0.005 in/min
Specimens 8.11 to 8.20
TENSILE STRESS LBF/IN^2
NEWTON/MM^2
AGE 15 DAYS
STRESS STRAIN RELATIONSHIP
FOR COMPOSITE MATRIX
-PERCENTAGE STRAIN- X10
0
50
100
150
200
250
300
350
400
450
500
550
0.500
1.
1.500
2.
2.500
3.
3.500
4.
0.
0.400
0.800
1.200
1.600
2.
2.400
2.800

Fig. 3.7

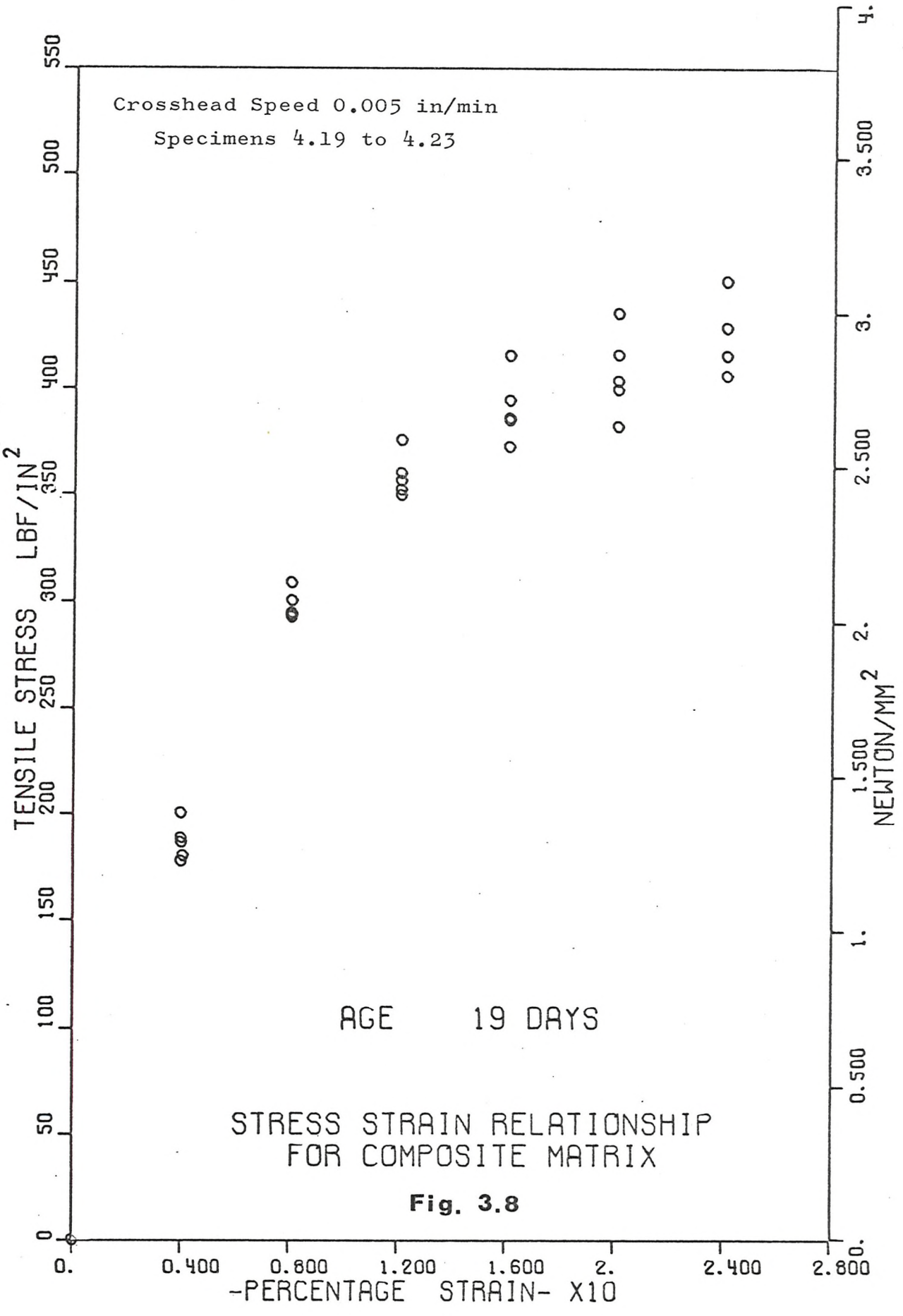
Crosshead Speed 0.005 in/min
Specimens 4.19 to 4.23
TENSILE STRESS LBF/IN2
NEWTON/MM2
AGE 19 DAYS
STRESS STRAIN RELATIONSHIP
FOR COMPOSITE MATRIX
-PERCENTAGE STRAIN- X10
0
50
100
150
200
250
300
350
400
450
500
550
0.500
1.
1.500
2.
2.500
3.
3.500
4.
0.
0.400
0.800
1.200
1.600
2.
2.400
2.800

Fig. 3.8

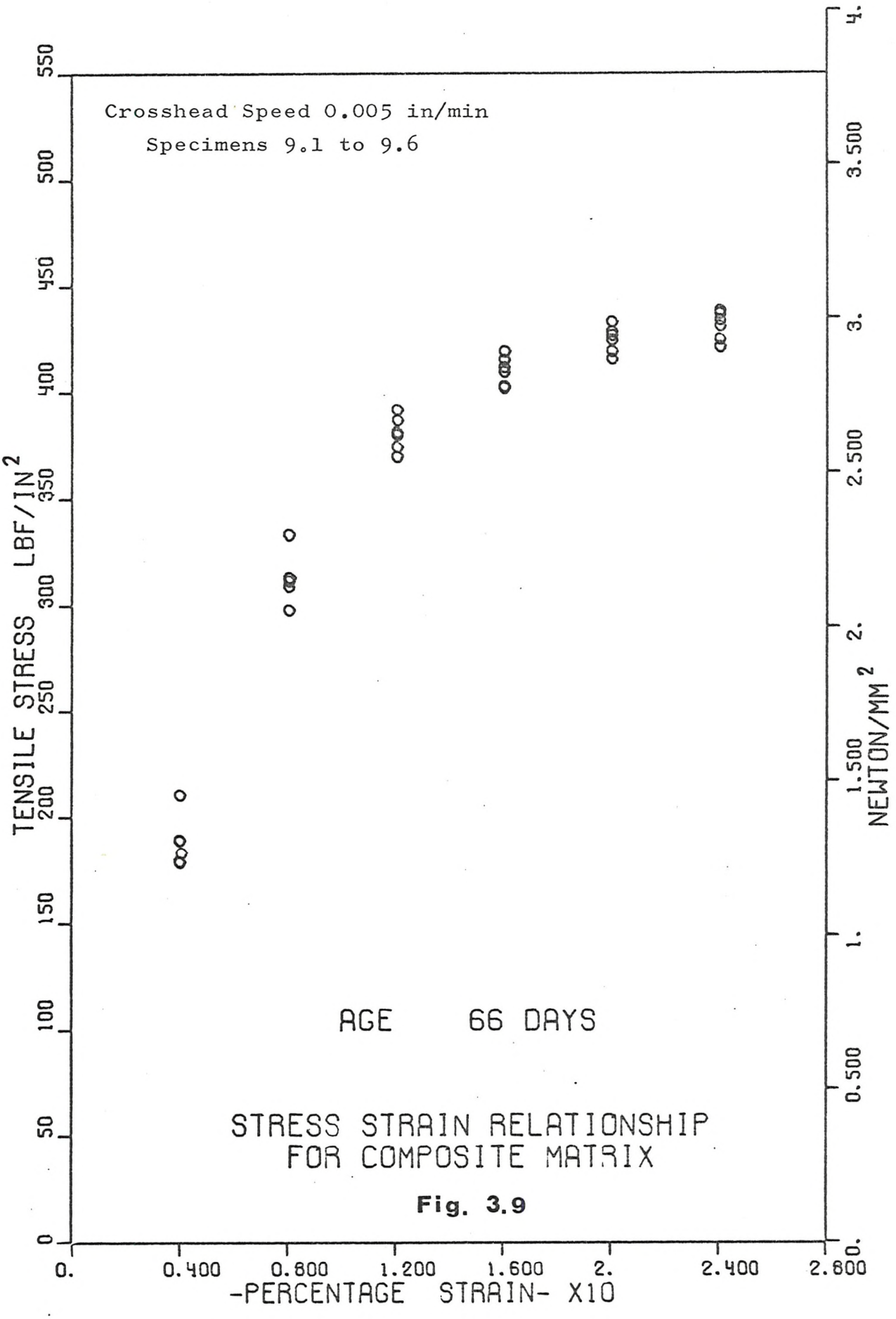
Crosshead Speed 0.005 in/min
Specimens 9.1 to 9.6
TENSILE STRESS LBF/IN 2
NEWTON/MM 2
AGE 66 DAYS
STRESS STRAIN RELATIONSHIP
FOR COMPOSITE MATRIX
-PERCENTAGE STRAIN- X10
0
50
100
150
200
250
300
350
400
450
500
550
0.500
1.
1.500
2.
2.500
3.
3.500
4.
0.
0.400
0.800
1.200
1.600
2.
2.400
2.800

Fig. 3.9

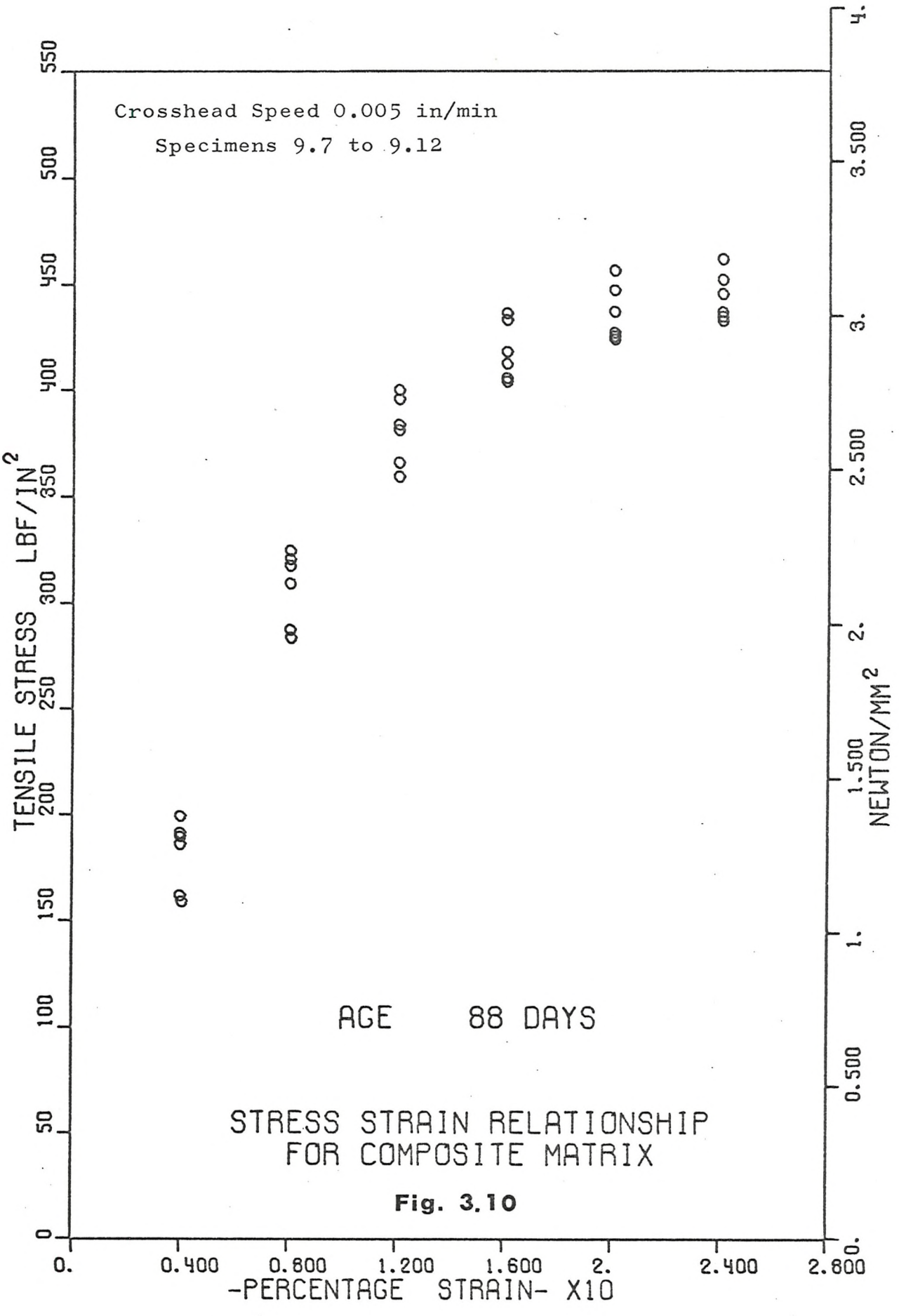
Crosshead Speed 0.005 in/min
Specimens 9.7 to 9.12
TENSILE STRESS LBF/IN^2
NEWTON/MM^2
-PERCENTAGE STRAIN- X10
AGE 88 DAYS
STRESS STRAIN RELATIONSHIP
FOR COMPOSITE MATRIX

Fig. 3.10

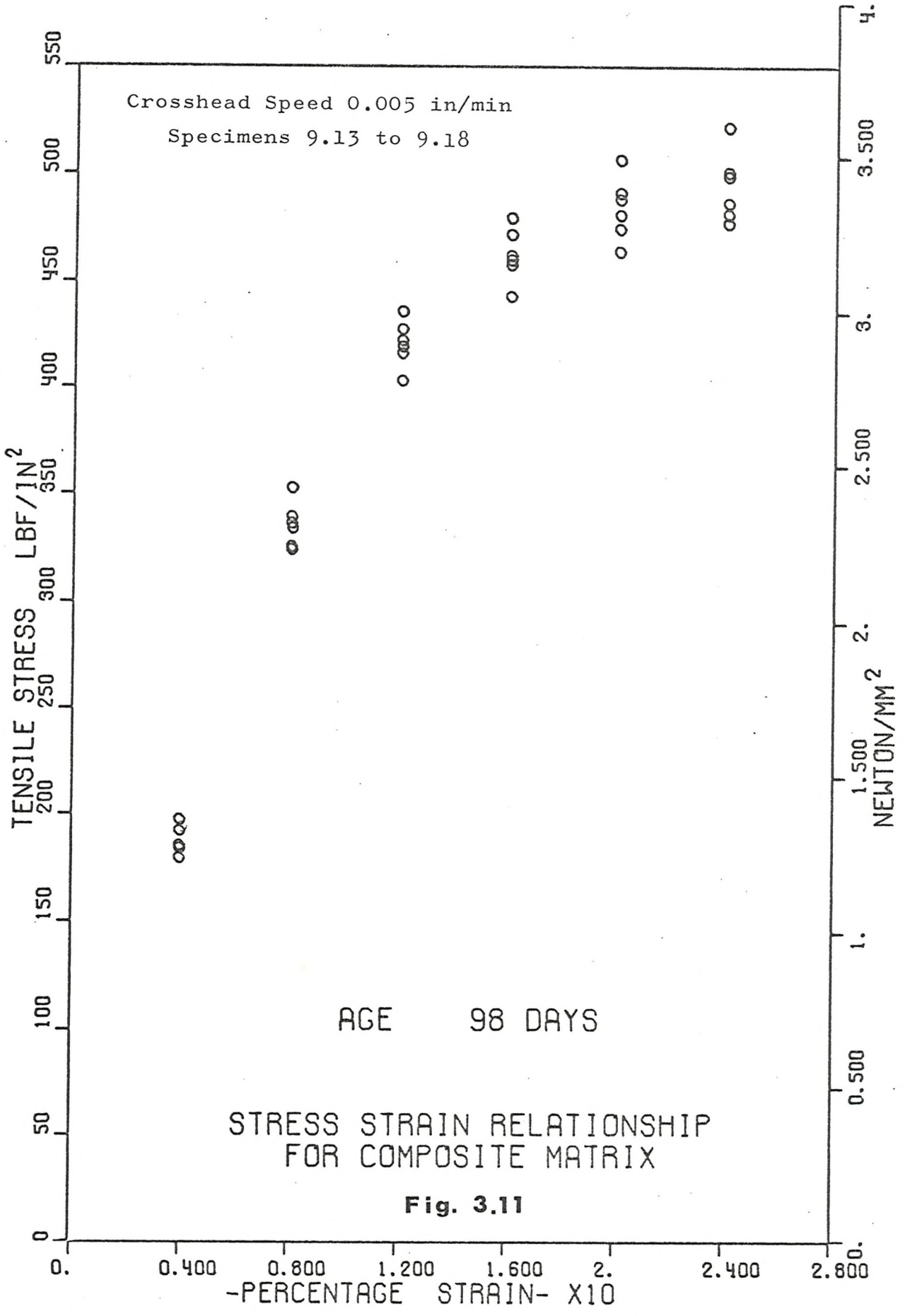
Crosshead Speed 0.005 in/min
Specimens 9.13 to 9.18
TENSILE STRESS LBF/IN^2
NEWTON/MM^2
AGE 98 DAYS
STRESS STRAIN RELATIONSHIP
FOR COMPOSITE MATRIX
-PERCENTAGE STRAIN- X10
0
50
100
150
200
250
300
350
400
450
500
550
0.500
1.
1.500
2.
2.500
3.
3.500
4.
0.
0.400
0.800
1.200
1.600
2.
2.400
2.800

Fig. 3.11

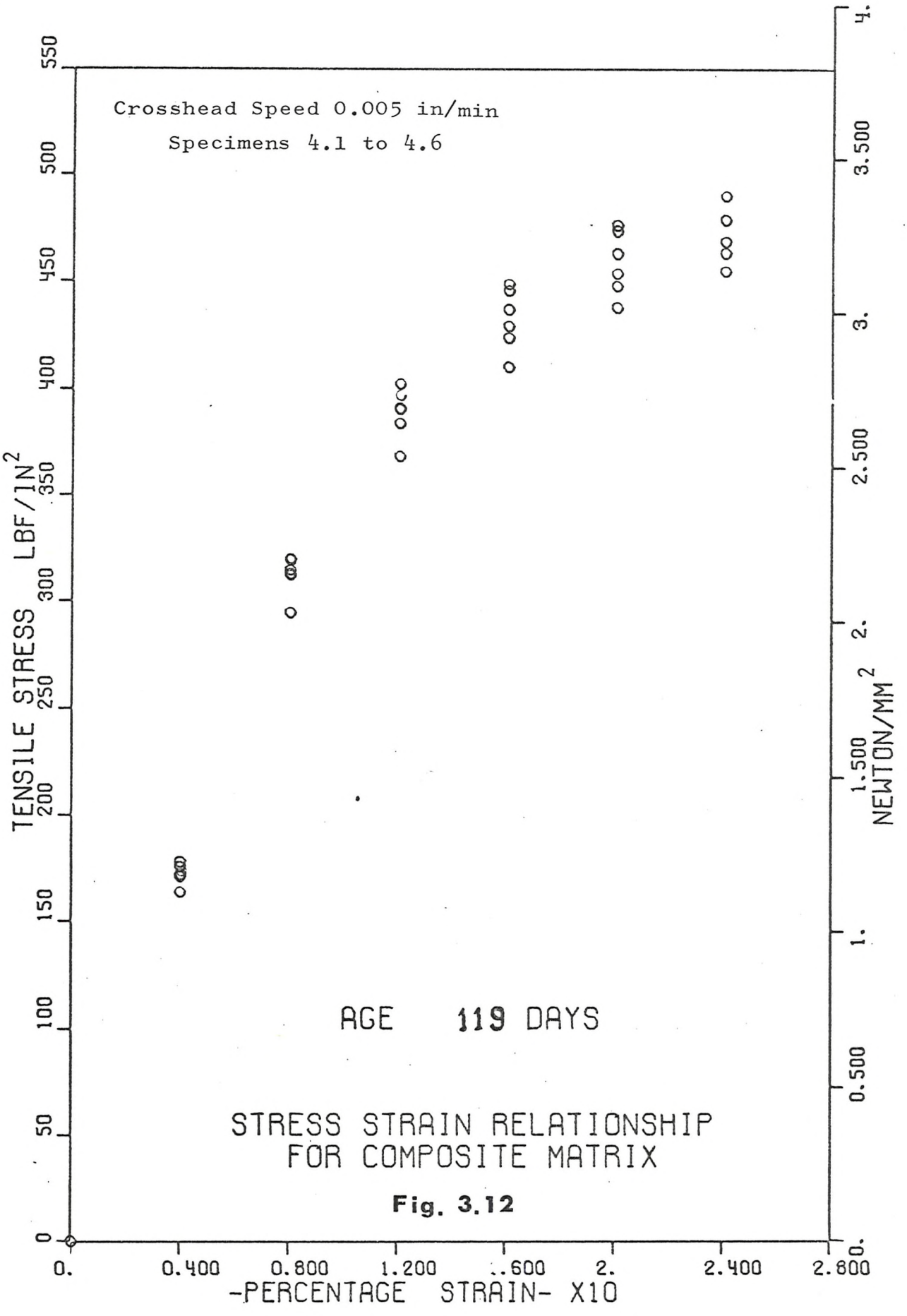
Crosshead Speed 0.005 in/min
Specimens 4.1 to 4.6
TENSILE STRESS LBF/IN^2
NEWTON/MM^2
AGE 119 DAYS
STRESS STRAIN RELATIONSHIP
FOR COMPOSITE MATRIX
-PERCENTAGE STRAIN- X10
0
50
100
150
200
250
300
350
400
450
500
550
0.500
1.
1.500
2.
2.500
3.
3.500
4.
0.
0.400
0.800
1.200
2.
2.400
2.800

Fig. 3.12

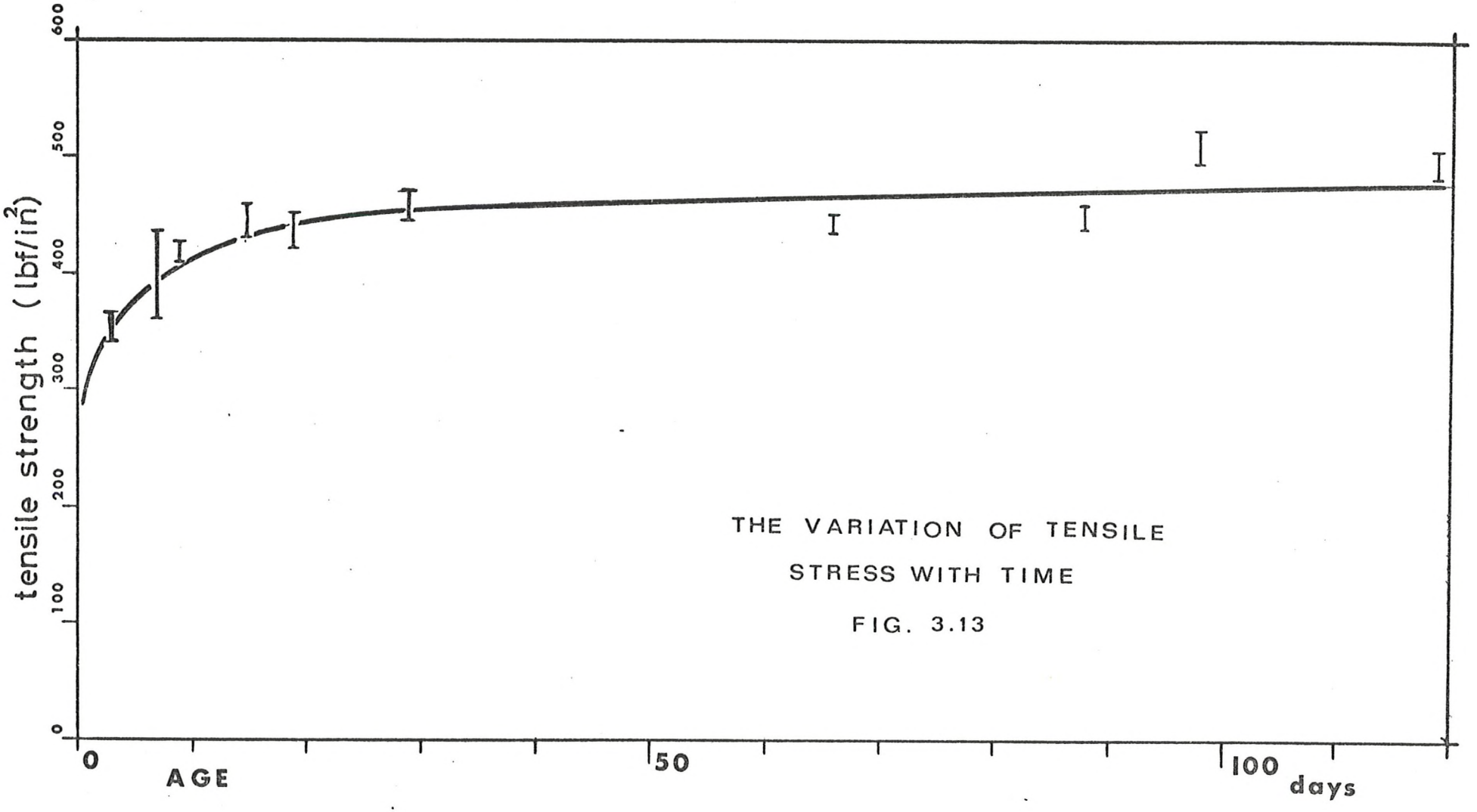

THE VARIATION OF TENSILE STRESS WITH TIME

FIG. 3.13

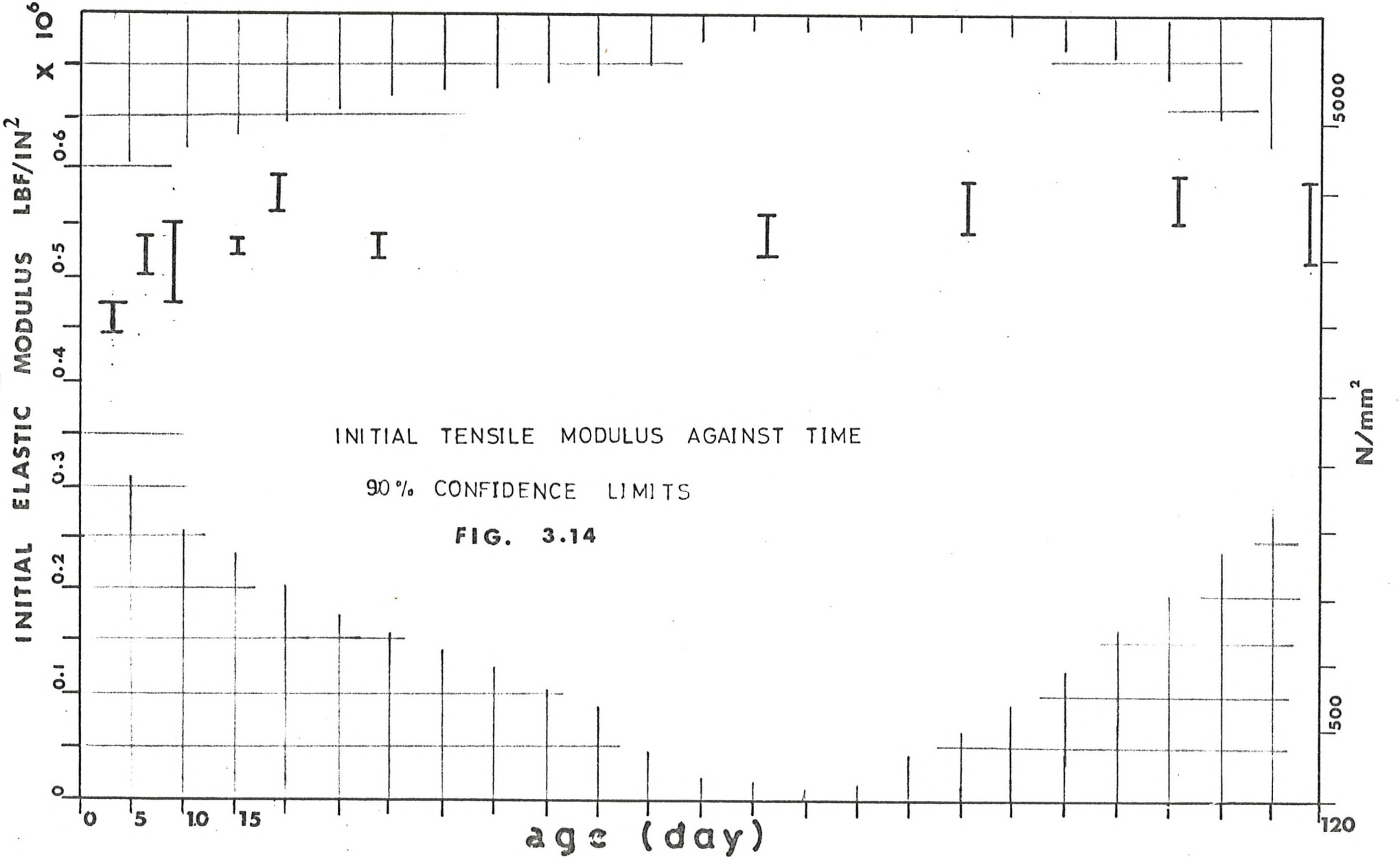

INITIAL TENSILE MODULUS AGAINST TIME

90 % CONFIDENCE LIMITS

FIG. 3.14

3.3.3 Experimental Results: Effect of Strain Rate

Tables 3.4, 3.5 and 3.6 summarise the results which are detailed in Appendix G (Table G2).

Figures 3.15 to 3.19 are the scatter stress-strain diagrams for the tensile tests conducted under various crosshead speeds ($\dot{\varepsilon}$) ranging from 0.002 to 0.2 in/min. All specimens had a constant free length between the grips of 6.5 in. so the crosshead speed was considered to be proportional to the applied strain rates 0.3077 to 30.7×10^{-3} strain/min. When comparing the scatter diagrams, secant modulus and strength increase at elevated crosshead speeds. The maximum and minimum strengths were 649.6 lbf/in^2 and 398.5 lbf/in^2 respectively.

Using the scatter diagrams (Figs. 3.15 to 3.19) the stresses at particular strains and crosshead speeds were recorded. From this information it was possible to plot the stress at particular strains and crosshead speeds against the log (crosshead speed), Fig. 3.20.

This semi-logrithmic plot indicates the relationship between these two variables as:

$$\sigma_i = k_i \log_{10} \dot{\varepsilon} + C_i \quad \ldots\ldots \quad 3.1$$

where σ_i i^{th} level of stress lbf/in^2

$\dot{\varepsilon}$ the crosshead speed in/min

k_i slope of line for a given strain and crosshead speed

C_i the constant which corresponds to the above parameters

The slopes of the lines in Fig. 3.20 (which all intersect at a stress of 164 lbf/in^2) were plotted as a function of strain to yield a smooth curve (Fig. 3.21) It is interesting to note from Fig. 3.21 that up to a strain of 0.35×10^{-3} the elastic modulus is not dependent upon the rate of strain. From Fig. 3.21 $k_i = 0$ for $\varepsilon < 0.035\%$. This indicates that any line on Fig. 3.21 which represents a strain of less than 0.035% is horizontal; i.e. there is only one stress corresponding to a given level of strain and the strain rate has no influence on the stress-strain relation. The fracture strain of ordinary Portland cement has been quoted as 0.35 to 0.6×10^{-3} (Appendix B, Sec. B3.4).

C_i may be expressed in terms of the slopes k_i

Thus $C_i = D + 4.8\ k_i$

Where D is the stress at which the lines intersect (164 lbf/in^2)

so $C_i = 164 + 4.8\ k_i$

$\therefore$ equation 3.1 now reads

$$\sigma_i = k_i(4.8 + \log_{10} \dot{\varepsilon}) + 164 \quad .... \ 3.2$$

It was then possible to construct empirical stress-strain curves (Fig. 3.22) at various crosshead speeds. The curves of Fig. 3.22 are superimposed upon the scatter diagrams of Figs. 3.15 to 3.19 and show good agreement.

Fig. 3.23 is a pictorial representation of the relationship between stress strain and time for this series of tests.

TABLE 3.4

SUMMARY OF TENSILE ULTIMATE STRENGTH RESULTS AT VARIOUS CROSSHEAD SPEEDS

Cut From Sheet	Crosshead Speed in/min	Mean Ultimate Strength (σ_u) lbf/in^2	Standard Deviation lbf/in^2	% Coeff. of Variation	Confidence Limit p = 0.1 lbf/in^2		Mean Estimated Specific Gravity
					Upper	Lower	
7.	0.002	405.36	9.438	2.33	413.1	397.6	1.645
3.	0.005	459.84	15.17	3.3	472.4	447.33	1.585
3.*	0.01	-	-	-	-	-	-
7.	0.02	482.45	20.025	4.15	498.96	465.93	1.646
3.	0.05	613.08	30.0	4.89	637.34	588.34	1.584
7.	0.2	641.97	25.38	3.95	637.82	621.0	1.646

* Full stress-strain diagram not recorded

TABLE 3.5

SUMMARY OF TENSILE INITIAL ELASTIC MODULUS VALUES AT VARIOUS CROSSHEAD SPEEDS

Cut From Sheet	Crosshead Speed in/min	Mean Initial Elastic Modulus lbf/in^2 (E_o) x 10^{-6}	Standard Deviation lbf/in^2 x 10^{-6}	% Coeff. of Variation	Confidence Limits p = 0.1 lbf/in^2 x 10^{-6}	
					Upper	Lower
7.	0.002	0.485	0.0132	2.73	0.496	0.475
3.	0.005	0.5267	0.01416	2.69	0.538	0.515
3.	0.01	0.569	0.0700	12.30	0.604	0.534
7.	0.02	0.5	0.0354	7.08	0.529	0.471
3.	0.05	0.544	0.0607	11.15	0.594	0.494
7.	0.2	0.496	0.0443	8.94	0.532	0.459

TABLE 3.6

SUMMARY OF ULTIMATE TENSILE STRAINS AT VARIOUS CROSSHEAD SPEEDS

(Age 29 days)

Cut From Sheet	Crosshead Speed in/min	Mean Ultimate Strain (ε_u) x 10^3	Standard Deviation x 10^3	% Coeff. of Variation	Confidence Limits p = 0.1, x 10^3	
					Upper	Lower
7.	0.002	4.475	0.387	8.65	4.794	4.155
3.	0.005	3.103	0.0789	25.43	3.75	2.453
3.*	0.1	-	-	-	-	-
7.	0.02	4.605	0.0481	10.45	5.0	4.208
3.	0.05	3.77	0.0861	22.81	4.483	3.063
7.	0.2	5.548	0.454	8.18	5.923	5.174

*No full stress-strain diagram recorded

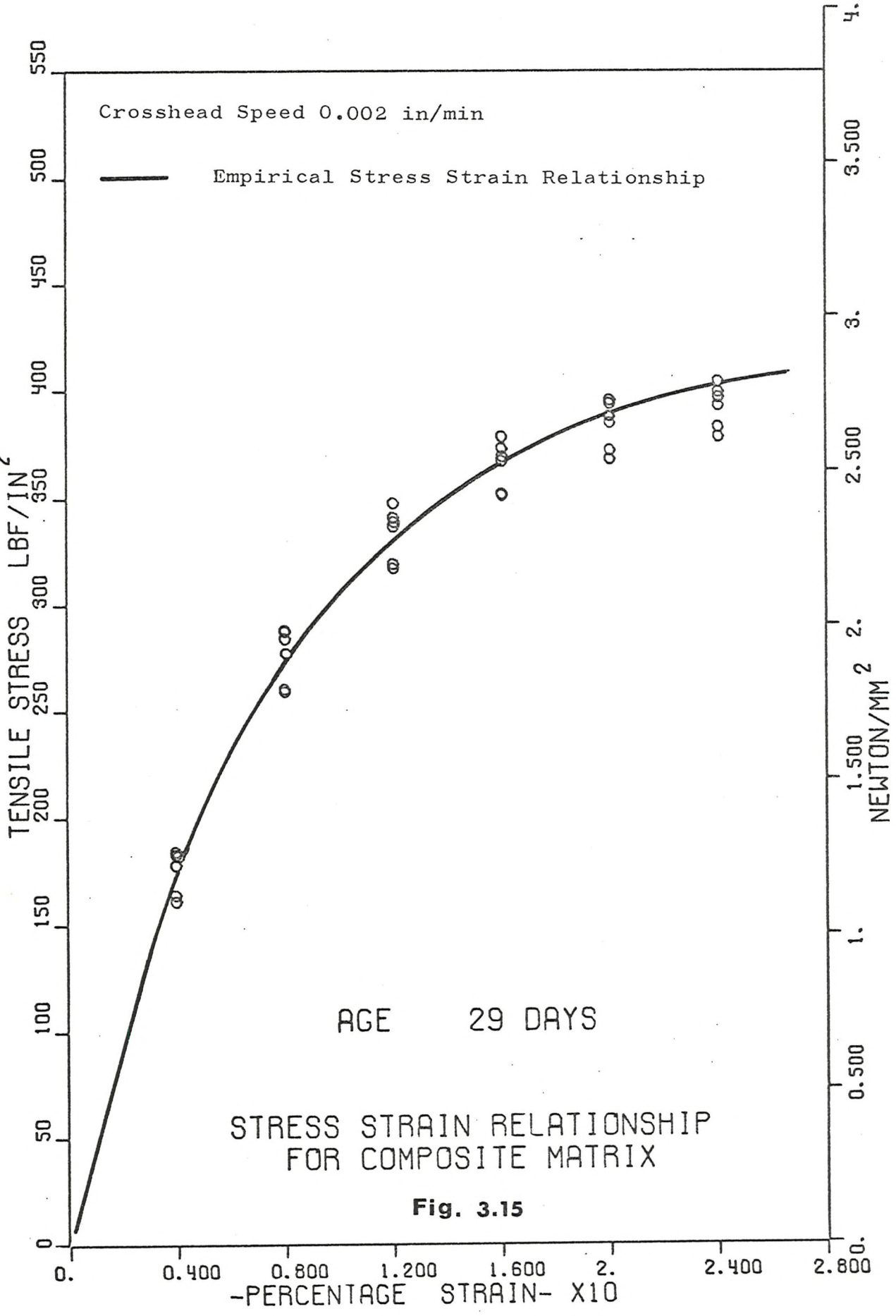
Crosshead Speed 0.002 in/min
Empirical Stress Strain Relationship
TENSILE STRESS LBF/IN^2
NEWTON/MM^2
-PERCENTAGE STRAIN- X10
AGE 29 DAYS
STRESS STRAIN RELATIONSHIP
FOR COMPOSITE MATRIX

Fig. 3.15

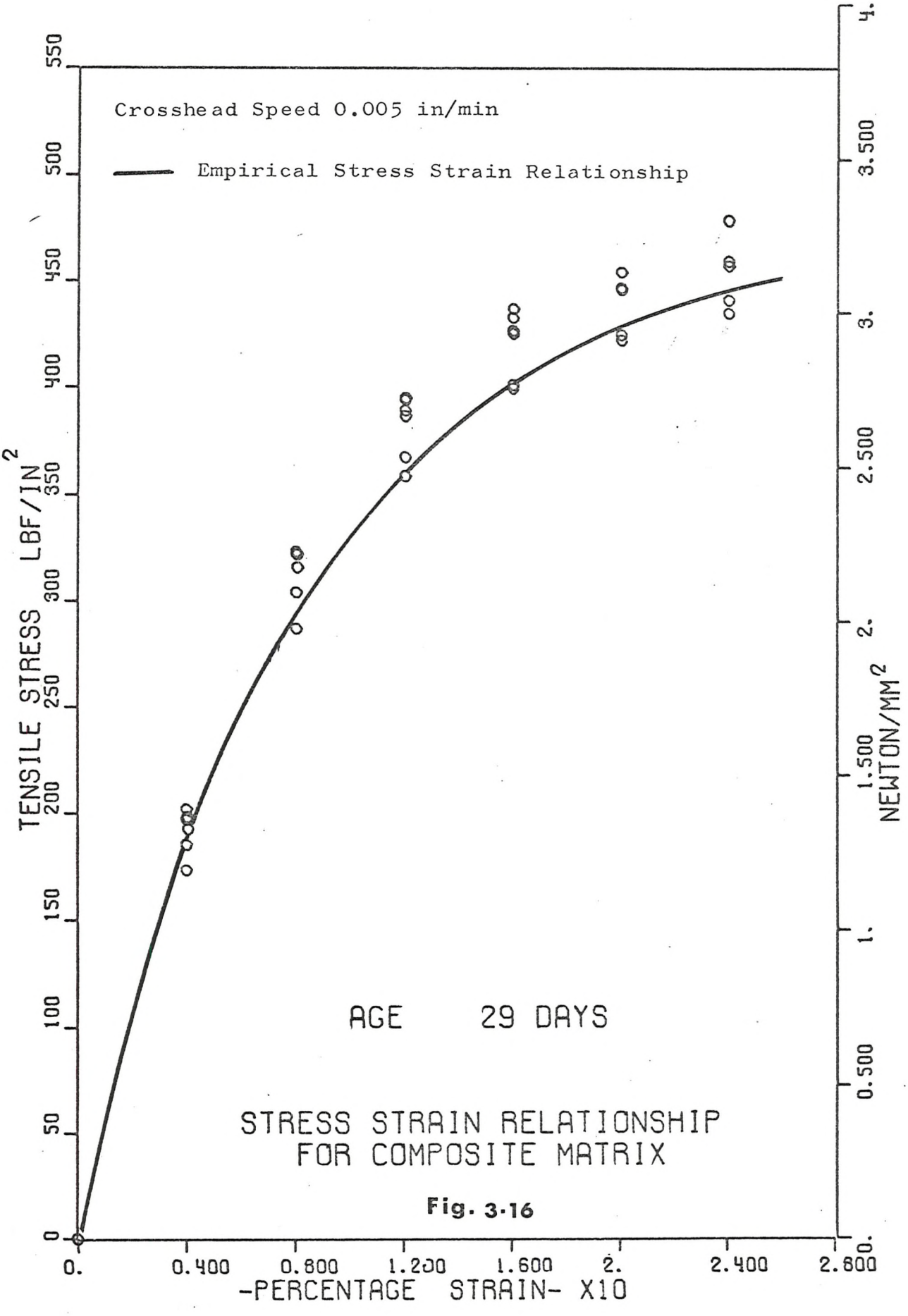
Crosshead Speed 0.005 in/min
Empirical Stress Strain Relationship
TENSILE STRESS LBF/IN^2
NEWTON/MM^2
-PERCENTAGE STRAIN- X10
0.
0.400
0.800
1.200
1.600
2.
2.400
2.800
0
50
100
150
200
250
300
350
400
450
500
550
0.500
1.
1.500
2.
2.500
3.
3.500
4.
AGE 29 DAYS
STRESS STRAIN RELATIONSHIP
FOR COMPOSITE MATRIX

Fig. 3.16

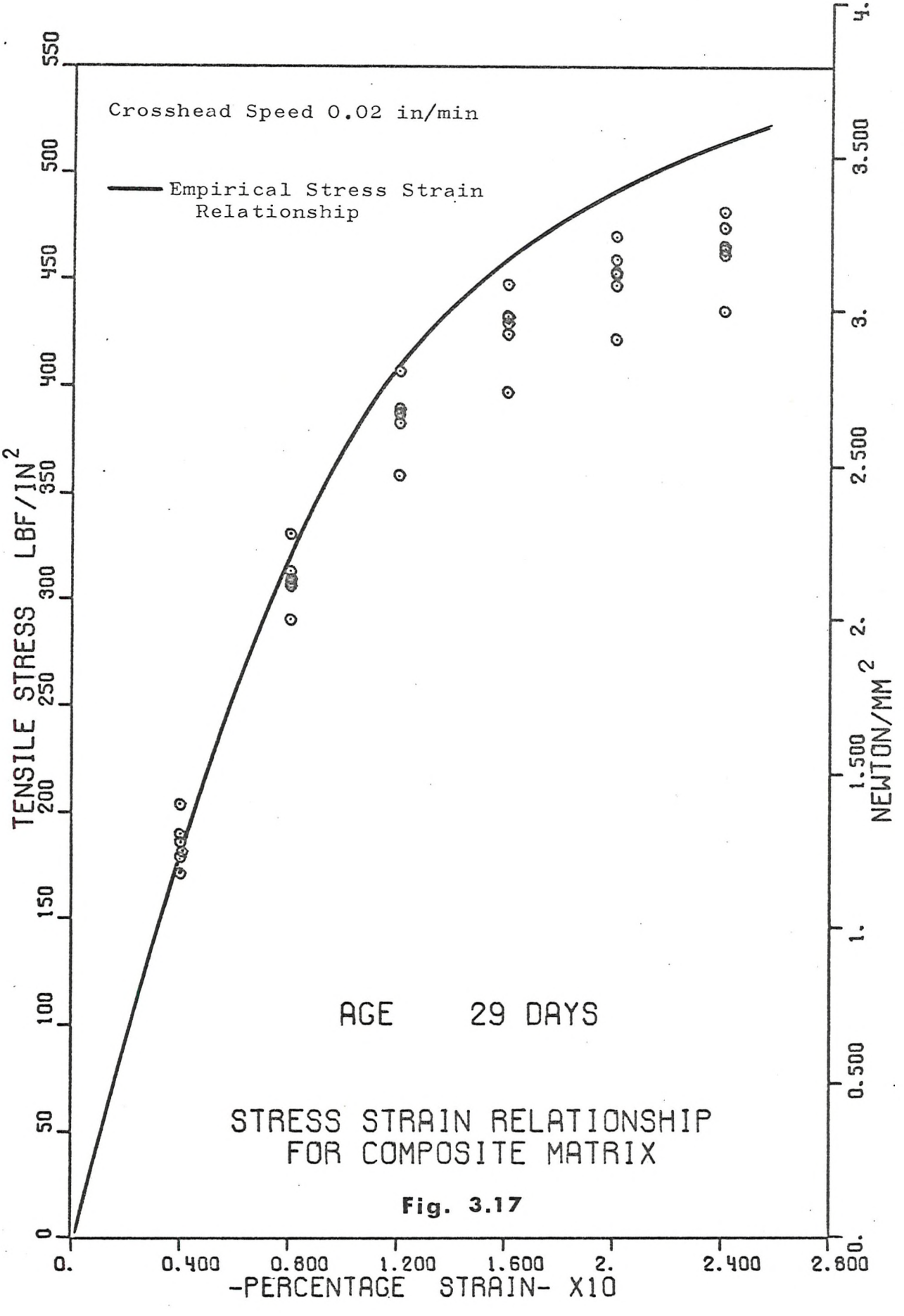
Crosshead Speed 0.02 in/min
Empirical Stress Strain Relationship
TENSILE STRESS LBF/IN^2
NEWTON/MM^2
-PERCENTAGE STRAIN- X10
0
50
100
150
200
250
300
350
400
450
500
550
0.
0.500
1.
1.500
2.
2.500
3.
3.500
4.
0.400
0.800
1.200
1.600
2.400
2.800
AGE 29 DAYS
STRESS STRAIN RELATIONSHIP
FOR COMPOSITE MATRIX

Fig. 3.17

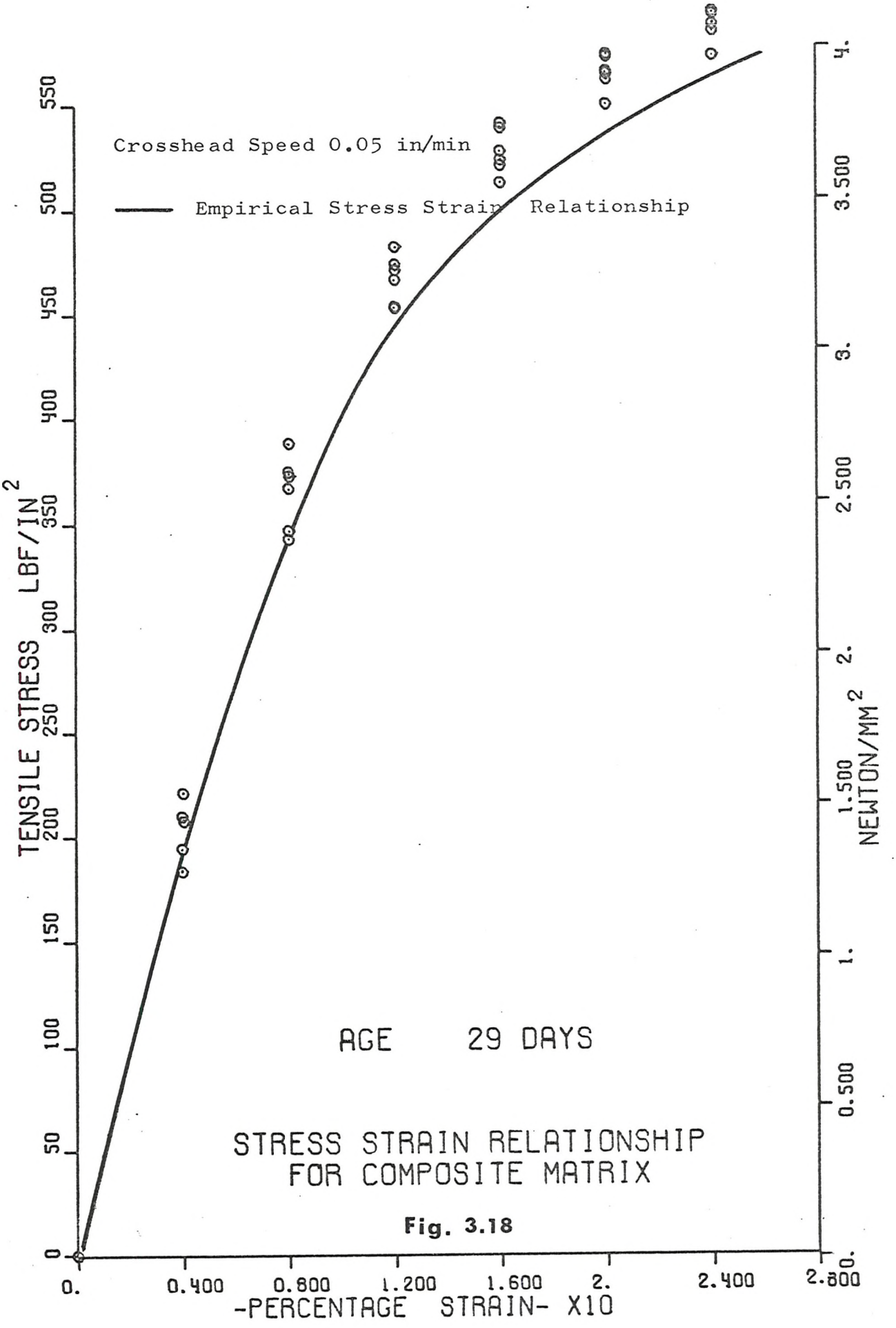
Crosshead Speed 0.05 in/min
Empirical Stress Strain Relationship
TENSILE STRESS LBF/IN 2
NEWTON/MM 2
-PERCENTAGE STRAIN- X10
0.
0.400
0.800
1.200
1.600
2.
2.400
2.800
0
50
100
150
200
250
300
350
400
450
500
550
0.500
1.
1.500
2.
2.500
3.
3.500
4.
AGE 29 DAYS
STRESS STRAIN RELATIONSHIP
FOR COMPOSITE MATRIX

Fig. 3.18

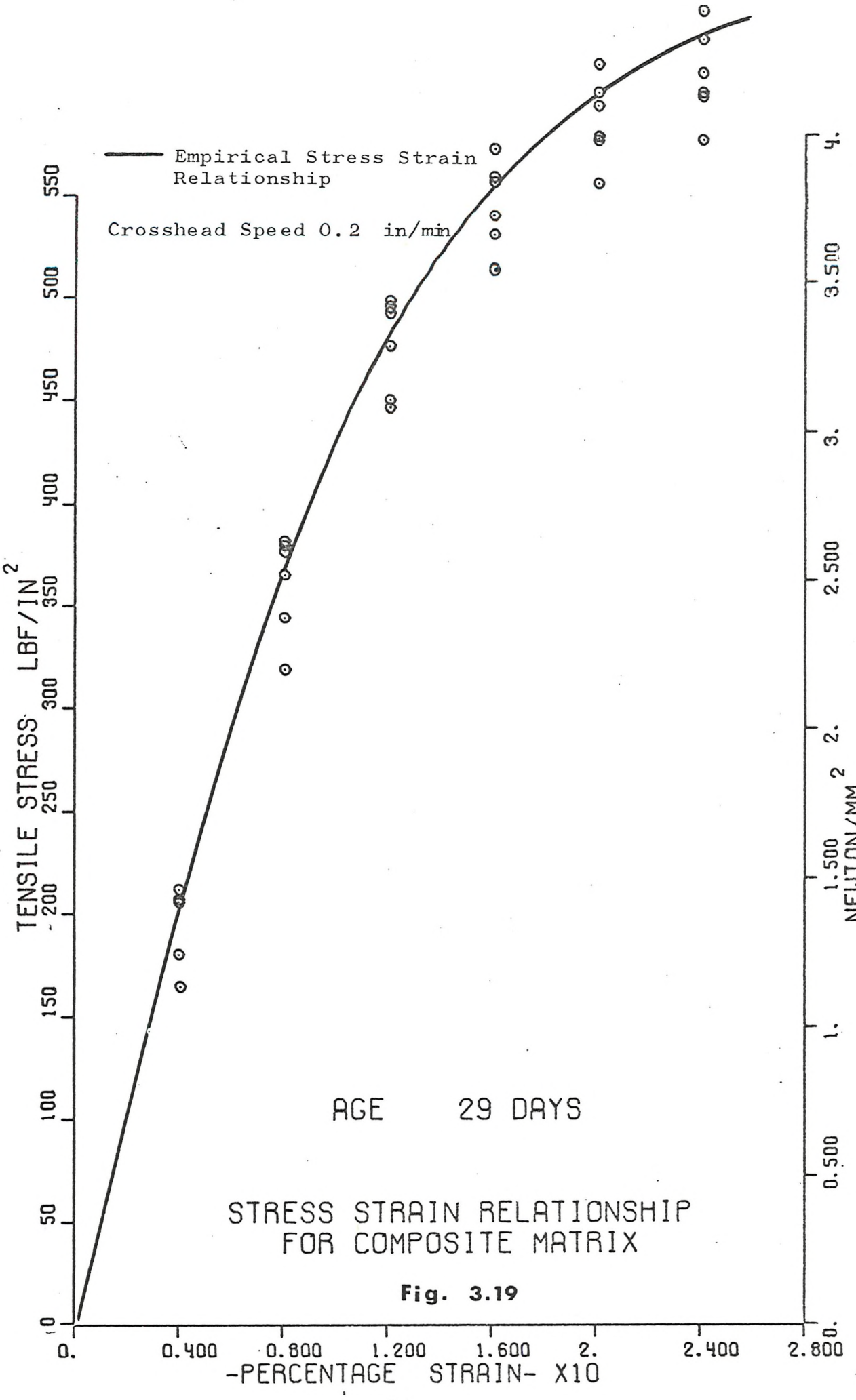
Empirical Stress Strain Relationship
Crosshead Speed 0.2 in/min
TENSILE STRESS LBF/IN^2
NEWTON/MM^2
-PERCENTAGE STRAIN- X10
0.
0.400
0.800
1.200
1.600
2.
2.400
2.800
0
50
100
150
200
250
300
350
400
450
500
550
0.500
1.
1.500
2.
2.500
3.
3.500
4.
AGE 29 DAYS
STRESS STRAIN RELATIONSHIP
FOR COMPOSITE MATRIX

Fig. 3.19

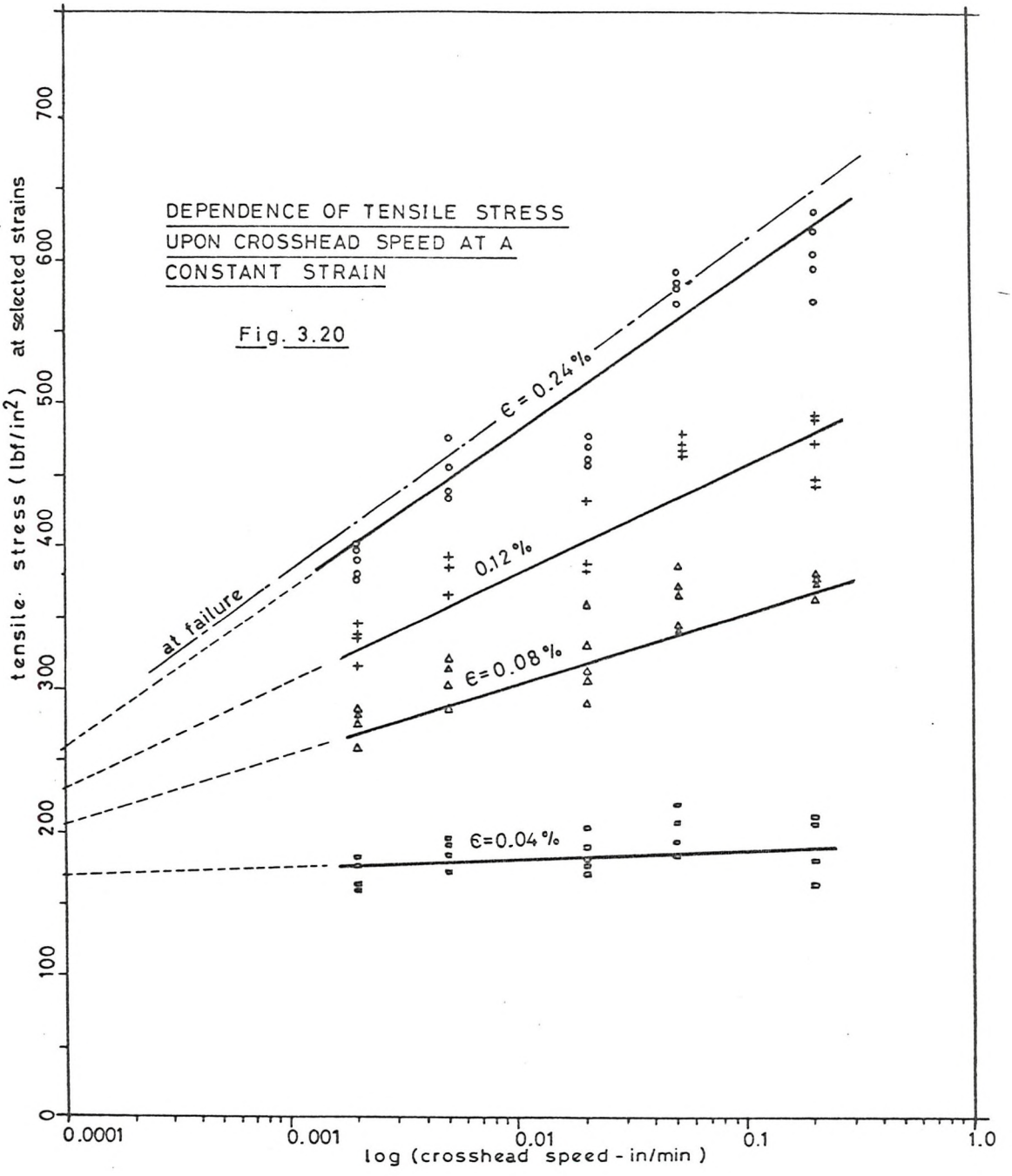
DEPENDENCE OF TENSILE STRESS
UPON CROSSHEAD SPEED AT A
CONSTANT STRAIN
Fig. 3.20
tensile stress (lbf/in2) at selected strains
log (crosshead speed - in/min)
at failure
ϵ = 0.24 %
0.12 %
ϵ=0.08 %
ϵ=0.04 %
0
100
200
300
400
500
600
700
0.0001
0.001
0.01
0.1
1.0

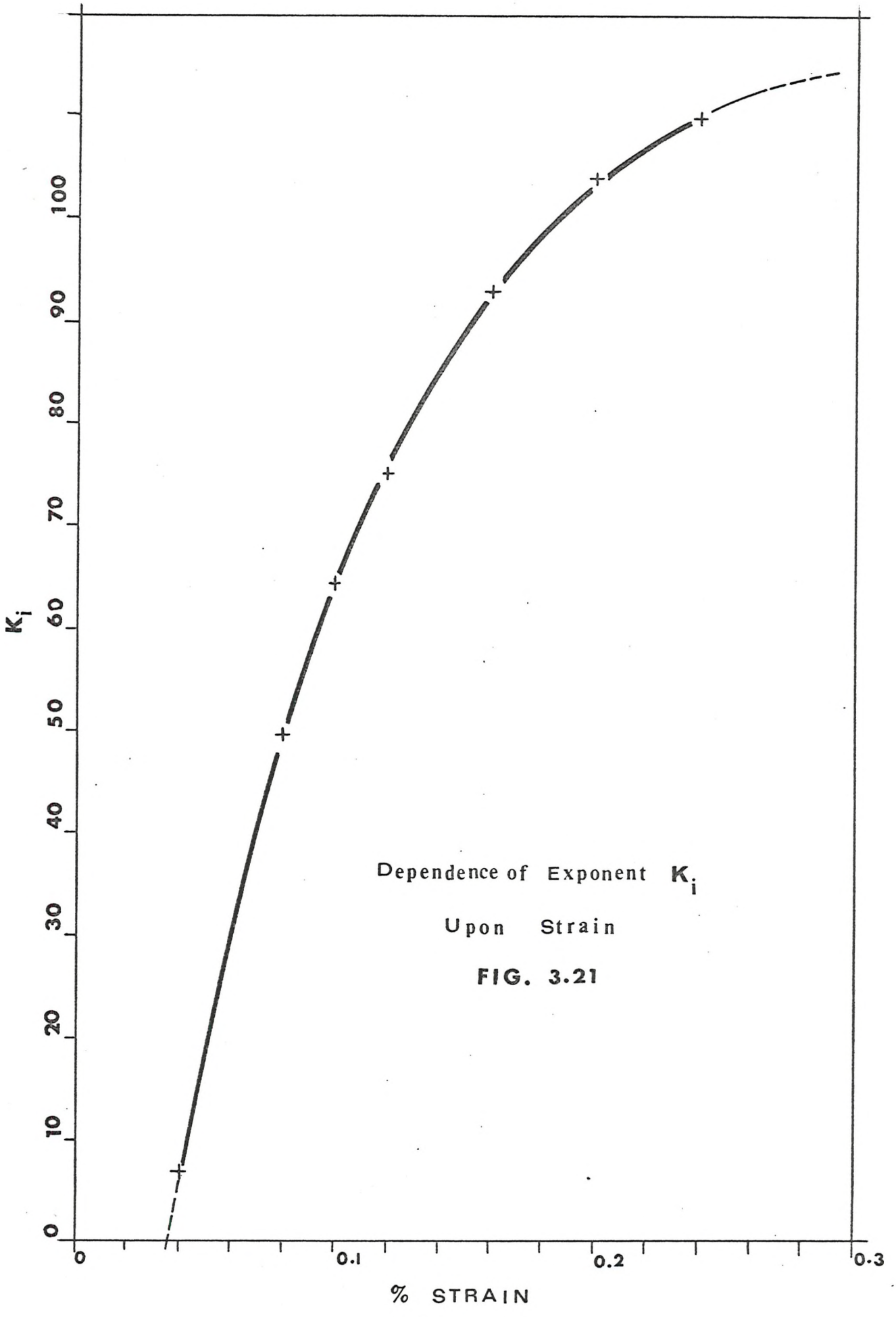

Dependence of Exponent K_i

Upon Strain

FIG. 3.21

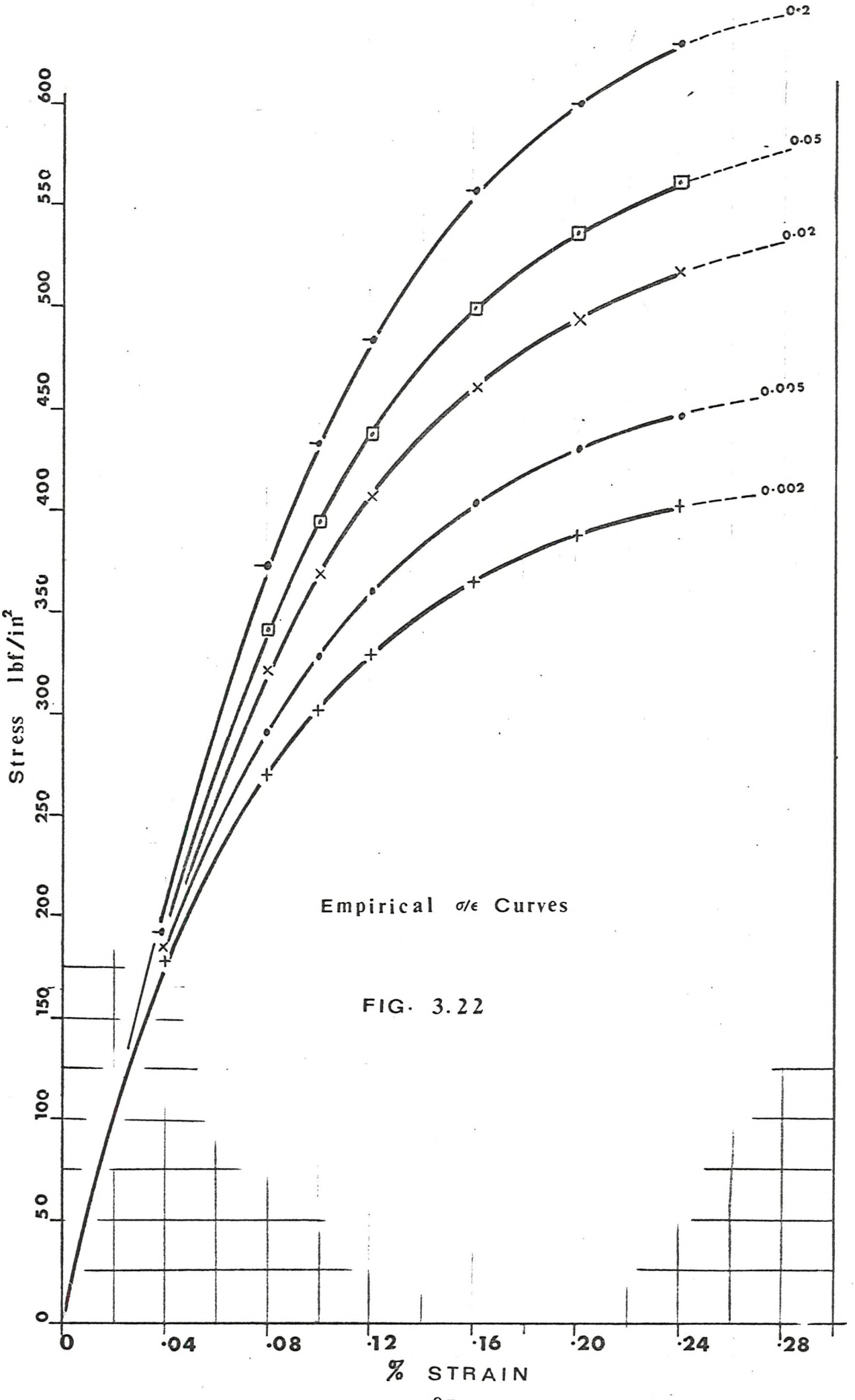

Empirical σ/ϵ Curves

FIG. 3.22

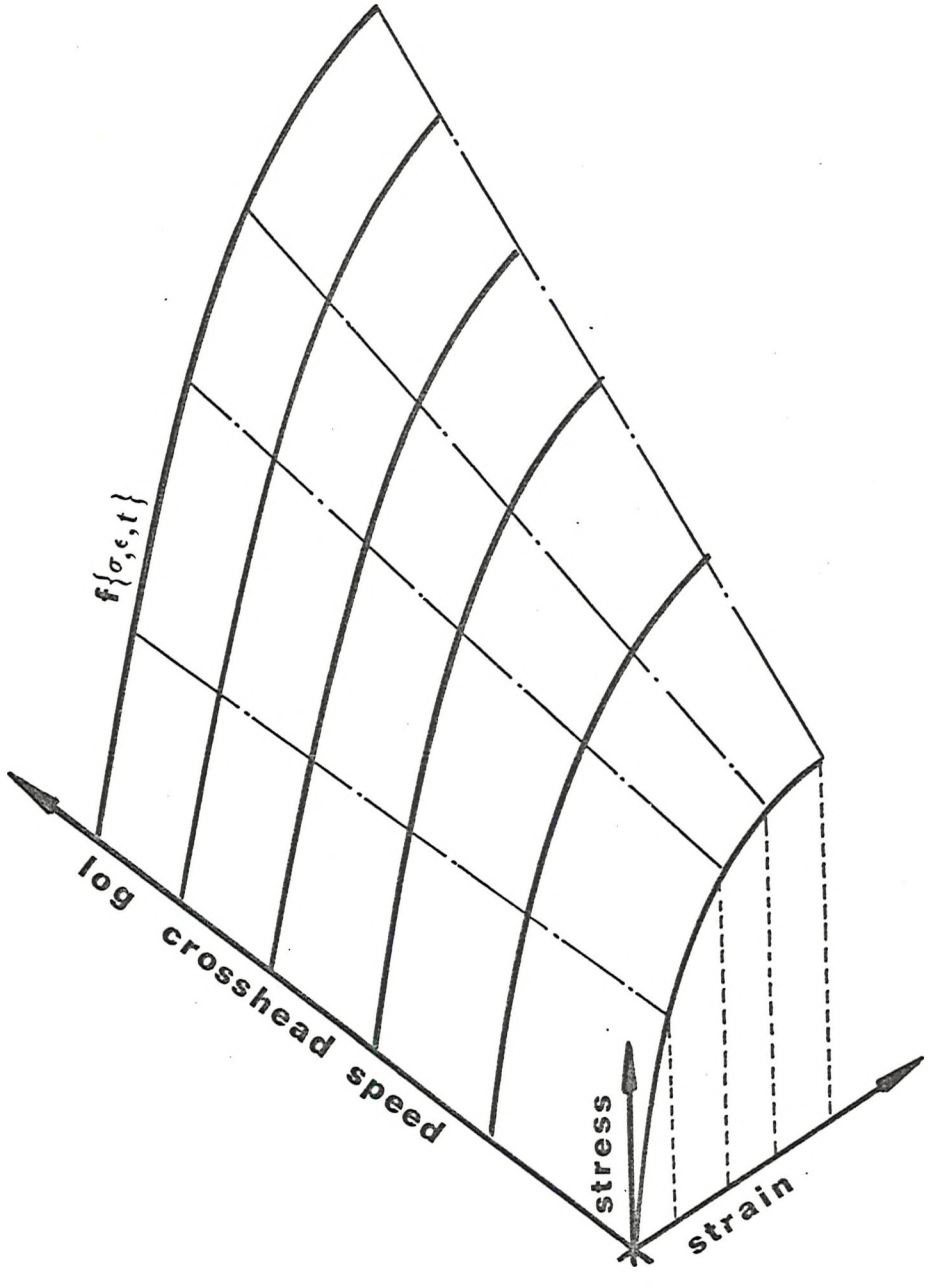

Pictorial Representation of the Relationship

Between Stress , Strain and Time

Fig. 3.23

3.3.4 Effects Due to Various Curing Histories

Two cement boards were manufactured (Sec. 3.2) cut and prepared (Appendix C, Sec. C2) to give 75 tensile specimens. The identity number and position of the specimen within the board are illustrated in Fig. 3.24. The specimens were arranged in a random manner. In general a test sample contained 3 specimens. These were tested in tension in the Instron machine with a crosshead speed of 0.005 in/min in conjunction with the strain gauge extensometer (Appendix C, Sec. C1.2) thus giving the full stress-strain diagram up to failure. This was not possible in all cases due to apparatus failure. Where this was so (marked +, Table 3.7) the Boulton Paul transducer and meter were used, thereby giving the initial modulus and ultimate strength only.

The standard curing conditions were:

1. A complete air cure: these were considered to be control samples and were stored at a temperature of 22°C and a relative humidity of approximately 40 to 60%. Various ages.
2. A complete wet cure: the specimens were fully immersed in water and removed just prior to testing. Various ages.

3. Specimens were tested at various ages, with different periods of wet cure, followed by a 6 day dry cure. Optimum strength values appear to have been reached after a 6 day dry cure as illustrated in Fig. 3.25.

4. Complex Cure: specimens were wet cured followed by an air cure. The periods of time in water and air varied, as detailed in Table 3.7 and illustrated in Fig. 3.26. All specimens were tested at a total age of 43 days.

The curing histories are detailed in Table 3.7 (column **4**) together with the ultimate tensile strengths (σ_u) lbf/in^2 (column **5**) and initial elastic modulus (E_o) lbf/in^2 (column **6**).

Fig. 3.26 shows the plot of tensile strength against specimen age for cures 1, 2 and 3. The lines on this graph are only graphical representations of the general trend for each curing history. The effect of curing history upon the tensile strength is quite marked. The wet cured specimens are weaker than the dry cured specimens (graph 1). However, specimens which have been wet cured and then finally dry cured appear to have strengths greater than the normal dry cure values (graph 3). This seems to suggest that when the specimens are soaked

in water the polymer weakens but the water is necessary to hydrate the cement particles. Upon drying, the polymer regains its strength and the cement particles are strengthened by the hydration process. Fig. 3.27 shows the plot of initial elastic modulus against specimen age. Here the specimens which have a cure period in water show a general increase of elastic modulus with age, although not marked. The line shown indicates the linear regression estimate calculated as a result of computer programme G44D, Appendix E.

Fig. 3.28 shows clearly the effect of different environments upon the polymer-cement. In the case where the material is cured immersed in water, it becomes weak and brittle. At the other extreme if the material is then allowed to dry out it becomes quite strong and ductile, which suggests that the strength of the polymer in the presence of water suffers damage but this is regained upon drying. The period of drying will depend very much upon the mass of the material and for sections such as the tensile specimen, 6 days were required. This was established by observing the sections after fracture during the type 4 cure series of tests.

10	59
49	34
30	52
6	27
4	35
61	39
17	56
13	47
65	68
50	12
75	66
67	73
7	14
16	25
64	9
28	33
72	54
46	2
40	11

48	15
5	20
69	60
71	26
24	58
23	31
3	14
36	18
43	21
8	55
42	62
76	1
44	37
22	51
29	74
70	32
57	63
38	53
45	19

Cutting Scheme for Sheets 10.

FIG 3.24

TABLE 3.7

PROPERTIES OF POLYMER-CEMENT UNDER VARYING CURING HISTORIES

Cure Type 1

1	2	3	4		5	6
Spec. No.	Thickness (in)	Total Age (Day)	Cure Time (Days)		Ultimate Strength (σ_u) lbf/in^2	Initial Elastic Modulus (E_o) lbf/in^2 x 10^6
			Wet	Air		
10.67	0.192	6	-	4	535	0.4770
10.68	0.189	6	-	4	560	0.4650
10.69 +	0.198	8	-	6	623	0.5330
10.70 +	0.162	8	-	6	741	0.6040
10.71 +	0.194	12	-	10	624	0.5950
10.72 +	0.195	12	-	10	591	0.5880
10.73	0.201	32	-	30	554	0.6900
10.74	0.157	32	-	30	546	0.6840
10.75	0.188	46	-	44	588	0.6020
10.76	0.169	46	-	44	597	0.6330

+ Full stress-strain graphs not obtained

Note: 48 hour moulding time not included in cure time

TABLE 3.7 (Continued)

Cure Type 2

1	2	3	4		5	6
Spec. No.	Thickness (in)	Total Age (Day)	Cure Time (Days)		Ultimate Strength (σ_u) lbf/in^2	Initial Elastic Modulus (E_o) $lbf/in^2 \times 10^6$
			Wet	Air		
10.1	0.19	3	1	-	192	0.3800
10.2 +	0.193	3	1	-	287	0.5220
10.3 +	0.174	3	1	-	220	0.4980
10.4 +	0.178	5	2	-	245	0.5030
10.5 +	0.193	5	2	-	265	0.5175
10.6 +	0.181	5	2	-	250	0.5050
10.7 +	0.187	5	3	-	246	0.5520
10.8 +	0.172	5	3	-	256	0.6020
10.9 +	0.202	5	3	-	237	0.4860
10.10 +	0.187	7	5	-	269	0.5920
10.11 +	0.189	7	5	-	258	0.4920
10.12 +	0.196	7	5	-	244	0.5130
10.13 +	0.189	9	7	-	277	0.5750
10.14 +	0.192	9	7	-	248	0.5140
10.15 +	0.152	9	7	-	365	0.6400
10.16	0.189	16	14	-	304	0.6270
10.17	0.186	16	14	-	307	0.6040
10.18	0.171	16	14	-	314	0.6180
10.19	Damaged					
10.20	0.149	30	28	-	381	0.7860
10.21	0.179	30	28	-	345	0.6230
10.22	0.167	44	42	-	415	0.6890
10.23	0.189	44	42	-	418	0.8550
10.24	0.202	44	42	-	428	0.8380

+ Full stress-strain graphs not obtained

Note: 48 hour moulding time not included in cure time

TABLE 3.7 (Continued)

Cure Type 3

1	2	3	4		5	6
Spec. No.	Thickness (in)	Total Age (Day)	Cure Time (Days)		Ultimate Strength (σ_u) lbf/in^2	Initial Elastic Modulus (E_o) lbf/in^2 x 10^6
			Wet	Air		
10.25 +	0.203	9	1	6	640	0.5270
10.26 +	0.175	9	1	6	650	0.6080
10.27 +	0.186	9	1	6	685	0.6840
10.28 +	0.195	10	2	6	692	0.6510
10.29 +	0.160	10	2	6	705	0.6500
10.30 +	0.181	10	2	6	722	0.5920
10.31	0.185	11	3	6	708	0.6280
10.32	0.144	11	3	6	727	0.6400
10.33	0.199	11	3	6	676	0.5100
10.34	0.186	13	5	6	870	0.7650
10.35	0.181	13	5	6	827	0.6760
10.36	0.165	13	5	6	828	0.5690
10.37	0.170	22	14	6	824	0.5950
10.38	0.163	22	14	6	902	0.7030
10.39	0.201	22	14	6	785	0.6150
10.40	0.192	30	22	6	924	0.8070
10.41	0.202	30	22	6	888	0.6400
10.42	0.172	30	22	6	950	0.9060
10.43	0.183	43	35	6	906	0.6920
10.44	0.176	43	35	6	940	0.6360

+ Full stress-strain graphs not obtained

Note: 48 hour moulding time not included in cure time

TABLE 3.7 (Continued)

Cure Type 4

1	2	3	4		5	6
Spec. No.	Thickness (in)	Total Age (Day)	Cure Time (Days)		Ultimate Strength (σ_u) lbf/in^2	Initial Elastic Modulus (E_o) lbf/in^2 x 10^6
			Wet	Air		
10.45	0.163	45	42	1	578	0.8060
10.46	0.206	45	42	1	508	0.7740
10.47	0.187	45	42	1	548	0.6710
10.48	0.195	45	43	-	455	0.6650
10.49	0.188	45	43	-	391	1.0040
10.50	0.195	45	43	-	331	0.7630
10.51	0.177	45	40	3	644	0.7140
10.52	0.192	45	40	3	730	0.7950
10.53	0.152	45	40	3	772	0.7190
10.54	0.195	45	39	4	767	0.7380
10.55	0.174	45	39	4	864	0.7900
10.56	0.182	45	39	4	863	0.6650
10.57	0.163	45	36	7	960	0.8250
10.58	0.187	45	36	7	898	0.6420
10.59	0.190	45	36	7	943	0.9630
10.60	0.163	45	29	14	909	0.6300
10.61	0.178	45	29	14	919	0.7900
10.62	0.165	45	29	14	910	0.7200
10.63	0.139	45	15	28	880	0.6820
10.64	0.197	45	15	28	832	0.7250
10.65	0.185	45	1	42	659	0.5740
10.66	0.197	45	1	42	634	0.6030

Note: 48 hour moulding time not included in cure time

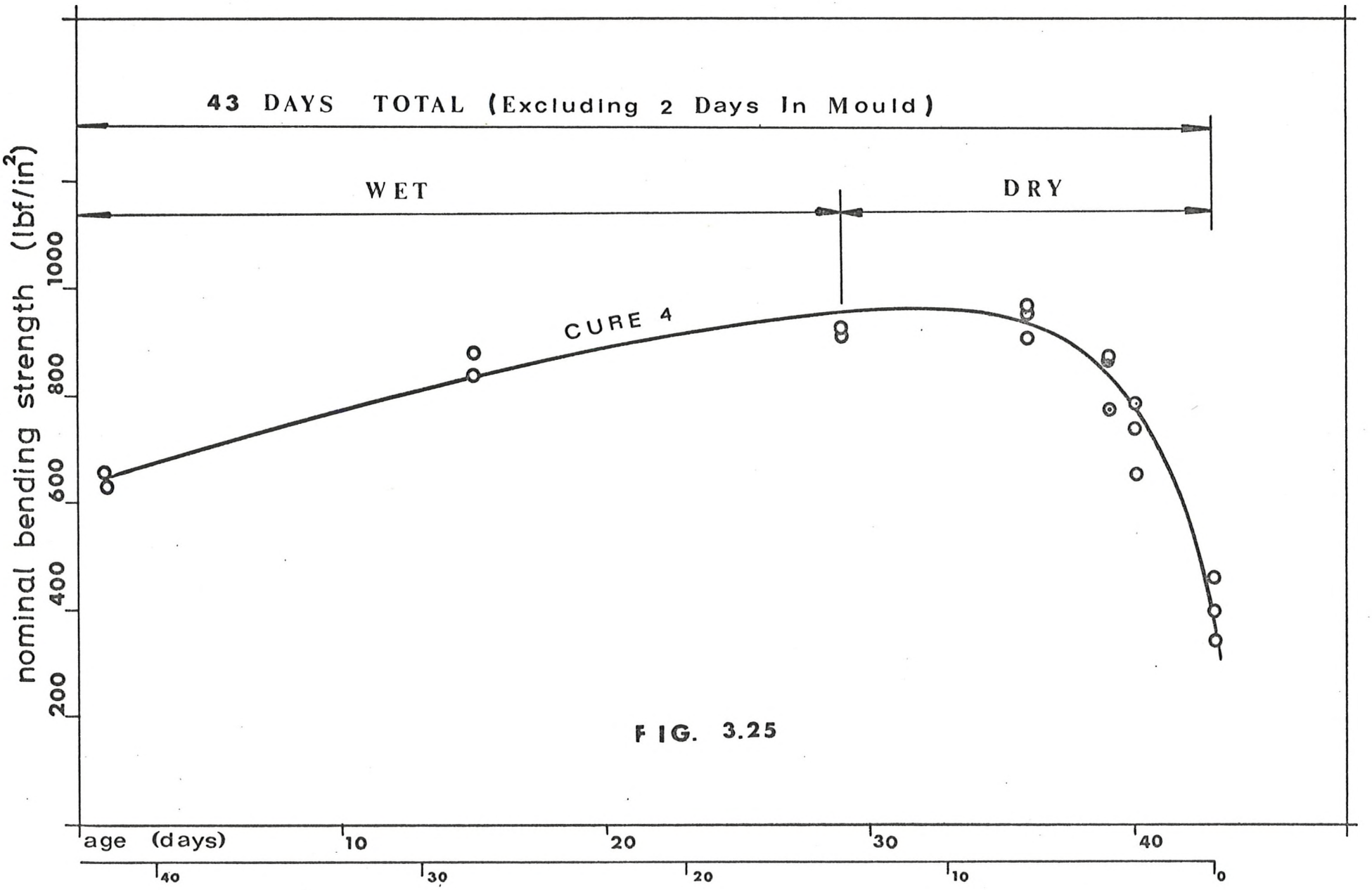
43 DAYS TOTAL (Excluding 2 Days In Mould)
WET
DRY
CURE 4
nominal bending strength (lbf/in²)
200
400
600
800
1000
age (days)
10
20
30
40
40
30
20
10
0

FIG. 3.25

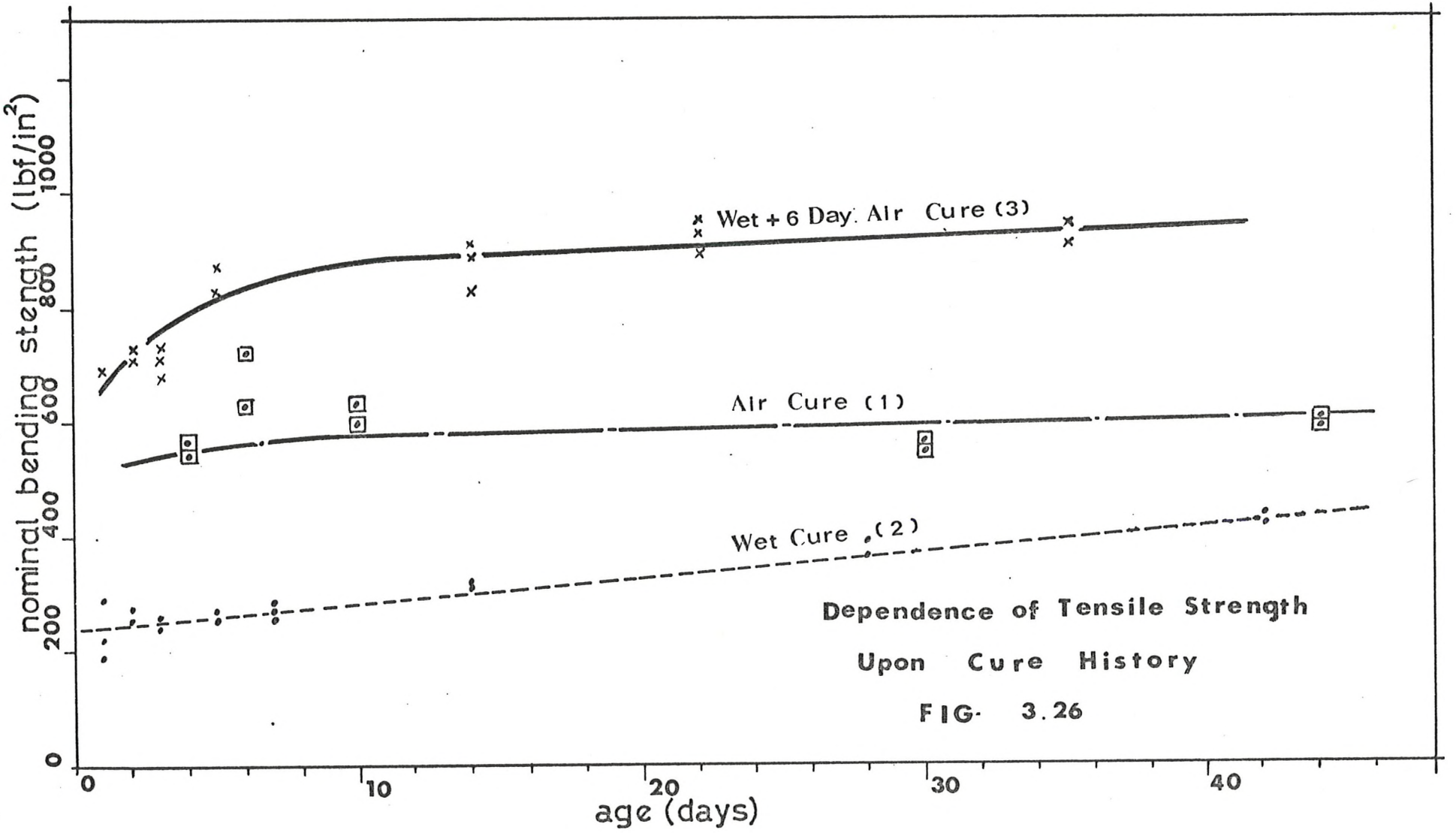

Dependence of Tensile Strength Upon Cure History

FIG. 3.26

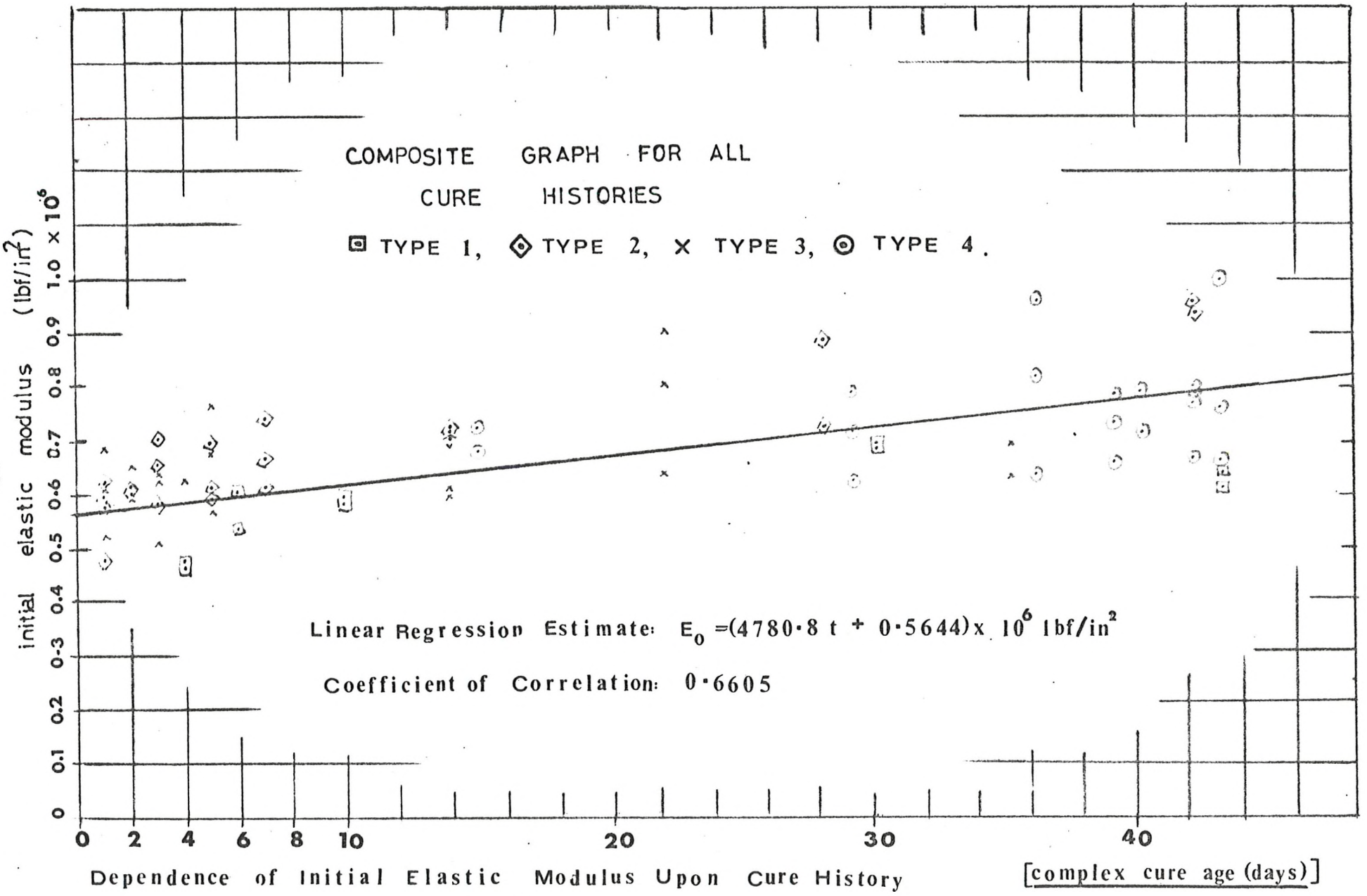

Dependence of Initial Elastic Modulus Upon Cure History

FIG. 3.27

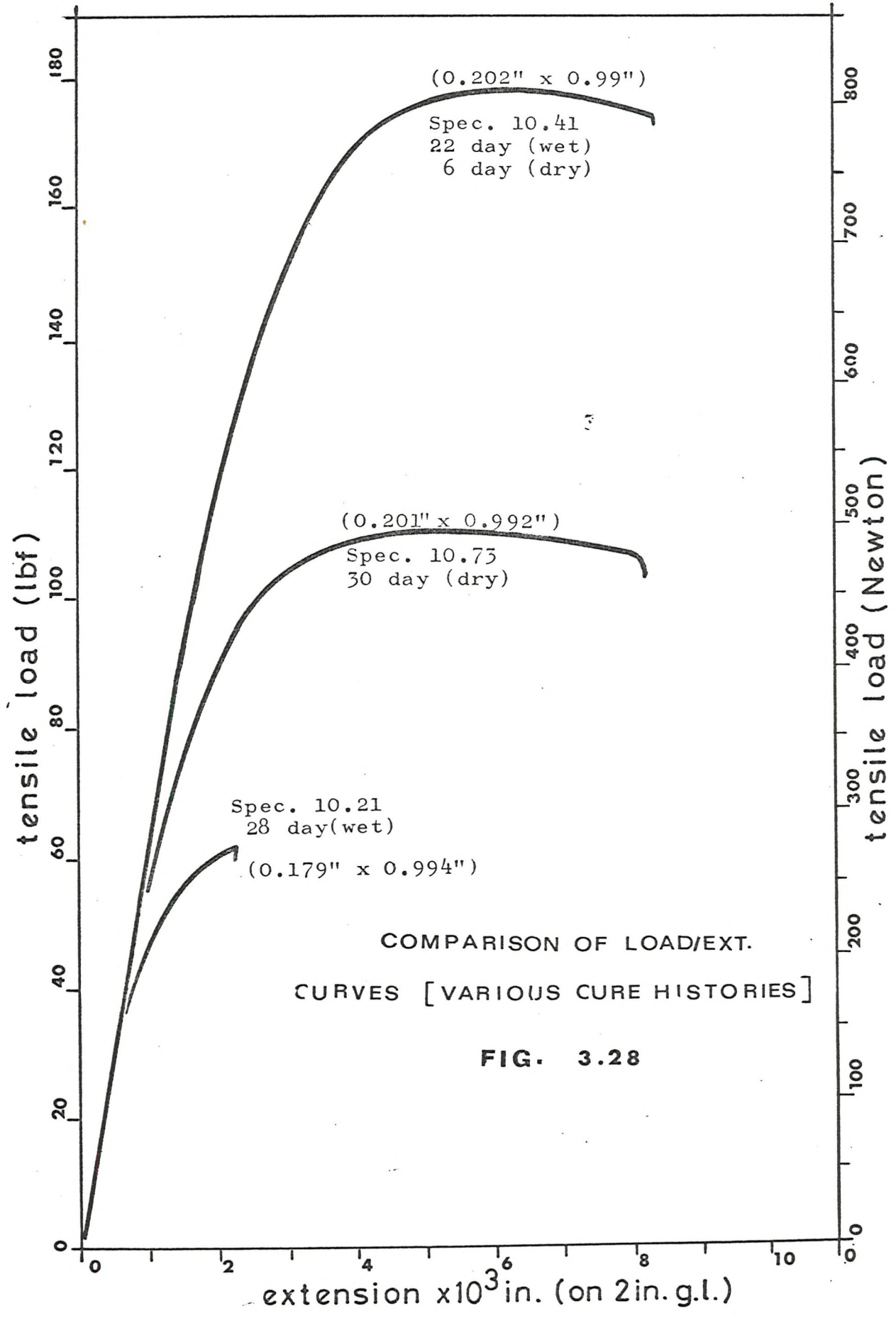

COMPARISON OF LOAD/EXT. CURVES [VARIOUS CURE HISTORIES]

FIG. 3.28

3.4 Compressive Stress Strain Investigation

3.4.1 The Experimental Method

Compression specimens were cut from the sheet as indicated on Fig. 3.2 when read in conjunction with Table 3.8. They were prepared as described in Appendix C (Sec. C2).

Each specimen was placed in a compression rig developed by ALLEN[3], as shown on plate 3.2 top. In order to measure the longitudinal contraction during loading, an extensometer (plate 3.2 bottom) was fitted around the rig in which was mounted a Baldwin microformer (Sec. C1.1). This gave a continuous plot of compressive load against contraction. An additional attachment (plate 3.3 top), having free lateral movement, allowed the simultaneous measurement of the lateral expansion. The transverse displacement of the specimen was detected by a transducer and the signal indicated on a transducer meter. By using the blipping device marks were made on the load-displacement graph at equal intervals of lateral expansion. From this information it was possible to plot the compressive load, lateral expansion graph and so, from the two plots, values for Poissons ratio in compression were derived.

The fully mounted rig is illustrated in plate 3.3 bottom.

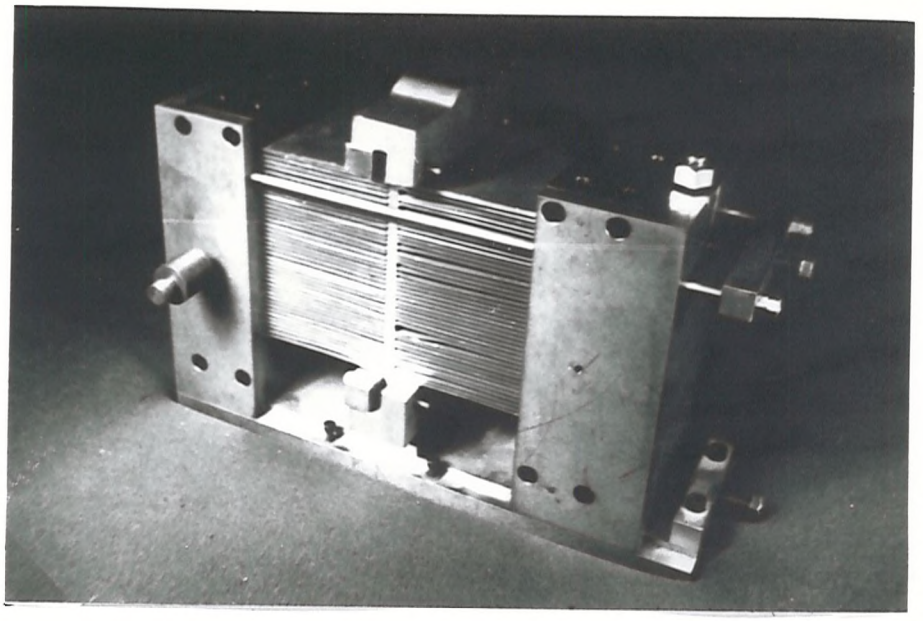

COMPRESSION RIG

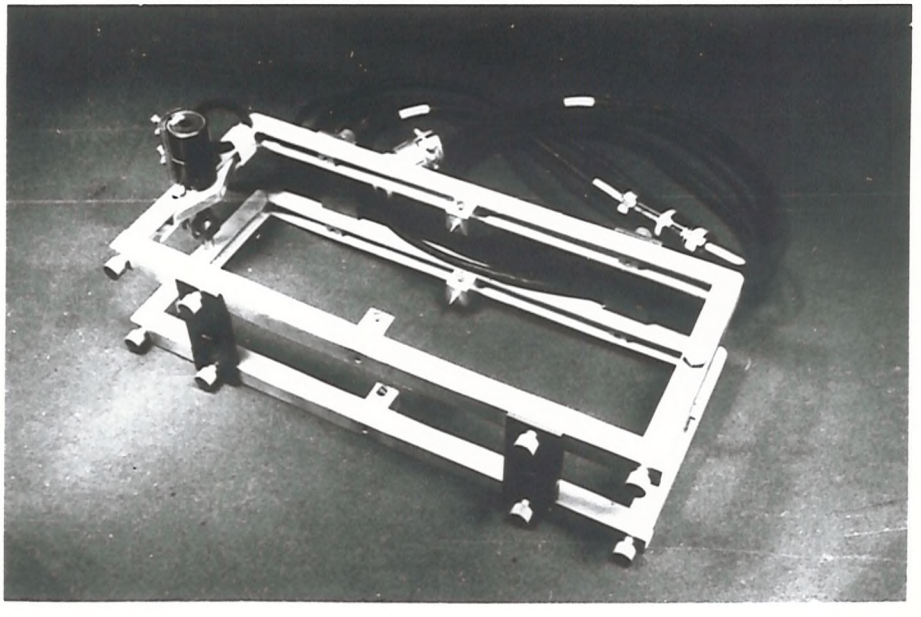

COMPRESSIVE LONG EXTENSOMETER

PLATE 3.2

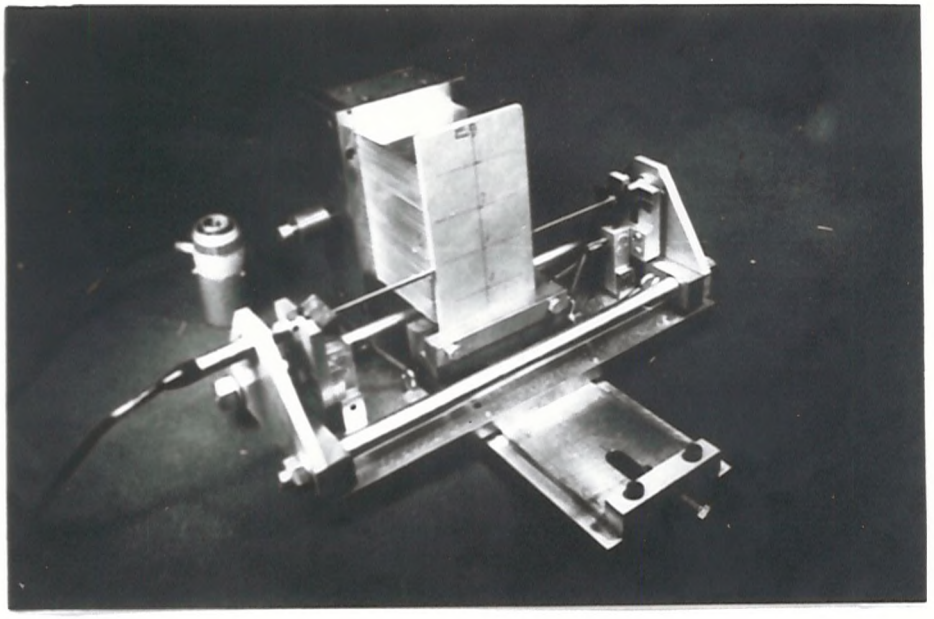

COMPRESSIVE LATERAL EXTENSOMETER

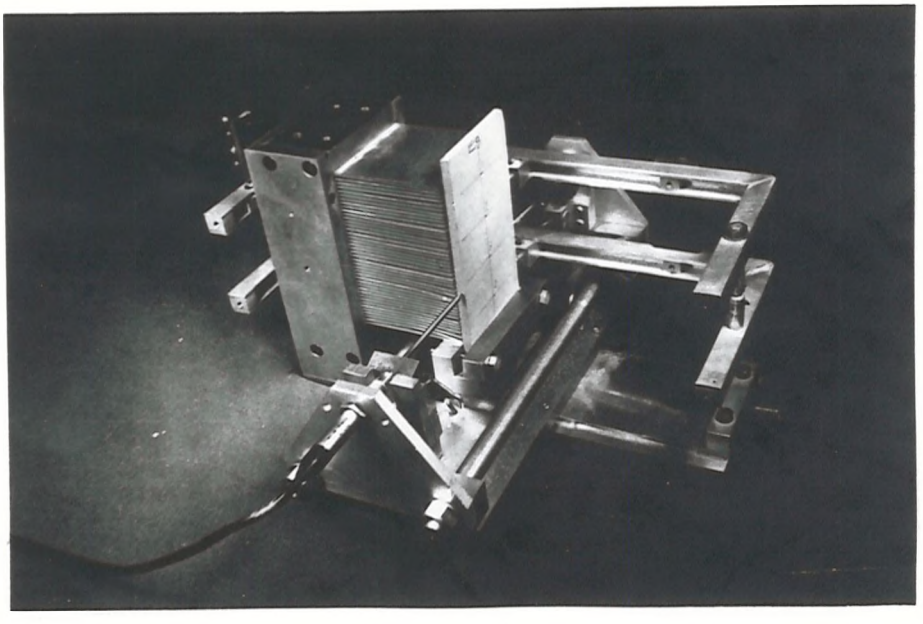

HALF COMPRESSION RIG & LONGITUDINAL EXTENSOMETER
COMPLETE WITH THE LATERAL EXTENSOMETER

PLATE 3.3

3.4.2 Experimental Results: Various Ages

The plots of Figs. 3.29, 3.30 and 3.31 show the compressive stress-strain curves to reach a maximum by 0.9% strain and then to remain almost at a constant stress for increased strains. This continuous yield was shown to exist in all compression tests of the polymer-cement. In view of this no values are quoted for strains at fracture. Tables 3.8 and 3.9 show the compressive strength and initial elastic modulus when tested under a constant crosshead speed but various ages. For detailed results see Appendix G (Table G3). When comparing the stress strain curves they are found to be almost identical, thus it is reasonable to assume that the effect of age upon the stress-strain curve is not marked.

Table 3.10 gives the values of the transverse/longitudinal strain ratio in compression. Difficulty was experienced here in view of the very small lateral displacements being measured. Therefore it was necessary to use the most sensitive range of the transducer meter. There was also a tendency for the measuring points to penetrate the specimen and temperature changes were detected by the meter which did not show good stability on this sensitive range. This particular test was discontinued for the present.

TABLE 3.8

COMPRESSIVE STRENGTHS AT VARIOUS AGES

(Crosshead Speed Constant at 0.005 in/min)

Specimen cut from sheet	Age (Days)	Cross-head speed in/min	Compressive Strength lbf/in^2	Standard Deviation lbf/in^2	% Coeff. of Variation	Confidence Limit p = 0.1 lbf/in^2		Estimated Specific Gravity
						Upper	Lower	
6*	8	0.005	-	-	-	-	-	1.653
5*	10	0.005	-	-	-	-	-	1.626
8.	14	0.005	1780.7	131.02	7.357	1888.9	1672.7	1.689
8.	75	0.005	1889.4	254.39	13.46	2131.7	1647.1	1.67
8.	142	0.005	1686.3	33.81	2.00	1726.0	1646.6	1.65

*Full compressive stress-strain diagrams were not recorded for these specimens

TABLE 3.9

COMPRESSIVE ELASTIC MODULUS AT VARIOUS AGES

(Crosshead Speed Constant at 0.005 in/min)

Specimen cut from sheet	Age (Days)	Cross-head speed in/min	Mean Initial Elastic Modulus $lbf/in^2 \times 10^{-6}$	Standard Deviation $lbf/in^2 \times 10^{-6}$	% Coeff. of Variation	Confidence Limits p = 0.1, $lbf/in^2 \times 10^{-6}$	
						Upper	Lower
6.	8	0.005	0.4751	0.0629	13.23	0.549	0.401
5.	10	0.005	0.4715	0.0206	4.38	0.488	0.454
8.	14	0.005	0.4983	0.0642	12.89	0.551	0.445
8.	75	0.005	0.4960	0.0778	15.69	0.570	0.422
4.	142	0.005	0.4391	0.0202	4.59	0.463	0.415

TABLE 3.10

EXPECTED VALUES OF TRANSVERSE/LONGITUDINAL STRAIN RATIO

Cut From Sheet	Crosshead Speed in/min	Age (Days)	Mean Poisson Ratio ν	Standard Deviation of ν	% Coeff. of Variation (p = 0.1)
6.	0.005	8	0.223	0.0308	13.82
5.	0.005	10	0.223	0.0507	22.75

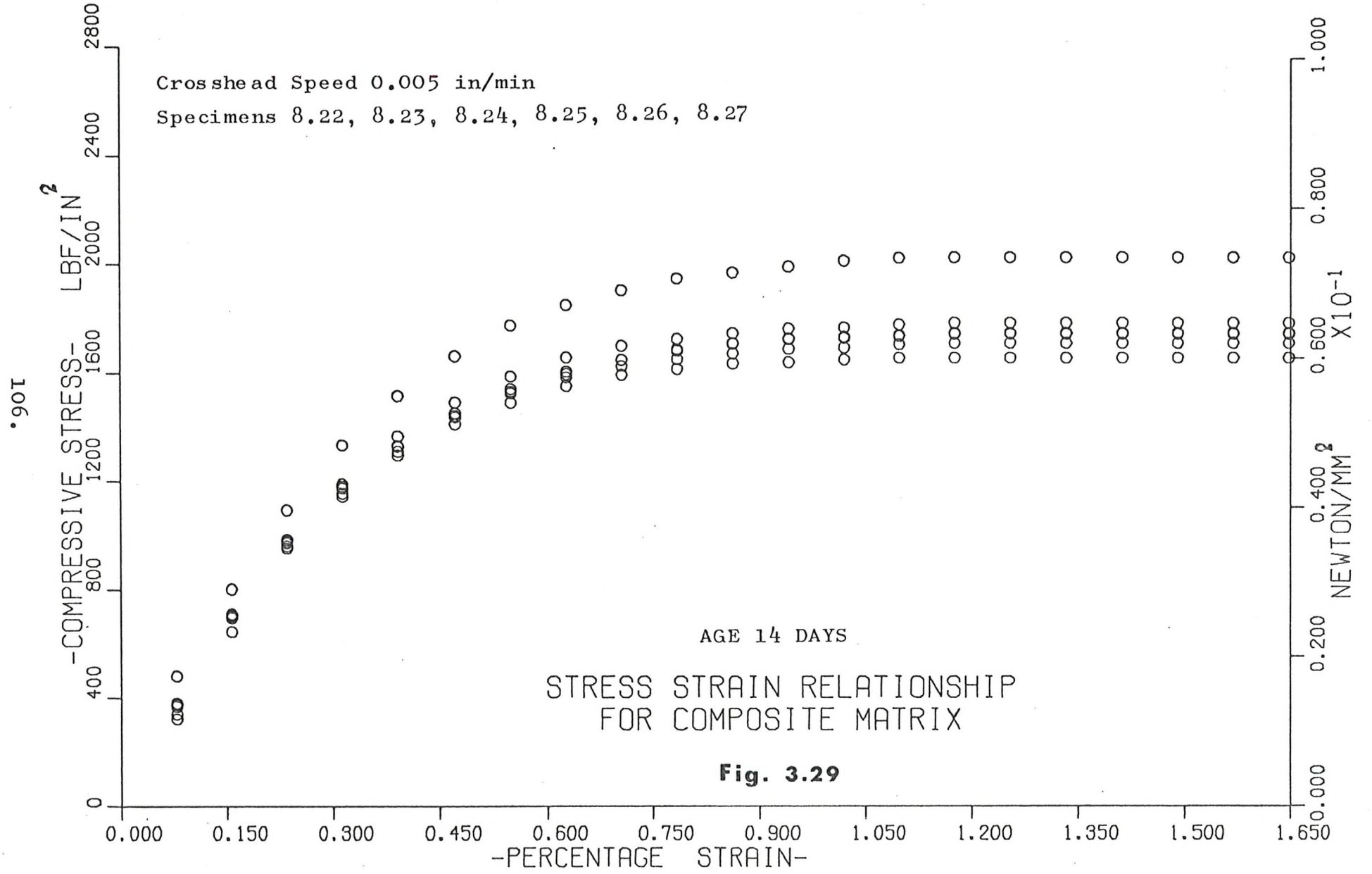
Crosshead Speed 0.005 in/min
Specimens 8.22, 8.23, 8.24, 8.25, 8.26, 8.27
AGE 14 DAYS
STRESS STRAIN RELATIONSHIP
FOR COMPOSITE MATRIX
-COMPRESSIVE STRESS- LBF/IN2
10^6
0
400
800
1200
1600
2000
2400
2800
0.000
0.150
0.300
0.450
0.600
0.750
0.900
1.050
1.200
1.350
1.500
1.650
-PERCENTAGE STRAIN-
0.000
0.200
0.400
0.600
0.800
1.000
X10-1
NEWTON/MM2

Fig. 3.29

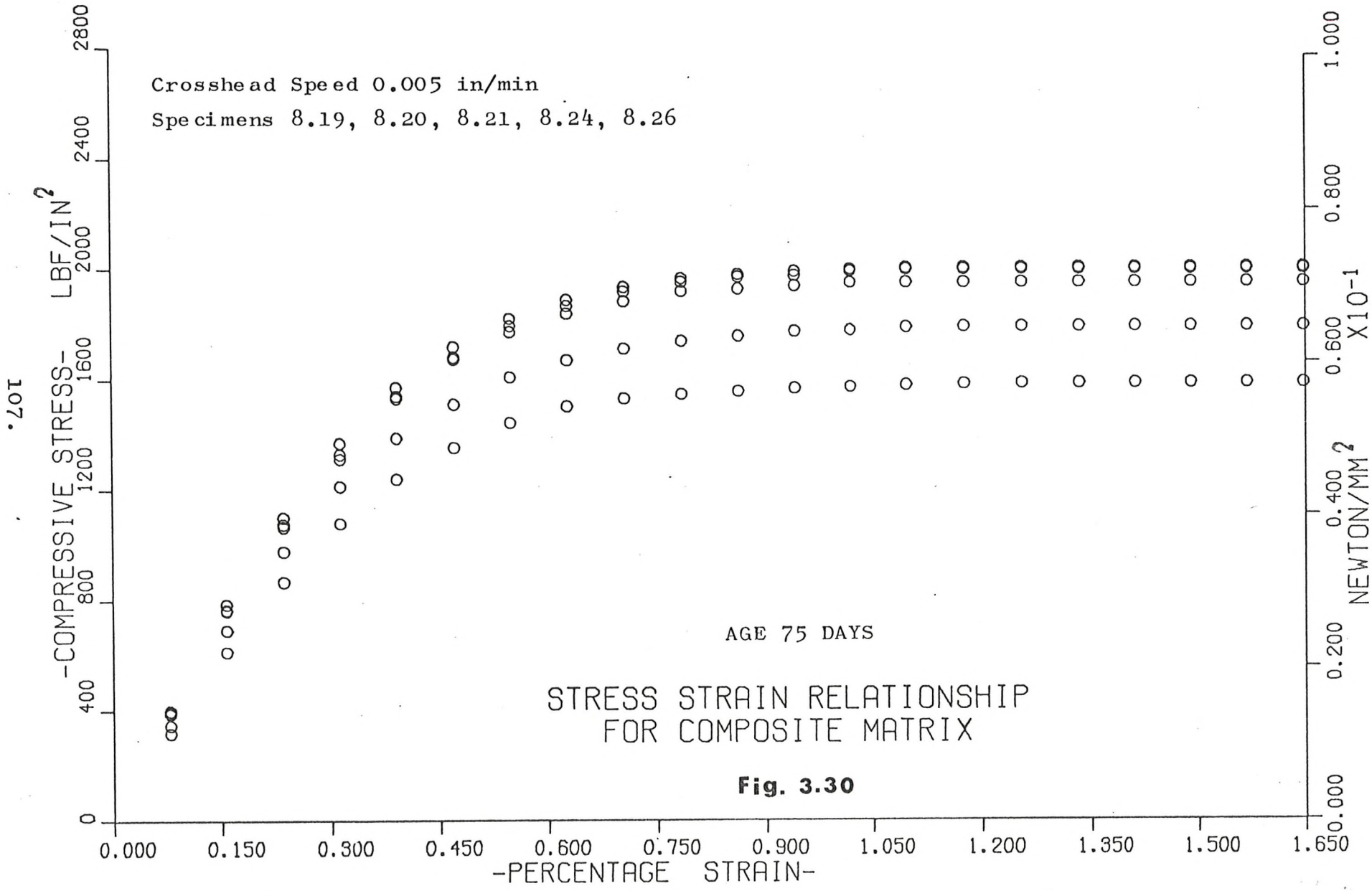
Crosshead Speed 0.005 in/min
Specimens 8.19, 8.20, 8.21, 8.24, 8.26
-COMPRESSIVE STRESS- LBF/IN2
0
400
800
1200
1600
2000
2400
2800
-PERCENTAGE STRAIN-
0.000
0.150
0.300
0.450
0.600
0.750
0.900
1.050
1.200
1.350
1.500
1.650
NEWTON/MM2 X10-1
0.000
0.200
0.400
0.600
0.800
1.000
AGE 75 DAYS
STRESS STRAIN RELATIONSHIP
FOR COMPOSITE MATRIX

Fig. 3.30

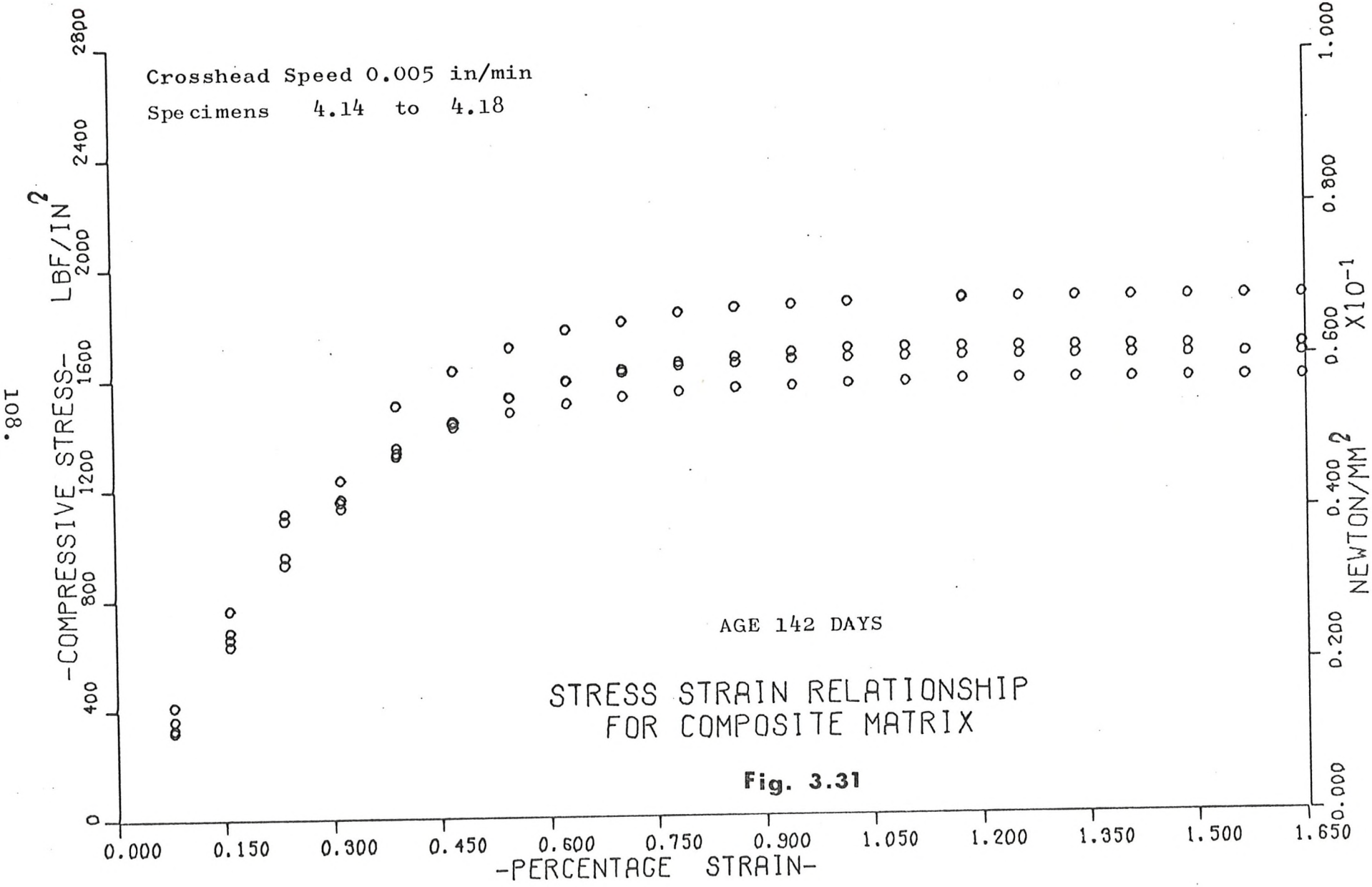
Crosshead Speed 0.005 in/min
Specimens 4.14 to 4.18
AGE 142 DAYS
STRESS STRAIN RELATIONSHIP
FOR COMPOSITE MATRIX
-COMPRESSIVE STRESS- LBF/IN2
NEWTON/MM2 X10-1
-PERCENTAGE STRAIN-
0
400
800
1200
1600
2000
2400
2800
0.000
0.150
0.300
0.450
0.600
0.750
0.900
1.050
1.200
1.350
1.500
1.650
0.000
0.200
0.400
0.600
0.800
1.000

Fig. 3.31

3.4.3 Experimental Results - Various Strain Rates

A summary of results is given in Tables 3.11 and 3.12 for compression tests run at various crosshead speeds from 0.01 to 0.5 in/min. Detailed results are given in Appendix G, Table G4.

Figs. 3.32 to 3.34 show sample stress-strain scatter diagrams for different crosshead speeds plotted by computer programme G44B (Appendix E).

No ultimate strain values have been quoted (refer page 77) but the effect upon ultimate strength due to various rates of strain is noticeable as illustrated by Fig. 3.35. When plotting Fig. 3.35 on a semi logrithmic basis (Fig. 3.36) a linear relationship may exist in the range of crosshead speeds 0.005 to 0.5 in/min.

TABLE 3.11

COMPRESSIVE STRENGTH SUMMARY

(Various Crosshead Speeds)

Specimen cut from sheet	Age (Days)	Cross-head speed in/min	Compressive Strength lbf/in^2	Standard Deviation lbf/in^2	% Coeff. of Variation	Confidence Limit p = 0.1 lbf/in^2		Estimated Specific Gravity
						Upper	Lower	
3.•	29	0.01	-	-	-	-	-	-
7.	29	0.02	1951.1	61.82	3.17	2002.0	1900.1	1.679
3.•	29	0.05	-	-	-	-	-	-
7.	29	0.20	2491.6	80.35	3.22	2557.8	2425.3	1.644
7.	29	0.5	2652.5	124.96	4.71	2755.6	2549.5	1.645

• No full compressive stress-strain plot recorded

TABLE 3.12

COMPRESSIVE INITIAL ELASTIC MODULUS SUMMARY

(Various Crosshead Speeds)

Specimen cut from sheet	Age (Days)	Cross-head speed in/min	Mean Initial Elastic Modulus $lbf/in^2 \times 10^{-6}$	Standard Deviation $lbf/in^2 \times 10^{-6}$	% Coeff. of Variation	Confidence Limits p = 0.1 $lbf/in^2 \times 10^{-6}$	
						Upper	Lower
3.	29	0.01	0.5487	0.088	16.04	0.6326	0.4649
7.	29	0.02	0.4573	0.0318	6.95	0.4835	0.4311
3.	29	0.05	0.4958	0.066	13.31	0.5503	0.4414
7.	29	0.20	0.5069	0.0438	8.64	0.5430	0.3707
7.	29	0.5	0.5578	0.0595	10.67	0.6069	0.5087

STRESS STRAIN RELATIONSHIP
FOR COMPOSITE MATRIX
AGE 29 DAYS
Crosshead Speed 0.02 in/min
Specimens 7.21, 7.23, 7.27,
7.32, 7.33, 7.34.
-COMPRESSIVE STRESS- LBF/IN2
-PERCENTAGE STRAIN-
NEWTON/MM2 X10-1

Fig. 3.32

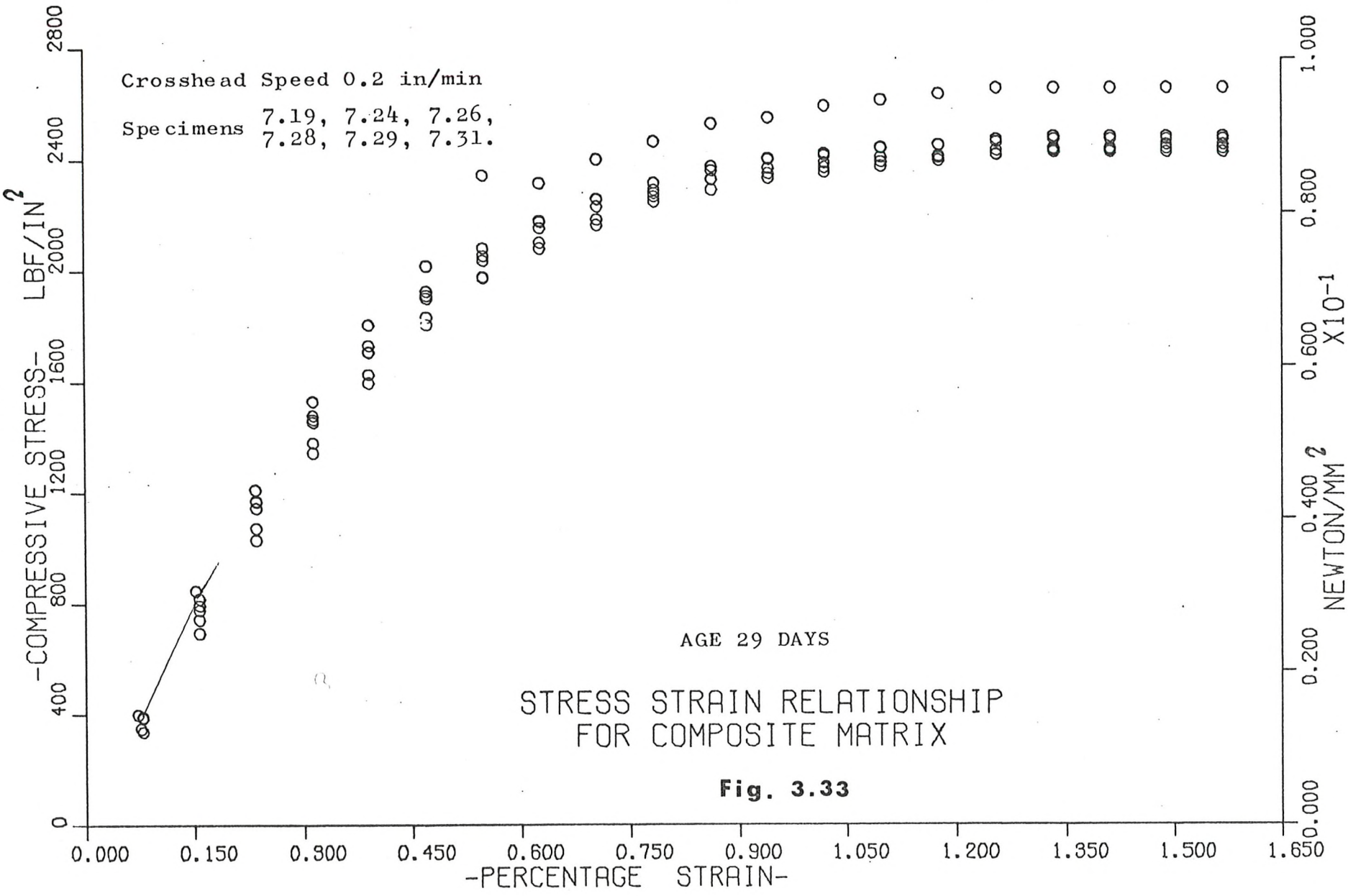
Crosshead Speed 0.2 in/min
Specimens 7.19, 7.24, 7.26, 7.28, 7.29, 7.31.
-COMPRESSIVE STRESS- LBF/IN2
NEWTON/MM2 X10-1
AGE 29 DAYS
STRESS STRAIN RELATIONSHIP FOR COMPOSITE MATRIX
-PERCENTAGE STRAIN-
0
400
800
1200
1600
2000
2400
2800
0.000
0.150
0.300
0.450
0.600
0.750
0.900
1.050
1.200
1.350
1.500
1.650
0.000
0.200
0.400
0.600
0.800
1.000

Fig. 3.33

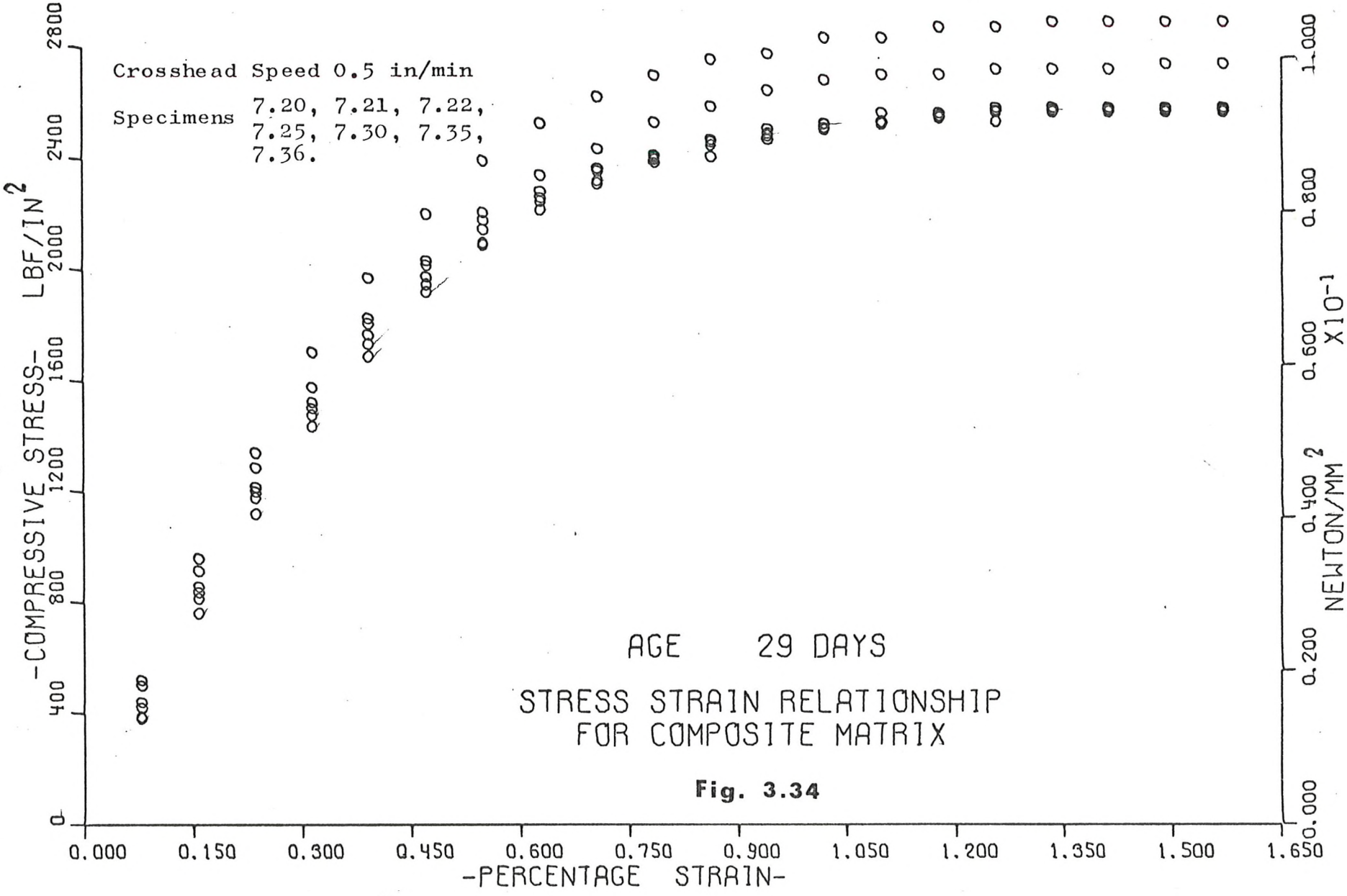
Crosshead Speed 0.5 in/min
Specimens 7.20, 7.21, 7.22, 7.25, 7.30, 7.35, 7.36.
-COMPRESSIVE STRESS- LBF/IN2
NEWTON/MM2 X10-1
-PERCENTAGE STRAIN-
0
400
800
1200
1600
2000
2400
2800
0.000
0.150
0.300
0.450
0.600
0.750
0.900
1.050
1.200
1.350
1.500
1.650
0.000
0.200
0.400
0.600
0.800
1.000
AGE 29 DAYS
STRESS STRAIN RELATIONSHIP
FOR COMPOSITE MATRIX

Fig. 3.34

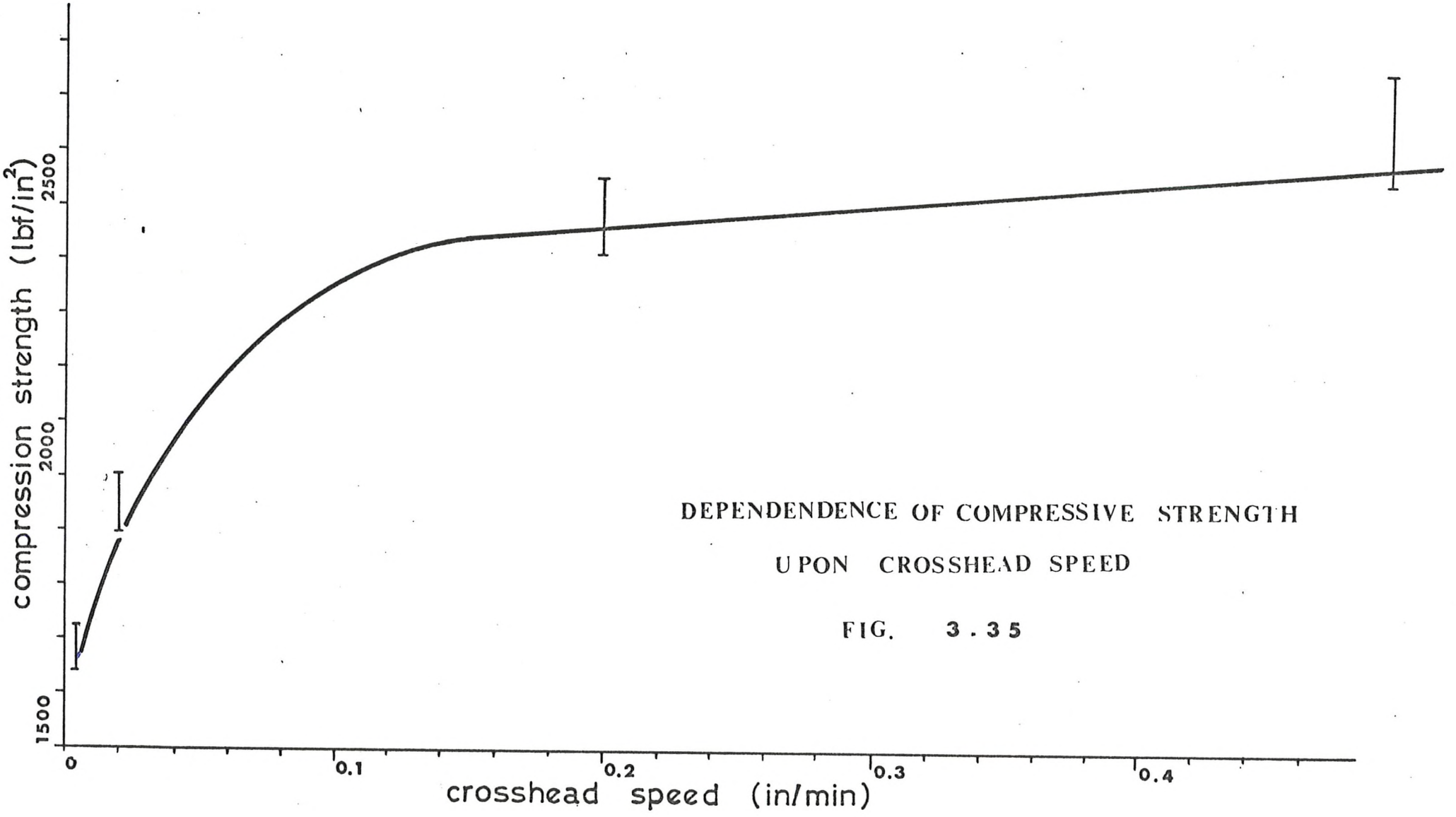

DEPENDENDENCE OF COMPRESSIVE STRENGTH

UPON CROSSHEAD SPEED

FIG. 3.35

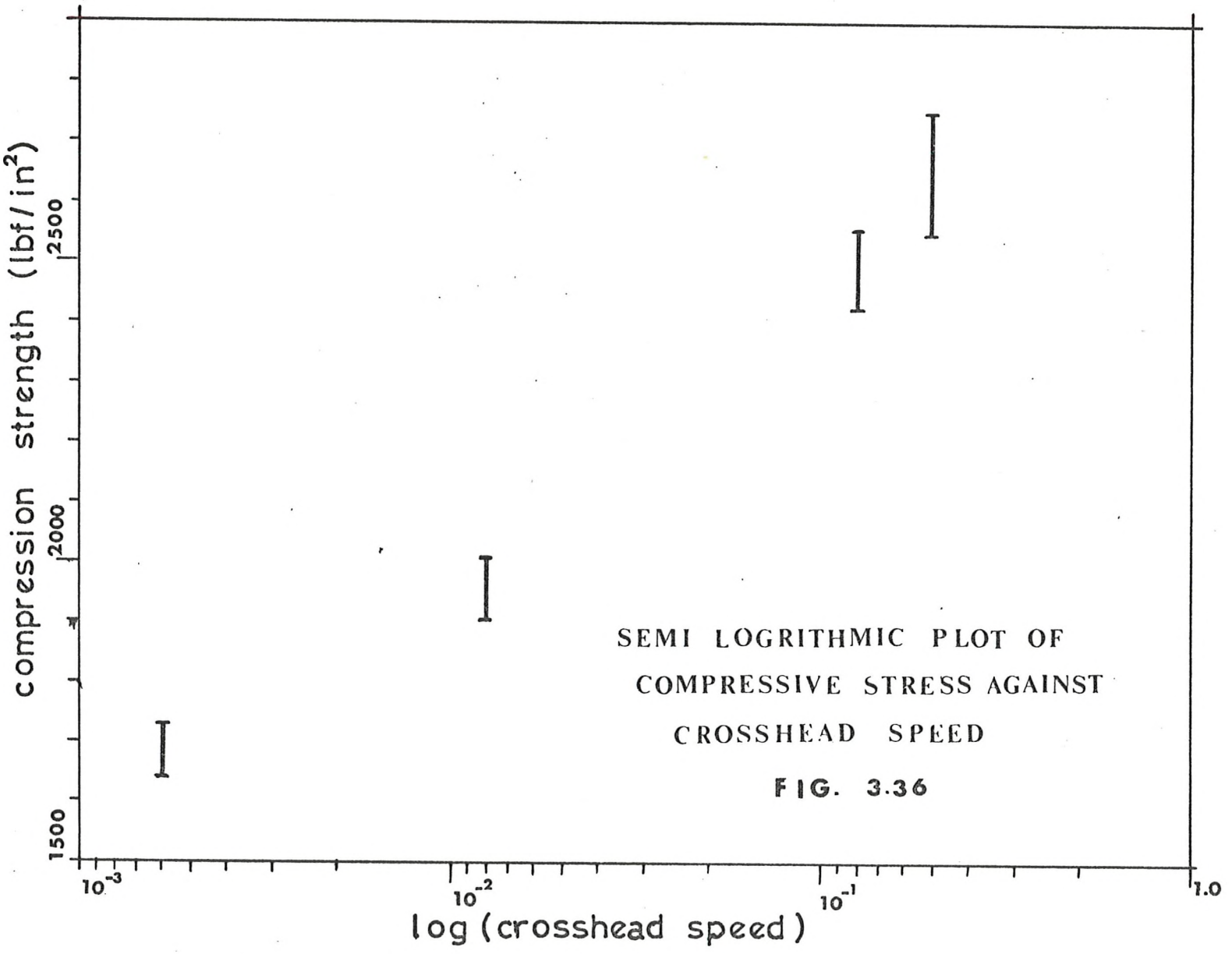

SEMI LOGRITHMIC PLOT OF COMPRESSIVE STRESS AGAINST CROSSHEAD SPEED

FIG. 3.36

3.5 Flexural Stress-Strain Investigation

3.5.1 The Experimental Method and Results

Flexural specimens selected were of the same dimensions and shape as the tensile specimens. Only two specimens were tested but the experimental method described here was used during the investigation of the reinforced material.

Plate 3.4 (bottom) shows the bending rig which was designed to give four point symmetrical loading. The top half of the rig was screwed into the moving crosshead of the Instron machine. Load was applied via four steel cylindrical rods positioned transversely in slots in the rig. The four rods were allowed to move freely in a vertical plane. The bottom portion of the rig was located by two dowel pins on the compression cell, thus ensuring central alignment. The distance between the rod centres was 10 inches and 6 inches.

Strain at the top and bottom faces of the beam was detected by foil strain gauges positioned at midspan (Fig. 3.37). Direct digital readings of strain were displayed on the static strain gauge indicator since it was fitted with a gauge factor adjustment. Simultaneously the applied load was

recorded on the Instron X-Y recorder (driven at a constant speed) and by using the blipping device it was possible to record the applied load and corresponding strain at the top and bottom faces of the beam. These readings are given in Tables 3.13 and 3.14.

Plate 3.4 (top) shows the assembled apparatus when placed in the Instron machine. If this photograph is read in conjunction with Fig. 3.37, the connection of the active and dummy strain gauges is quite clear.

The load for both flexural tests was applied at a constant speed of 0.005 in/min. and conducted in a constant environment of temperature 22^{o}C and 40 to 60% relative humidity.

Figs. 3.38 and 3.39 illustrate the applied load-strain graphs for the bending tests. It is seen that the strain developed in the tension face is greater than the strain at the compression face especially at elevated loads.

ASSEMBLED FLEXURAL APPARATUS

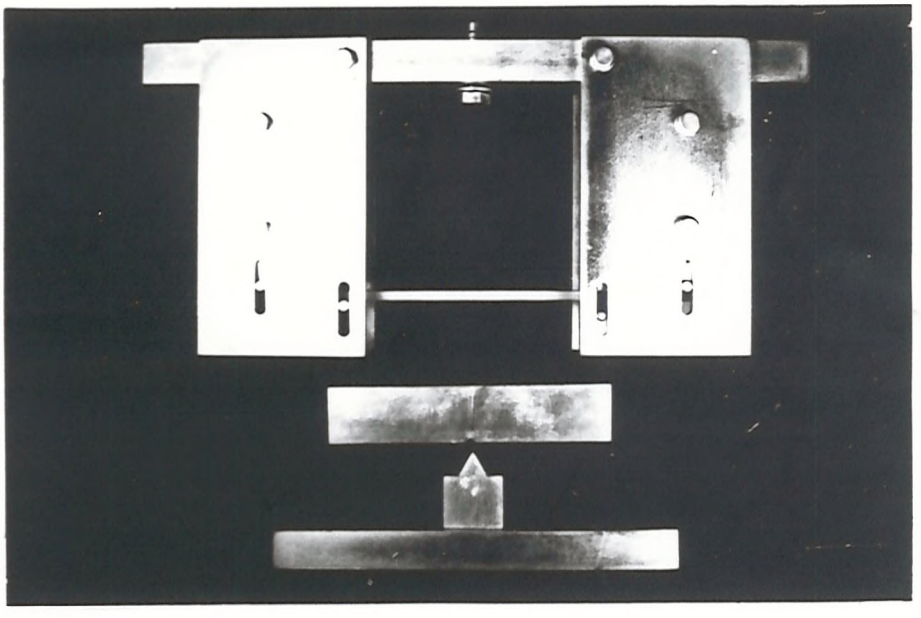

THE BENDING RIG

PLATE 3.4

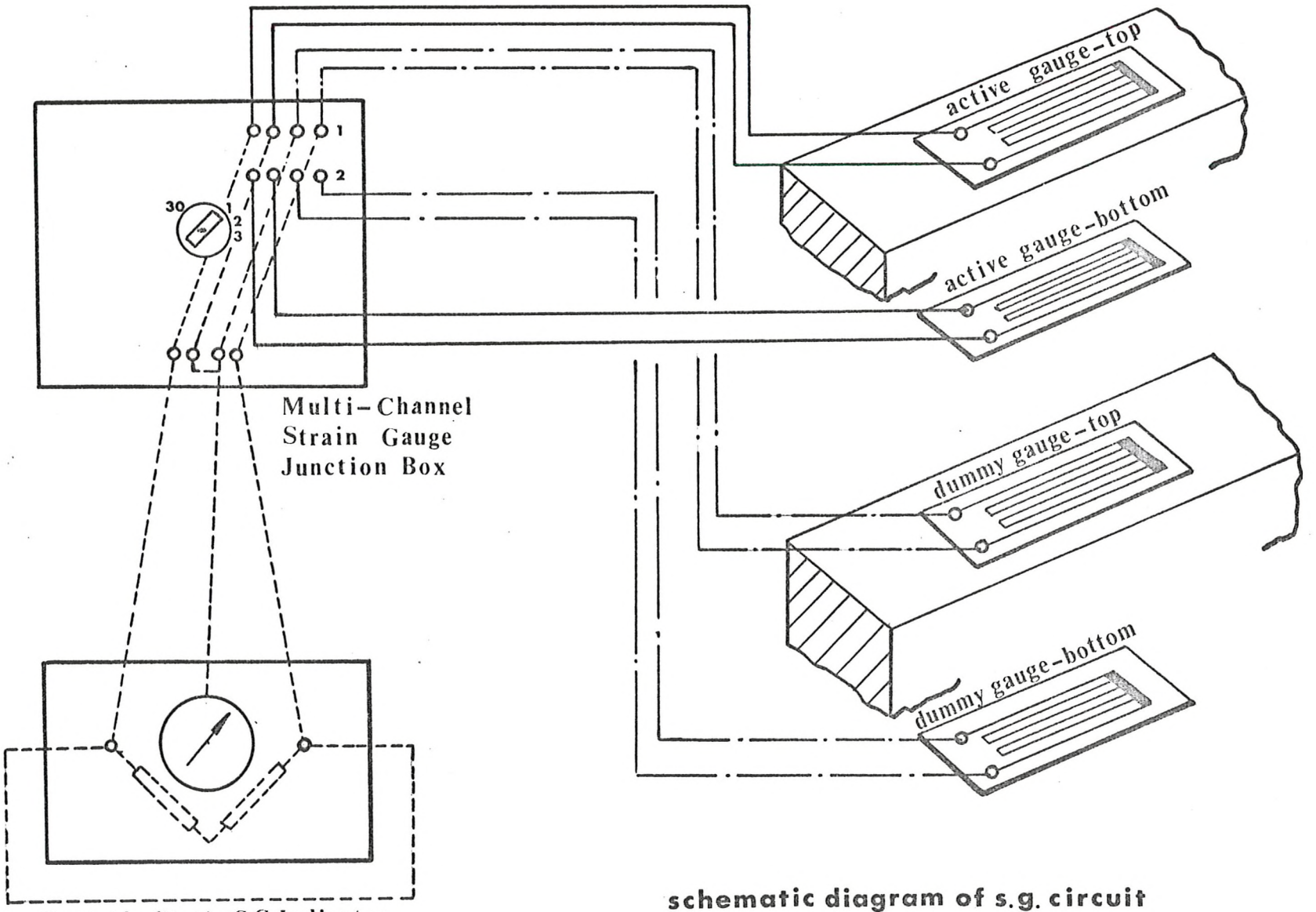

schematic diagram of s.g. circuit
-flexural experiment-
fig. 3.37

TABLE 3.13

FLEXURAL TEST (SPECIMEN 1.19)

No. of Load Points		4
Gauge Factor		2.16
Strain Gauge	G.L. ..	10 mm. 120 $\pm$ 0.3 Ω
	Type ..	Foil-Fla-10-11
Width		0.995 in.
Depth		0.250 in.
Crosshead Speed		0.005 in/min

Load lbf.	TENSION FACE Strain x 10^3	COMPRESSION FACE Strain x 10^3
0.34	0.038	0.048
0.74	0.093	0.113
1.14	0.148	0.169
1.54	0.203	0.226
1.94	0.268	0.285
2.34	0.322	0.345
2.74	0.381	0.398
3.14	0.455	0.470
3.54	0.522	0.522
4.64	0.725	0.725
5.64	0.923	0.885
6.64	1.153	1.080
7.64	1.438	1.295
8.64	1.758	1.535
9.44	2.048	1.695
10.44	2.528	2.020
11.54	3.588	2.540
11.94	4.368	2.915

TABLE 3.14

FLEXURAL TEST (SPECIMEN 1.20)

No. of Load Points		4
Gauge Factor		2.16
Strain Gauge	G.L. ..	10 mm. $120 \pm 0.3\Omega$
	Type ..	Foil-Fla-10-11
Width		1.001 in
Depth		0.241 in
Crosshead Speed		0.005 in/min

Load lbf	TENSION FACE	COMPRESSION FACE
	Strain x 10^3	Strain x 10^3
0.36	0.054	0.050
0.76	0.110	0.121
1.16	0.172	0.180
1.56	0.230	0.247
1.96	0.290	0.310
2.36	0.352	0.375
2.76	0.424	0.435
3.16	0.491	0.510
3.56	0.568	0.572
4.56	0.795	0.740
5.56	0.980	0.930
6.56	1.270	1.137
7.56	1.550	1.323
8.56	1.950	1.600
9.56	2.400	1.895

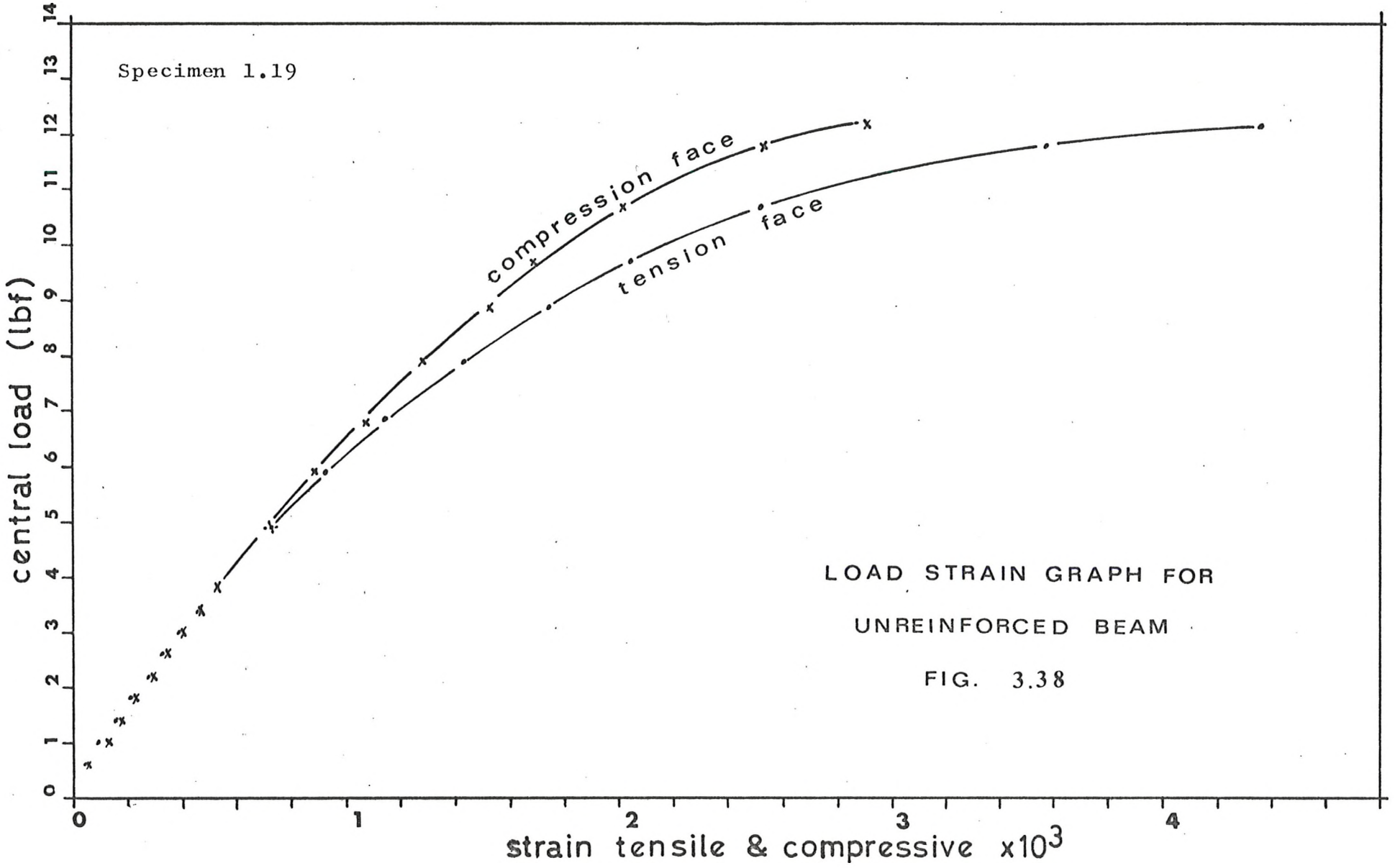

LOAD STRAIN GRAPH FOR

UNREINFORCED BEAM

FIG. 3.38

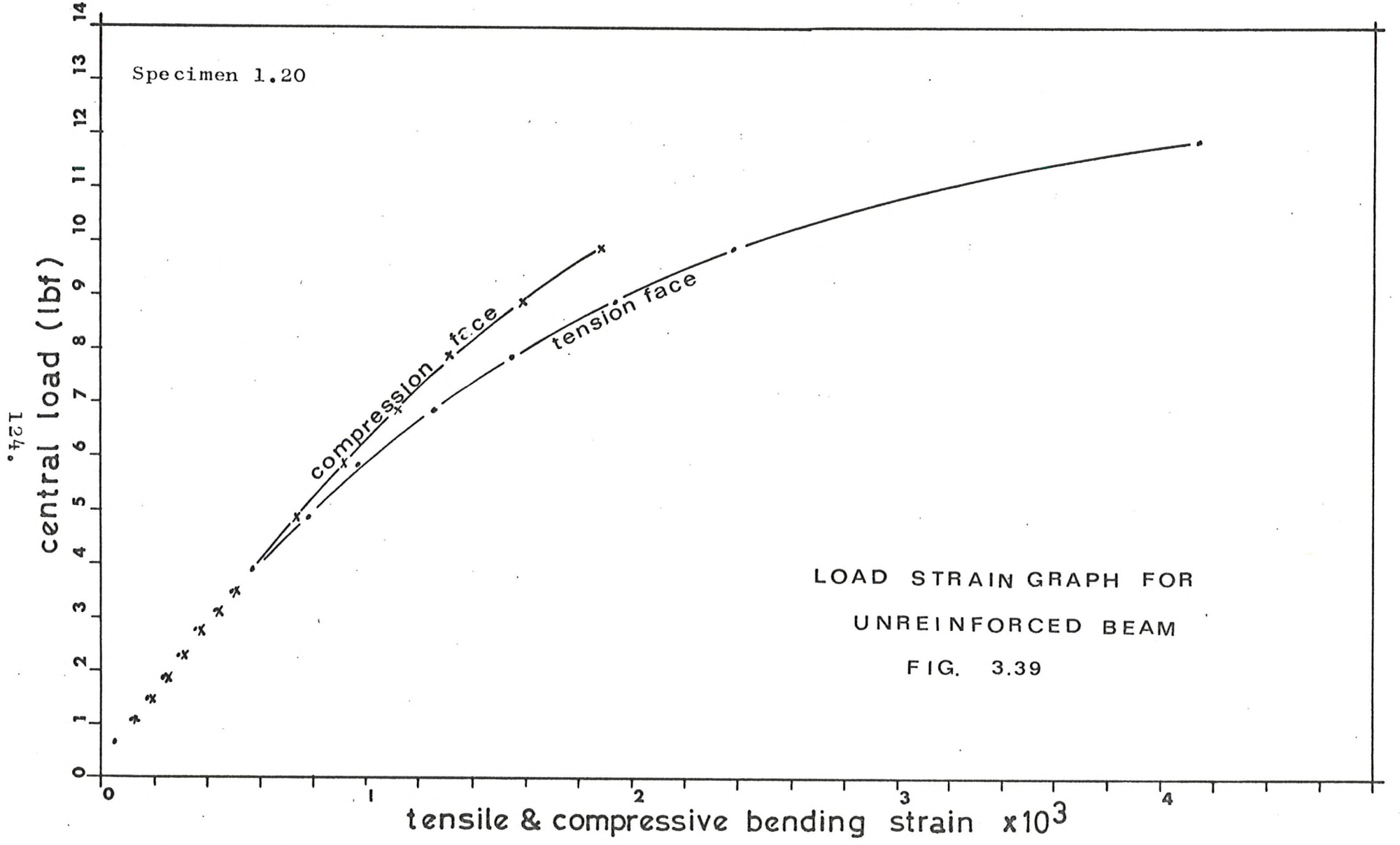

LOAD STRAIN GRAPH FOR
UNREINFORCED BEAM
FIG. 3.39

3.6 Shrinkage of Unreinforced Polymer-Cement

To examine the shrinkage, five unreinforced polymer cement specimens were prepared. The shape of the specimens was identical with that of the specimens used in the creep investigations (Sec. 3.7). Shrinkage strains were detected by using a Demec extensometer. The two Demec markers were attached to one surface of each specimen using strain gauge glue. The alignment of the markers was coincident with the centre line of the specimen and spanned their length symmetrically. The Demec gauge displayed direct readings of shrinkage strain upon a dial gauge where 1 division was equivalent to 0.99×10^{-5} strain. These strains (Table 3.15) were recorded over a period of 122 days (approximately 10.5×10^{6} s.). A linear regression estimate of the shrinkage was made over the period 6 to 122 days using the least squares method (Appendix A) and was found to be 17.8×10^{-12} strain/s. Data of shrinkage are illustrated graphically in Fig. 3.40 and the linear regression estimate is shown upon it.

All the specimens used for shrinkage tests were stored vertically at a constant temperature of $22^{\circ}C$ and relative humidity of 40-60%.

TABLE 3.15

SHRINKAGE OF UNREINFORCED POLYMER CEMENT

AGE (DAYS)	TOTAL SHRINKAGE STRAIN X 10^3				
	EX 1	EX 2	EX 3	EX 4	EX 5
1	0.457	0.480	0.248	0.450	0.495
2	0.644	0.576	0.575	0.826	0.684
3	0.744	0.577	0.754	0.685	0.762
4	1.176	0.837	1.822	1.762	1.911
5	1.839	1.817	1.822	1.796	1.990
6	1.841	1.802	1.871	1.891	1.888
8	1.837	1.919	1.937	1.950	1.980
10	1.901	1.941	1.870	1.901	1.931
12	1.832	1.837	1.788	1.851	1.911
13	1.982	1.911	1.857	1.911	1.866
14	1.965	1.907	1.916	1.886	1.988
19	1.940	1.990	2.010	1.965	2.030
30	1.957	1.982	2.021	1.969	2.038
48	2.000	1.990	1.980	2.010	2.045
64	2.030	2.030	2.000	1.970	2.109
74	1.980	1.980	1.921	1.940	1.990
76	2.178	2.070	2.168	2.039	2.099
79	2.049	1.960	1.990	1.901	1.990
81	2.039	1.960	2.000	1.990	2.059
89	2.049	2.030	1.980	1.970	2.109
90	2.039	2.049	2.020	1.980	2.069
114	2.129	2.109	2.039	2.059	2.228
122	2.070	2.039	2.020	1.990	2.139

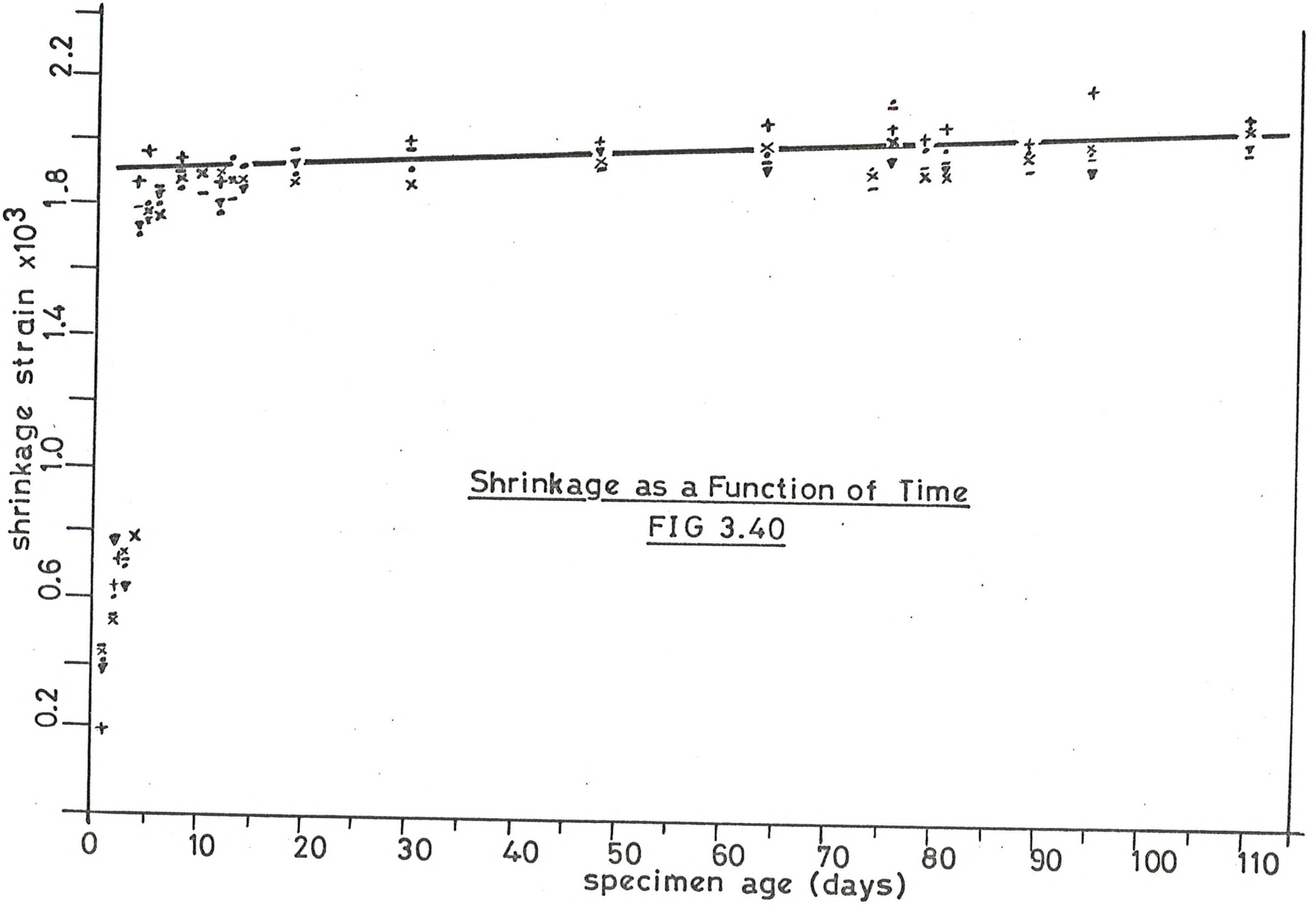

Shrinkage as a Function of Time

FIG 3.40

3.7 The Investigation of Long Term Creep

3.7.1 The Experiment

Unreinforced creep specimens were dumb-bell in shape, cut from the cement boards as indicated in Fig. 3.2. The dimensions of the creep specimen are shown in Fig. 3.43 and this was prepared as described in Appendix C (Sec. C2).

The long term creep investigation was carried out in the machine shown in Fig. 3.41. Here the specimens were hung in pairs coupled to the machine and the dead load by clamps (Fig. 3.42). The weights which were suspended at the end of the specimen and underneath the machine imposed stresses at various levels upon the specimen ranging from 52.5 lbf/in^2 to 252 lbf/in^2. Plate 3.5 (bottom) shows the creep specimens assembled in the machine.

The extension of the specimen was detected by a mechanical extensometer (10 in. gauge length) in which was mounted a dial gauge extensometer (each division indicating 0.001 in.) (Plate 3.5, top).

Stress was applied gradually to the specimen by removing the dead load support. Time was considered zero when the full load was applied so extensions were recorded before and at the end of this operation to yield the instantaneous strain. Creep readings for the unreinforced material were recorded up to 33 603 600 s.

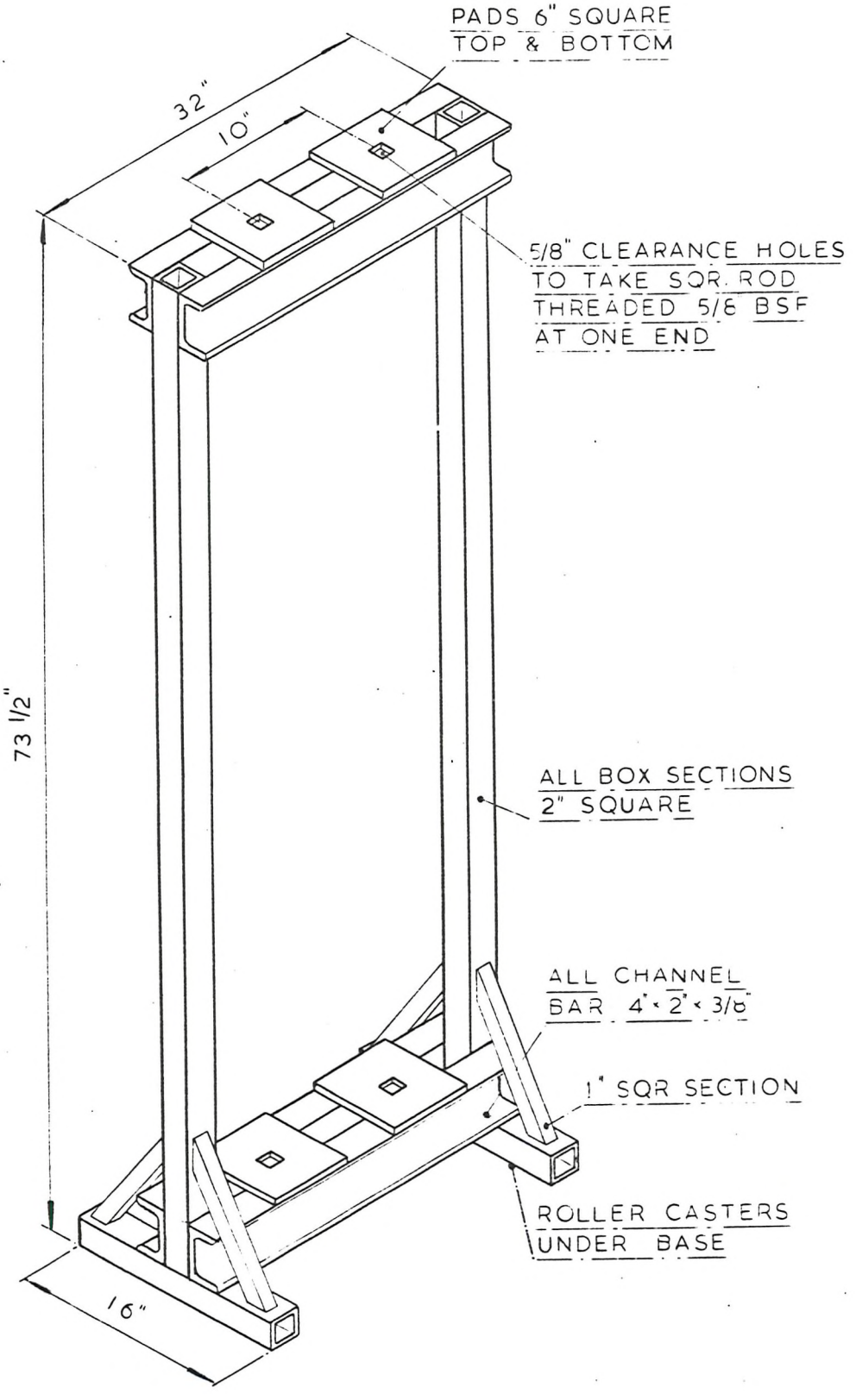

THE CREEP MACHINE

FIGURE **3.41**

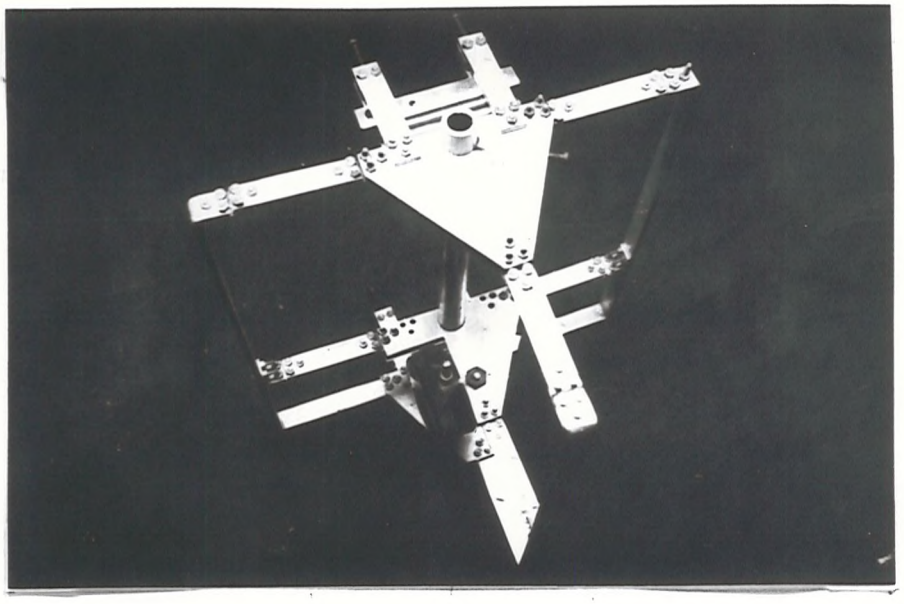

CREEP SPECIMEN EXTENSOMETER

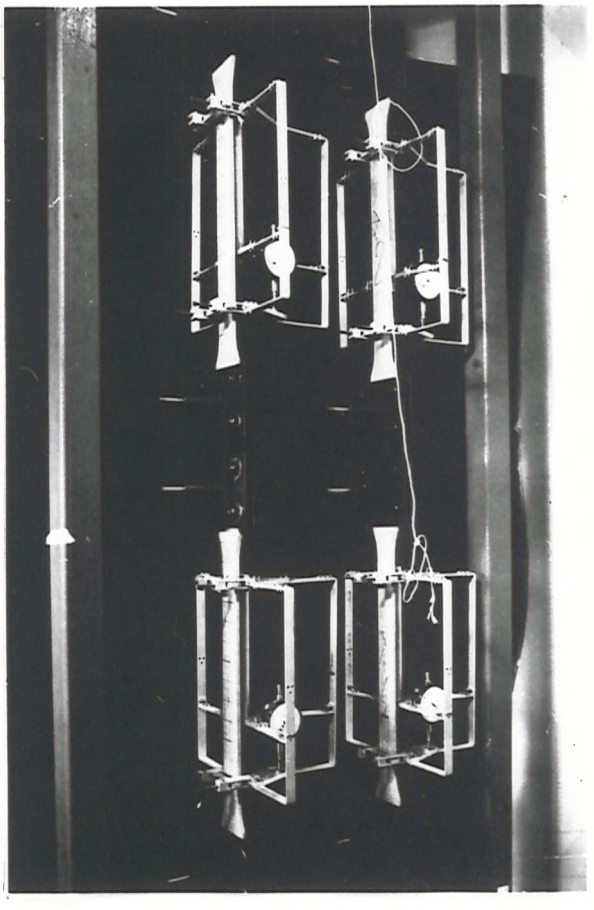

CREEP SPECIMENS ASSEMBLED IN MACHINES

PLATE 3.5

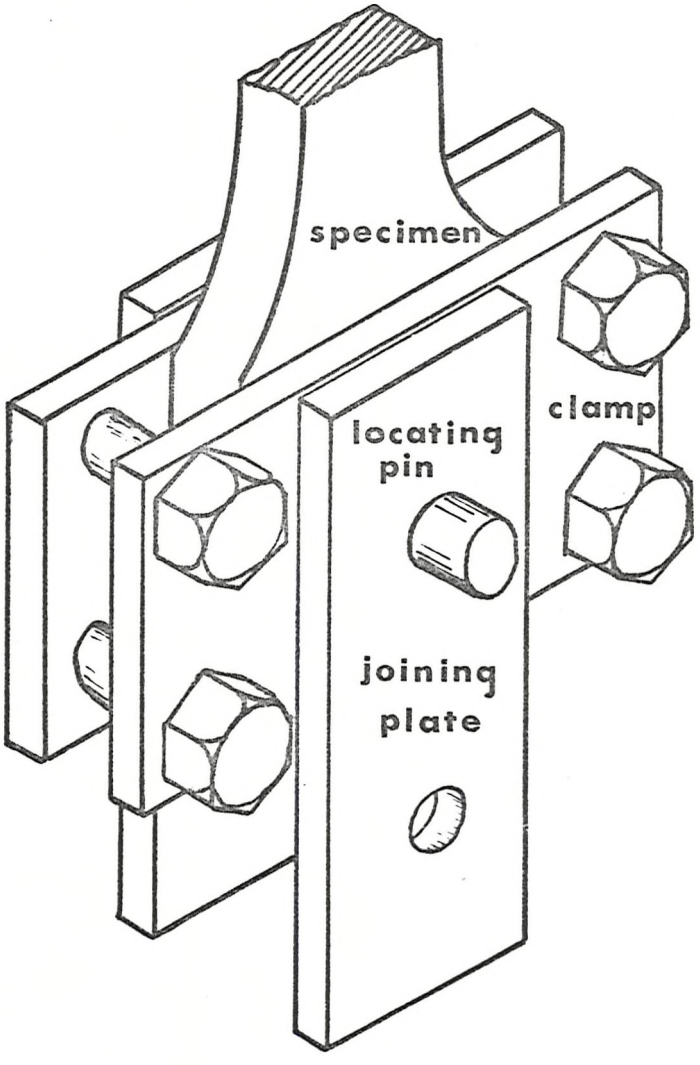

Clamping device for creep specimen
FIG 3.42

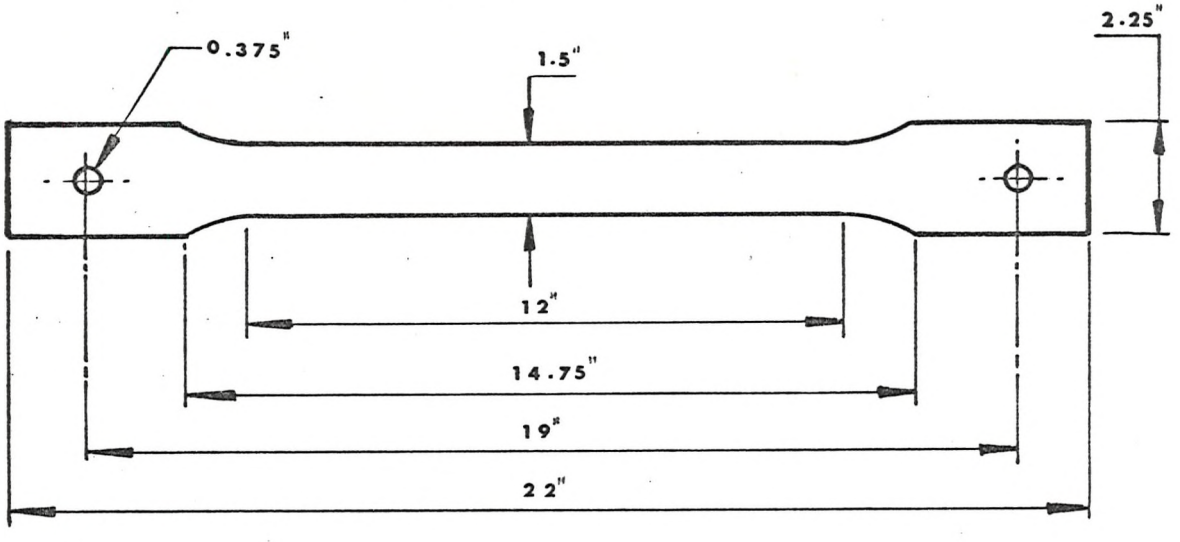

creep specimen
FIG 3.43

3.7.2 Results of the Creep Experiment

Recorded and calculated results of the creep experiments are given in Appendix G. (Table G4).

The unreinforced polymer cement specimens were subjected to constant stresses ranging from 65 lbf/in^2 (Specimen 1.1) to 265 lbf/in^2 (Specimen 2.2). By comparing the tensile strengths of specimens cut from the same sheets (Table 3.16) the above stresses correspond to stress levels of 11 % to 45 %. The maximum duration of the experiments was 34×10^6 s. (Table 3.17).

Fig. 3.44 shows the total strain of the polymer-cement at the various stress levels as a function time and illustrates the inelastic behaviour of the material. Fig. 3.45 is the same graph but shows the creep data up to 14×10^6 s.

It is assumed that the creep curves reach a steady rate of creep by 10×10^6 s ; these rates were estimated using the method of least squares (Sec. A2.1) within the range of times 14×10^6 to 10×10^6 s. This yielded the secondary creep strain (ε_2) and secondary creep strain/unit stress (secondary creep compliance - J_2).

It was not possible to record the exact instantaneous deformation of the specimens upon loading. A fairly accurate estimate of this

instantaneous extension was made in the following manner.

If it is assumed that the recorded value of strain at 10s. is approximately equal to the instantaneous strain it is then possible to make an initial estimate of the primary creep strain (ε_1). This was done by subtracting the secondary creep strain (ε_2) and the estimated instantaneous strain (ε_o) from the total strain (ε_t).

Then $\varepsilon_1 = \varepsilon_t - \varepsilon_o - \varepsilon_2$

which are the components of the deformation curve suggested by Pao and Marin[35] (Fig. 3.50).

When plotting the log (estimated ε_1) against log (time) a linear relationship is given at large times (Fig. 3.46). Deviation from the straight line occurs at small times and this is brought about by the error in the estimated instantaneous strain. By extrapolation of the straight line at large times a closer estimate of the instantaneous strain may be made. If this procedure is repeated two or three times a reasonable degree of accuracy in estimating the instantaneous strain results.

Table 3.17 lists the various stress levels for the creep investigation, together with the creep duration. Also given in this table are the total strains for times 0, 10, 100 and 1000s. and the applied stresses. This results in the isochronous curves of Figs. 3.47, 3.48 and 3.49 which indicate the non linear nature of the polymer cement. The curves shown on these figures merely represent their general character and should not be interpreted further.

TABLE 3.16

TENSILE CONTROL CREEP SPECIMEN

Spec. No.	Mean dimensions (inch)		Specimen Weight (g)	Ultimate Stress lbf/in^2
	Width	Thick.		
1.7	0.947	0.237	71.45	562
1.8	0.995	0.246	73.57	574
1.9	0.991	0.250	75.13	571
1.10	1.001	0.255	76.32	563
				567.5 (Mean)
2.8	0.991	0.244	73.25	575
2.9	0.999	0.236	73.44	573
2.10	0.993	0.256	75.47	512
2.11	0.990	0.257	76.13	570
				557.5 (Mean)

Total Specimen Length: 11.2 inch

TABLE 3.17

INSTANTANEOUS CREEP DATA

Spec. No.	Notation	Static Stress lbf/in^2	% Stress Level	Total Strain x 10^3				Min. Creep Rate ($\dot{e} \times 10^{12}$) strain/s	Creep Duration (seconds)	$E_i \times 10^6$ lbf/in^2
				t = 0s	t = 10s	t = 100s	t = 1000s			
1.1	●	65.0	11.44	0.1	0.21	0.239	0.24	6.49	33522900	0.65
1.2	×	97.3	14.35	0.113	0.2	0.217	0.233	10.77	33522900	0.732
2.6	⊙	115.8	20.0	0.125	0.19	0.23	0.27	13.04	33603600	0.926
2.7	●	146.5	25.45	0.15	0.2	0.21	0.27	26.8	33603600	0.977
2.4ψ	◢	176.0	30.6	0.144	0.32	0.35	0.41	29.5 s	716220	0.994
1.3†	△	200.0	35.2	0.232	0.37	0.43	0.49	54.67	17532000	0.862
2.3†	◇	206.0	35.8	0.202	0.48	0.50	0.62	40.0 s	716220	1.02
2.1ψ	▽	229.0	39.8	0.250	0.47	0.49	0.55	50.0 s	8100	0.916
1.4ψ	⊡	230.0	40.5	0.250	0.45	0.50	0.55	38.51	17532000	0.92
2.2†	+	256.0	44.5	0.274	0.67	0.76	0.88	64.0 s	8100	0.967

† Specimen Failed

ψ Termination due to parent specimen failure

s Estimate

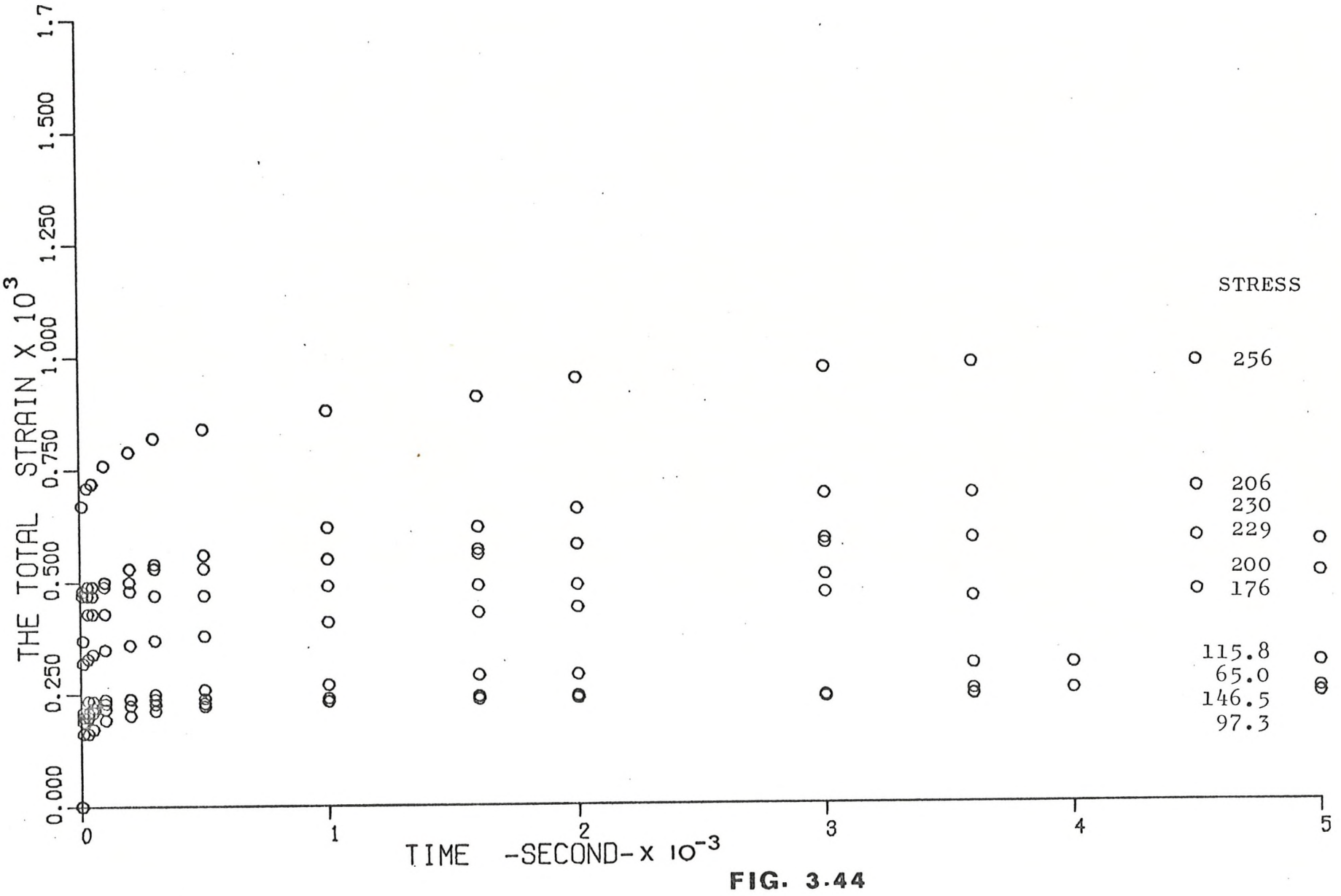

FIG. 3.44

CREEP CURVES FOR POLYMER-CEMENT

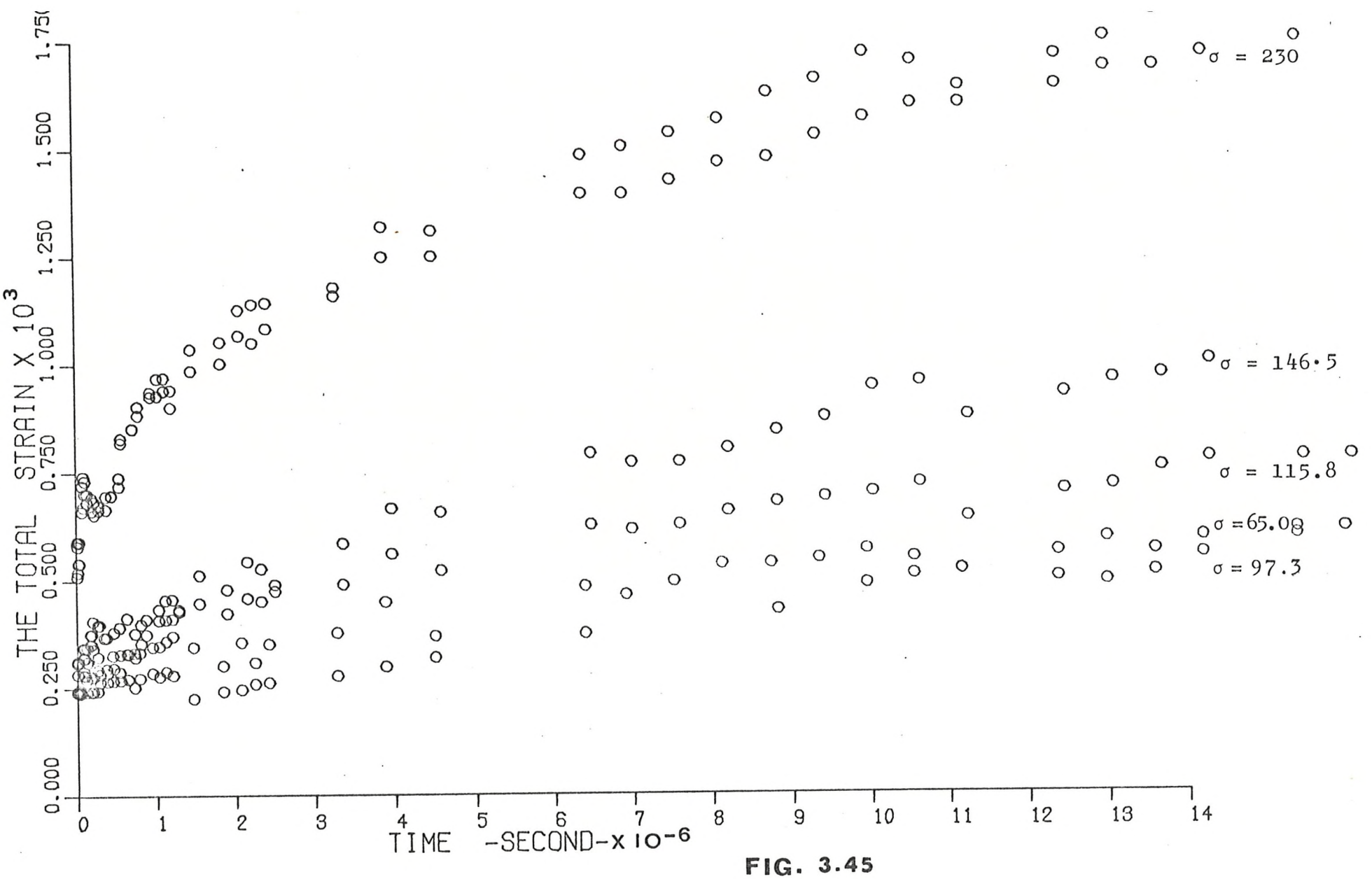

FIG. 3.45

CREEP CURVES FOR POLYMER-CEMENT

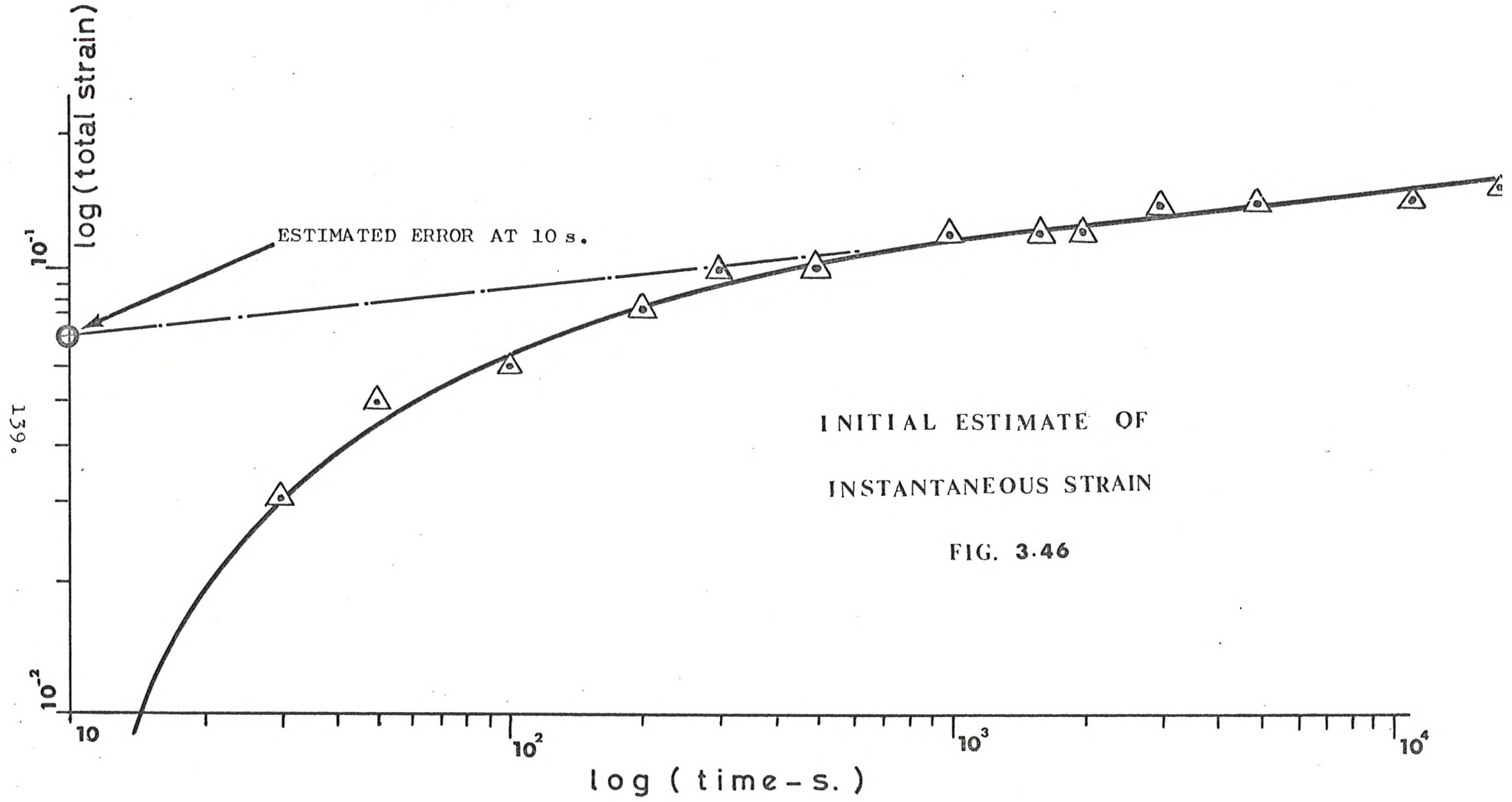

INITIAL ESTIMATE OF

INSTANTANEOUS STRAIN

FIG. 3.46

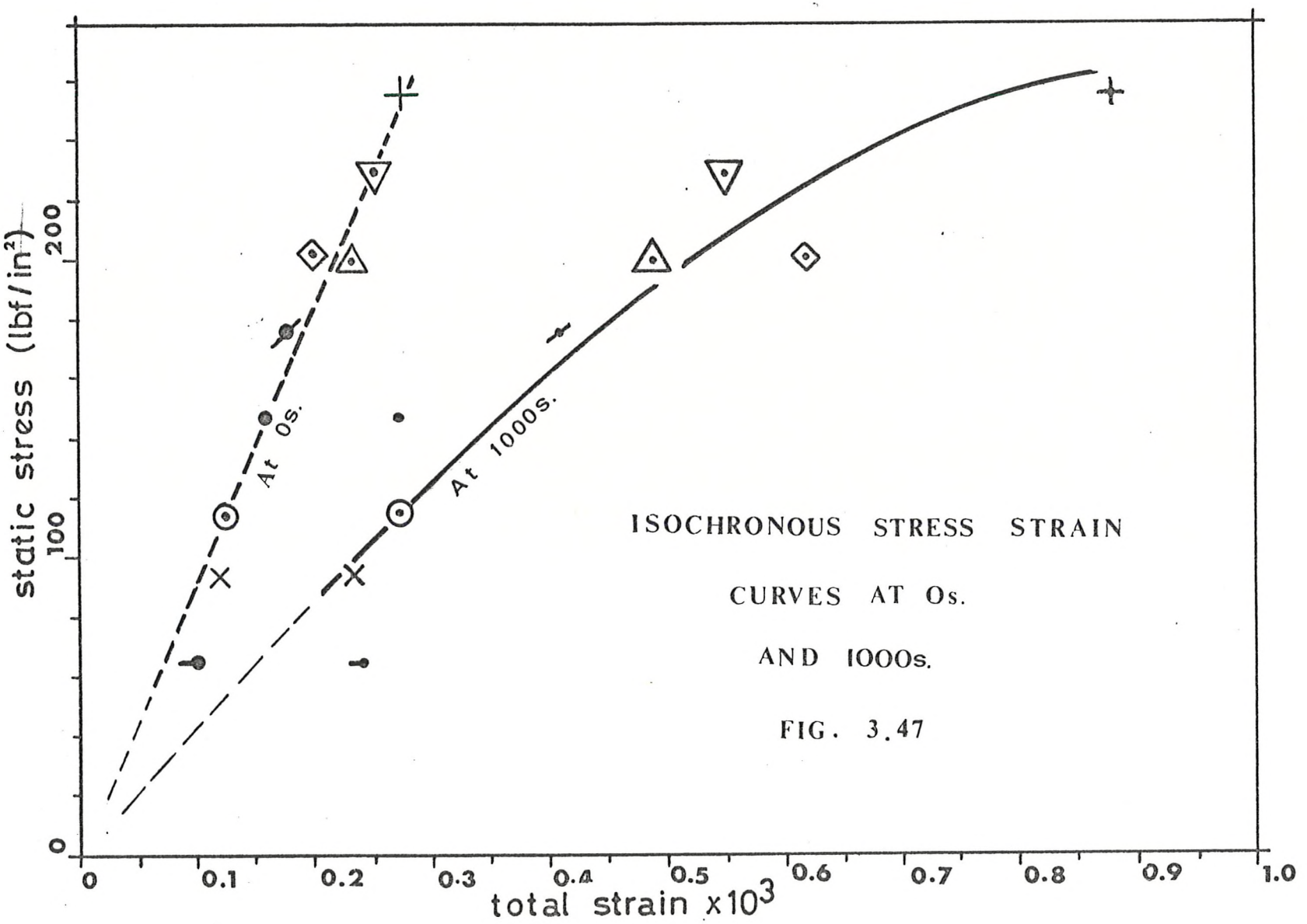

ISOCHRONOUS STRESS STRAIN

CURVES AT Os.

AND 1000s.

FIG. 3.47

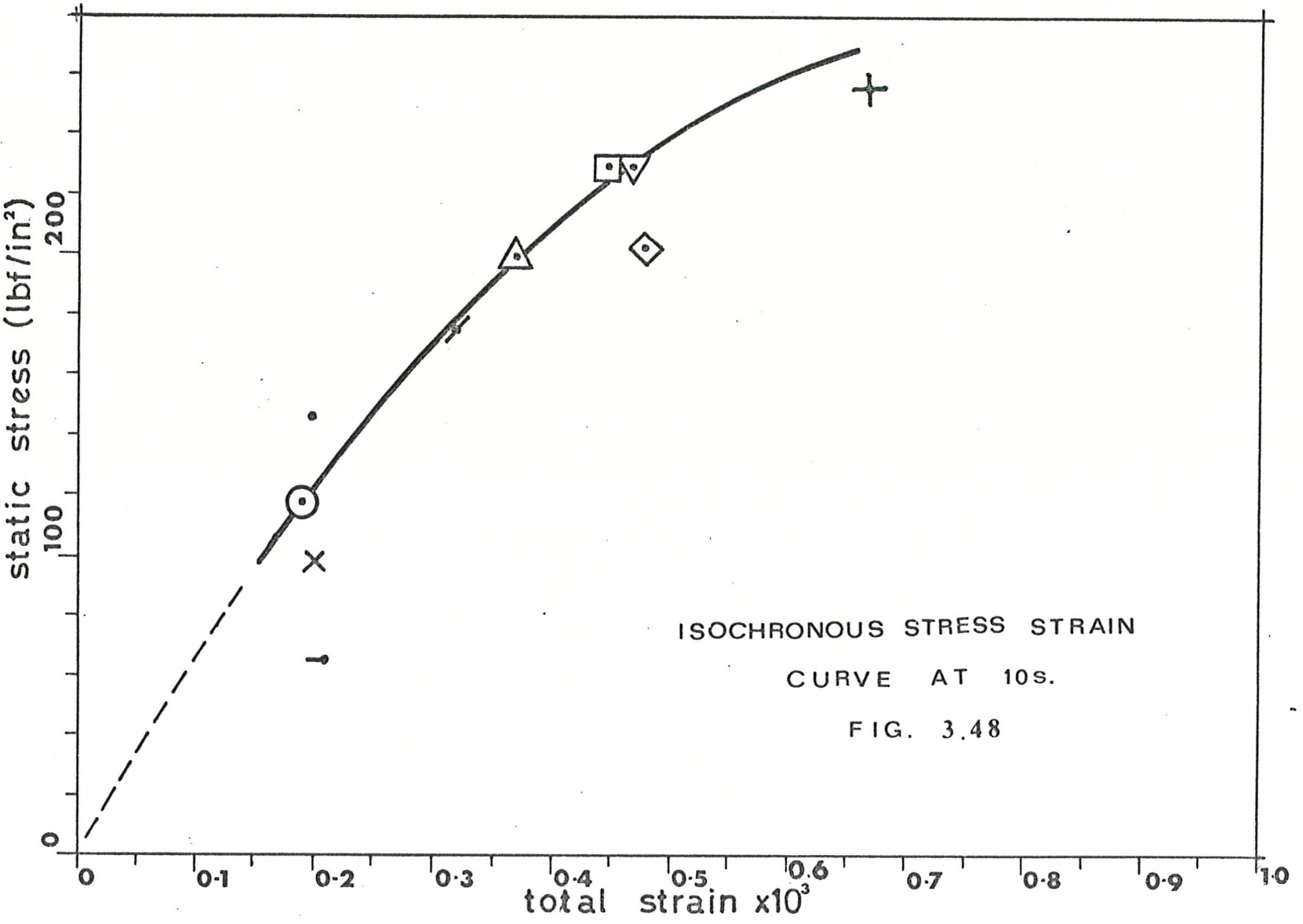

ISOCHRONOUS STRESS STRAIN CURVE AT 10s.

FIG. 3.48

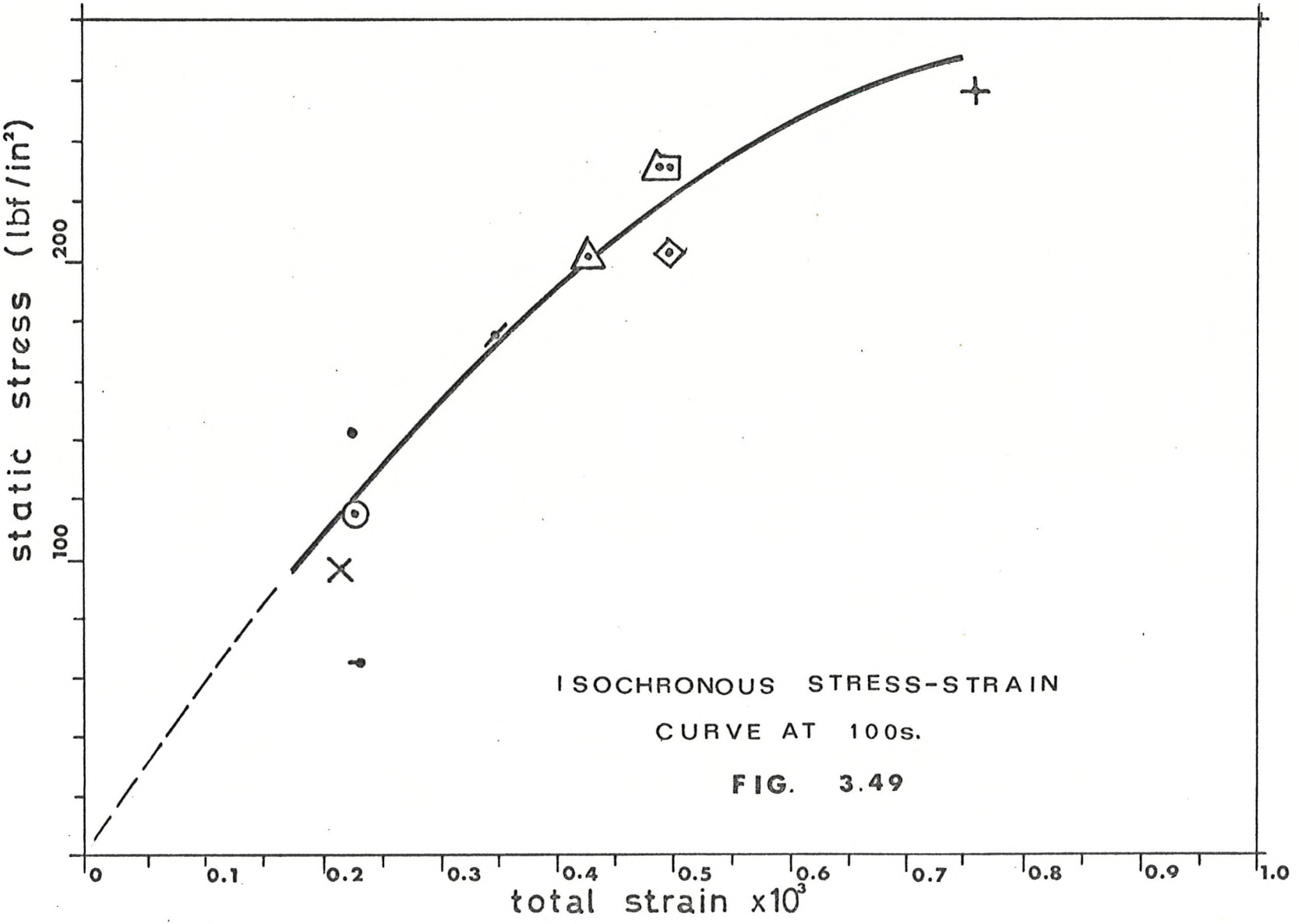

ISOCHRONOUS STRESS-STRAIN CURVE AT 100s.

FIG. 3.49

3.7.3 Analysis of Creep Data

Following Pao and Marin[35] the creep curves for the polymer-cement were reduced to three components of strain (Fig. 3.50)

I) Elastic strain (ε_o), which is proportional to the applied stress.

II) Transient creep strain or primary creep (ε_1)

III) Secondary creep strain shown as a linear function of time (ε_2)

The total creep strain ε_t is given by:

$$\varepsilon_o + \varepsilon_1 + \varepsilon_2 \qquad \ldots 3.3$$

These three components were analysed in the following manner:

Elastic Strain (ε_o)

This is defined as

$$\varepsilon_o = \frac{\sigma_i}{E_o} \qquad \ldots 3.4$$

where σ_i is the applied constant stress at the i^{th} level.

E_o the corresponding initial elastic modulus

Primary Creep (ε_1)

Primary creep strainswere obtained in the manner described in Section 3.7.2.

When plotting the log (primary creep compliance) $\frac{\varepsilon_{1i}}{\sigma_i}$ against the $\log_{10}$ (time) a family of straight lines was assumed (Fig. 3.51).

This yields the relationship between stress, strain and time

$$\frac{\varepsilon_{1i}}{\sigma_i} = A_i \; t^{B_i} \qquad \ldots 3.5$$

where B_i is the slope of each line

and A_i constant compliance value given

at t = 1s. for each line

The slopes of the straight lines of Fig. 3.51 were then plotted against their corresponding stresses. This indicated a linear relationship (Fig. 3.52) of the form:

$$\sigma_i = k\, B_i ,$$

where k is a linear regression estimate (equal to 2620) and B_i is as before.

By substitution, equation 3.5 gives

$$\varepsilon_{1i} = \sigma_i \, A_i \, t^{\left\{\frac{\sigma_i}{2620}\right\}} \qquad \ldots 3.6$$

Secondary Creep Strain (ε_2)

A linear relationship was assumed to exist between the secondary creep strain and time

$$\therefore \quad \varepsilon_{2i} = \dot{e}_i t \qquad \ldots\ 3.7$$

where $\dot{e}_i$ is the minimum creep rate for the i^{th} stress level.

Fig. 3.54 is the log plot of Fig. 3.53 i.e. log (σ_i) against log ($\dot{e}_i$), thus the graph obeys the law

$$\sigma_i = C \dot{e}_i^{D}$$

where C and D are constants computed to be (16.275×10^{-6}) and 0.48107 respectively. Hence by substitution into equation 3.7, the secondary creep strain (ε_2) at the i^{th} level of stress (σ_i)

$$\varepsilon_{2i} = t \left[\frac{\sigma_i \times 10^{-6}}{16.275} \right]^{2.0793} \qquad \ldots\ 3.8$$

By combining equations 3.4, 3.6 and 3.8 the total strain is given by

$$\varepsilon_t = \varepsilon_o + \varepsilon_1 + \varepsilon_2$$

$$= \frac{\sigma_i}{E_o} + \sigma_i A_i t^{\left\{\frac{\sigma_i}{2620}\right\}} + t\left[\frac{\sigma_i \times 10^{-6}}{16.275}\right]^{2.0793}$$

$$\ldots\ 3.9$$

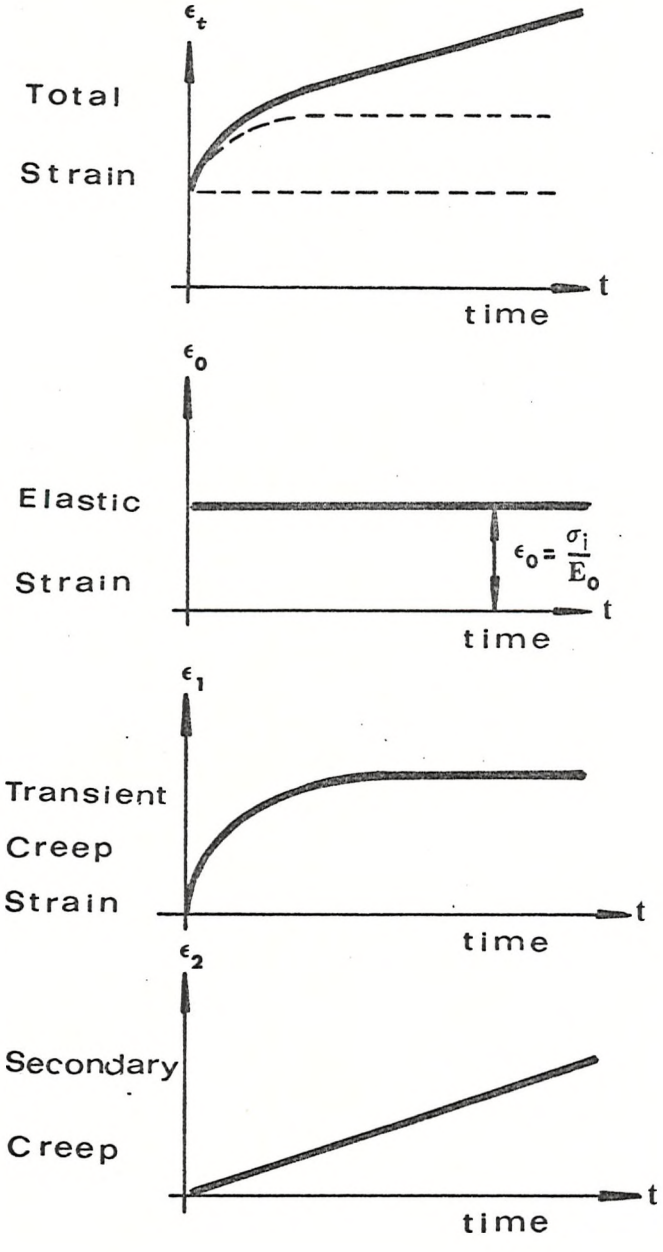

COMPONENTS OF CREEP STRAIN

FIG. 3.50

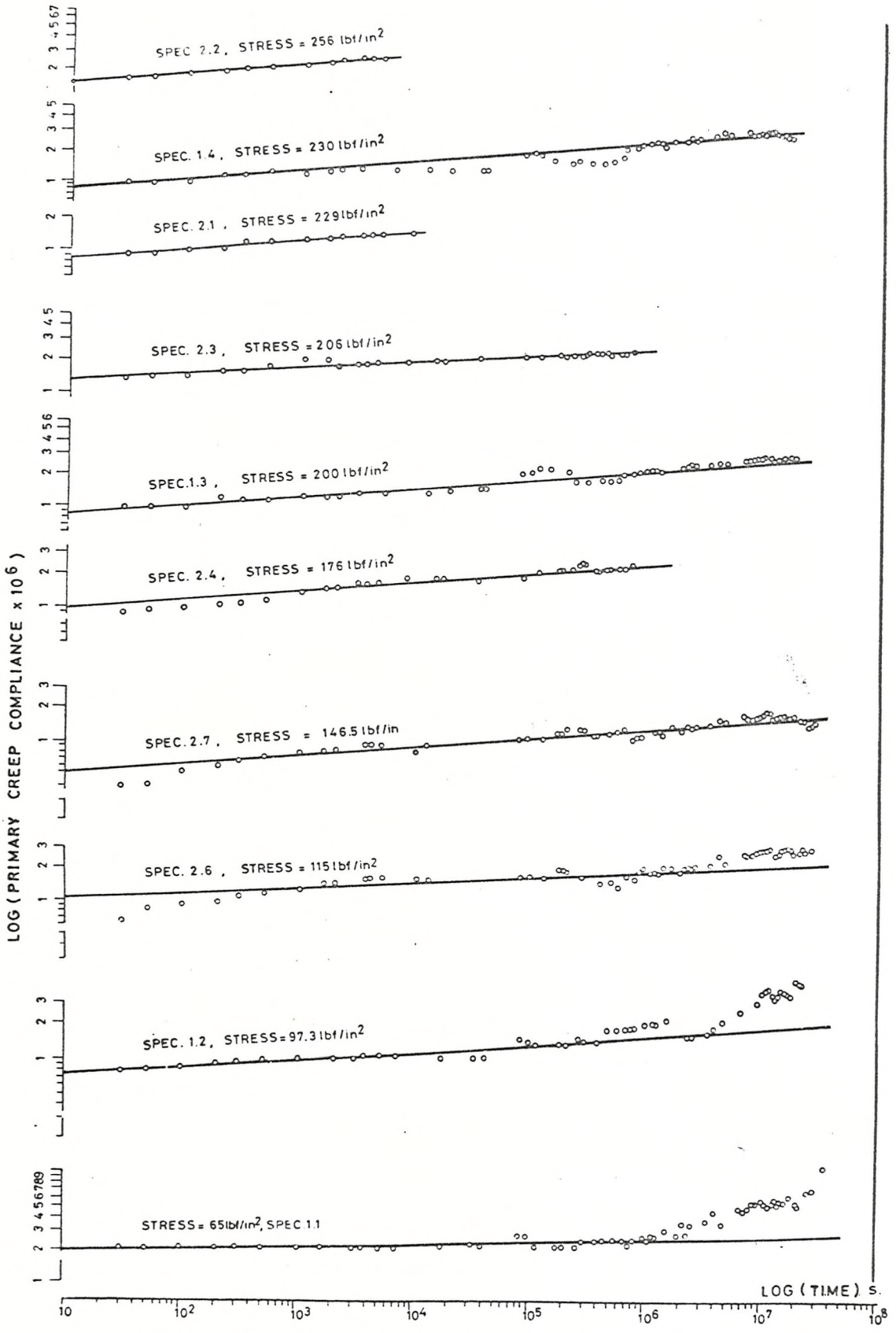

LOG-LOG RELATIONSHIP BETWEEN PRIMARY CREEP COMPLIANCE AND TIME

FIG. 3.51

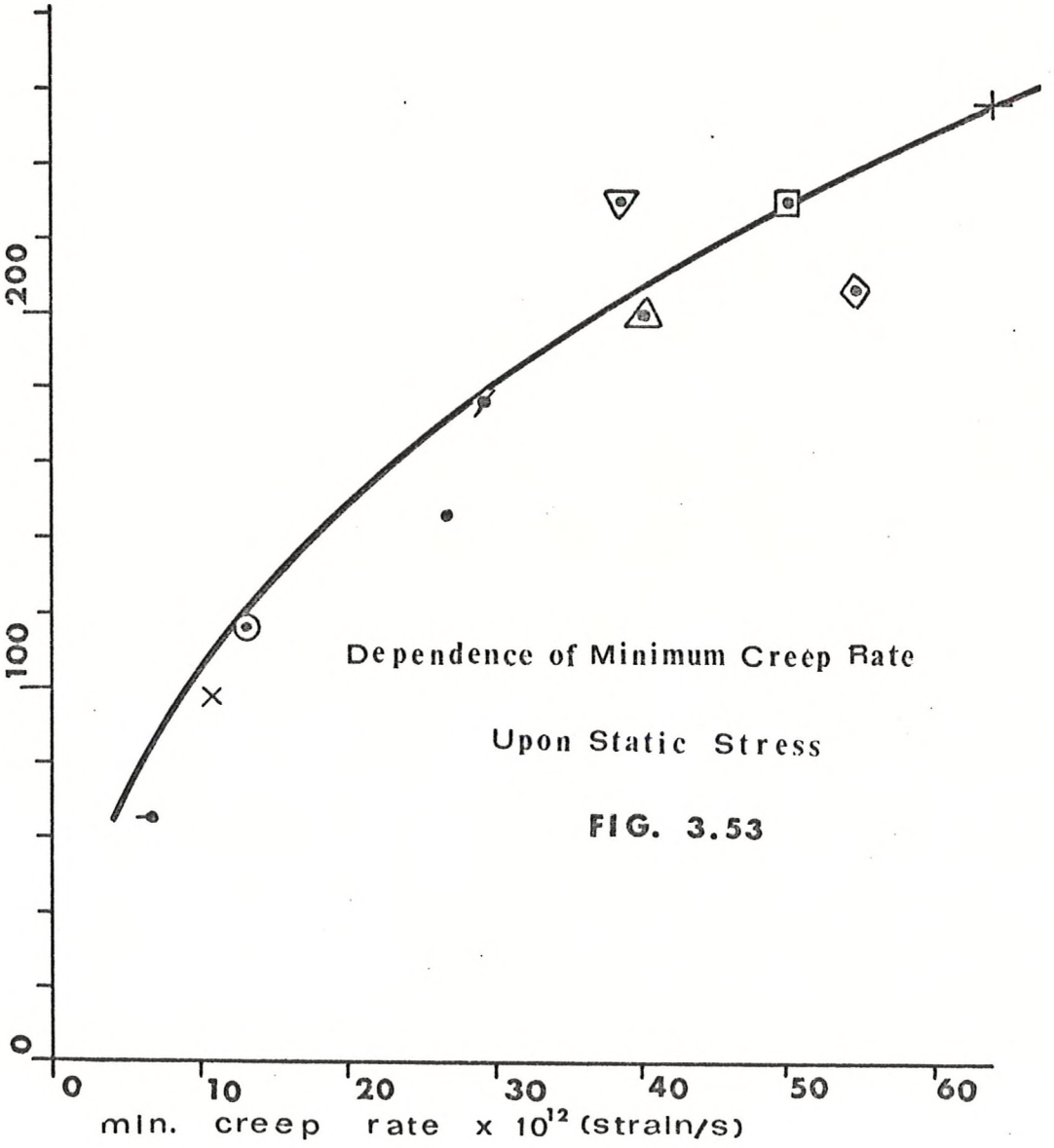

Dependence of Minimum Creep Rate

Upon Static Stress

FIG. 3.53

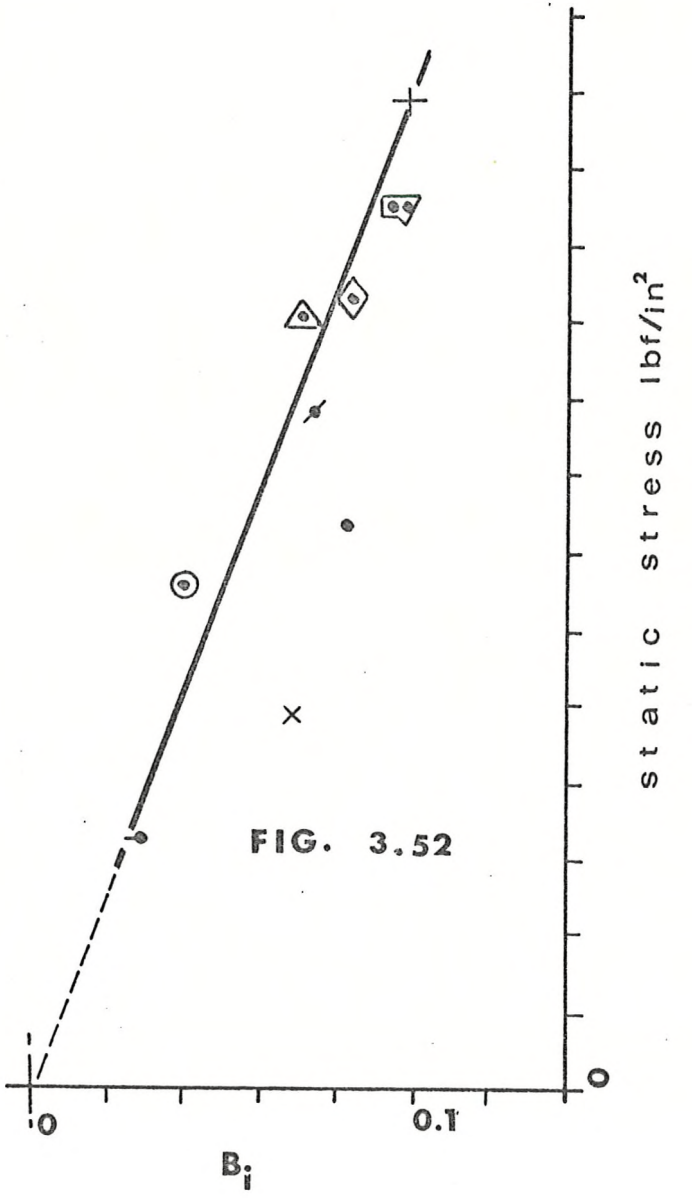

FIG. 3.52

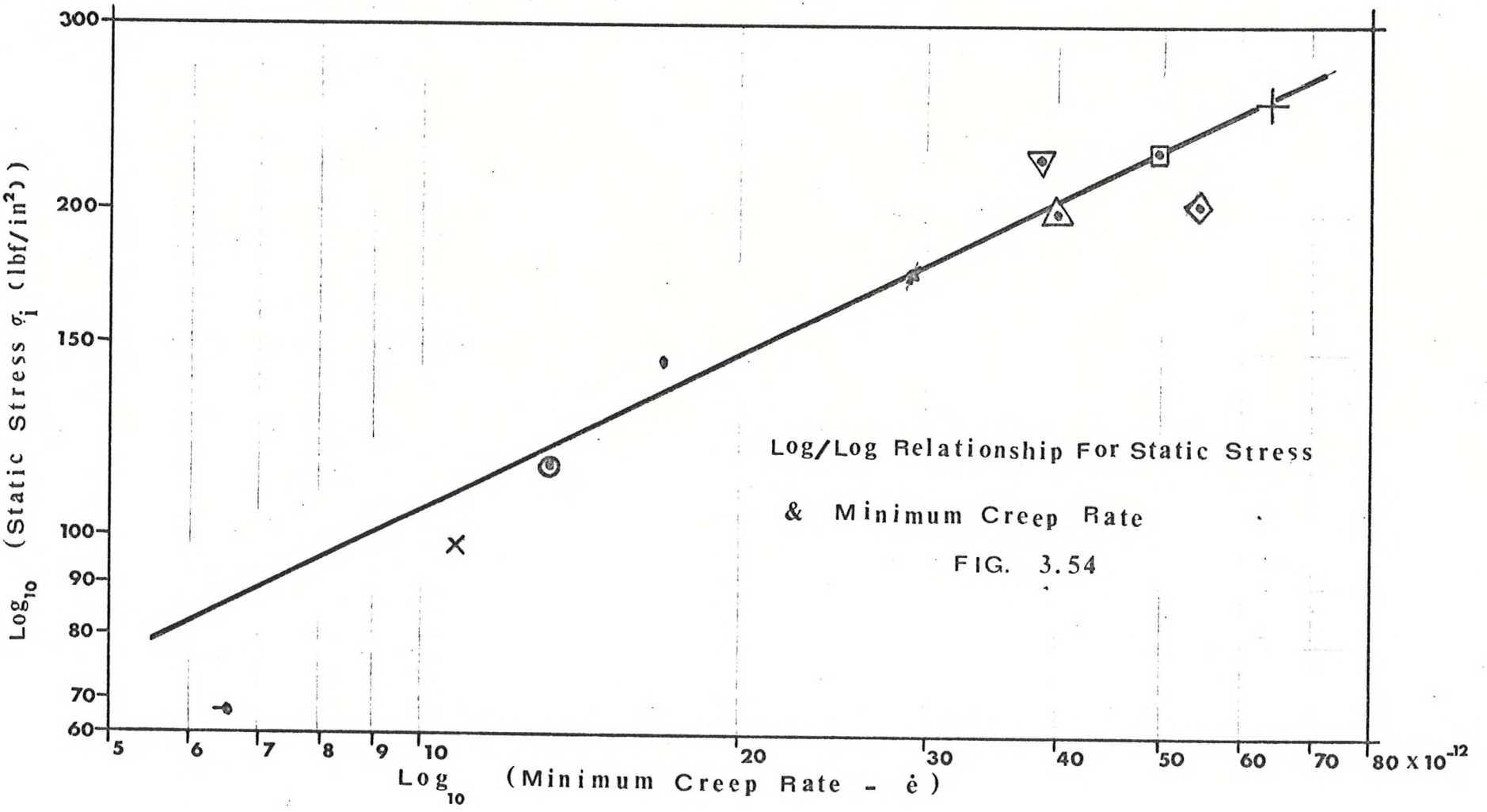

Log/Log Relationship For Static Stress & Minimum Creep Rate

FIG. 3.54

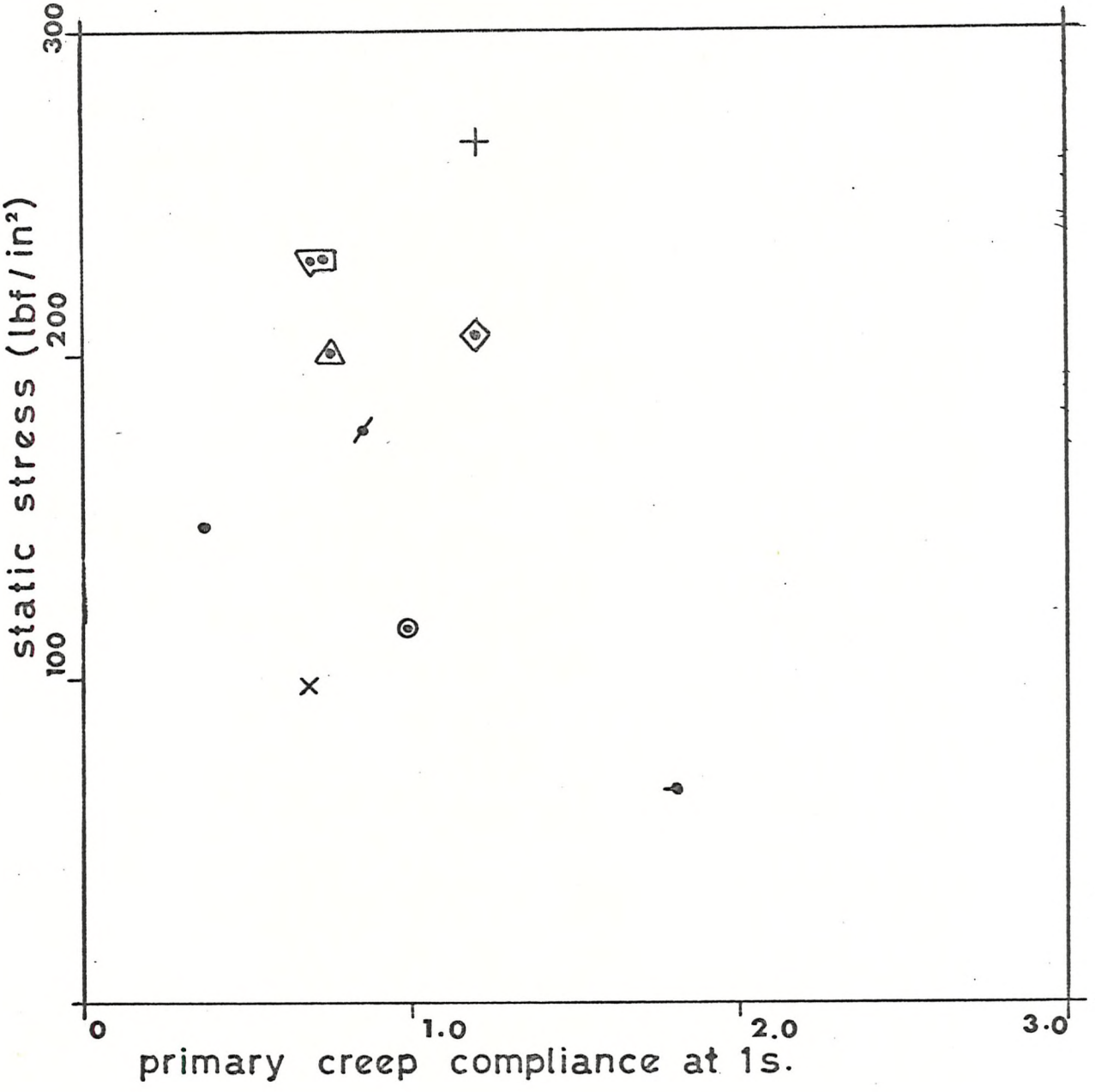

DEPENDENCE OF CREEP COMPLIANCE AT 1s.

UPON APPLIED STATIC STRESS

FIG. - 3.55

3.8 Non Destructive Testing

The mechanical testing of the polymer-cement showed a general improvement of tensile strength and ductility over ordinary hardened Portland cement paste. This was brought about by the introduction of the 100% acrylic dispersion (Primal E330). The question was then asked, was the polymer dispersed within the hardened Portland cement paste or, alternatively, did some chemical change of the Portland cement take place when combined with Primal E330? The latter possibility was tentatively investigated by employing X-ray diffraction techniques and the former by micro examination using thin slide techniques.

3.8.1 X-Ray Diffraction Scanning

The X-ray wide angled diffractometer supplied by Philips and Company Limited was coupled to a recorder which produced the spectograms of Fig. 3.56. The angle, rate of scan, chart speed and amplitude of peaks were all adjustable.

Three samples were prepared as follows:

a) Dry Portland cement powder

b) Hardened Portland cement paste with a w/c ratio of 0.3 (ground to a powder)

c) Hardened Primal - Portland cement paste with a w/c ratio of 0.3, s/c ratio of 0.2, a/c ratio of 0.02 (ground to a powder).

The X-ray diffraction patterns (a, b, c, Fig. 3.56) did not show any significant deviations except, of course, the peaks which appear on patterns b and c which are expected (calcium hydroxide and ettringite). This seemed to indicate that no apparent major chemical changes took place by the introduction of the polymer into the fresh cement paste. The indication here is towards studies of the structure of the material by optical or electron microscopic inspection[33] rather than X-ray diffraction techniques. The chart (Fig. 3.57) will assist in the identification of the chemical compounds from the peaks at various diffraction angles. Table 3.18 gives the chemical composition of the major compounds in full, together with their corresponding mineral names[33]. The cement chemists abbreviations are also shown for reference.

TABLE 3.18

MINERALS AND PHASES LIKELY TO OCCUR IN HARDENED PORTLAND CEMENT AND POLYMER-PORTLAND CEMENT

MINERAL NAME	
C_4AF	(Calcium Aluminum ferrite) $Ca_4Al_2Fe_2O_{10}$
C_3A	(tricalcium aluminate) $Ca_3Al_2O_6$
αC_2S	(dicalcium silicate) Ca_2SiO_4
C_2S	(dicalcium silicate) Ca_2SiO_4
Calcium aluminate monosulphate hydrate	$Ca_3Al_2O_7 \cdot CaSO_4 \cdot 12H_2O$
Ettringite	$Ca_3Al_2O_7 \cdot 3CaSO_4 \cdot 32H_2O$
C_3S	Ca_3SiO_5
Alite	Ca_3SiO_5

CEMENT CHEMISTS ABBREVIATIONS:

C	=	CaO
A	=	Al_2O_3
S	=	SiO_2
H	=	H_2O
F	=	Fe_2O_3
S_oC_3S	=	$3 \cdot CaO \cdot SiO_2$ or $Ca_3 Si O_5$

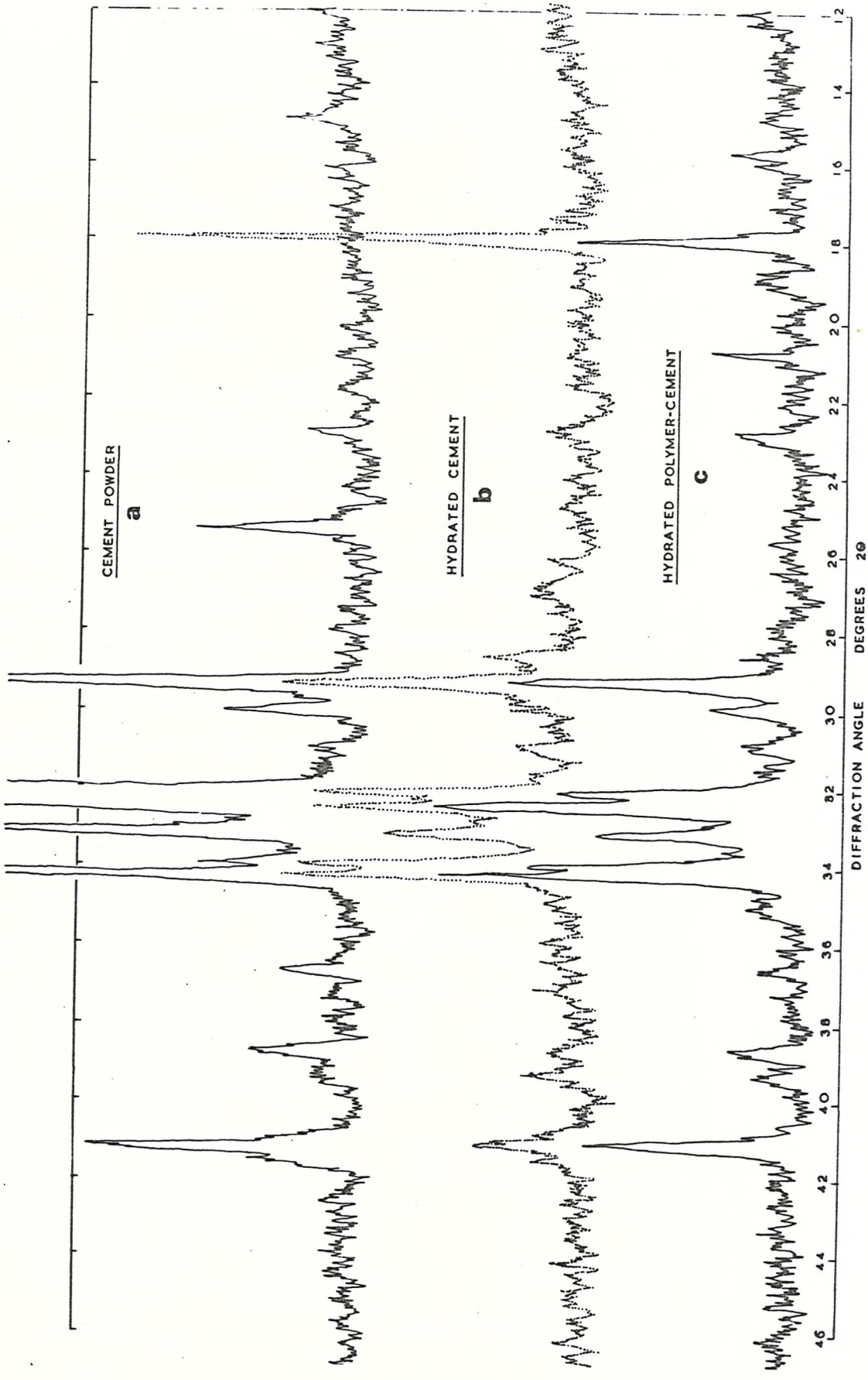

X-RAY DIFFRACTION PATTERNS
figure 3.56

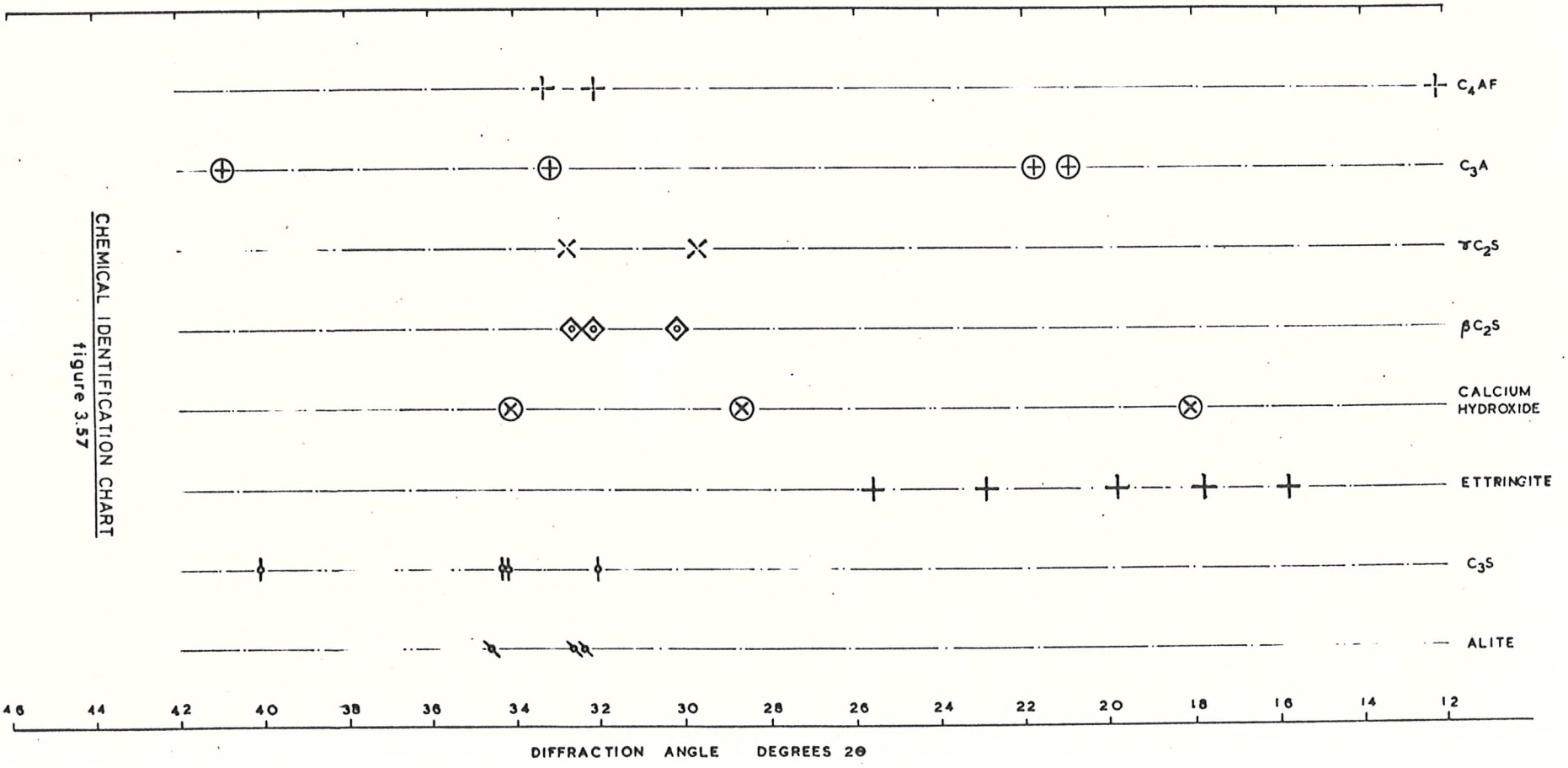

CHEMICAL IDENTIFICATION CHART
figure 3.57

3.8.2 Micro Examination

Preparation of Thin Section:

Several prisms were prepared having various solid/cement ratios but a constant water/cement ratio of 0.3. Using a motta cutter a slice was taken from each prism. These were ground on glass plates until flat and smooth, then dried on a hot plate. Each slice was placed on a glass slide, covered with lakeside and set. This was followed by a further grinding with carborundum paste until a thickness of about 30 micron was obtained. The sample was then covered with a durafix film and removed from slide by melting lakeside. Another slide was prepared with Canada Balsam to receive the sample. A cover slip was placed and the completed slide allowed to cool, then washed.

Plate 3.6 shows the micrograph of a sample with a solid/cement ratio of 0.25 using transmitted light through the glass slide. Plate 3.7 is a specimen with a solid/cement ratio 0.1 under the same conditions. When using crossed nicols (Plate 3.8) a crystalline material is seen to exist. Plate 3.9 shows a specimen with a solid/cement ratio of 0.2 (crossed nicols).

Upon inspection of the range of thin slides with solid/cement ratios from 0.1 to 0.25 a

birefrigent material in the form of startlets is evident. These starlets are dispersed interstitial to the cement grains and they increase in density per unit area with an increase of solid/cement ratio. This leads to the possible conclusion that the polymer exists as concentrations dispersed throughout the hardened paste. It also suggests that the polymer concentrations act as a ductile aggregate and may even surround some cement particles. This supports the thought that, during wet curing conditions, the polymer strength reduces and with it that of the polymer cement specimen. However, upon drying, the polymer regains its strength and ductility.

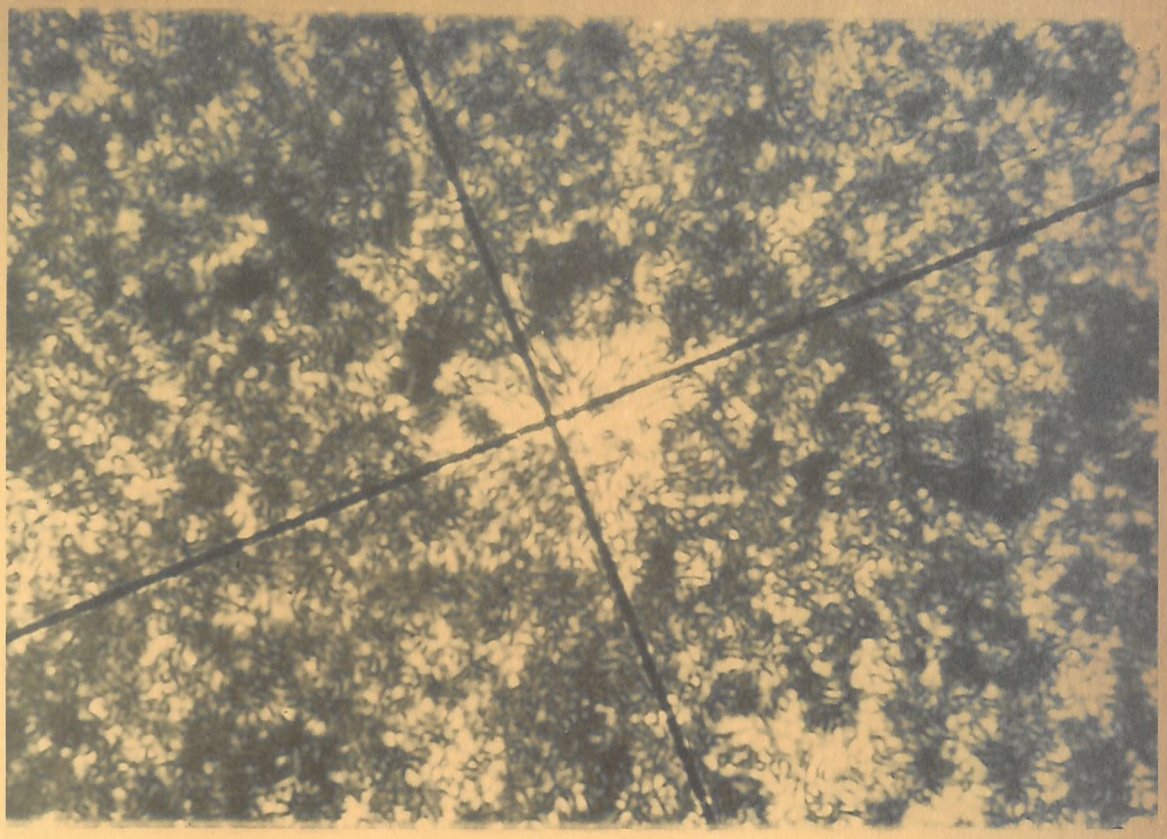

PLAIN LIGHT

w/c = 0.3 s/c = 0.25

PLATE 3.6

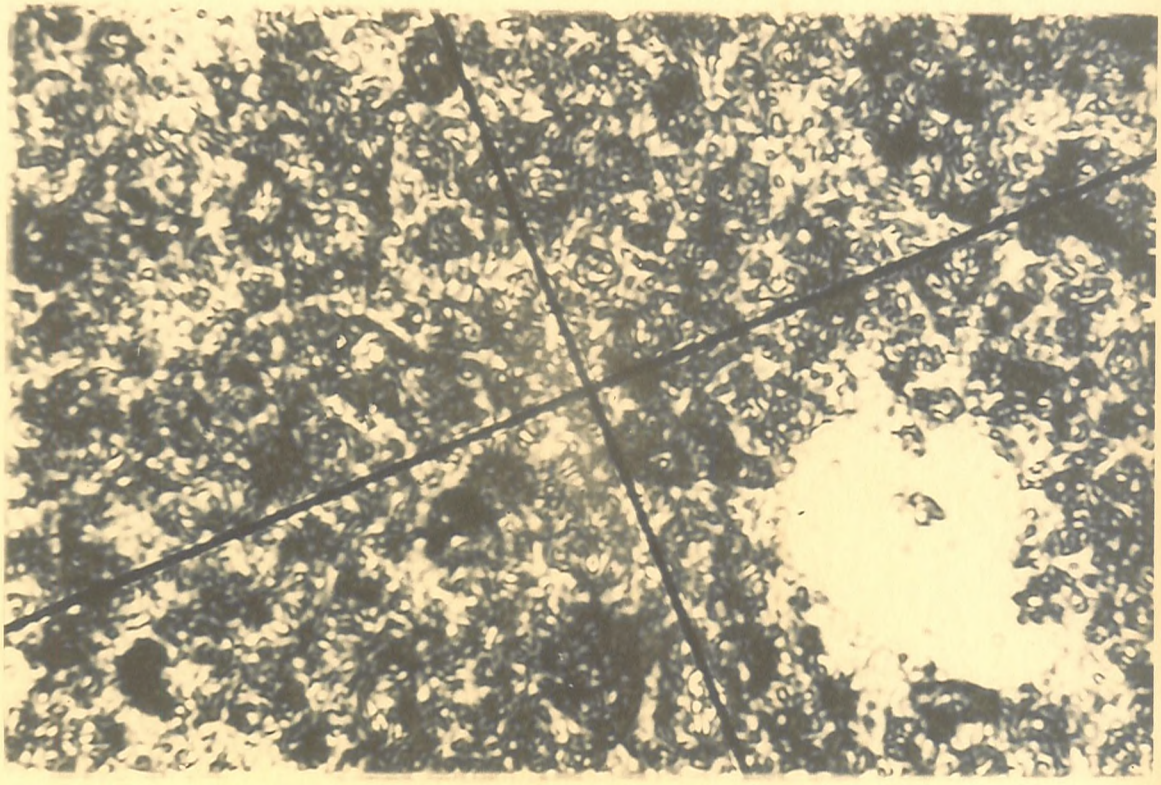

PLAIN LIGHT

w/c = 0.3 s/c = 0.1

PLATE 3.7

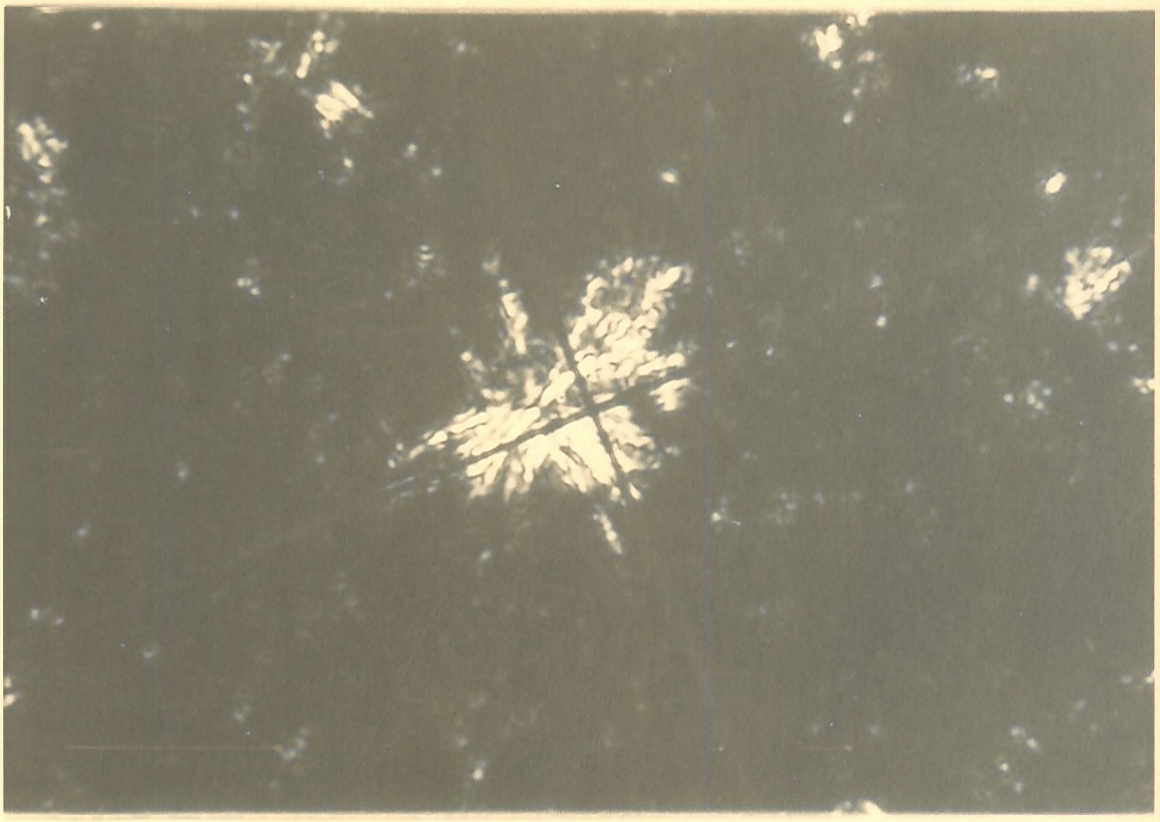

POLARIZED LIGHT

w/c = 0.3 s/c = 0.25

PLATE 3.8

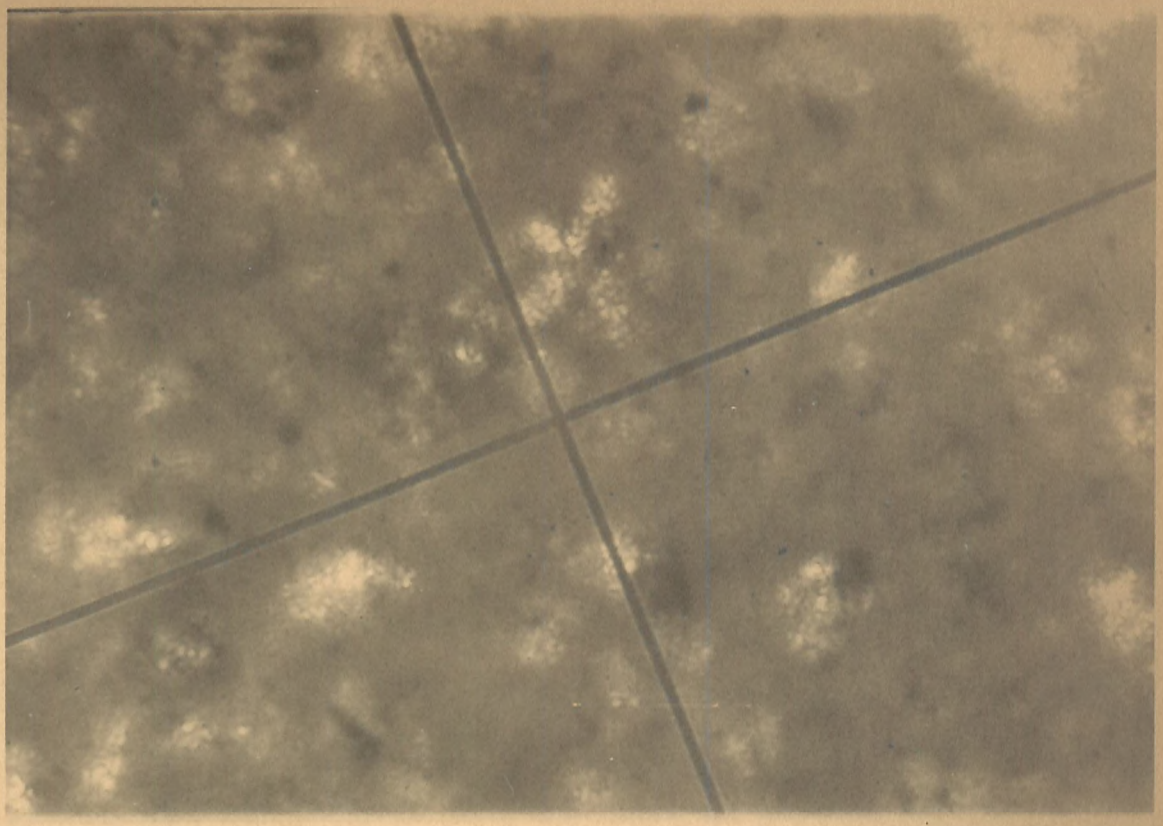

POLARIZED LIGHT

w/c = 0.3 s/c = 0.2

PLATE 3.9

CHAPTER 4

REINFORCED MATERIAL

(Chopped Strand Mat)

4.1 Outline

This chapter reports investigations of some of the mechanical properties of the material described in Chapter 3 when reinforced by an approximately random distribution of E-glass fibres. This reinforcement was provided in the form of chopped strand mat (Appendix B1) supplied by Fibreglass Limited.

Eight sheets (approximately 24 in x 18 in) were manufactured to provide the test pieces (Fig. 4.1). Each sheet consisted of a polymer-cement matrix with a w/c ratio 0.3, s/c ratio 0.2 and a/c ratio 0.002 (page 44), and was reinforced by two layers of C.S.M. Sheet 11 was an exception in which three layers of C.S.M. were used.

Fig. 4.1 gives a complete description of the eight laminates, including nomenclature, nature of reinforcement and the tests to which the various sheets were subjected.

All the sheets of material were stored vertically in air at a constant temperature of

22°C and 40-60% relative humidity (and were tested in the same environment).

Fig. 4.2 shows the experimental plan for the testing of the C.S.M.-reinforced polymer-cement.

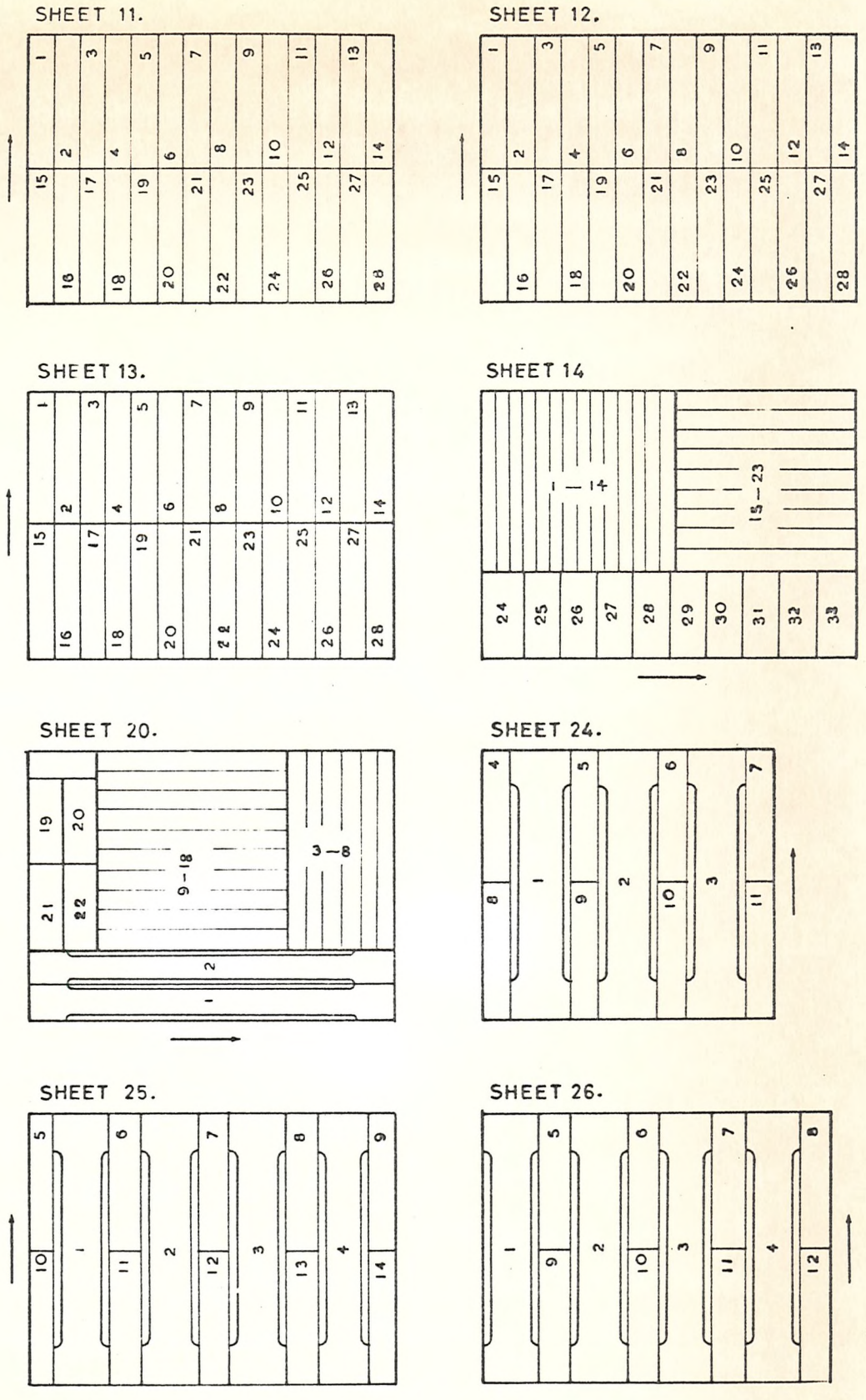

Cutting Plan of Polymer-Cement Sheets Reinforced by glass chopped strand mat

FIG. 4.1

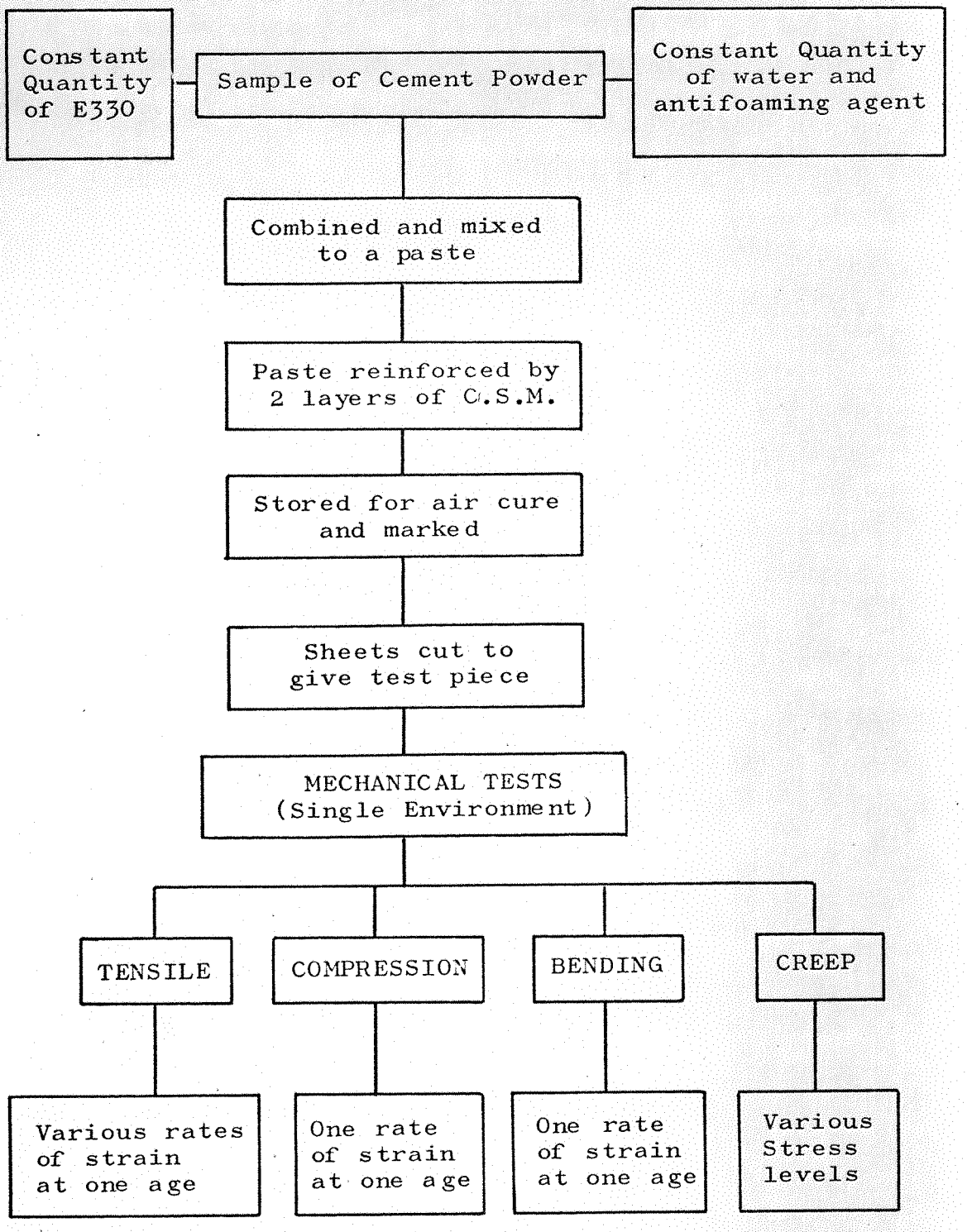

experimental flow chart
fig 4.2

4.2 Properties of the Chopped Strand Mat

4.2.1 General

The chopped strand mat used in this investigation was supplied by Fibreglass Limited (FGE 2000; E glass; see Appendix B). The manufacturers quote a nominal weight of 1.5 ozf/ft^2 for this mat.

The strength and modulus of elasticity of E glass are given as 300 to 400 x 10^3 lbf/in^2 and 10 to 14 x 10^6 lbf/in^2 respectively. At Southampton, using a long single strand of E-glass (about 204 filaments), the elastic modulus was found to be between 10 and 11 x 10^6 lbf/in^2 with a specific gravity of 2.53.

The glass content of the laminate cannot be determined by burning off the matrix as is done with G.R.P. laminates.

The composite was placed in a quantity of concentrated Hydrochloric acid which appeared to remove the cement particles, leaving a sample of glass and polymer. Unfortunately it was not possible then to ignite the polymer and so retain the glass reinforcement alone.

These difficulties were not overcome and the alternative was to obtain a measure of the weight of the glass in a particular sample by

estimating the quantity of glass in each layer of reinforcement before fabrication.

4.2.2 Random Sample

A sample of C.S.M. 7 feet long and approximately 3 feet wide was cut into 6 inch squares (numbered 1 to 84) and the weight of each square was recorded (Table 4.1). It was immediately seen from the distribution of weights (Table 4.1) that the mat weight varied across its width. If the mat were cut down the centre along the roll direction and superimposed upon the other half (with the centre of one half adjacent to the outside edge of the other), then the variation across the width would be reduced (Table 4.2). The ANOVA (analysis of variance) tables shown on Tables 4.1 and 4.2 indicate the column and row effects of each distribution using the F distribution as a test of significance (Appendix A, Sec A2.3).

In order to draw an unbiased sample the 14 x 6 array of Table 4.1 was arranged in random order (Table 4.3). The ANOVA table then shows the column and row effects not to be significant. From the arrangement of Table 4.3 the first row was selected as the random sample.

TABLE 4.1

WEIGHTS (g) OF 6 X 6 IN. SQUARES OF A SINGLE LAYER OF C.S.M. AS CUT FROM ROLL

(i.e. Including Size, Binder and Moisture)

10.10 (1)	10.60 (2)	11.70 (3)	11.00 (4)	10.00 (5)	10.90 (6)	10.60 (7)	11.20 (8)	10.60 (9)	10.80 (10)	9.70 (11)	11.20 (12)	10.80 (13)	10.60 (14)	
8.50 (15)	9.80 (16)	10.90 (17)	9.60 (18)	10.00 (19)	10.00 (20)	10.20 (21)	10.50 (22)	10.00 (23)	9.70 (24)	9.20 (25)	10.70 (26)	10.60 (27)	10.60 (28)	A
12.10 (29)	12.10 (30)	10.70 (31)	11.40 (32)	11.70 (33)	11.20 (34)	11.40 (35)	11.80 (36)	11.50 (37)	12.00 (38)	11.80 (39)	11.80 (40)	11.50 (41)	11.90 (42)	
10.80 (43)	11.00 (44)	11.60 (45)	12.20 (46)	13.00 (47)	12.50 (48)	13.60 (49)	12.70 (50)	12.40 (51)	12.40 (52)	11.80 (53)	12.50 (54)	12.50 (55)	11.60 (56)	
11.40 (57)	11.80 (58)	12.20 (59)	11.70 (60)	11.70 (61)	11.50 (62)	11.70 (63)	12.00 (64)	11.70 (65)	12.30 (66)	11.10 (67)	12.00 (68)	11.80 (69)	12.50 (70)	B
12.20 (71)	12.30 (72)	12.80 (73)	12.90 (74)	12.40 (75)	12.10 (76)	11.50 (77)	11.60 (78)	11.90 (79)	12.40 (80)	12.00 (81)	12.70 (82)	12.40 (83)	11.70 (84)	

→ roll direction

ANOVA TABLE

Source	Degrees of Freedom-ν	Mean Squares	Computed F Number	Critical F Number
Between cols	13	0.428	1.6279	1.79
Between rows	5	10.87	41.33	2.293
Errors	65	0.263		

Since 41.33 >>2.293 row effects significant

TABLE 4.2

WEIGHTS (g) OF 6 X 6 IN. SQUARES OF DOUBLE LAYER OF C.S.M.

(Obtained by Superimposing Region A on B in Table 4.1)

20.90	21.60	23.30	23.20	23.00	23.40	24.20	23.90	23.00	23.20	21.50	23.70	23.30	22.20
19.90	21.60	23.10	21.30	21.70	21.50	21.90	22.50	21.70	22.00	20.30	22.70	22.40	23.10
24.30	24.40	23.50	24.30	24.10	23.30	22.90	23.40	23.40	24.40	23.80	24.50	23.90	23.60

→ roll direction

ANOVA TABLE

Source	Degrees of Freedom-ν	Mean Squares	Computed F Number	Critical F Number
Between cols	13	0.831	1.52	1.79
Between rows	2	16.25	29.74	2.293
Errors	41	0.547		

Significance of row effects reduced since
29.74 > 2.293

TABLE 4.3

RANDOM DISTRIBUTION OF GLASS WEIGHTS

10.00 (20)	10.90 (17)	11.90 (42)	10.60 (28)	10.00 (23)	12.20 (59)	12.30 (66)	12.00 (38)	11.70 (61)	10.60 (2)	10.80 (10)	12.40 (51)	12.50 (55)	12.40 (52)
11.00 (44)	9.20 (25)	12.90 (74)	13.60 (49)	11.00 (4)	11.70 (3)	11.70 (33)	11.80 (53)	12.50 (70)	9.70 (11)	12.50 (54)	12.50 (48)	11.70 (63)	11.70 (60)
11.40 (57)	10.70 (31)	11.10 (67)	12.10 (29)	11.70 (65)	11.80 (40)	11.60 (78)	12.20 (71)	11.50 (37)	9.60 (18)	12.00 (64)	10.90 (6)	10.50 (22)	8.50 (15)
11.80 (69)	11.70 (84)	11.40 (32)	11.20 (12)	10.10 (1)	10.60 (27)	12.10 (30)	12.70 (50)	11.80 (58)	11.80 (36)	11.60 (45)	11.50 (77)	10.60 (14)	12.40 (83)
11.60 (56)	11.80 (39)	12.30 (72)	10.70 (26)	11.20 (8)	9.80 (16)	10.00 (19)	13.00 (47)	9.70 (24)	12.70 (82)	11.20 (34)	12.80 (73)	10.60 (7)	12.00 (81)
11.50 (41)	10.20 (21)	11.50 (62)	12.00 (68)	12.10 (76)	10.60 (9)	12.40 (80)	11.90 (79)	10.00 (5)	11.40 (35)	10.80 (43)	12.40 (75)	12.20 (46)	10.80 (13)

→ roll direction

ANOVA TABLE

Source	Degrees of Freedom-ν	Mean Squares	Computed F Number	Critical F Number
Between cols	13	0.483	1.265	1.79
Between rows	5	1.159	0.527	2.293
Errors	65	0.916		

Col and row effects not significant
Since $1.265 < 1.79$ and $0.527 < 2.293$

4.2.3 Weight of Chopped Strand Mat

Most chopped strand mats use a binding agent and contain a certain amount of moisture (Appendix B1). To find the weight of the glass per unit area it was necessary first to calculate the moisture and size contents of the mat.

Each selected square was placed in a dessicator for a period of 24 hours and then weighed accurately (weight A). The squares were then placed in an oven at 105°C for 20 minutes to evaporate the moisture within the mat, to give the weight of the glass plus binder (weight B). Finally the glass mat samples were put into a furnace at 635 to 650°C. This ignited the resin binder on the glass to give the weight of the glass alone (weight C).

The weights A, B and C are recorded in Table 4.4 which also gives the moisture and binder contents. The mean moisture and binder contents are 0.496 and 5.631 both being percentages of the final glass weight. The average weight of glass in the mat was computed to be 1.519 ozf/ft^2 which gives an equivalent thickness of 0.0144 inches if a specific gravity of 2.53 is assumed; this compares favourably with the manufacturer's value of 1.5 ozf/ft^2.

TABLE 4.4

WEIGHT OF 6 x 6 INCH SINGLE LAYER SAMPLES OF C.S.M.

(Before drying (A), after drying (B) and after burning (C))

Sample Number	Initial Weight (g) (A)	Weight (g) (B)	Weight (g) (C)	A-B(g)	B-C(g)	$\frac{A-B}{C}$%	$\frac{B-C}{C}$%
2	10.65	10.5698	10.008	0.0602	0.5618	0.6015	5.613
10	10.85	10.7950	10.2229	0.0650	0.5721	0.5918	5.596
17	10.9582	10.9071	10.3310	0.0511	0.5761	0.4946	5.576
20	10.0792	10.0113	9.4461	0.0679	0.5652	0.7188	5.983
23	10.0122	10.0034	9.4255	0.0088	0.5779	0.0934	6.131
28	10.757	10.7121	10.0948	0.0449	0.6173	0.4448	6.1149
38	12.0797	12.0278	11.3892	0.0519	0.6386	0.4557	6.0022
42	12.0294	11.9812	11.3711	0.0482	0.6101	0.4239	5.3654
51	12.566	12.5152	11.8629	0.1398	0.6523	1.178	5.4986
52	12.5466	12.5058	11.8692	0.0408	0.6366	0.3437	5.363
55	12.1296	12.0826	11.4462	0.0407	0.6364	0.4106	5.56
59	12.6744	12.6346	11.9706	0.0398	0.664	0.3325	5.5467
61	11.6462	11.5952	11.000	0.0510	0.592	0.4636	5.4109
66	12.1574	12.1122	11.5272	0.0452	0.585	0.3921	5.075
				Mean Values		0.4961	5.6311

Column 7 Standard Deviation = 0.24436 Coeff. of Variation = 49%
Column 8 Standard Deviation = 0.31379 Coeff. of Variation = 5.5725%
∴ total % correction = 6.127

4.3 Preparation of Thin Glass Reinforced Laminates

A simple hand layup method (Appendix D (Sec. D3)) was used as follows. A sheet of p.v.c. was laid flat and coated with a mould oil. The polymer-cement, prepared as described on page 50, was applied to the p.v.c. as a thin layer with a brush. The first piece of chopped strand mat was placed upon the cement and rolled in order to push the cement up through the mat and to expel trapped air. Additional cement was applied where necessary to give a smooth surface. The second layer of mat was placed and the procedure was repeated. After five minutes a sheet of transparent Cobex was placed on the laminate and by rolling from the centre outwards the excess cement and the trapped air were expelled. The glass mats were placed in the particular manner shown in Table 4.2 and the roll direction of the mat was recorded. When 24 hours had elapsed the p.v.c. and cobex sheets were peeled from the laminate to reveal a mirror-like surface finish with the glass mat showing at the surface in a vein-like manner.

4.4 Tensile Stress-Strain Properties

4.4.1 The Experimental Method

The purpose of this experiment was to study the effect upon the stress-strain diagram of variations in the rate of applied strain.

Tensile specimens selected from sheets 11, 12 and 13 (as shown in Fig 4.1 when read with Table 4.5) were cut and prepared as described in Appendix C (Sec. C2).

The experiment was performed using the Instron testing machine (Appendix C (Sec. C1)) as described on page 54. Tensile strains were detected over a gauge length of 2 inches and a load-extension diagram was obtained up to fracture. The tests were conducted at crosshead speeds ranging from 0.002 in/min to 1.0 in/min. Since the free length between the testing machine jaws in all cases was 6.38 inches then the crosshead speeds correspond to strain rates of 0.313 to 156.74 x 10^{-3} strain/min.

4.4.2 Experimental Results

The results are summarised in Table 4.5 (tensile strength), Table 4.6 (ultimate strain) and Table 4.7 (initial elastic modulus). Figures for sheet 12 (2 layers of C.S.M.) are shown in

parenthesis; figures for sheet 13 (2 layers of C.S.M.) are not. Tables 4.8 (tensile strength) and 4.9 (initial elastic modulus) show the summary of results for tensile specimens cut from sheet 11 (3 layers of C.S.M.). These tables indicate the % coefficients of variance which are considerably greater than those for the unreinforced material of Tables 3.4, 3.5 and 3.6. The tables also give the 90% confidence limits. Detailed results of these tests may be seen in Appendix H, Tables H2 and H3.

Figures 4.3 to 4.10 show the scatter stress strain diagram of the specimens cut from sheets 12 and 13. Each series of tests is run at constant crosshead speed ($\dot{\varepsilon}$) which is indicated on the appropriate diagrams. In every case the stress-strain diagram starts with an approximately linear slope which decreases with respect to strain until it reaches a constant value. The upper portion of the stress-strain diagram is quite linear. The tensile strength is plotted against log (crosshead speed) in Fig. 4.11, and this shows the effect of crosshead speed upon tensile strength to be small. Figure 4.11 emphasises the increase in variation of strengths for the reinforced material using a 90% confidence limit. (Compare Fig. 3.20).

Tensile specimens were tested from sheets 20, 24, 25 and 26 (Fig. 4.1) and a summary of the tensile properties is given in Tables 4.10 and 4.11 (detailed Appendix H, Table H4). Sheets 20, 24, 25 and 26 were also used to provide the long term creep and flexural specimens. Sheet 20 was manufactured so that it had a low glass content and specimens were cut parallel and normal to the roll direction of the glass fibre mat. The scatter tensile stress-strain diagrams (of specimens cut from sheet 20) are given in Figures 4.12 and 4.13. These two diagrams clearly illustrate the weakness in assuming that the fibres of a C.S.M. are distributed in a completely random manner.

Figures 4.14 to 4.21 show the dependence of secant modulus (stress/corresponding strain) upon strain at the various crosshead speeds. Each curve shows the same general character.

Figures 4.22 to 4.28 illustrate the dependence of chord elastic modulus (change of stress/corresponding change of strain) upon the stress at various crosshead speeds and indicates the same character as Figures 4.14 to 4.21.

TABLE 4.5

SUMMARY OF TENSILE STRENGTHS

(2 Layers of C.S.M.)

Specimen Numbers	Cross-head Speed $\dot{\varepsilon}$ in/min	Tensile Strength σ_u lbf/in^2	Standard Deviation lbf/in^2	% Coeff. of Var.	Confidence Limits p =0.1, lbf/in^2		Mean % Glass Content	Est. Mean Specific Gravity	Strength per layer of glass lbf/in^2
					Upper	Lower			
13.1 - 13.7 Sheet 12	0.005	2170.8 (2701.8)	378.18 (236.37)	17.42 (8.74)	2448.1 (2875.2)	1893.5 (2528.5)	9.43 (8.96)	1.777 (1.656)	1035.4
13.8 - 13.10	0.01	2715.6	297.46	10.95	3217.1	2214.2	10.31	1.749	1357.8
13.11 - 13.13 Sheet 12	0.02	2368.7 (3166.1)	420.97 (216.9)	17.77 (6.85)	3078.4 (3325.2)	1659.0 (3007.1)	9.57 (8.95)	1.75 (1.677)	1184.4
13.14 - 13.16	0.05	2396.9	671.94	28.033	3529.7	1264.1	8.63	1.777	1198.5
13.17 - 13.19	0.1	2671.9	110.45	4.134	2858.1	2485.7	8.95	1.790	1335.9
13.20 - 13.22 Sheet 12	0.2	2834.3 (3357.4)	207.83 (299.15)	7.333 (8.910)	3184.7 (3576.7)	2484.0 (3138.0)	9.82 (9.01)	1.779 (1.667)	1417.2
13.23 - 13.25 Sheet 12	0.5	2592.2 (3457.1)	138.18 (204.45)	5.33 (5.91)	2825.2 (3625.7)	2359.3 (3288.5)	9.44 (9.03)	1.78 (1.661)	1296.1
13.26 - 13.28	1.0	2764.6	304.87	11.028	3154.8	2374.4	9.06	1.772	1382.3

Figures in parenthesis are selected from specimens 12.1 to 12.28 (See Table H2 and Fig. 4.1)

TABLE 4.6

SUMMARY OF ULTIMATE STRAINS

(2 Layers of C.S.M.)

Specimen Numbers	Crosshead Speed $\dot{\varepsilon}$ (in/min)	Ultimate Strain x 10^3	Standard Deviation x 10^3	% Coeff. of Var.	Confidence Limits p = 0.1 x 10^3	
					Upper	Lower
13.1 - 13.7	0.005	6.253	0.962	15.38	6.958	5.548
13.8 - 13.10	0.01	7.017	0.960	13.69	8.636	5.398
13.11 - 13.13	0.02	7.8866	0.873	11.07	9.359	6.415
13.14 - 13.16	0.05	6.0666	0.503	8.29	6.915	5.218
13.17 - 13.19	0.1	6.2634	0.872	13.93	7.734	4.793
13.20 - 13.22	0.2	7.2300	0.602	8.33	8.355	6.215
13.23 - 13.25	0.5	6.7866	0.412	6.069	7.481	6.092
13.26 - 13.27	1.0	9.5000	1.556	18.302	10.491	6.509

(Specimens cut from Sheet 12 Failed at Strains $>10 \times 10^{-3}$

TABLE 4.7

SUMMARY OF INITIAL ELASTIC MODULUS VALUES

(2 Layers C.S.M.)

Specimen Numbers	Crosshead Speed $\dot{\varepsilon}$ (in/min)	Initial Elastic Modulus $lbf/in^2 \times 10^{-6}$	Standard Deviation $lbf/in^2 \times 10^{-6}$	% Coeff. of Var.	Confidence Limits p = 0.1, $lbf/in^2 \times 10^{-6}$	
					Upper	Lower
13.1 - 13.7 Sheet 12	0.005	0.9929 (0.6128)	0.0958 (0.0814)	9.65 (13.28)	1.0631 (0.6724)	0.9226 (0.5531)
13.8 - 13.10	0.01	0.875	0.0322	3.68	0.9294	0.8206
13.11 - 13.13 Sheet 12	0.02	0.9085 (0.6919)	0.1089 (0.1122)	11.99 (16.22)	1.0922 (0.7742)	0.7248 (0.6096)
13.14 - 13.16	0.05	1.3119	0.4020	30.64	1.9896	0.6342
13.17 - 13.19	0.1	1.0424	0.0105	1.009	1.0602	1.0247
13.20 - 13.22 Sheet 12	0.2	0.9490 (0.6952)	0.3447 (0.0623)	36.32 (8.96)	1.5302 (0.7409)	0.3679 (0.6495)
13.23 - 13.25 Sheet 12	0.5	0.8774 (0.7641)	0.358 (0.1049)	40.76 (13.74)	1.4803 (0.8506)	0.2744 (0.6775)
13.26 - 13.28	1.0	1.4799	0.338	22.85	1.9128	1.0470

Figures in parenthesis are specimens cut from sheet 12 (1 to 28)

TABLE 4.8

SUMMARY OF ULTIMATE STRENGTHS

(3 Layers C.S.M.)

Crosshead Speed $\dot{\varepsilon}$ (in/min)	Tensile Strength σ_u lbf/in^2	Standard Deviation lbf/in^2	% Coeff. of Var.	Confidence Limits p = 0.1, lbf/in^2 Upper	Lower	Mean % Glass Content By Vol.	Estimated Mean Specific Gravity	Strength per layer of glass, lbf/in^2
0.005	3611.7	307.7	8.52	3837.3	3386.1	7.06	1.762	1203.9
0.02	3786.4	387.4	10.23	4105.8	3466.9	7.238	1.763	1262.1
0.2	4111.2	194.6	4.73	4253.9	3968.5	7.32	1.782	1370.3
0.5	4177.5	487.4	11.67	4579.4	3775.6	6.923	1.753	1392.5

SPECIMENS CUT FROM SHEET 11 (SEE FIG. 4.1, TABLE H1)

TABLE 4.9

SUMMARY OF INITIAL ELASTIC MODULUS VALUES

(3 Layers of C.S.M.)

Crosshead Speed $\dot{\varepsilon}$ (in/min)	Initial Elastic Modulus (E_o) $lbf/in^2 \times 10^{-6}$	Standard Deviation $lbf/in^2 \times 10^{-6}$	% Coeff. of Var.	Confidence Limits p = 0.1, $lbf/in^2 \times 10^{-6}$	
				Upper	Lower
0.005	0.7729	0.1225	15.85	0.8627	0.6831
0.02	0.8139	0.0593	7.28	0.8628	0.7650
0.2	0.7981	0.1196	14.99	0.8858	0.7104
0.5	0.7936	0.1094	13.78	0.8838	0.7034

SPECIMENS CUT FROM SHEET 11 (SEE FIG. 4.1, TABLE H1)

TABLE 4.10

SUMMARY OF TENSILE STRENGTHS

(Control Specimens for Creep Experiment)

Specimen Numbers	Tensile Strength σ_u lbf/in^2	Standard Deviation lbf/in^2	% Coeff. of Var.	Confidence Limits p = 0.1, lbf/in^2		Mean % Glass Content By Vol.	Estimated Mean Specific Gravity
				Upper	Lower		
+20.3 - 20.8	2189.6	499.9	22.83	2601.8	1777.3	6.88	1.735
•20.9 - 20.14	1282.9	106.5	8.30	1370.7	1195.1	6.59	1.758
•24.4 - 24.6	3230.7	290.4	8.99	3720.3	2741.2	11.33	1.724
•25.5 - 25.7	2115.4	111.2	5.26	2302.8	1927.9	9.11	1.664
•26.5 - 26.7	2913.2	485.1	16.65	3730.9	2095.4	10.78	1.725

• Cut Parallel to Roll Direction of C.S.M.

+ Cut Normal to Roll Direction of C.S.M.

TABLE 4.11

SUMMARY OF INITIAL ELASTIC MODULII

(Control Specimens for Creep Experiment)

Specimen Numbers	Initial Elastic Modulus (E_o) $lbf/in^2 \times 10^{-6}$	Standard Deviation $lbf/in^2 \times 10^{-6}$	% Coeff. of Var.	Confidence Limits p = 0.1, lbf/in^2	
				Upper	Lower
+20.3 - 20.8	1.2622	0.224	17.77	1.447	1.077
•20.9 - 20.14	0.9825	0.1064	10.83	1.070	0.895
•24.4 - 24.6	0.5785	0.0242	4.176	0.619	0.538
•25.5 - 25.7	1.0221	0.1899	18.58	1.342	0.702
•26.5 - 26.7	0.7155	0.0912	12.74	0.869	0.562

Crosshead Speed Constant at 0.005 in/min

• Cut Parallel to the Roll Direction of the C.S.M.

+ Cut Normal to the Roll Direction of the C.S.M.

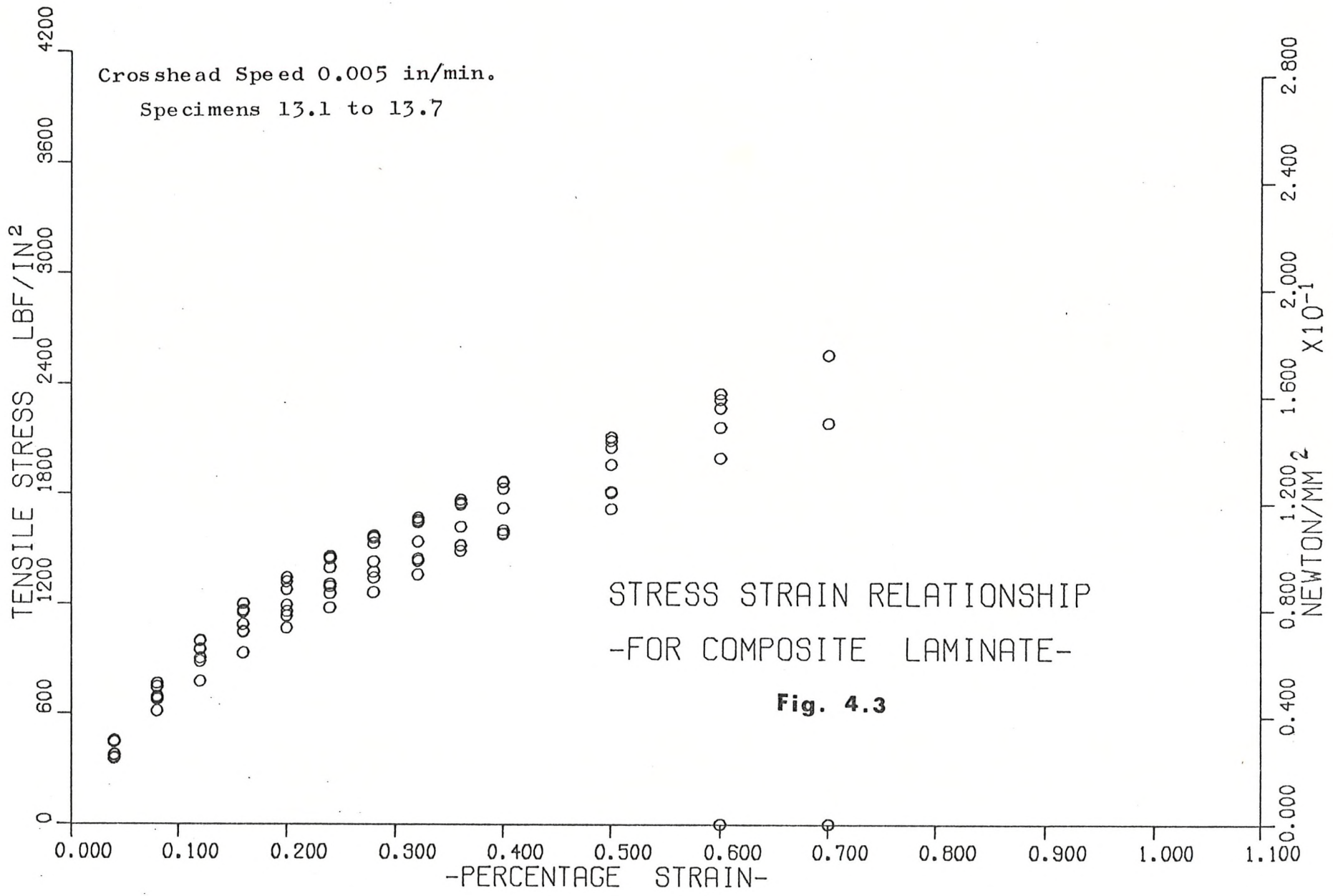
Crosshead Speed 0.005 in/min.
Specimens 13.1 to 13.7
TENSILE STRESS LBF/IN2
0
600
1200
1800
2400
3000
3600
4200
0.000
0.100
0.200
0.300
0.400
0.500
0.600
0.700
0.800
0.900
1.000
1.100
-PERCENTAGE STRAIN-
0.000
0.400
0.800
1.200
1.600
2.000
2.400
2.800
NEWTON/MM2 X10-1
STRESS STRAIN RELATIONSHIP
-FOR COMPOSITE LAMINATE-

Fig. 4.3

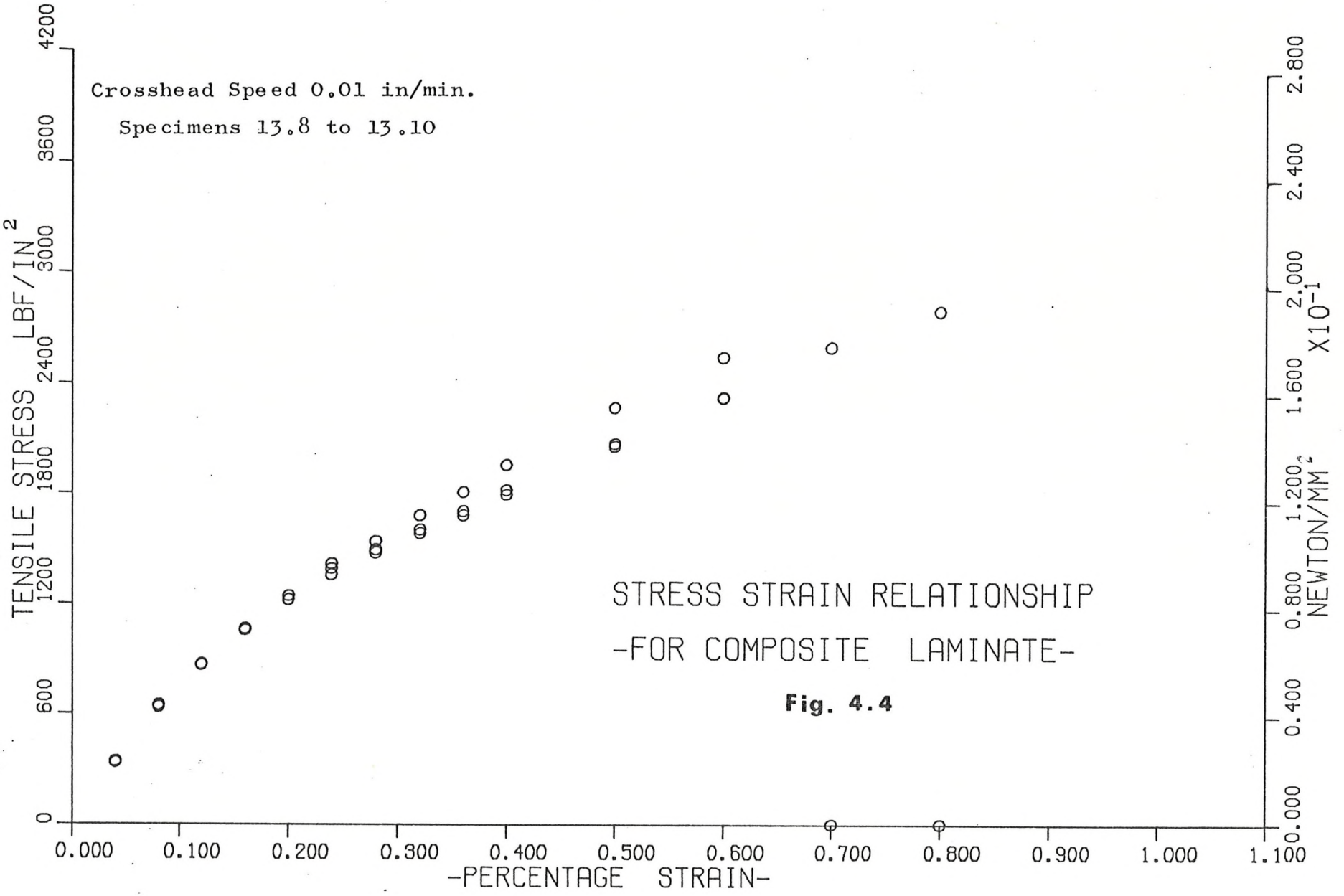
Crosshead Speed 0.01 in/min.
Specimens 13.8 to 13.10
TENSILE STRESS LBF/IN 2
0
600
1200
1800
2400
3000
3600
4200
0.000
0.100
0.200
0.300
0.400
0.500
0.600
0.700
0.800
0.900
1.000
1.100
-PERCENTAGE STRAIN-
0.000
0.400
0.800
1.200
1.600
2.000
2.400
2.800
X10-1
NEWTON/MM2
STRESS STRAIN RELATIONSHIP
-FOR COMPOSITE LAMINATE-

Fig. 4.4

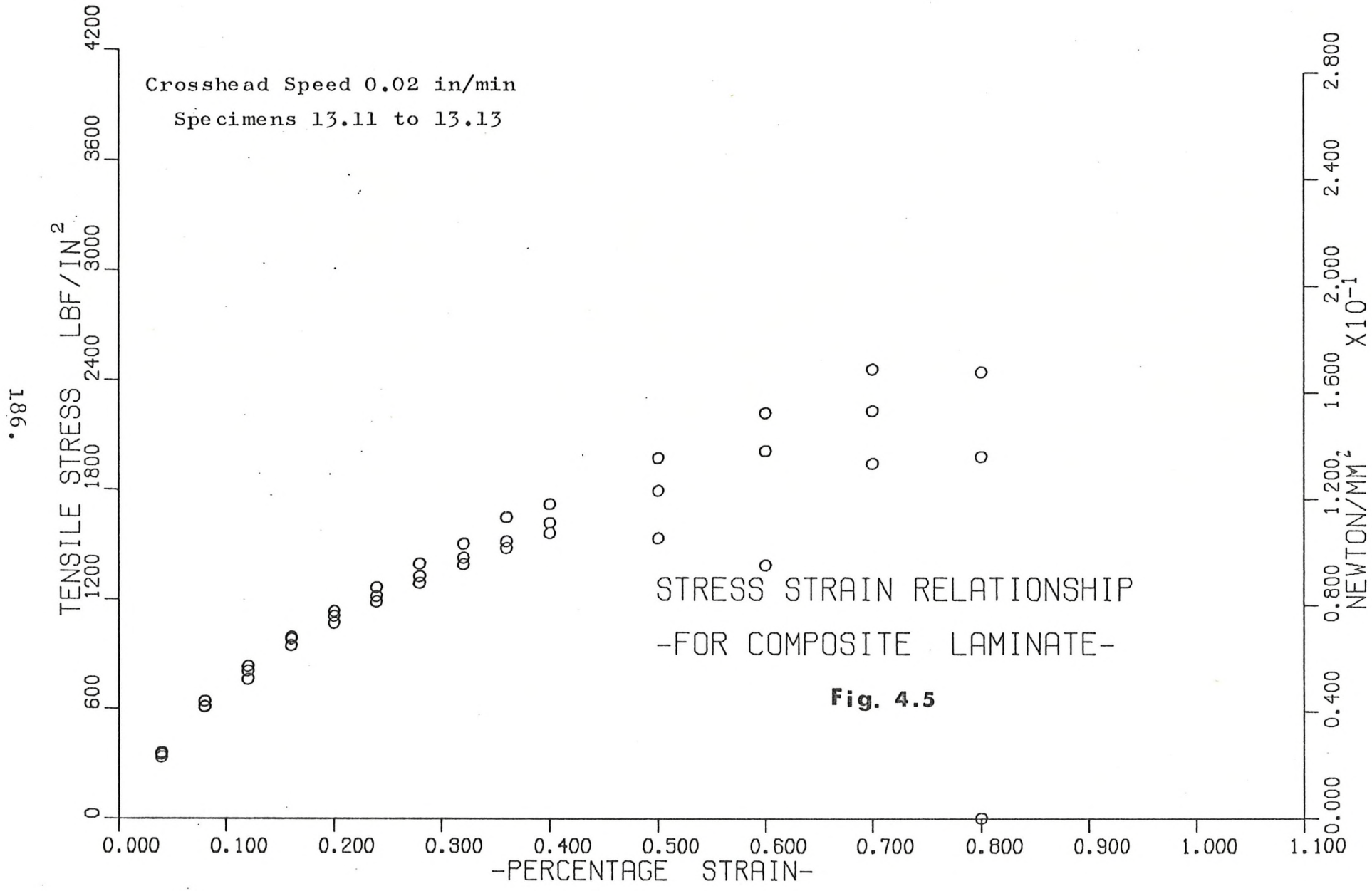
Crosshead Speed 0.02 in/min
Specimens 13.11 to 13.13
TENSILE STRESS LBF/IN^2
0
600
1200
1800
2400
3000
3600
4200
0.000
0.100
0.200
0.300
0.400
0.500
0.600
0.700
0.800
0.900
1.000
1.100
-PERCENTAGE STRAIN-
0.000
0.400
0.800
1.200
1.600
2.000
2.400
2.800
NEWTON/MM^2 X10^{-1}
STRESS STRAIN RELATIONSHIP
-FOR COMPOSITE LAMINATE-

Fig. 4.5

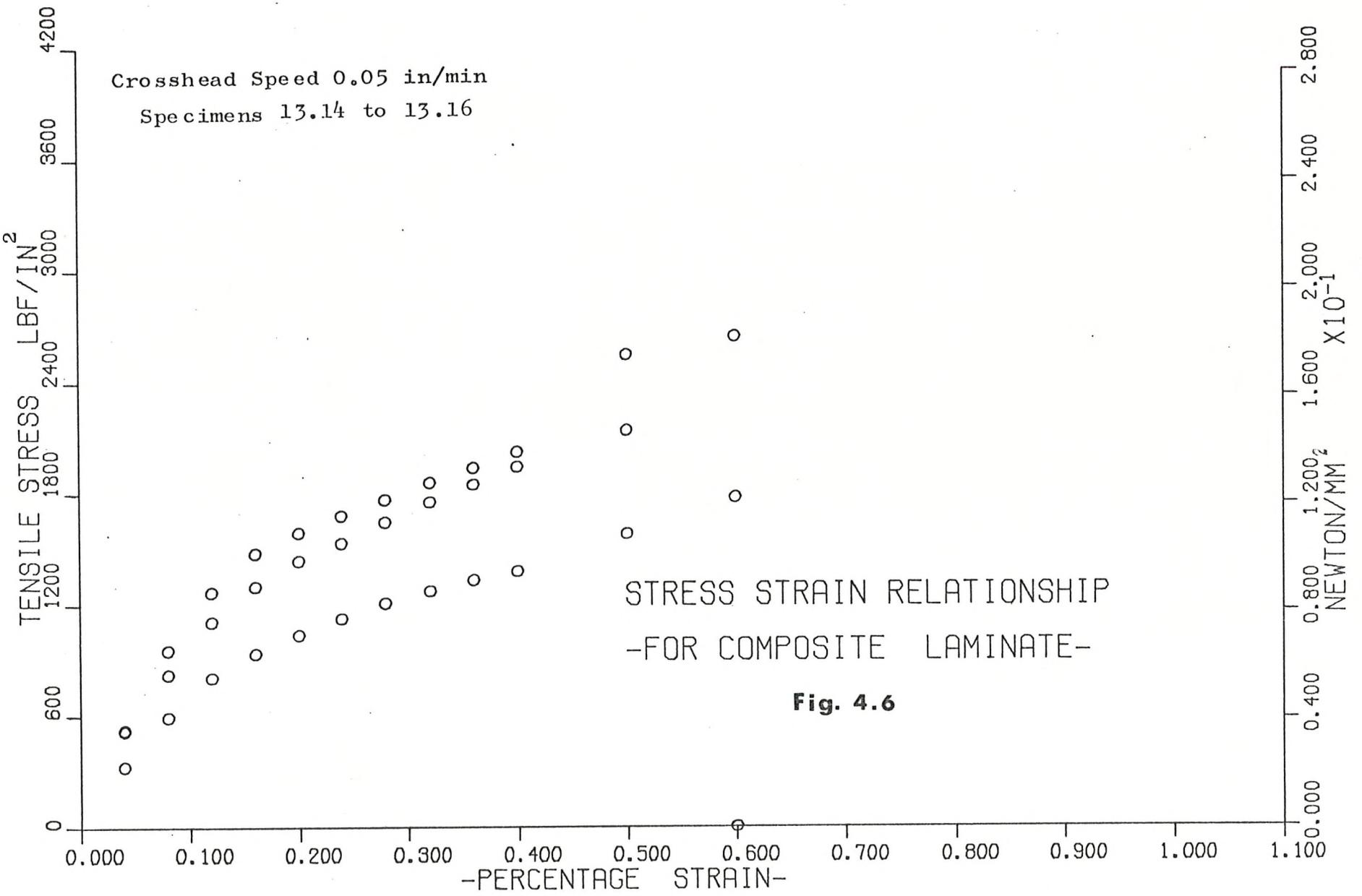
Crosshead Speed 0.05 in/min
Specimens 13.14 to 13.16
TENSILE STRESS LBF/IN^2
0
600
1200
1800
2400
3000
3600
4200
0.000
0.100
0.200
0.300
0.400
0.500
0.600
0.700
0.800
0.900
1.000
1.100
-PERCENTAGE STRAIN-
0.000
0.400
0.800
1.200
1.600
2.000
2.400
2.800
X10^{-1}
NEWTON/MM^2
STRESS STRAIN RELATIONSHIP
-FOR COMPOSITE LAMINATE-

Fig. 4.6

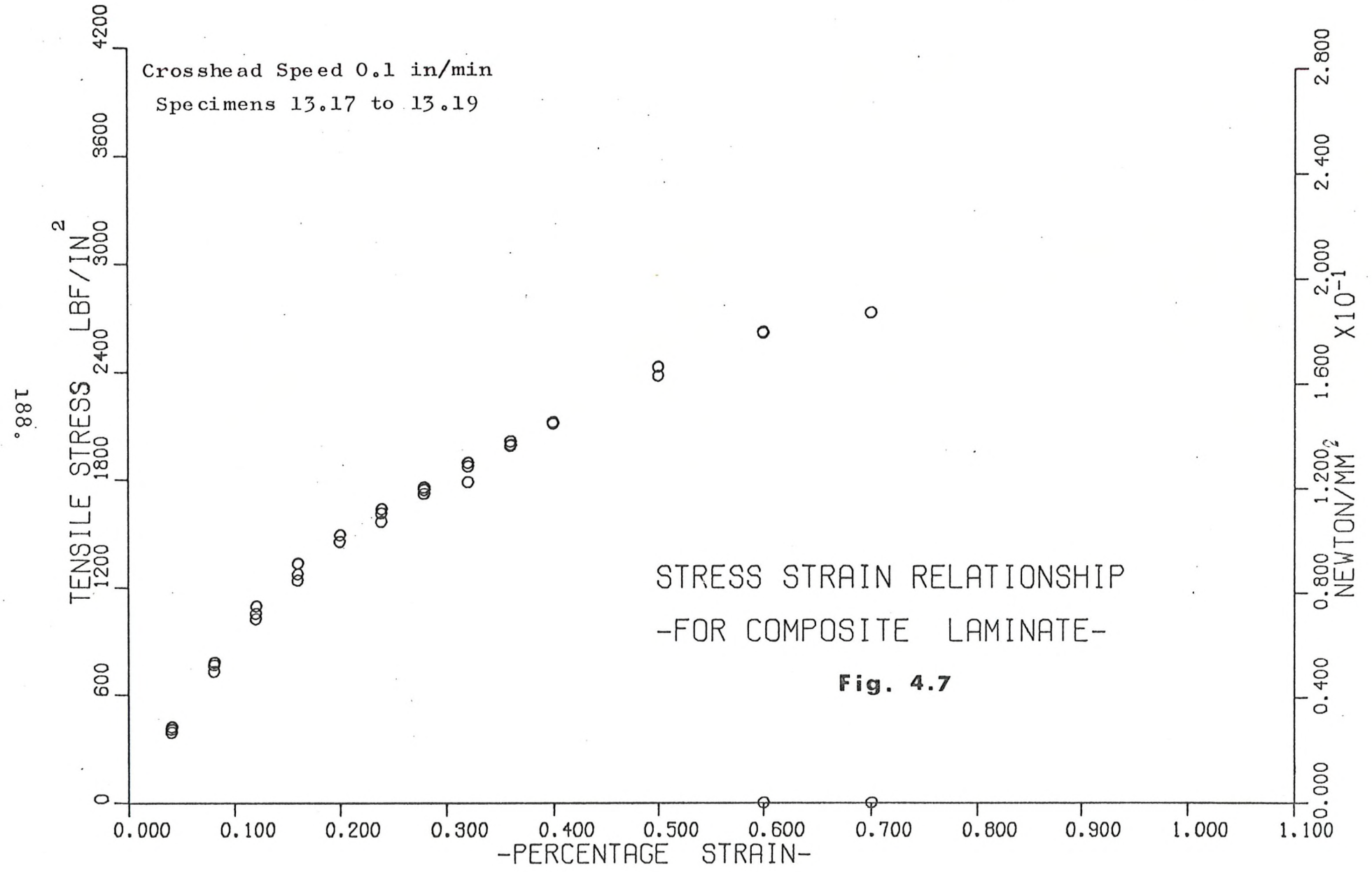
Crosshead Speed 0.1 in/min
Specimens 13.17 to 13.19
TENSILE STRESS LBF/IN2
0
600
1200
1800
2400
3000
3600
4200
0.000
0.100
0.200
0.300
0.400
0.500
0.600
0.700
0.800
0.900
1.000
1.100
-PERCENTAGE STRAIN-
0.000
0.400
0.800
1.200
1.600
2.000
2.400
2.800
X10-1
NEWTON/MM2
STRESS STRAIN RELATIONSHIP
-FOR COMPOSITE LAMINATE-

Fig. 4.7

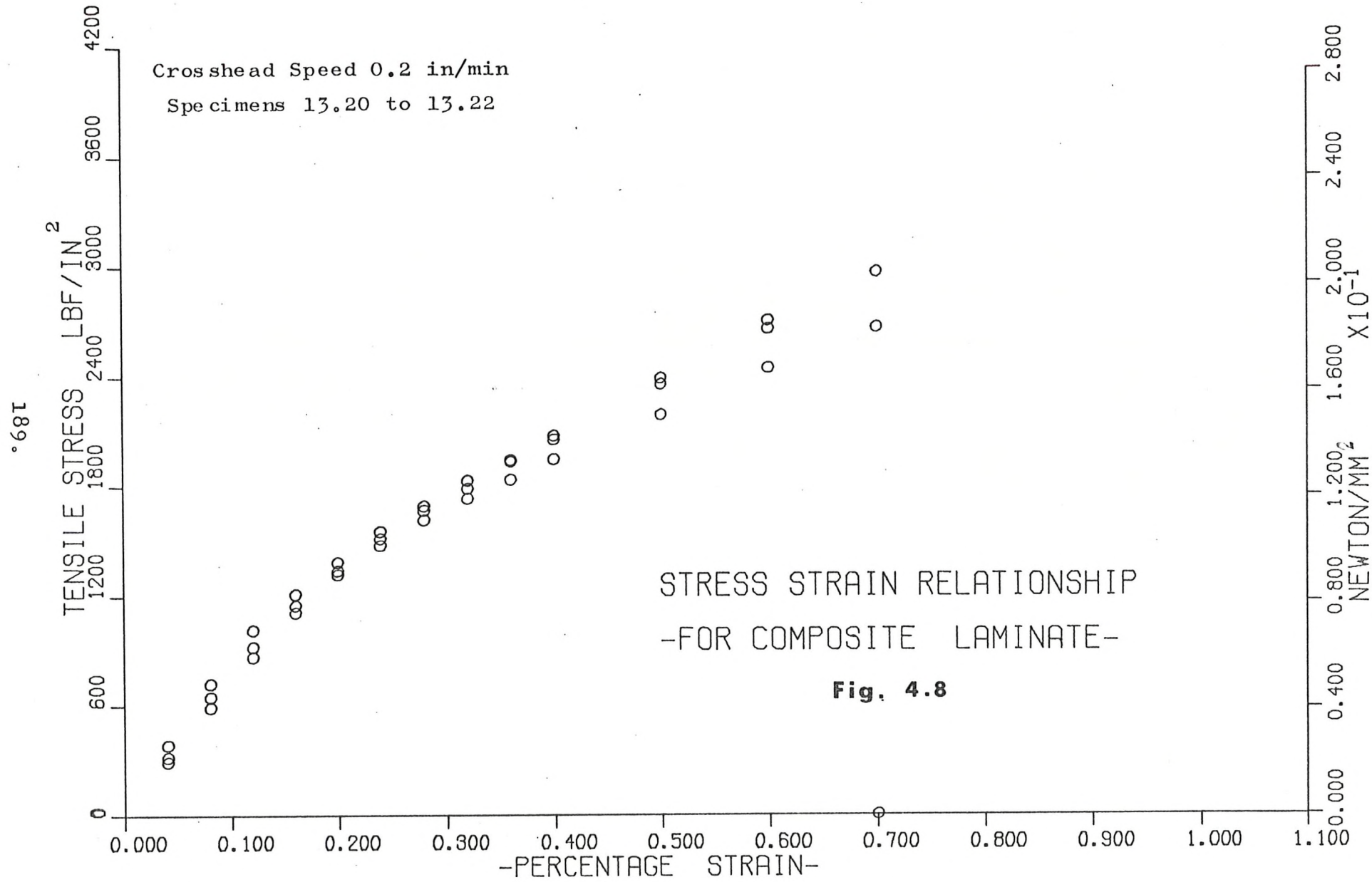

STRESS STRAIN RELATIONSHIP

-FOR COMPOSITE LAMINATE-

Fig. 4.8

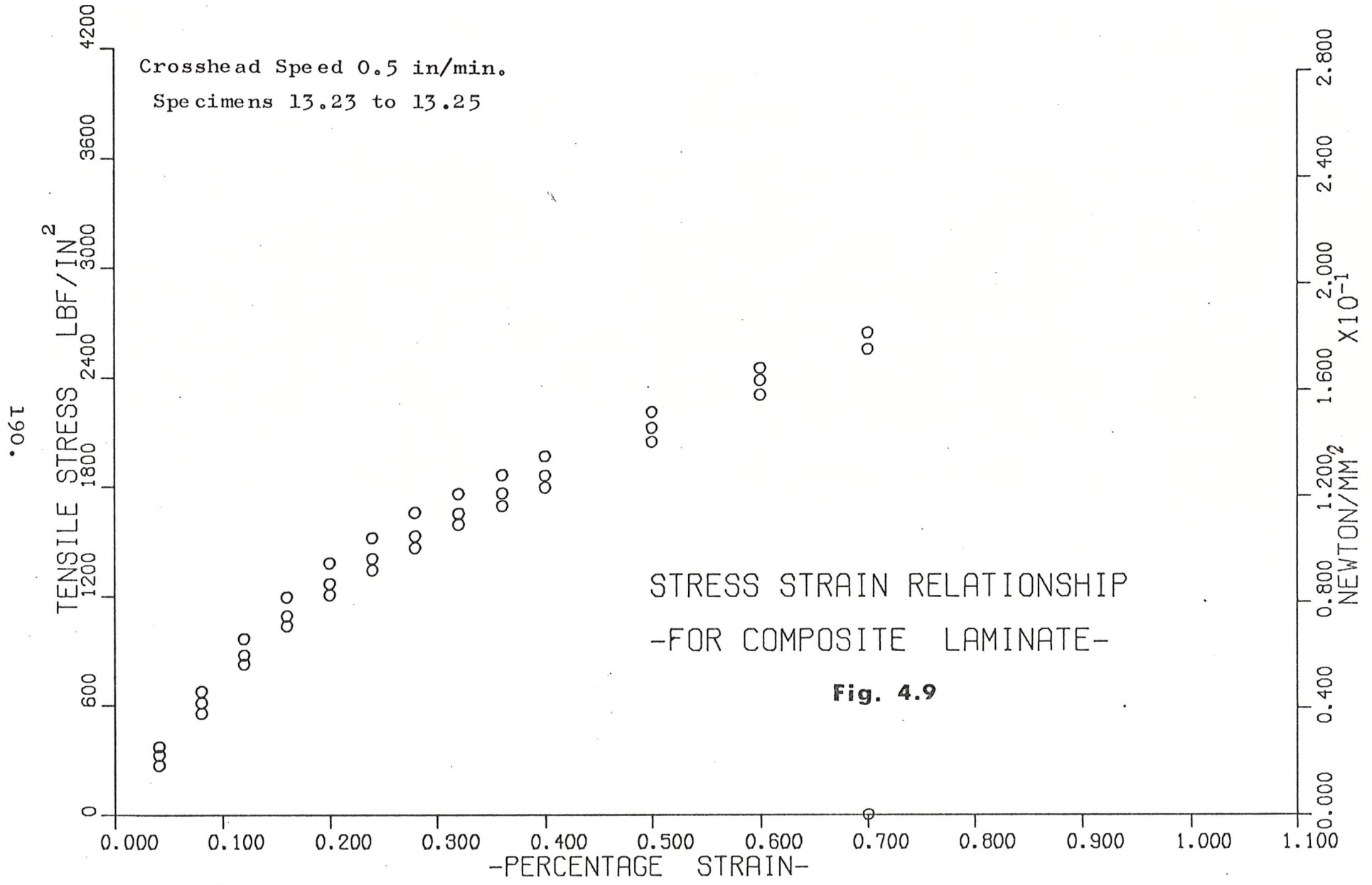
Crosshead Speed 0.5 in/min.
Specimens 13.23 to 13.25
TENSILE STRESS LBF/IN2
NEWTON/MM2
X10-1
-PERCENTAGE STRAIN-
0
600
1200
1800
2400
3600
4200
0.000
0.100
0.200
0.300
0.400
0.500
0.600
0.700
0.800
0.900
1.000
1.100
0.400
0.800
1.200
1.600
2.000
2.400
2.800
STRESS STRAIN RELATIONSHIP
-FOR COMPOSITE LAMINATE-

Fig. 4.9

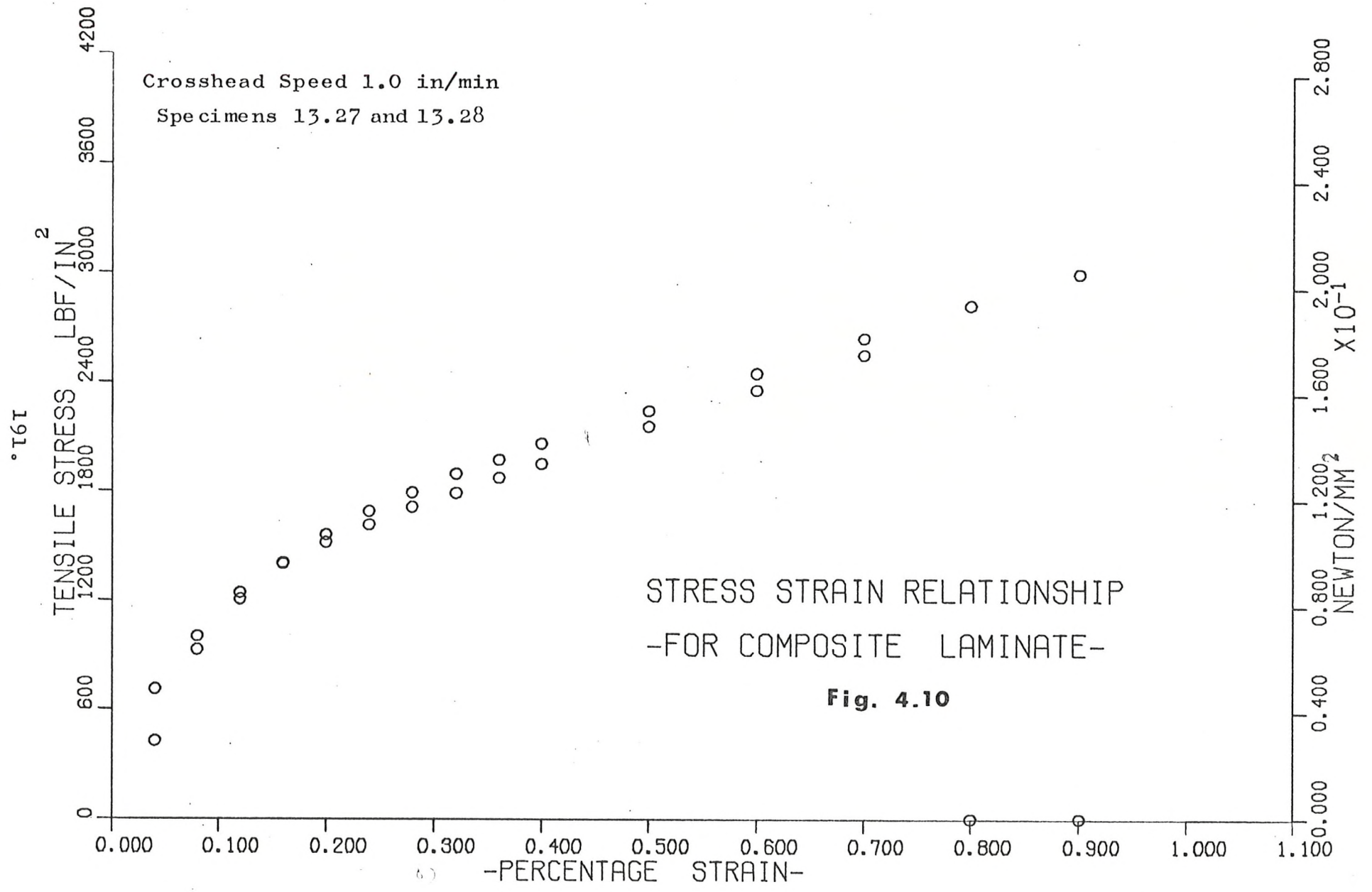
Crosshead Speed 1.0 in/min
Specimens 13.27 and 13.28
TENSILE STRESS LBF/IN2
0
600
1200
1800
2400
3000
3600
4200
0.000
0.100
0.200
0.300
0.400
0.500
0.600
0.700
0.800
0.900
1.000
1.100
-PERCENTAGE STRAIN-
NEWTON/MM2 X10-1
0.000
0.400
0.800
1.200
1.600
2.000
2.400
2.800
STRESS STRAIN RELATIONSHIP
-FOR COMPOSITE LAMINATE-

Fig. 4.10

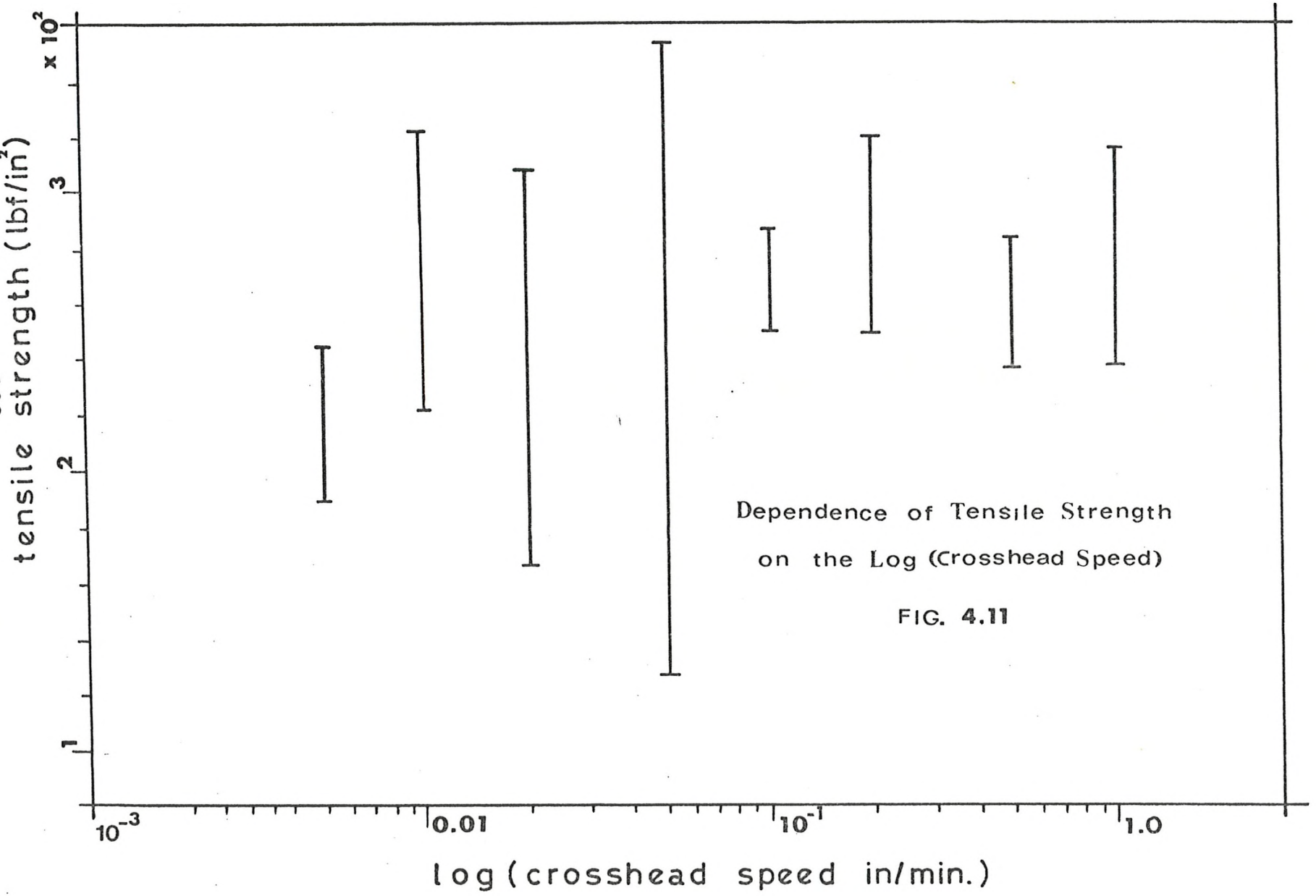

Dependence of Tensile Strength on the Log (Crosshead Speed)

FIG. 4.11

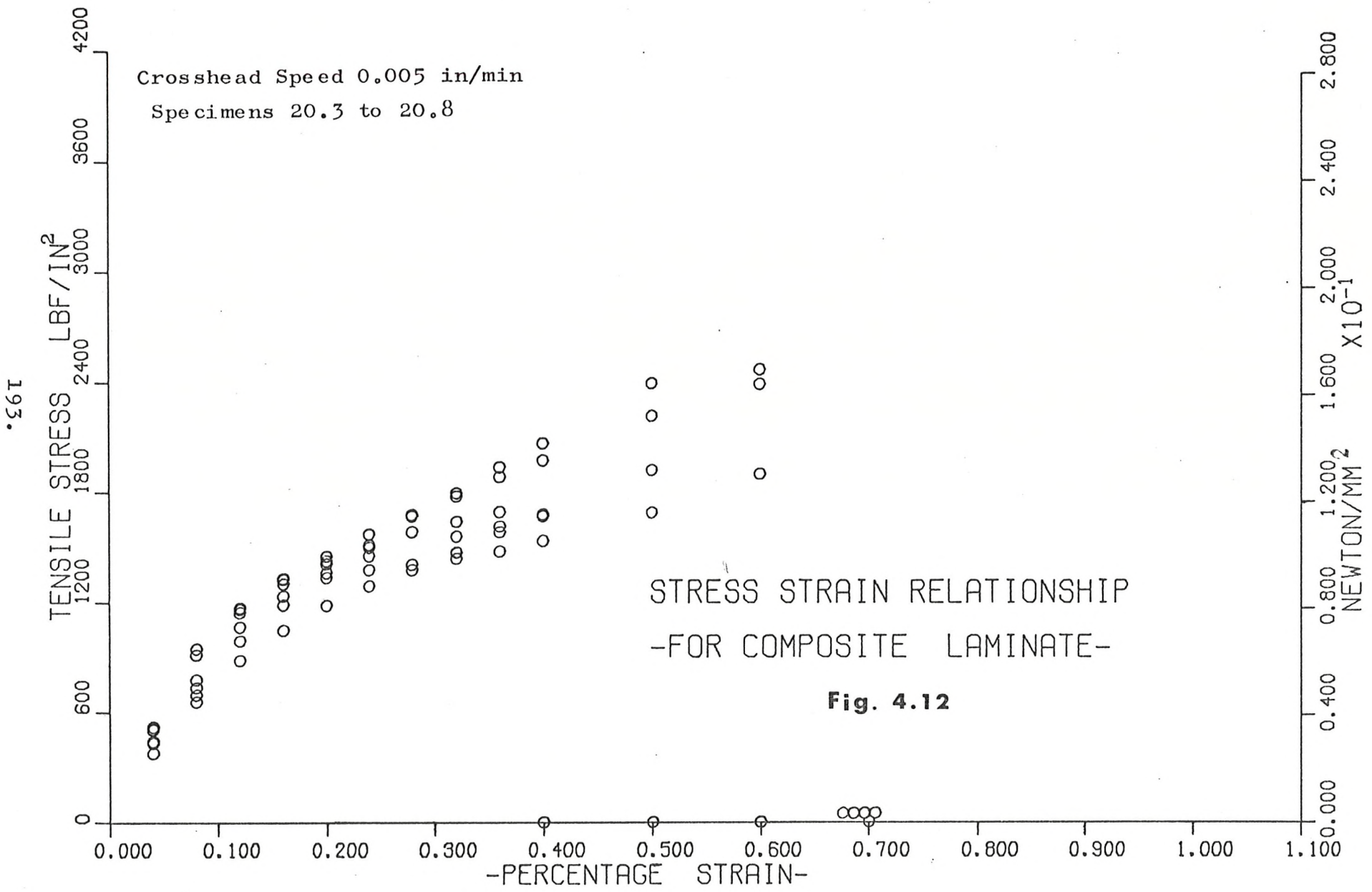

STRESS STRAIN RELATIONSHIP

-FOR COMPOSITE LAMINATE-

Fig. 4.12

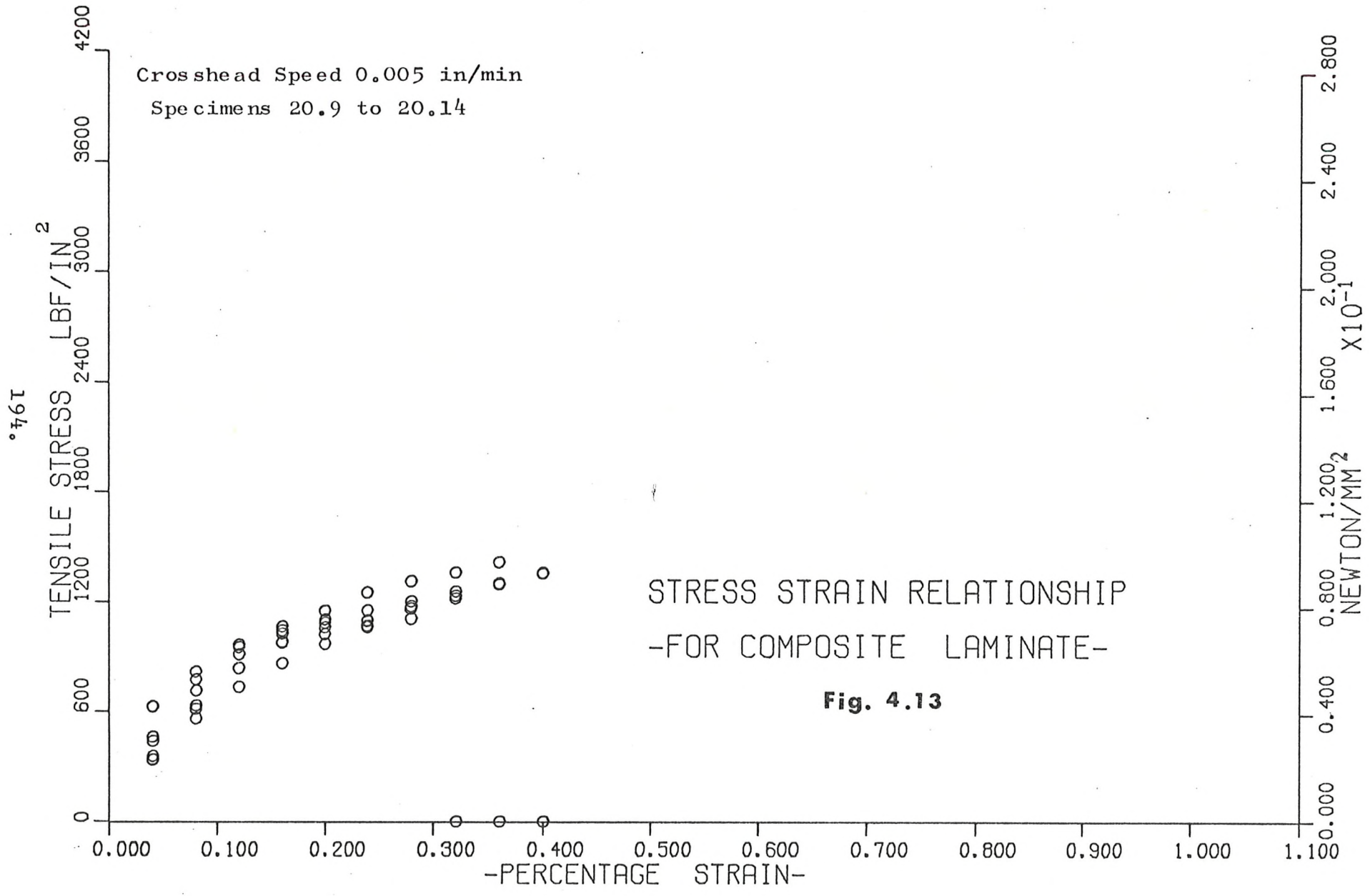

STRESS STRAIN RELATIONSHIP

-FOR COMPOSITE LAMINATE-

Fig. 4.13

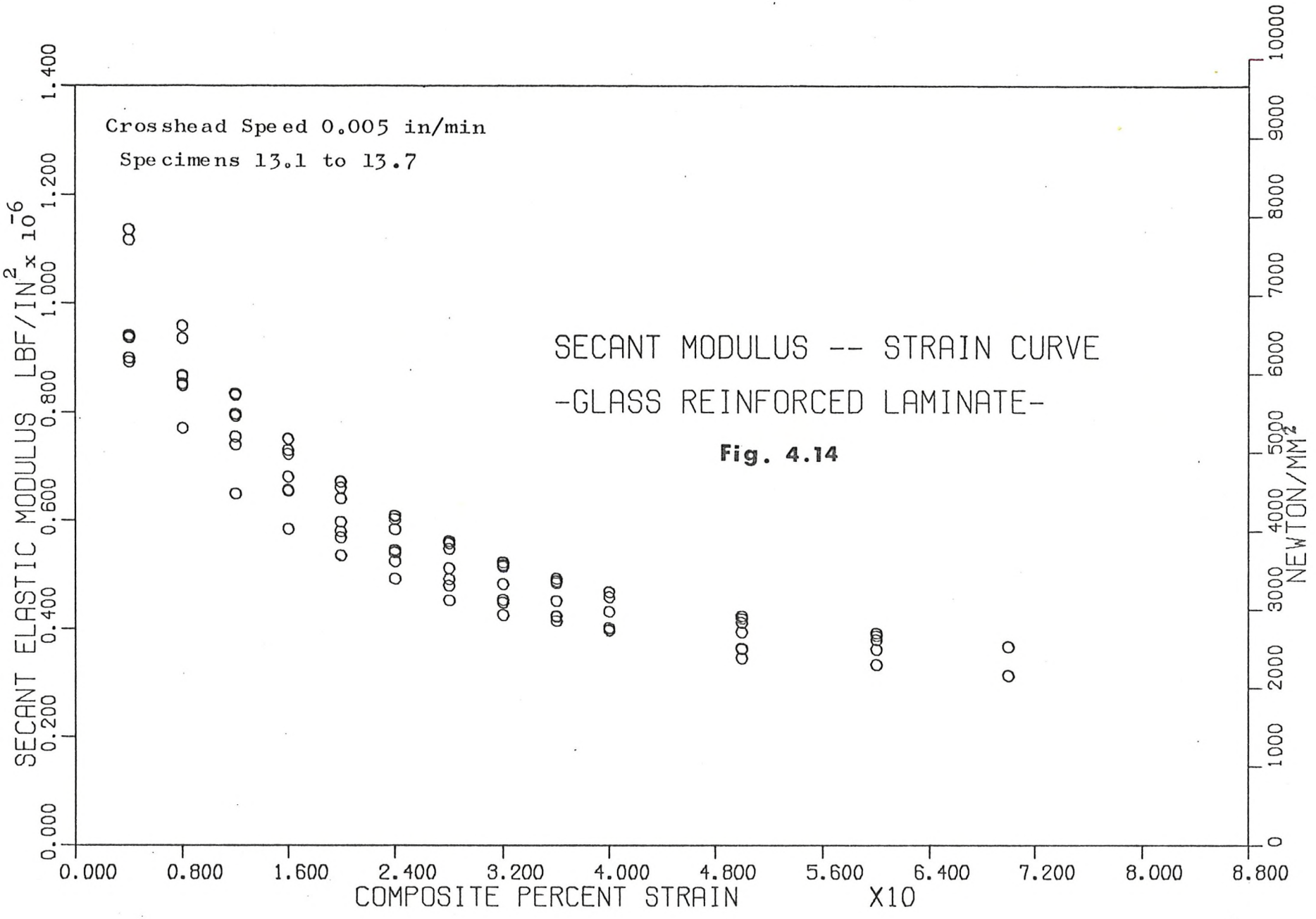
Crosshead Speed 0.005 in/min
Specimens 13.1 to 13.7
SECANT MODULUS -- STRAIN CURVE
-GLASS REINFORCED LAMINATE-
Fig. 4.14
SECANT ELASTIC MODULUS LBF/IN^2 x 10^{-6}
NEWTON/MM^2
COMPOSITE PERCENT STRAIN X10
0.000
0.200
0.400
0.600
0.800
1.000
1.200
1.400
0
1000
2000
3000
4000
5000
6000
7000
8000
9000
10000
0.000
0.800
1.600
2.400
3.200
4.000
4.800
5.600
6.400
7.200
8.000
8.800

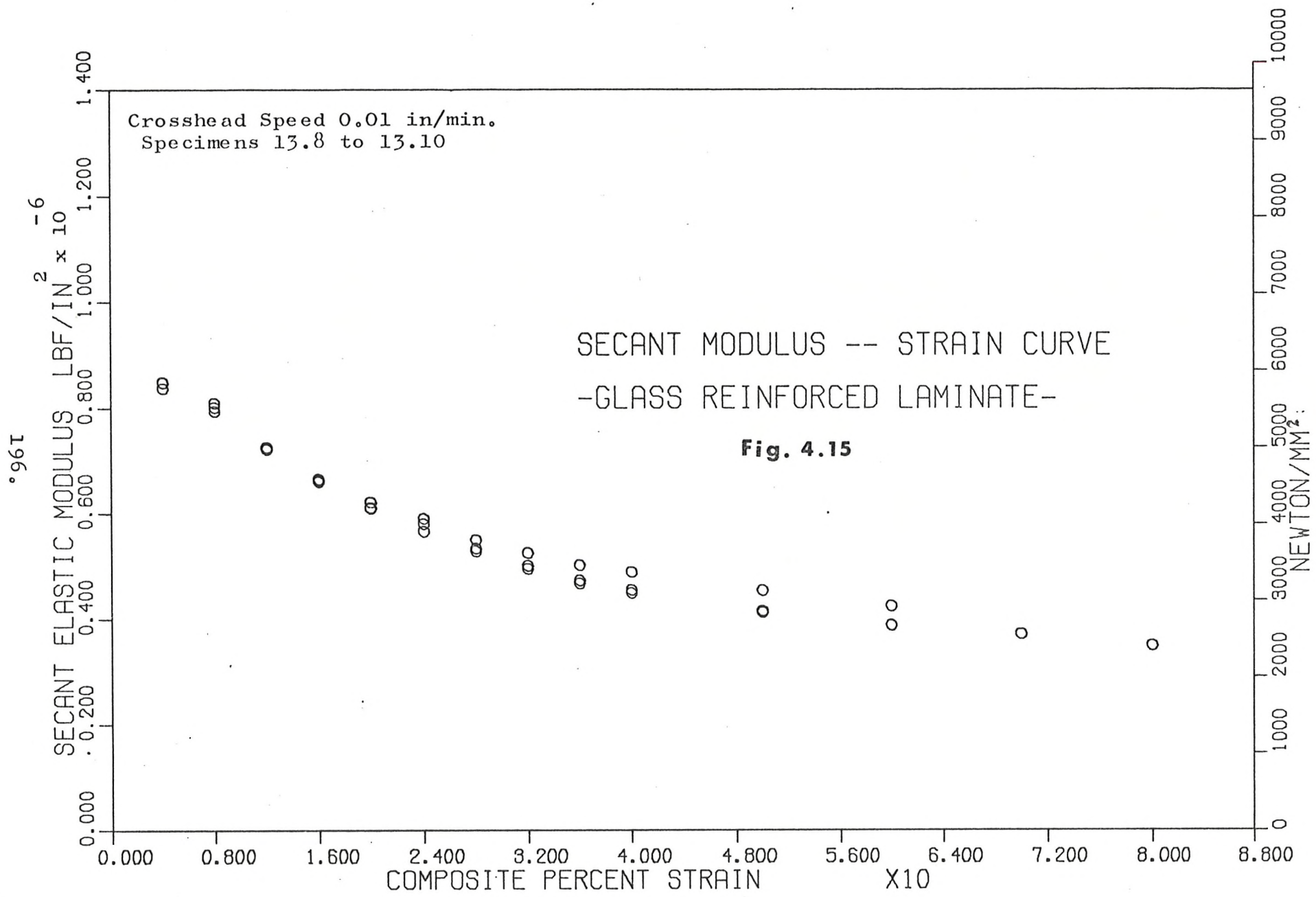
Crosshead Speed 0.01 in/min.
Specimens 13.8 to 13.10
SECANT MODULUS -- STRAIN CURVE
-GLASS REINFORCED LAMINATE-
Fig. 4.15
SECANT ELASTIC MODULUS LBF/IN^2 x 10^{-6}
NEWTON/MM^2
COMPOSITE PERCENT STRAIN X10
0.000
0.200
0.400
0.600
0.800
1.000
1.200
1.400
0
1000
2000
3000
4000
5000
6000
7000
8000
9000
10000
0.000
0.800
1.600
2.400
3.200
4.000
4.800
5.600
6.400
7.200
8.000
8.800

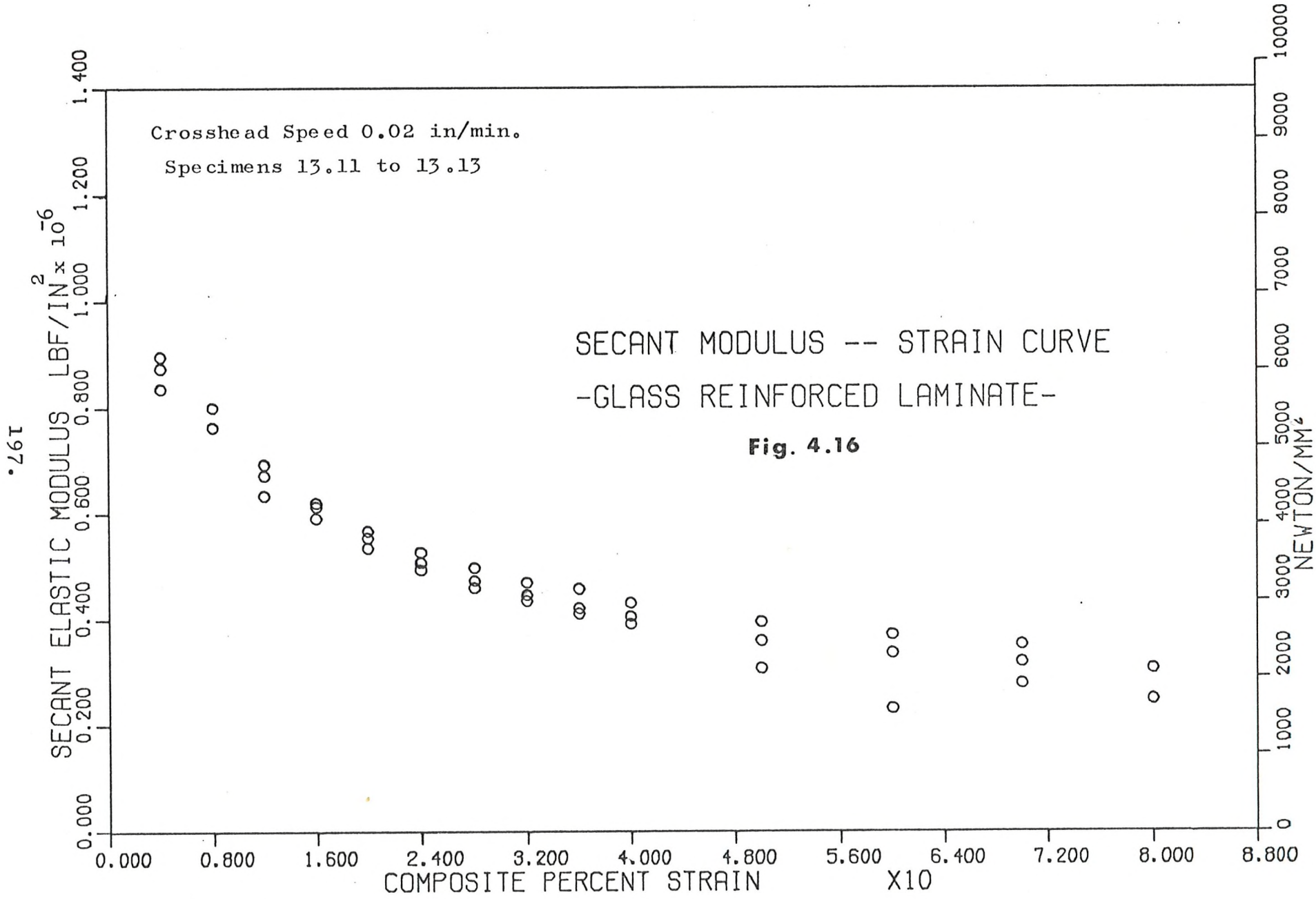
Crosshead Speed 0.02 in/min.
Specimens 13.11 to 13.13
SECANT MODULUS -- STRAIN CURVE
-GLASS REINFORCED LAMINATE-
Fig. 4.16
SECANT ELASTIC MODULUS LBF/IN^2 x 10^{-6}
NEWTON/MM^2
COMPOSITE PERCENT STRAIN X10
0.000
0.200
0.400
0.600
0.800
1.000
1.200
1.400
0
1000
2000
3000
4000
5000
6000
7000
8000
9000
10000
0.000
0.800
1.600
2.400
3.200
4.000
4.800
5.600
6.400
7.200
8.000
8.800

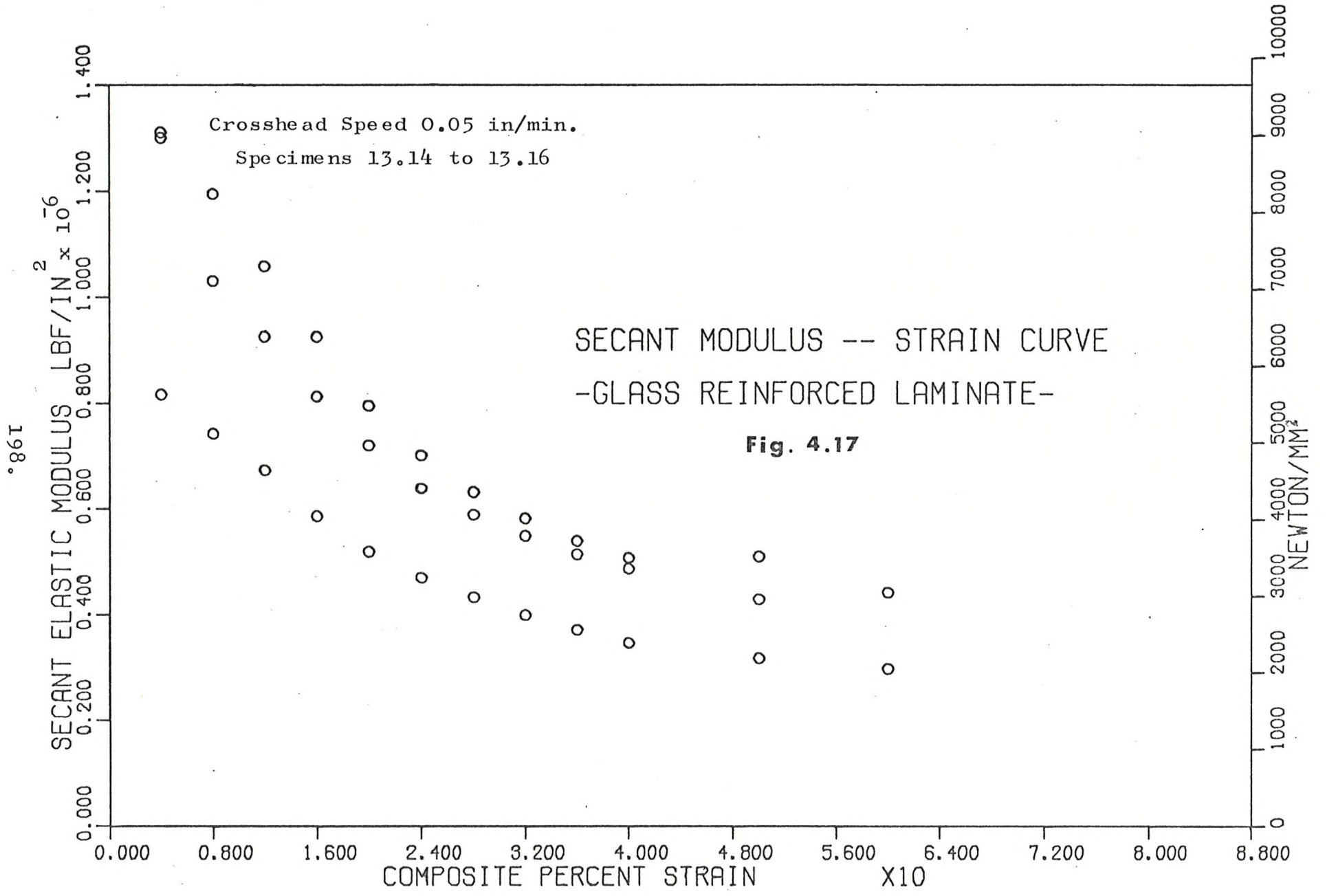
Crosshead Speed 0.05 in/min.
Specimens 13.14 to 13.16
SECANT MODULUS -- STRAIN CURVE
-GLASS REINFORCED LAMINATE-
Fig. 4.17
SECANT ELASTIC MODULUS LBF/IN^2 x 10^{-6}
NEWTON/MM^2
COMPOSITE PERCENT STRAIN X10
0.000
0.200
0.400
0.600
0.800
1.000
1.200
1.400
0
1000
2000
3000
4000
5000
6000
7000
8000
9000
10000
0.000
0.800
1.600
2.400
3.200
4.000
4.800
5.600
6.400
7.200
8.000
8.800
1981

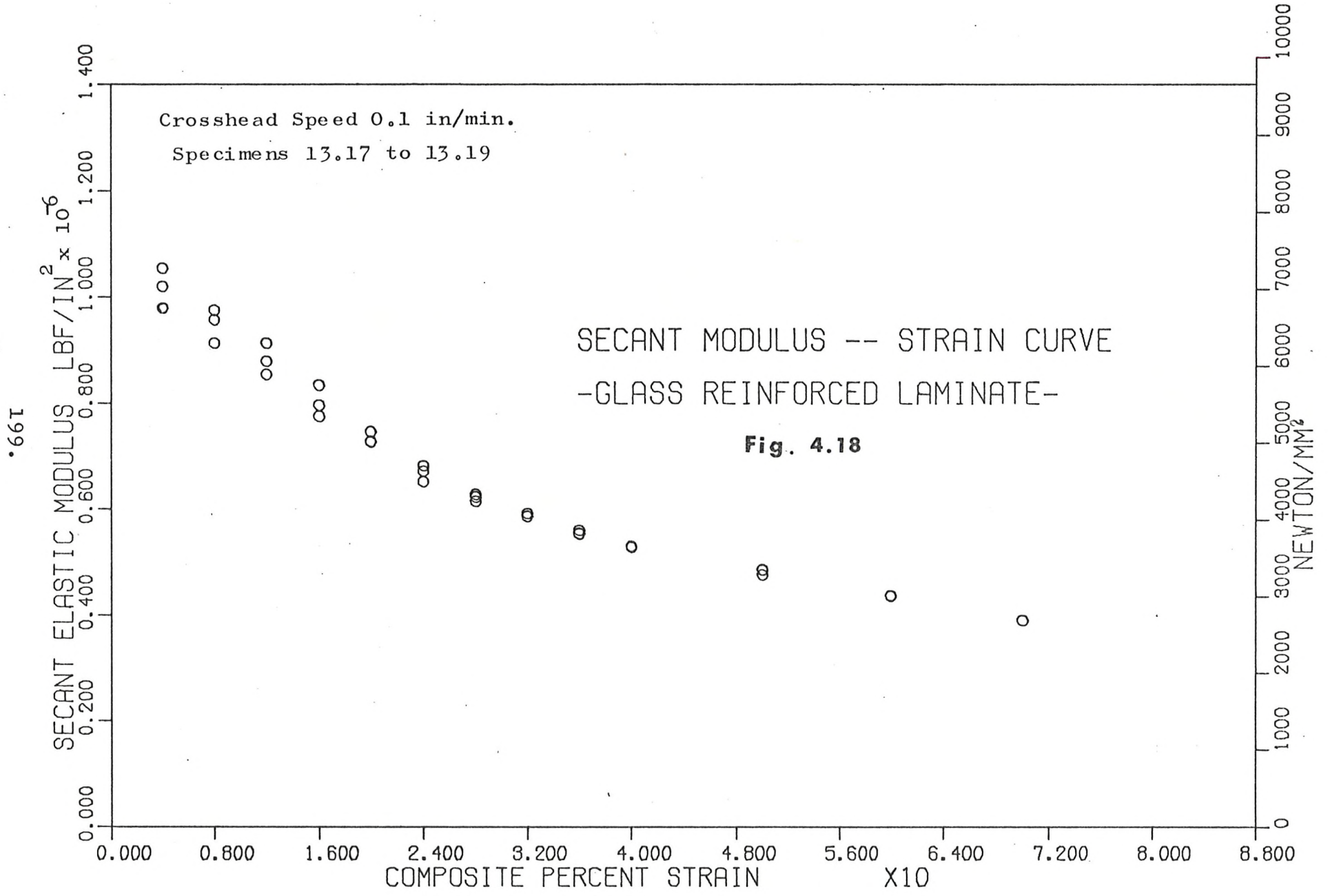
Crosshead Speed 0.1 in/min.
Specimens 13.17 to 13.19
SECANT MODULUS -- STRAIN CURVE
-GLASS REINFORCED LAMINATE-
Fig. 4.18
SECANT ELASTIC MODULUS LBF/IN^2 x 10^{-6}
NEWTON/MM^2
COMPOSITE PERCENT STRAIN X10
0.000
0.200
0.400
0.600
0.800
1.000
1.200
1.400
0
1000
2000
3000
4000
5000
6000
7000
8000
9000
10000
0.000
0.800
1.600
2.400
3.200
4.000
4.800
5.600
6.400
7.200
8.000
8.800

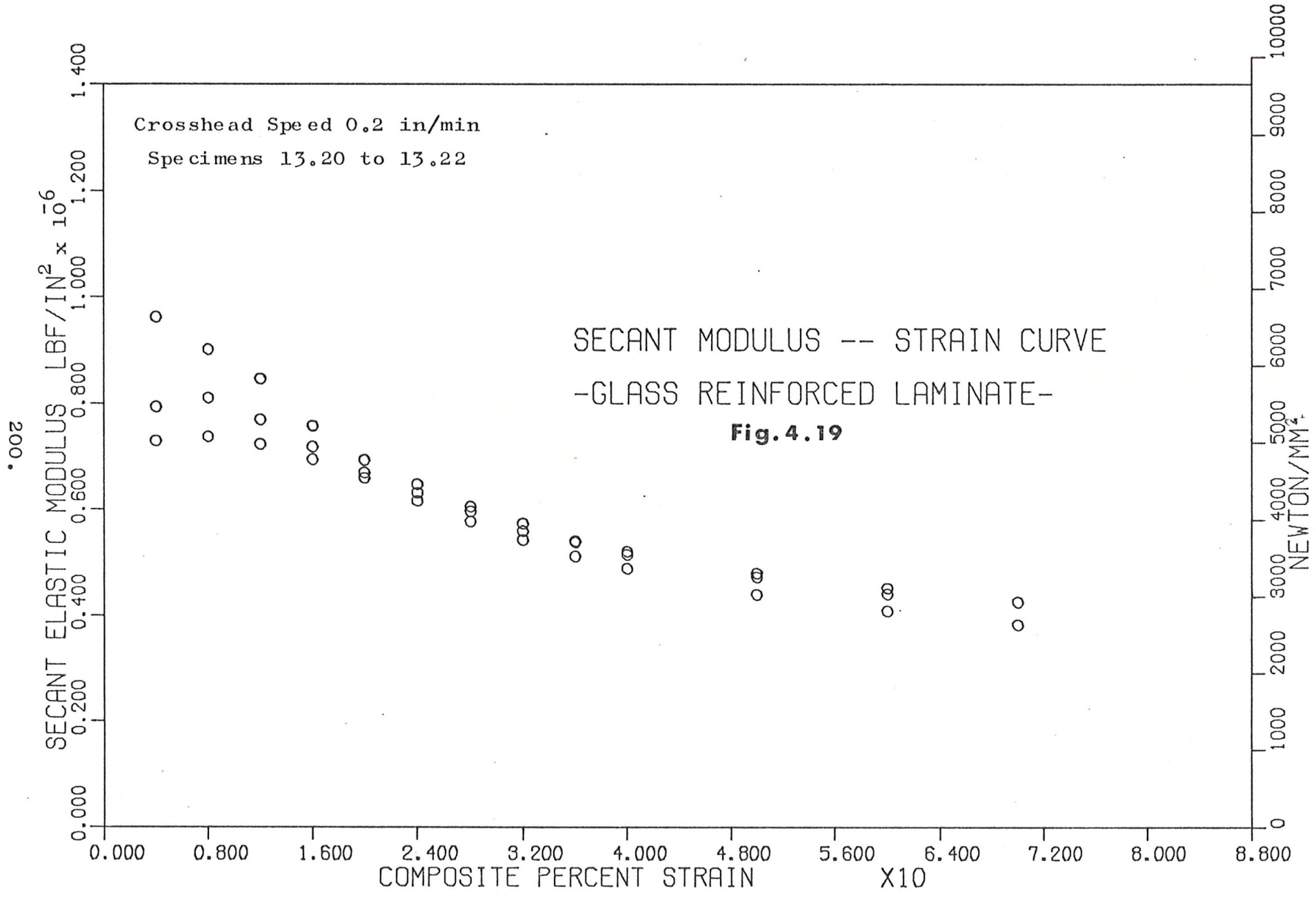
Crosshead Speed 0.2 in/min
Specimens 13.20 to 13.22
SECANT MODULUS -- STRAIN CURVE
-GLASS REINFORCED LAMINATE-
Fig.4.19
SECANT ELASTIC MODULUS LBF/IN^2 x 10^{-6}
NEWTON/MM^2
COMPOSITE PERCENT STRAIN X10
0.000
0.200
0.400
0.600
0.800
1.000
1.200
1.400
0
1000
2000
3000
4000
5000
6000
7000
8000
9000
10000
0.000
0.800
1.600
2.400
3.200
4.000
4.800
5.600
6.400
7.200
8.000
8.800

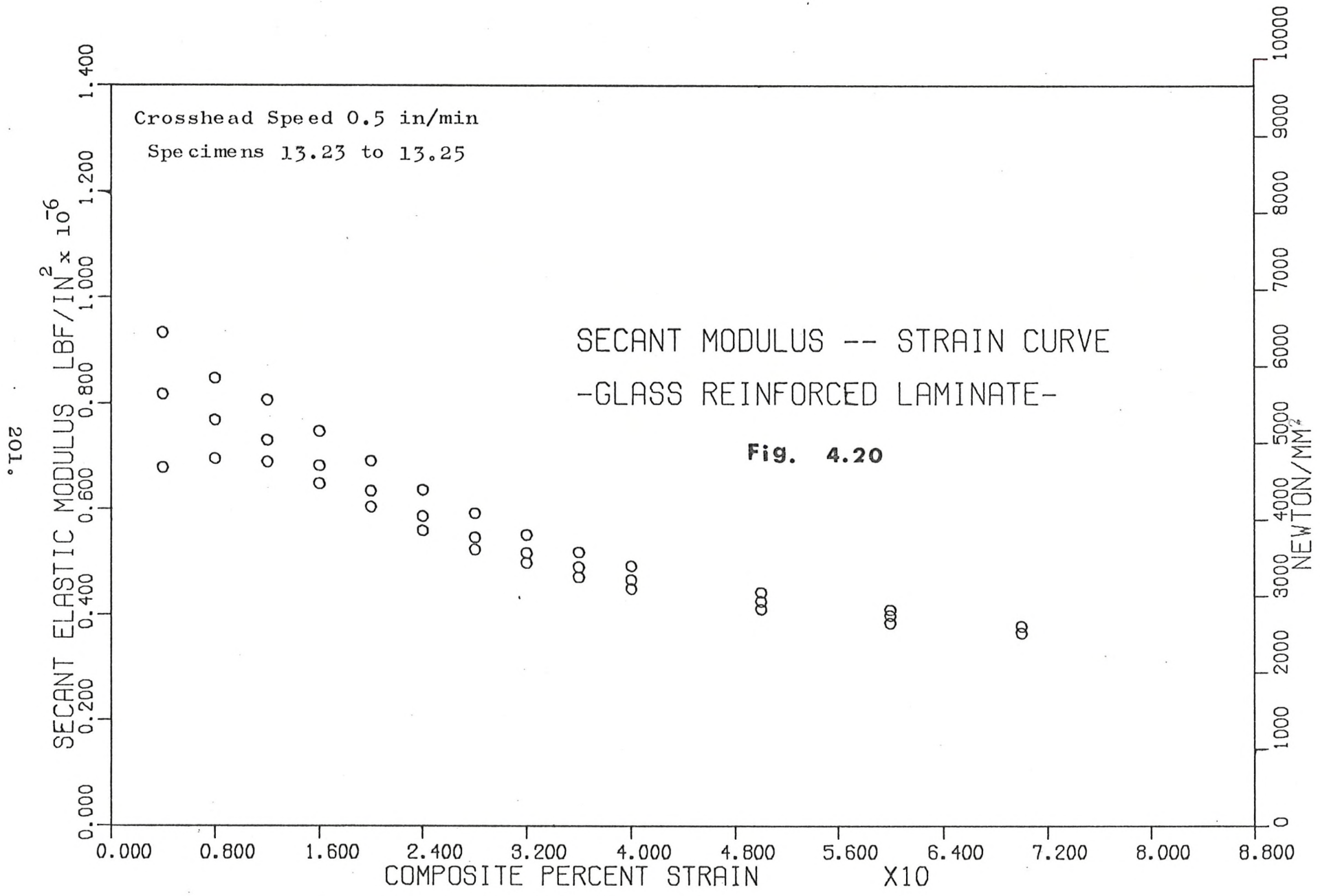
Crosshead Speed 0.5 in/min
Specimens 13.23 to 13.25
SECANT MODULUS -- STRAIN CURVE
-GLASS REINFORCED LAMINATE-
Fig. 4.20
SECANT ELASTIC MODULUS LBF/IN^2 x 10^{-6}
NEWTON/MM^2
COMPOSITE PERCENT STRAIN X10
0.000
0.200
0.400
0.600
0.800
1.000
1.200
1.400
0
1000
2000
3000
4000
5000
6000
7000
8000
9000
10000
0.000
0.800
1.600
2.400
3.200
4.000
4.800
5.600
6.400
7.200
8.000
8.800

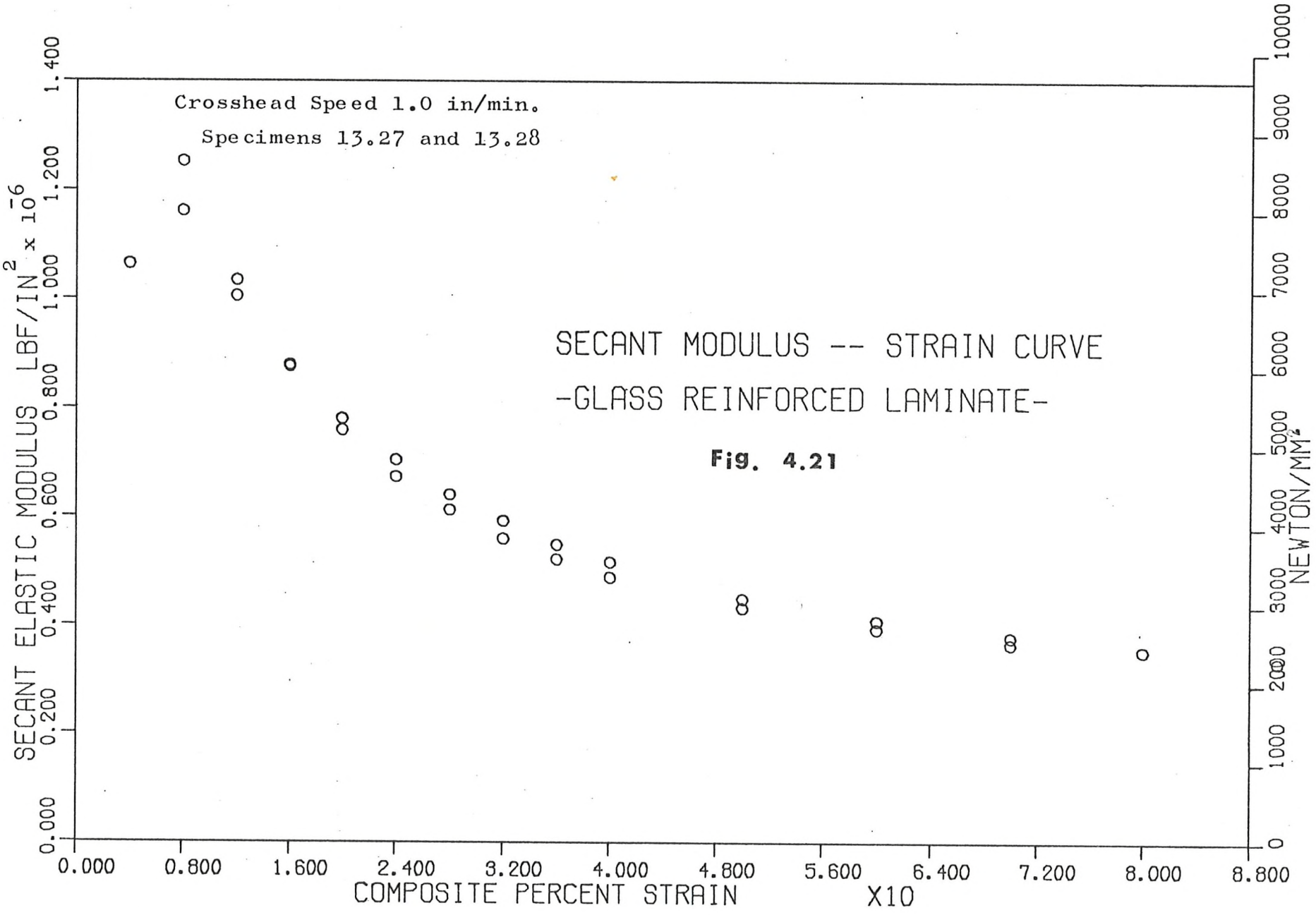
Crosshead Speed 1.0 in/min.
Specimens 13.27 and 13.28
SECANT MODULUS -- STRAIN CURVE
-GLASS REINFORCED LAMINATE-
SECANT ELASTIC MODULUS LBF/IN^2 x 10^{-6}
NEWTON/MM^2
COMPOSITE PERCENT STRAIN
X10
0.000
0.200
0.400
0.600
0.800
1.000
1.200
1.400
0
1000
2000
3000
4000
5000
6000
7000
8000
9000
10000
0.000
0.800
1.600
2.400
3.200
4.000
4.800
5.600
6.400
7.200
8.000
8.800

Fig. 4.21

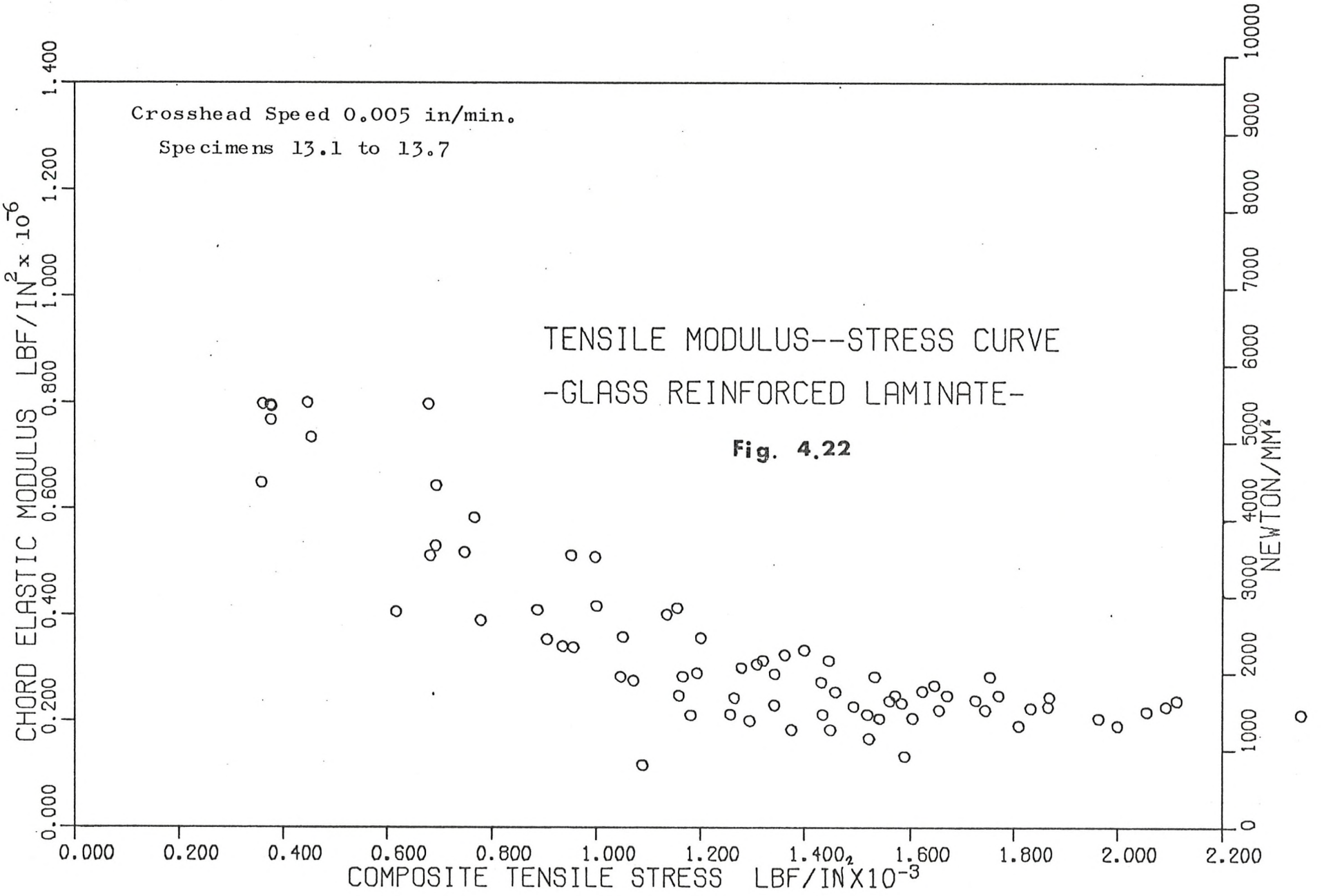
Crosshead Speed 0.005 in/min.
Specimens 13.1 to 13.7
TENSILE MODULUS--STRESS CURVE
-GLASS REINFORCED LAMINATE-
CHORD ELASTIC MODULUS LBF/IN^2 x 10^6
NEWTON/MM^2
COMPOSITE TENSILE STRESS LBF/INX10^{-3}
0.000
0.200
0.400
0.600
0.800
1.000
1.200
1.400
1.600
1.800
2.000
2.200
0
1000
2000
3000
4000
5000
6000
7000
8000
9000
10000

Fig. 4.22

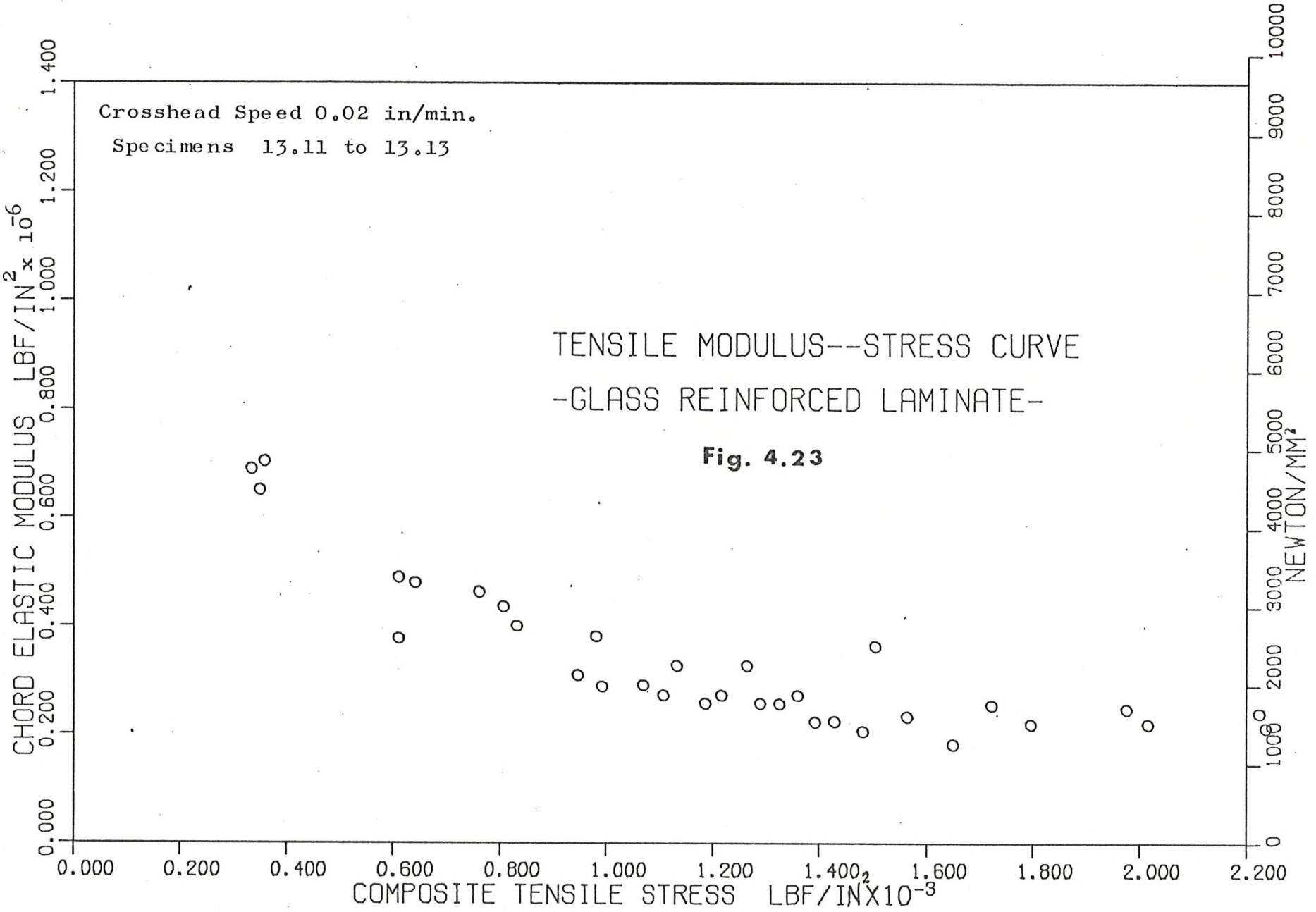
Crosshead Speed 0.02 in/min.
Specimens 13.11 to 13.13
TENSILE MODULUS--STRESS CURVE
-GLASS REINFORCED LAMINATE-
CHORD ELASTIC MODULUS LBF/IN^2 x 10^{-6}
COMPOSITE TENSILE STRESS LBF/INX10^{-3}
NEWTON/MM^2
0.000
0.200
0.400
0.600
0.800
1.000
1.200
1.400
1.600
1.800
2.000
2.200
0
1000
2000
3000
4000
5000
6000
7000
8000
9000
10000

Fig. 4.23

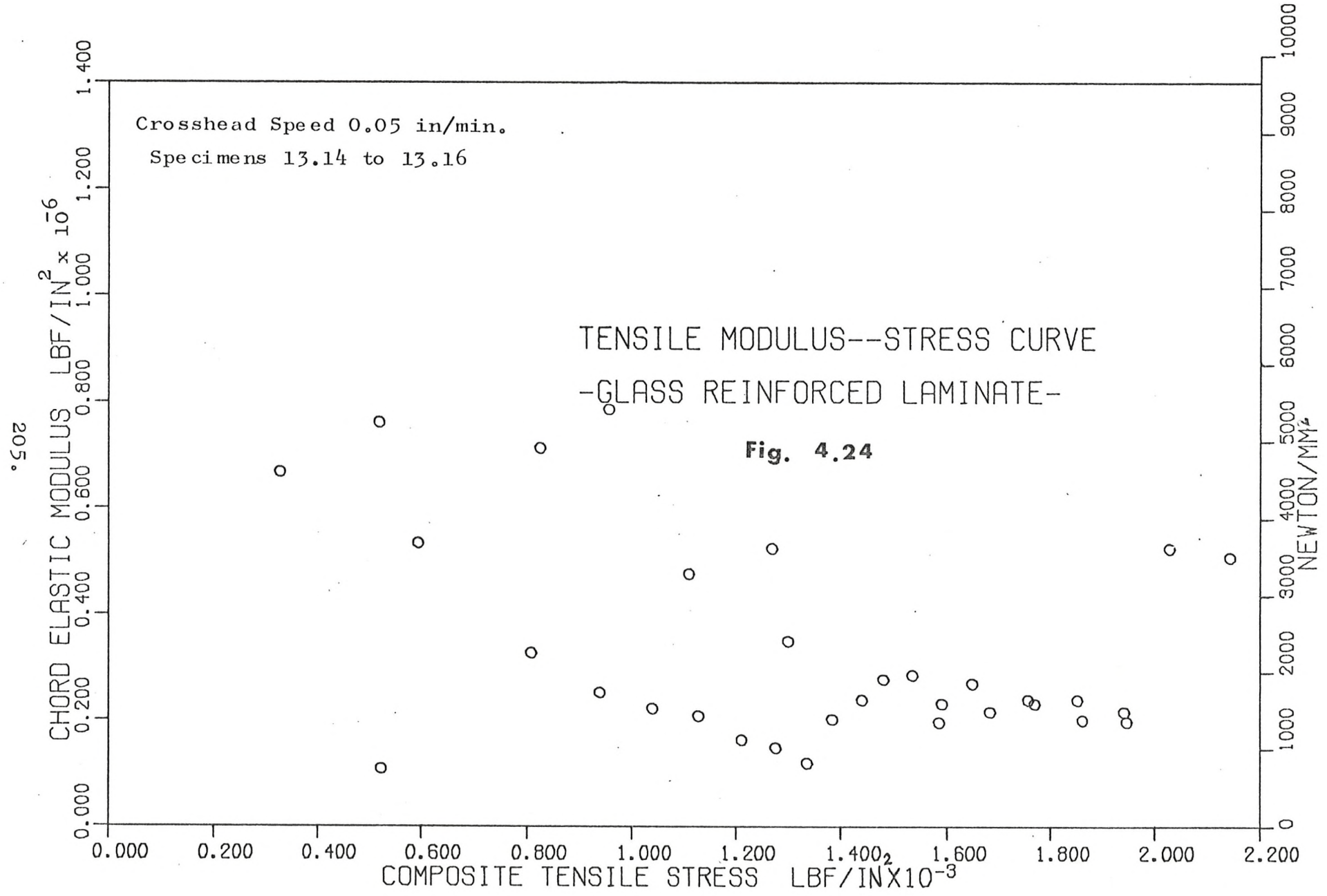
Crosshead Speed 0.05 in/min.
Specimens 13.14 to 13.16
TENSILE MODULUS--STRESS CURVE
-GLASS REINFORCED LAMINATE-
Fig. 4.24
205.
CHORD ELASTIC MODULUS LBF/IN^2 x 10^{-6}
0.000
0.200
0.400
0.600
0.800
1.000
1.200
1.400
NEWTON/MM^2
0
1000
2000
3000
4000
5000
6000
7000
8000
9000
10000
0.000
0.200
0.400
0.600
0.800
1.000
1.200
1.400
1.600
1.800
2.000
2.200
COMPOSITE TENSILE STRESS LBF/INX10^{-3}

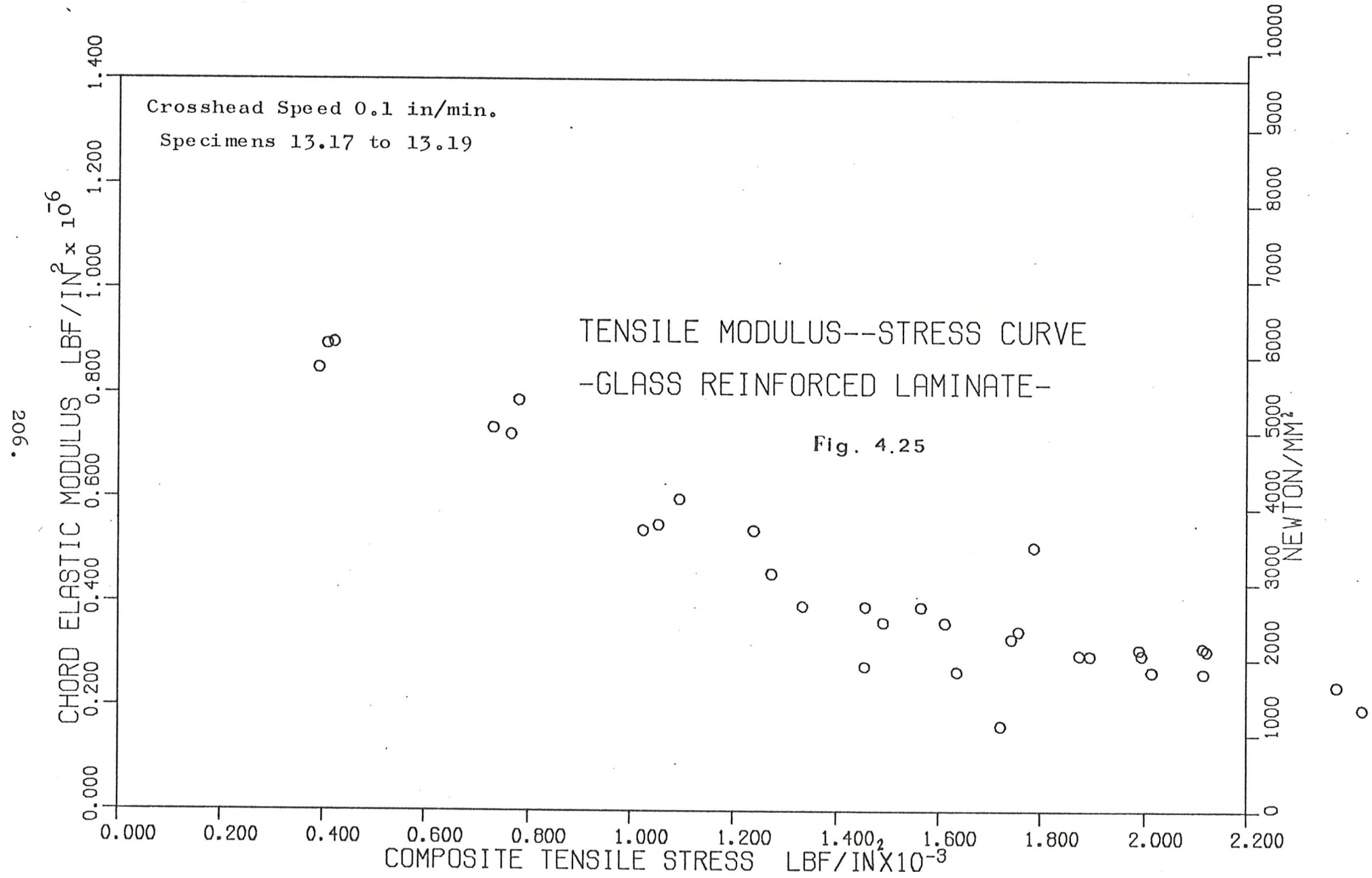
Crosshead Speed 0.1 in/min.
Specimens 13.17 to 13.19
TENSILE MODULUS--STRESS CURVE
-GLASS REINFORCED LAMINATE-
CHORD ELASTIC MODULUS LBF/IN^2 x 10^{-6}
NEWTON/MM^2
COMPOSITE TENSILE STRESS LBF/INX10^{-3}
0.000
0.200
0.400
0.600
0.800
1.000
1.200
1.400
1.600
1.800
2.000
2.200
0
1000
2000
3000
4000
5000
6000
7000
8000
9000
10000

Fig. 4.25

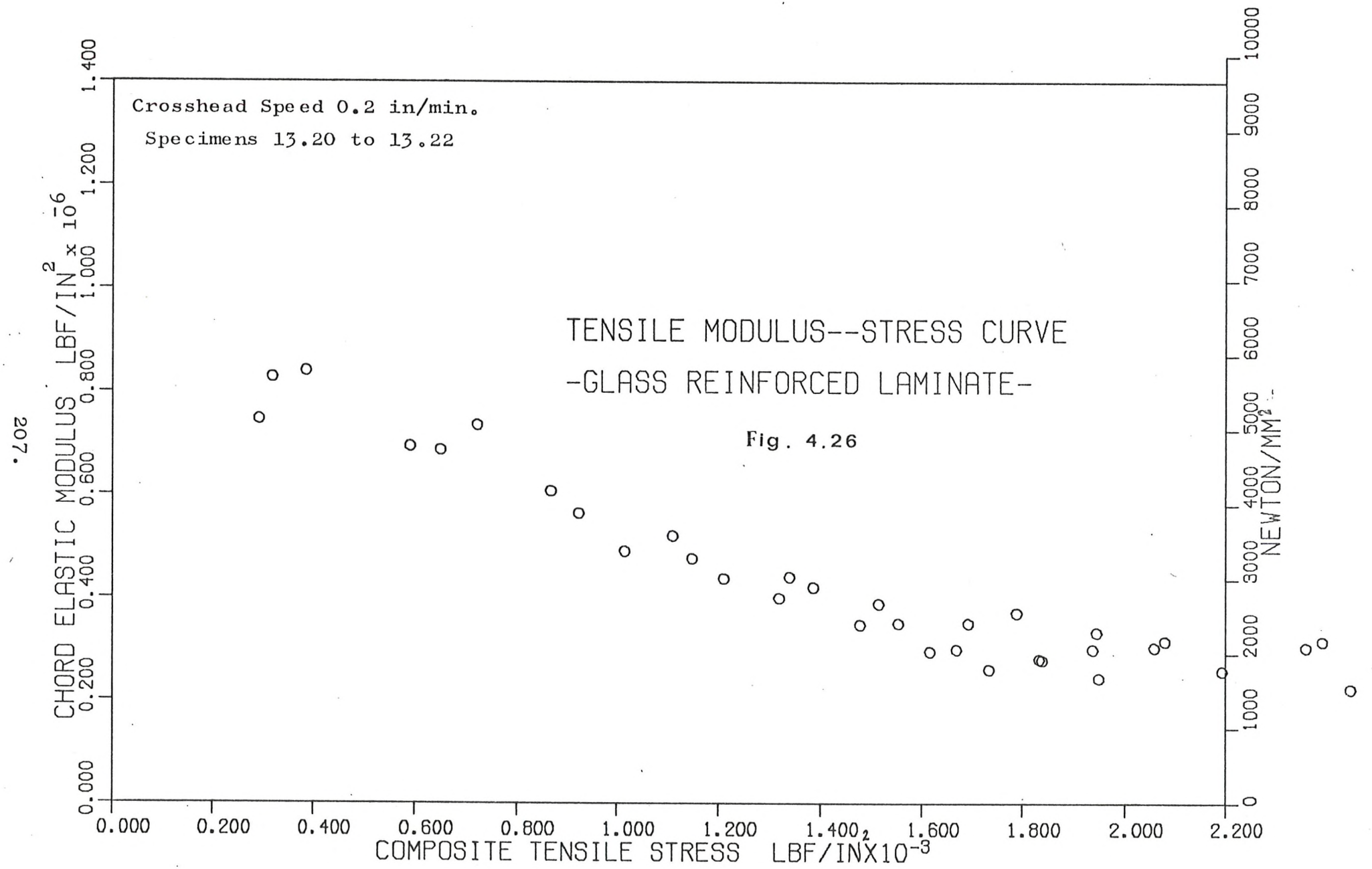
Crosshead Speed 0.2 in/min.
Specimens 13.20 to 13.22
TENSILE MODULUS--STRESS CURVE
-GLASS REINFORCED LAMINATE-
CHORD ELASTIC MODULUS LBF/IN^2 x 10^{-6}
NEWTON/MM^2
COMPOSITE TENSILE STRESS LBF/INX10^{-3}
0.000
0.200
0.400
0.600
0.800
1.000
1.200
1.400
1.600
1.800
2.000
2.200
0
1000
2000
3000
4000
5000
6000
7000
8000
9000
10000

Fig. 4.26

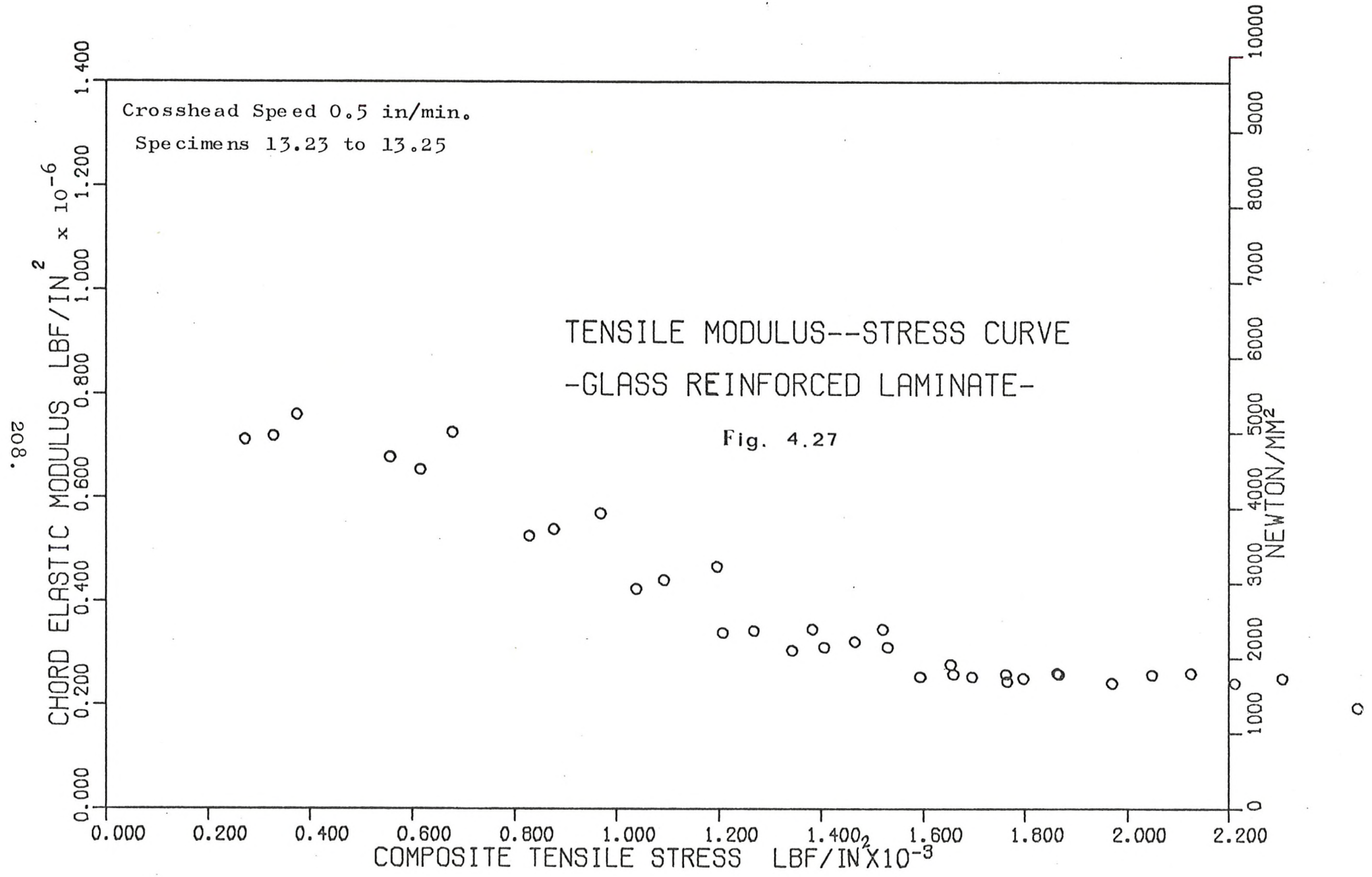
Crosshead Speed 0.5 in/min.
Specimens 13.23 to 13.25
TENSILE MODULUS--STRESS CURVE
-GLASS REINFORCED LAMINATE-
Fig. 4.27
CHORD ELASTIC MODULUS LBF/IN² x 10⁻⁶
NEWTON/MM²
COMPOSITE TENSILE STRESS LBF/IN²X10⁻³
0.000
0.200
0.400
0.600
0.800
1.000
1.200
1.400
1.600
1.800
2.000
2.200
0
1000
2000
3000
4000
5000
6000
7000
8000
9000
10000

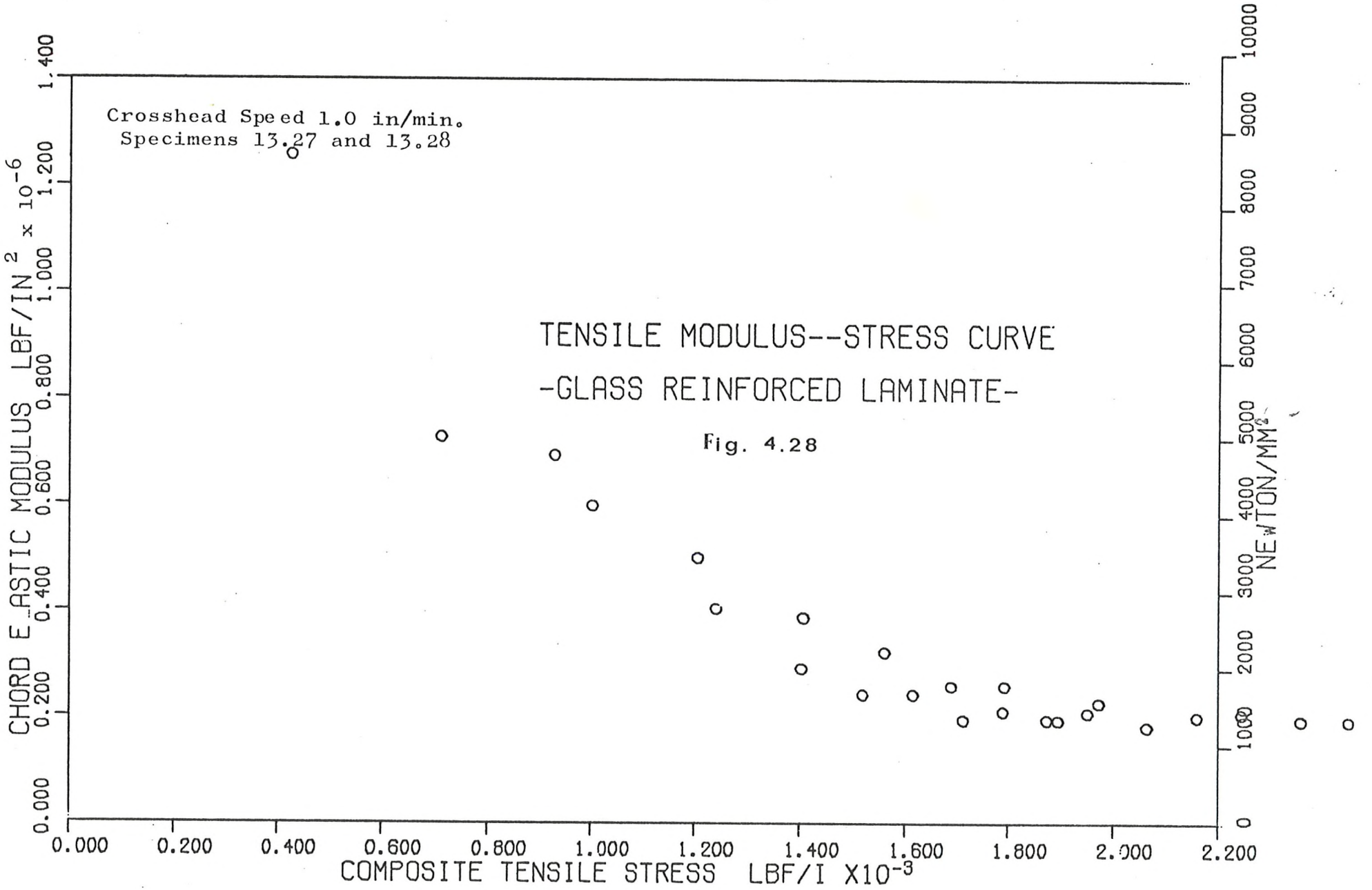
Crosshead Speed 1.0 in/min.
Specimens 13.27 and 13.28
TENSILE MODULUS--STRESS CURVE
-GLASS REINFORCED LAMINATE-
Fig. 4.28
CHORD ELASTIC MODULUS LBF/IN^2 x 10^{-6}
NEWTON/MM^2
COMPOSITE TENSILE STRESS LBF/I X10^{-3}
0.000
0.200
0.400
0.600
0.800
1.000
1.200
1.400
1.600
1.800
2.000
2.200
0
1000
2000
3000
4000
5000
6000
7000
8000
9000
10000

4.5 Compressive Tests

4.5.1 Experimental Results

The experimental method has been described in Section 3.5.1 but no lateral measurements were recorded during this series of tests. Only one set of reinforced compression specimens was tested, at a crosshead speed of 0.005 in/min. This was because the tensile tests on the reinforced material suggested that the influence of crosshead speed was not marked. The compression specimens were cut from sheet 14 as indicated in Figure 4.1.

Table 4.12 shows the calculated results of initial elastic modulus and ultimate strength for each specimen, together with the standard deviation and 90% confidence limits for the full set of specimens.

Figure 4.29 illustrates the scatter compressive stress-strain diagram for the above specimens. Greater strain could have been achieved but they were beyond the range of the apparatus.

TABLE 4.12

RESULTS OF COMPRESSION TEST ON REINFORCED MATERIAL

(2 Layers of C.S.M.)

Specimen Number	Maximum Stress lbf/in^2	Initial Elastic Modulus $lbf/in^2 \times 10^{-6}$
14.83	4809.2	0.7631
14.84	4497.0	0.6377
14.85	4506.5	0.6386
14.86	5720.2	0.4635
14.87	5562.2	0.5679
14.88	5521.7	0.4366

Stress $\frac{lbf}{in^2}$	Mean maximum	5102.8
	Standard deviation:	561.52
	% Coeff. of variation	11.0
	Upper limit } p = 0.1	5568.9
	Lower limit } p = 0.1	4689.7
Initial Elastic Modulus $\frac{lbf}{in^2} \times 10^{-6}$	Mean	0.5846
	Standard deviation:	0.122
	% Coeff. of variation	20.87
	Upper limit } p = 0.1	0.6852
	Lower limit } p = 0.1	0.4839

STRESS STRAIN RELATIONSHIP
FOR COMPOSITE
-COMPRESSIVE STRESS- LBF/IN2
0
800
1600
2400
3200
4000
4800
5600
-PERCENTAGE STRAIN-
0.000
0.150
0.300
0.450
0.600
0.750
0.900
1.050
1.200
1.350
1.500
1.650
NEWTON/MM2 X10-1
0.000
0.400
0.800
1.200
1.600
2.000

Fig. 4.29

4.6 Flexural Tests

4.6.1 Experimental Results

The experimental method adopted for the flexural tests is described in Section 3.5.1.

Tables H5.1 to H5.5, Appendix H, give the nominal bending stresses for the reinforced beams. These nominal stresses were calculated by assuming linear stress distribution, according to simple bending theory. They are merely a measure of the load applied to the specimen and do not necessarily represent stresses actually present. These tables also show the corresponding strain at the top and bottom faces of the beams, detected by foil strain gauges.

The experimental results are shown graphically in Figures 4.30 to 4.34 where it can be seen that greater strains exist at the tension face than the compression face for the same nominal bending stress. Due to very large deflections, therefore leading to a limitation of the bending rig, the specimens were not loaded to fracture.

Larger bending stresses are developed in specimen 20.18 (Fig. 4.30) which has a greater thickness than the other specimens and lower glass content (Table 4.10).

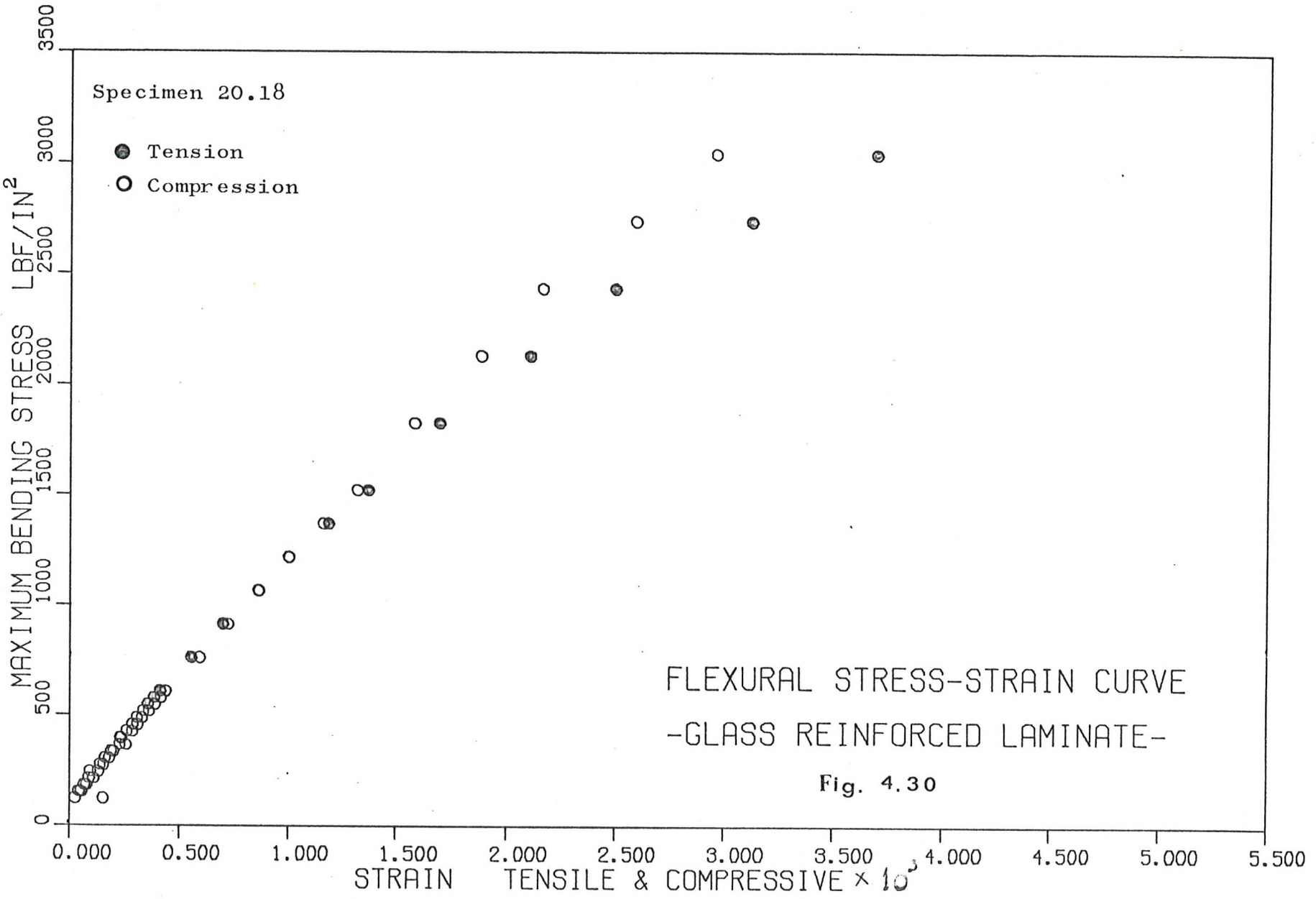

FLEXURAL STRESS-STRAIN CURVE

-GLASS REINFORCED LAMINATE-

Fig. 4.30

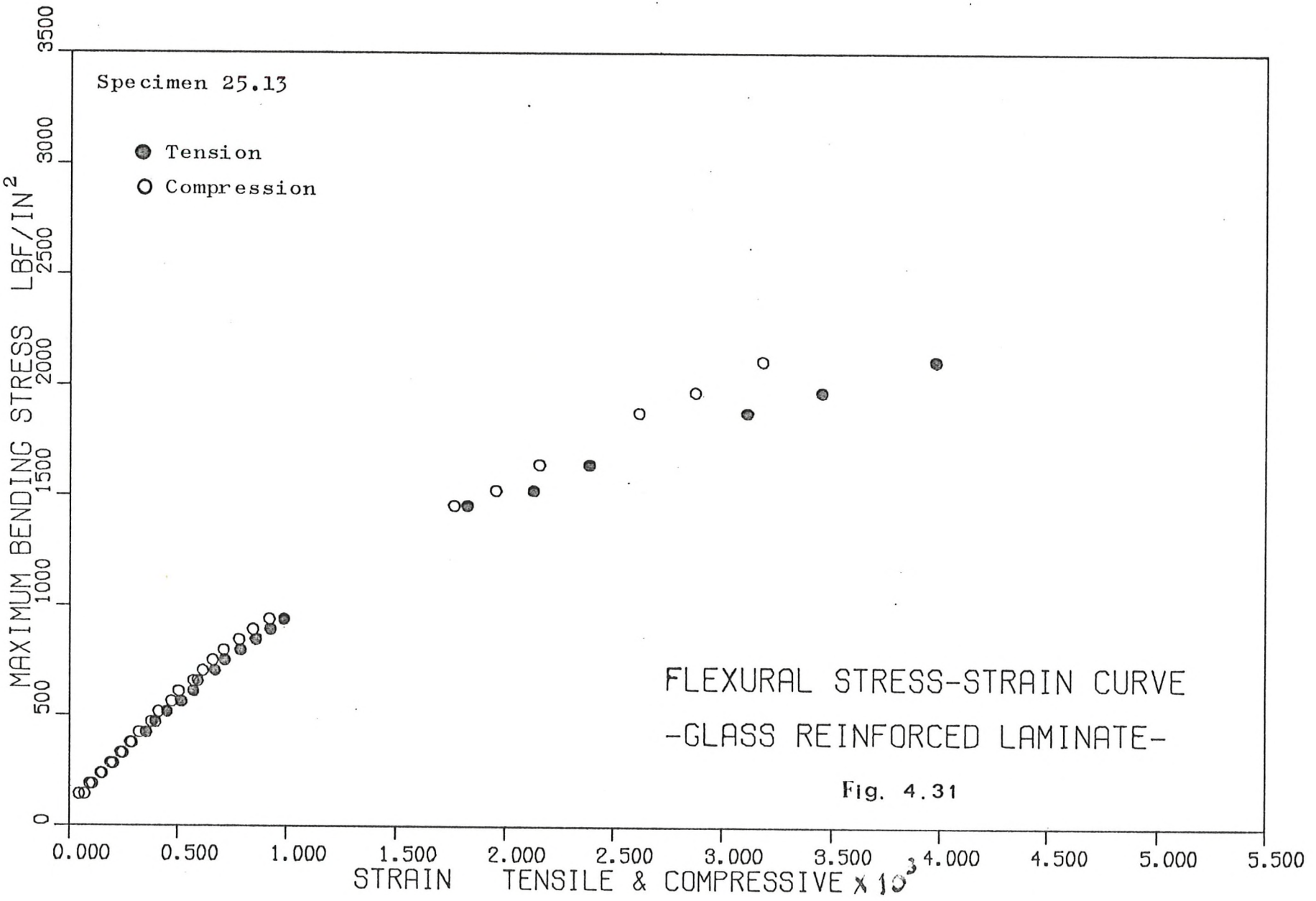

FLEXURAL STRESS-STRAIN CURVE

-GLASS REINFORCED LAMINATE-

Fig. 4.31

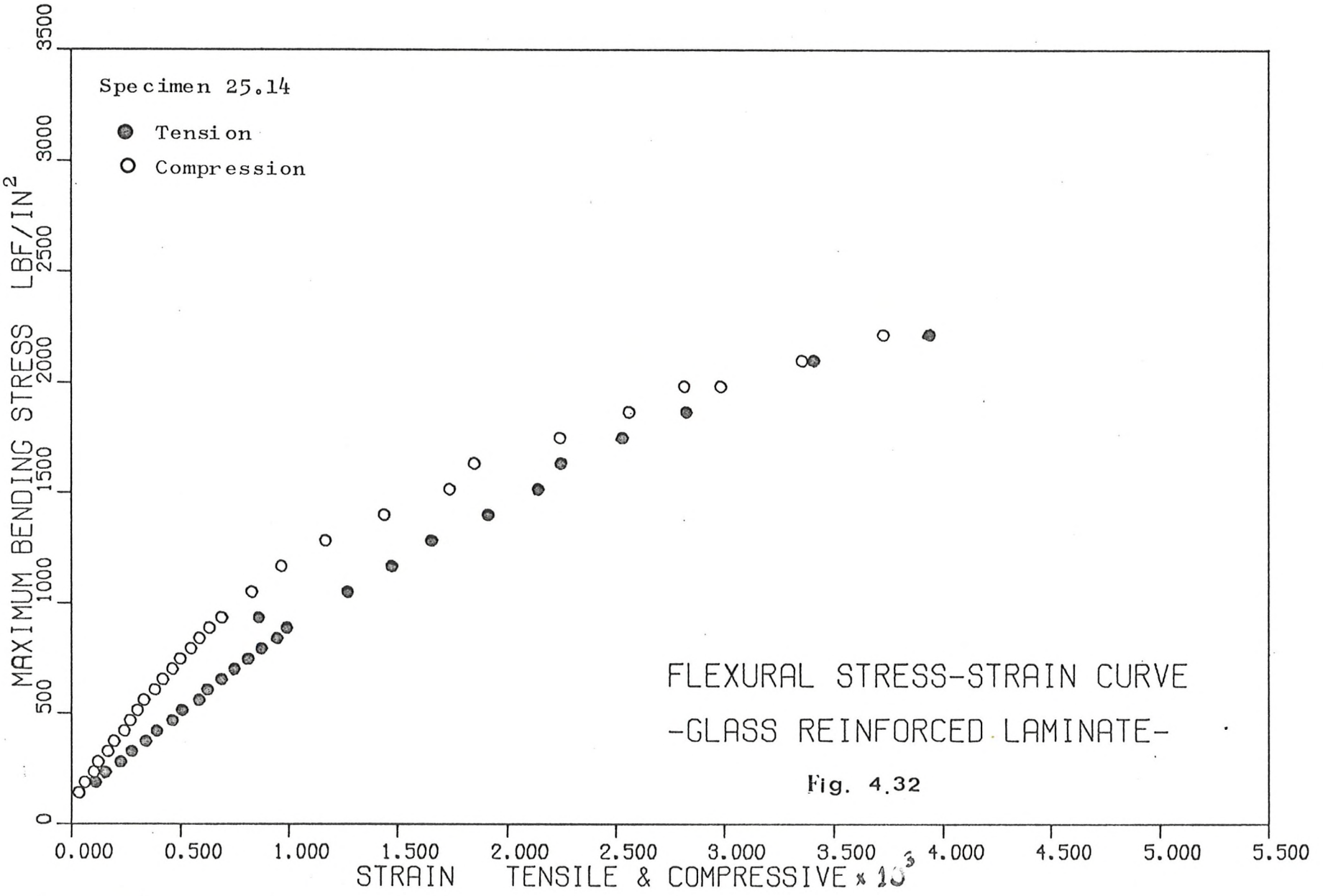

FLEXURAL STRESS-STRAIN CURVE

-GLASS REINFORCED LAMINATE-

Fig. 4.32

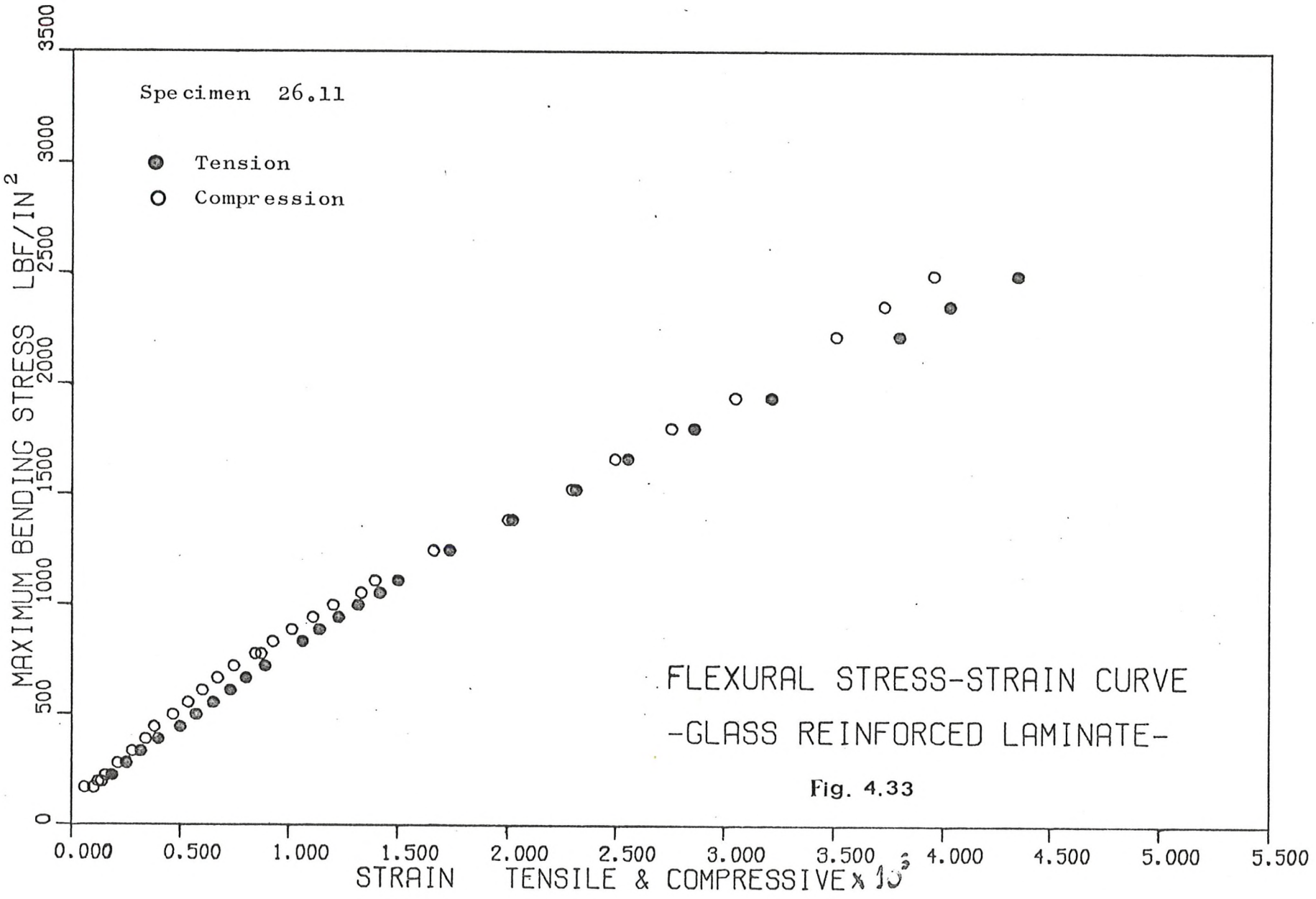
Specimen 26.11
Tension
Compression
MAXIMUM BENDING STRESS LBF/IN^2
0
500
1000
1500
2000
2500
3000
3500
0.000
0.500
1.000
1.500
2.000
2.500
3.000
3.500
4.000
4.500
5.000
5.500
STRAIN TENSILE & COMPRESSIVE x 10^3
FLEXURAL STRESS-STRAIN CURVE
-GLASS REINFORCED LAMINATE-

Fig. 4.33

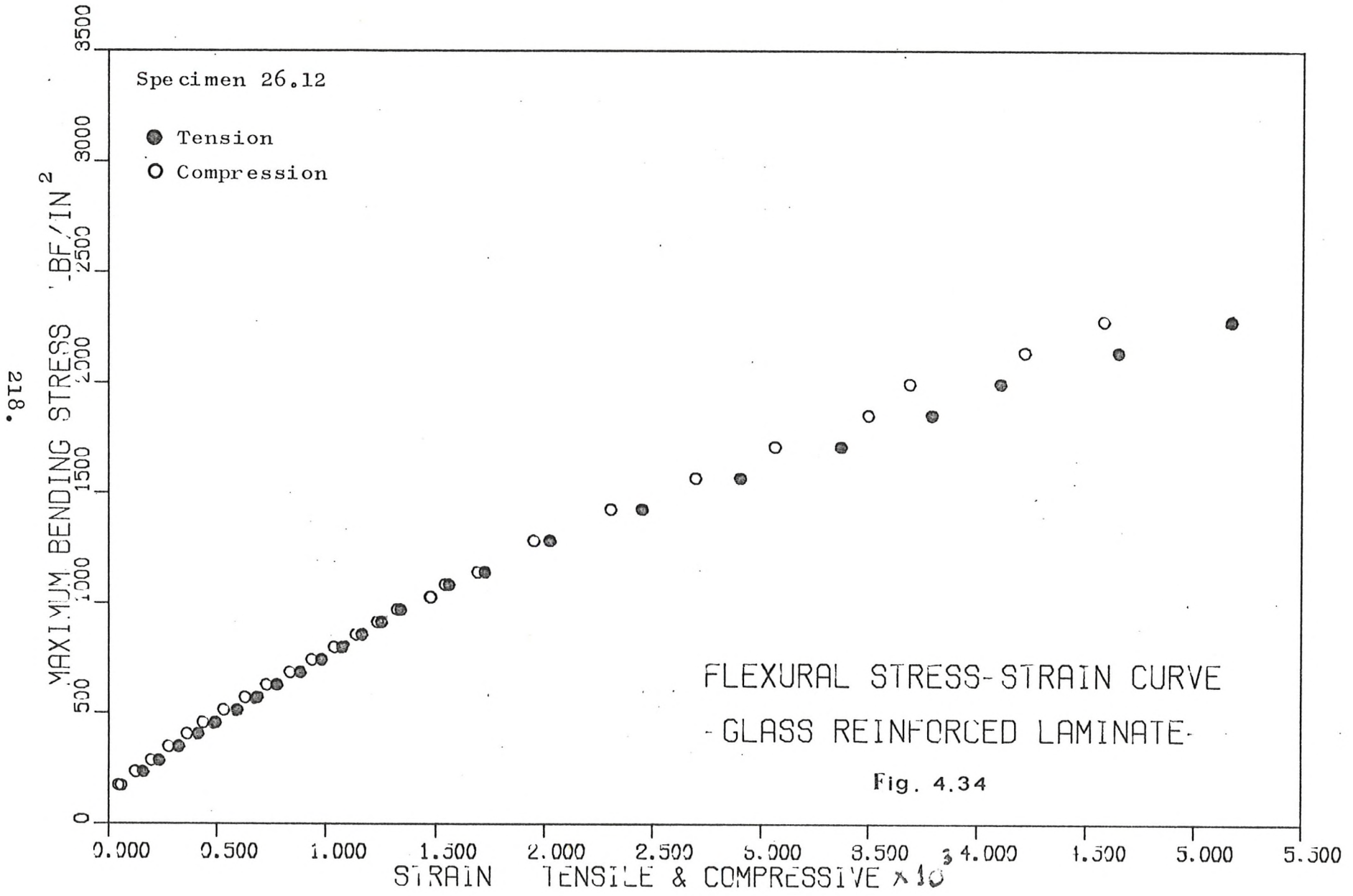
Specimen 26.12
Tension
Compression
MAXIMUM BENDING STRESS LBF/IN2
0
500
1000
1500
2000
2500
3000
3500
0.000
0.500
1.000
1.500
2.000
2.500
3.000
3.500
4.000
4.500
5.000
5.500
STRAIN TENSILE & COMPRESSIVE X 10
FLEXURAL STRESS-STRAIN CURVE
-GLASS REINFORCED LAMINATE-

Fig. 4.34

4.7 Long Term Creep Study of Thin Reinforced Polymer-Cement Laminates

4.7.1 Experimental Method

The experimental technique employed for the study of long term creep properties has been described in Chapter 3 (Sec. 3.7.1). The creep specimens described in this section were cut from sheets 20, 24, 25 and 26 (Fig. 4.1). Each pair of creep specimens, coupled as shown in Fig. 4.35, was subjected to a static stress in the range 315 lbf/in^2 to 1220 lbf/in^2. These are from 24.5% to 42% of the tensile strengths in Table 4.10. The tests were carried out at a temperature of 22^{o}C and relative humidity of 60-65%. It should be noted that specimens 20.1 and 20.2 contain the same number of layers of C.S.M. as the other specimens but had a markedly lower glass content. Total strains (ε_t) were measured over a gauge length of 10 inches by the extensometer in Plate 3.5. Creep measurements were recorded up to a time of approximately 33 x 10^6 s.• Figures 4.36 and 4.37 illustrate the creep curves of all the reinforced specimens up to 5000 s. and 14 x 10^6 s. The total strains at 0, 10, 100 and 1000 s. at the various stress levels are recorded

---

• 604800 seconds = 1 week

in Table 4.13, together with mean dimensions of the specimens. Minimum creep rates (Table 4.13) were calculated in the range 10 x 10^6 s. to 14 x 10^6 s. using the method of least squares (Appendix A and Computer Programme G44D). Isochronous curves for 0, 10, 100 and 1000 s. (Figures 4.38 to 4.41) illustrate the non linear nature of the material.

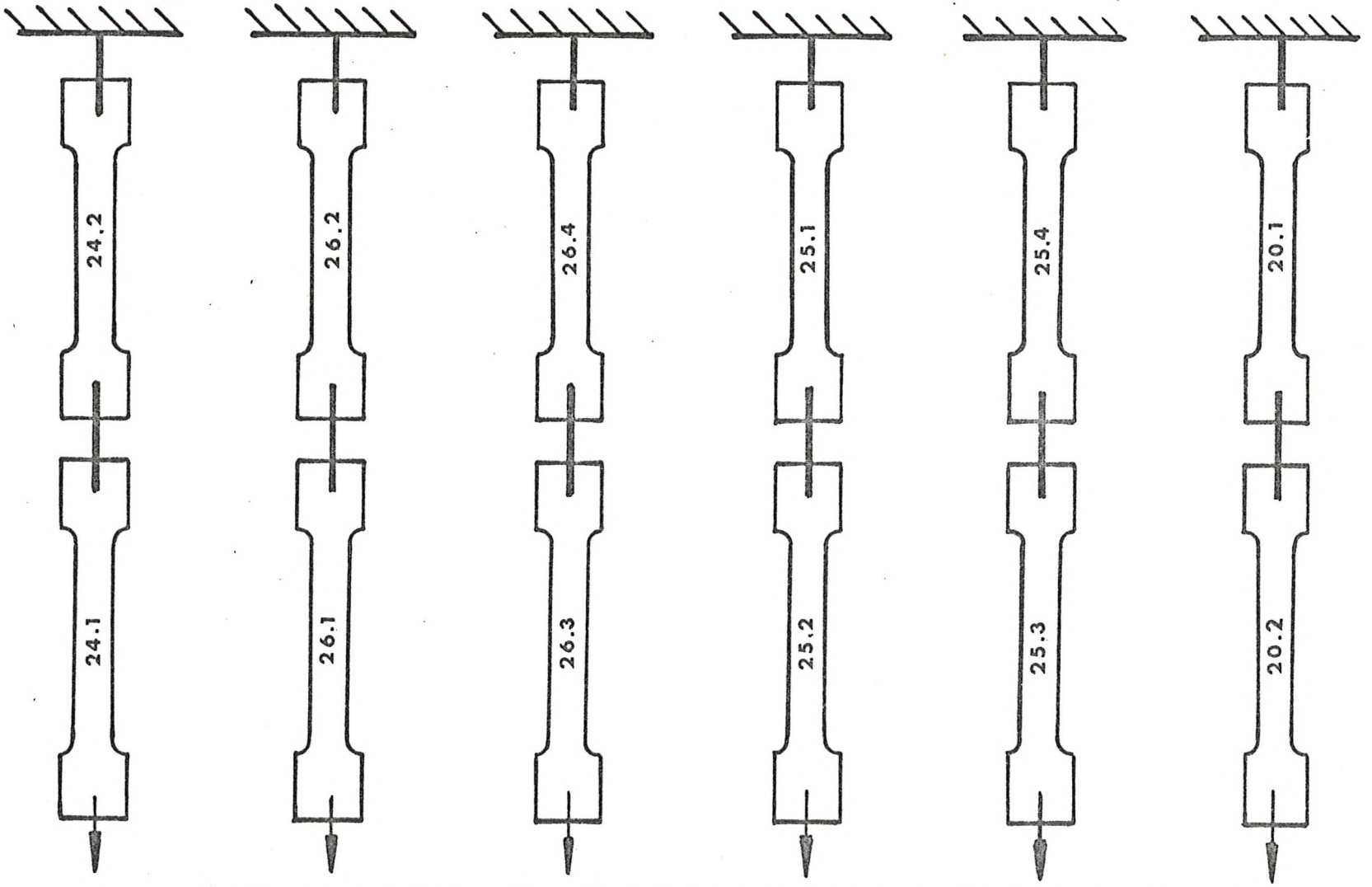

Arrangement for Testing of Glass Reinforced Creep Specimen

FIG 4.35

TABLE 4.13

INSTANTANEOUS CREEP DATA

Spec. No.	Tensile Stress lbf/in^2	Notation	Total Strain x 10^3				J_o x 10^6 (at 0s)	Slope A_i	Min. Creep Rate x 10^{12} strain/s	Mean Dimensions Inches	
			0s.	10s.	100s.	1000s.				Width	Thick-ness
20.2	315.0	×	0.16	0.17	0.23	0.24	–	–	20.46	1.495	0.211
20.1	347.0	◥	0.226	0.25	0.28	0.28	–	–	16.56	1.492	0.210
25.4	475.0	⊡	0.31	0.4	0.52	0.57	0.365	0.11	22.82	1.491	0.151
25.3	481.0	●	0.286	0.44	0.51	0.56	0.24	0.127	20.34	1.487	0.139
25.1	633.0	◈	0.49	0.55	0.63	0.72	0.33	0.113	21.44	1.488	0.154
25.2	684.0	◬	0.59	0.86	0.94	1.05	0.31	0.109	31.08	1.48	0.137
26.4	960.0	◈	1.62	1.93	2.06	2.18	0.31	0.087	42.8	1.492	0.141
26.3	1038.0	■	1.82	2.04	2.15	2.27	0.19	0.117	38.22	1.493	0.126
24.1	1070.0	+	1.78	2.19	2.38	2.6	0.44	0.087	43.3	1.488	0.1344
24.2	1125.0	⊙	1.93	2.4	2.62	2.84	0.48	0.075	43.46	1.488	0.1323
26.1	1170.0	●	2.19	2.64	2.87	3.08	0.43	0.089	37.46	1.490	0.140
26.2	1220.0	●	2.02	3.06	3.4	3.66	0.52	0.087	46.69	1.490	0.138

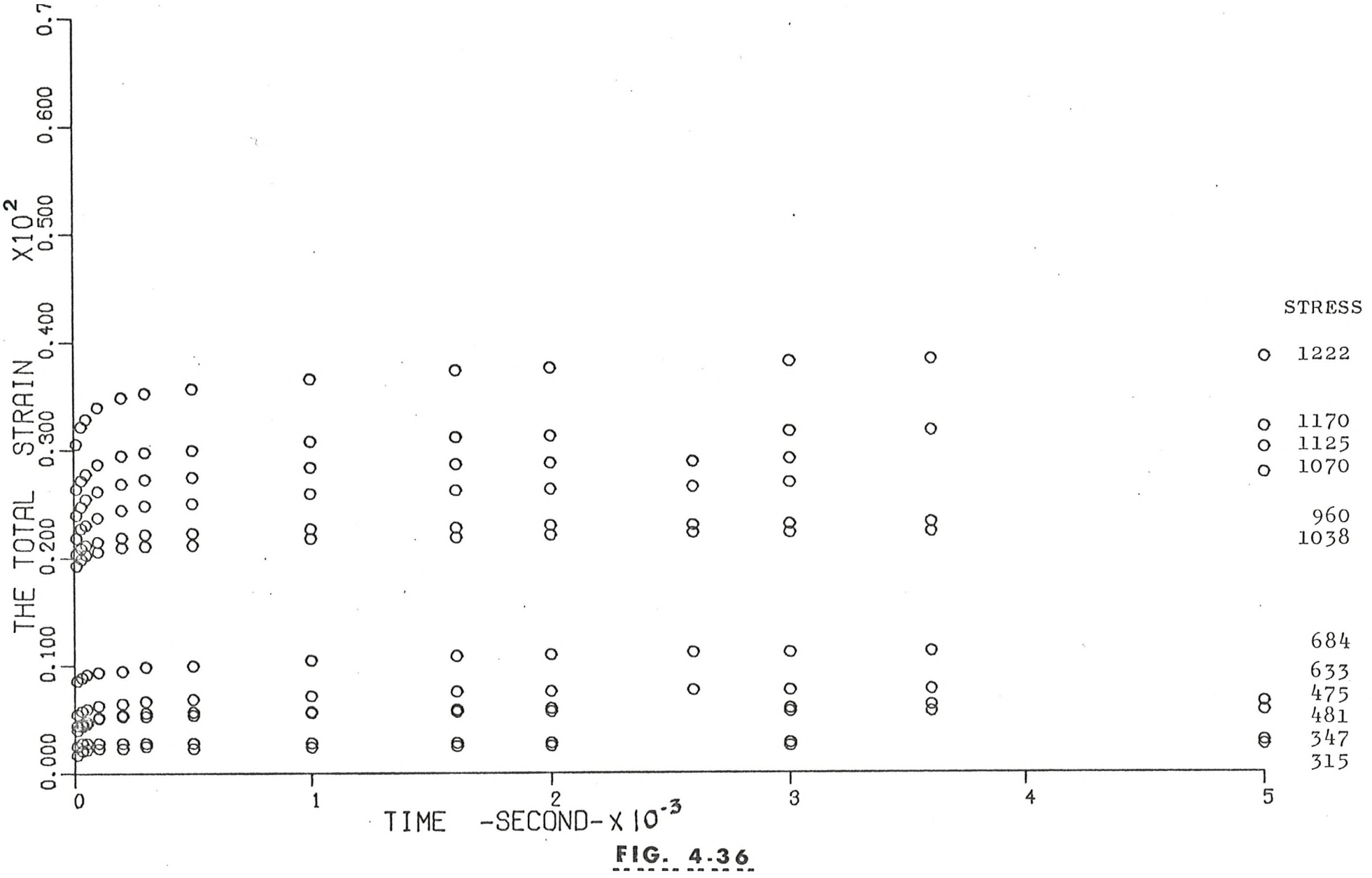

FIG. 4-36

CREEP CURVES FOR REINFORCED POLYMER-CEMENT LAMINATES

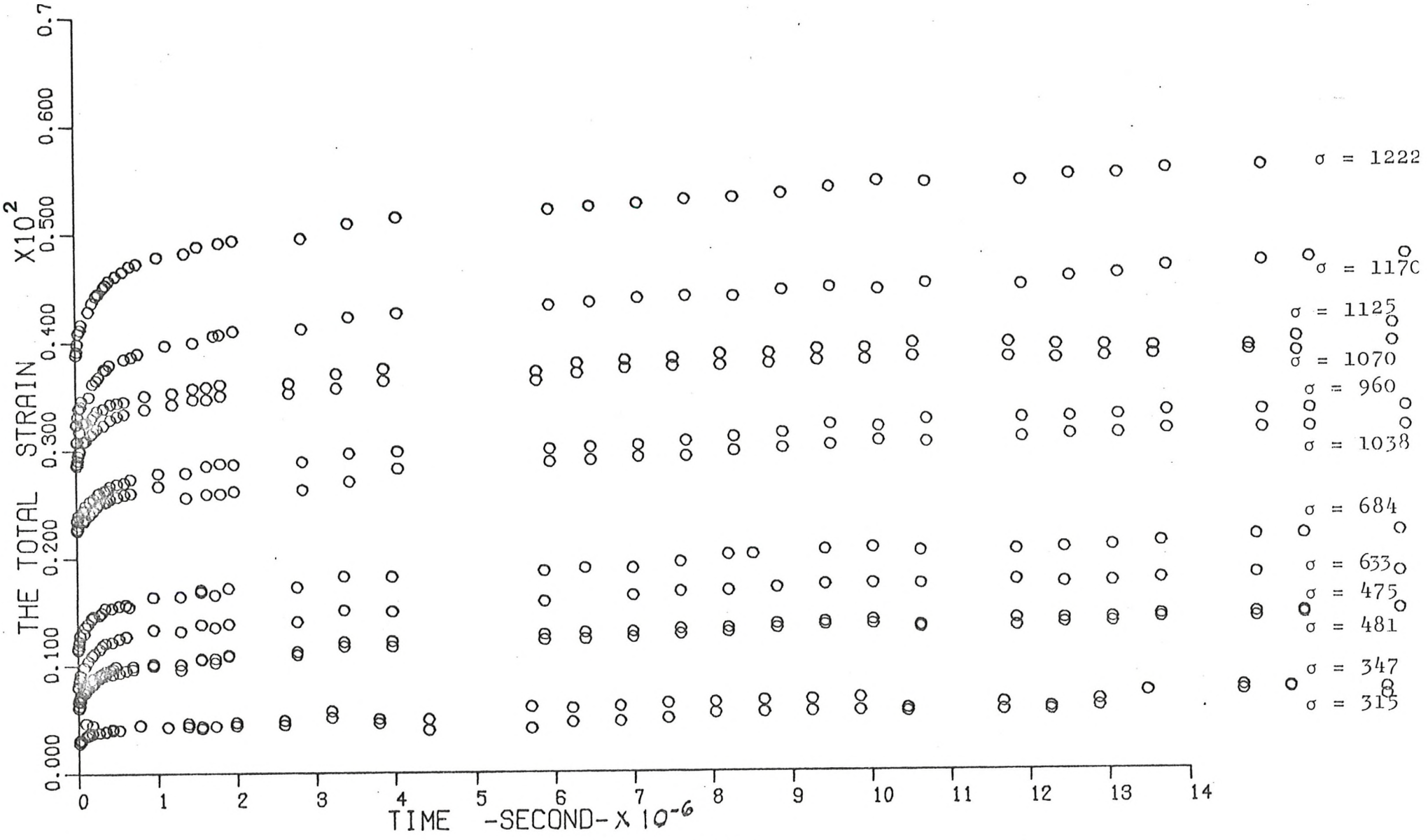

FIG. 4.37

CREEP CURVES FOR REINFORCED POLYMER-CEMENT LAMINATES

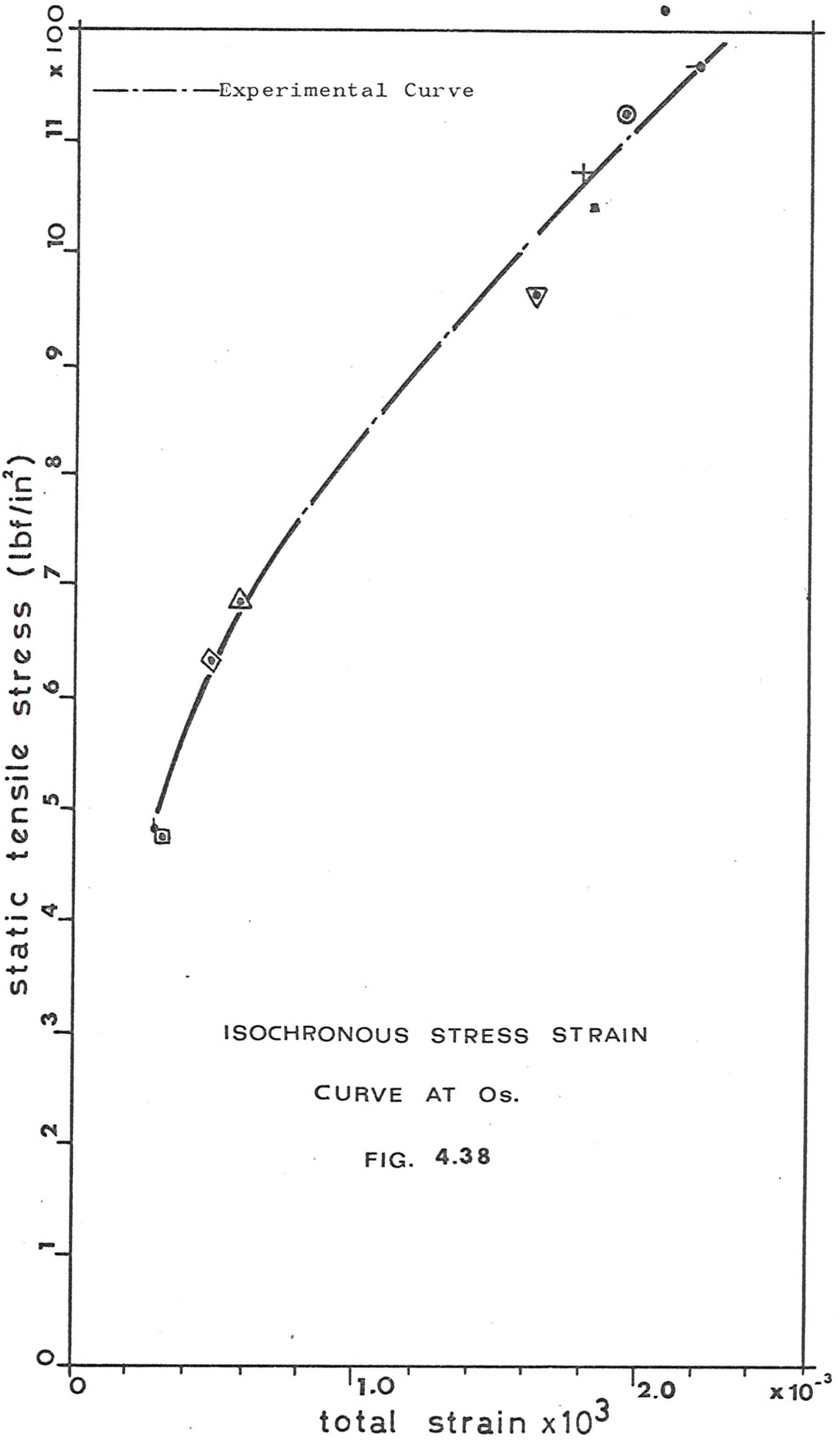

ISOCHRONOUS STRESS STRAIN CURVE AT Os.

FIG. 4.38

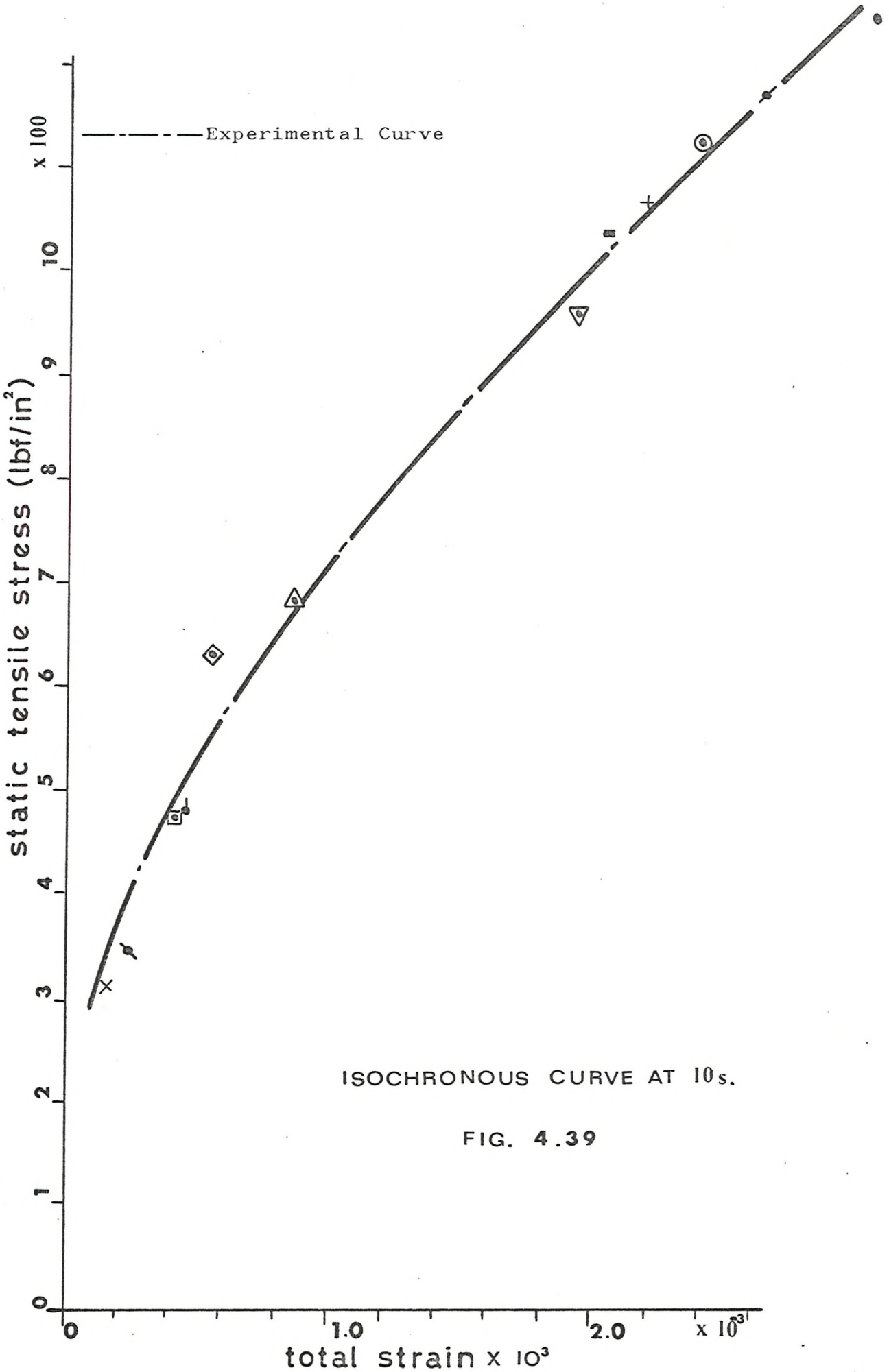

ISOCHRONOUS CURVE AT 10s.

FIG. 4.39

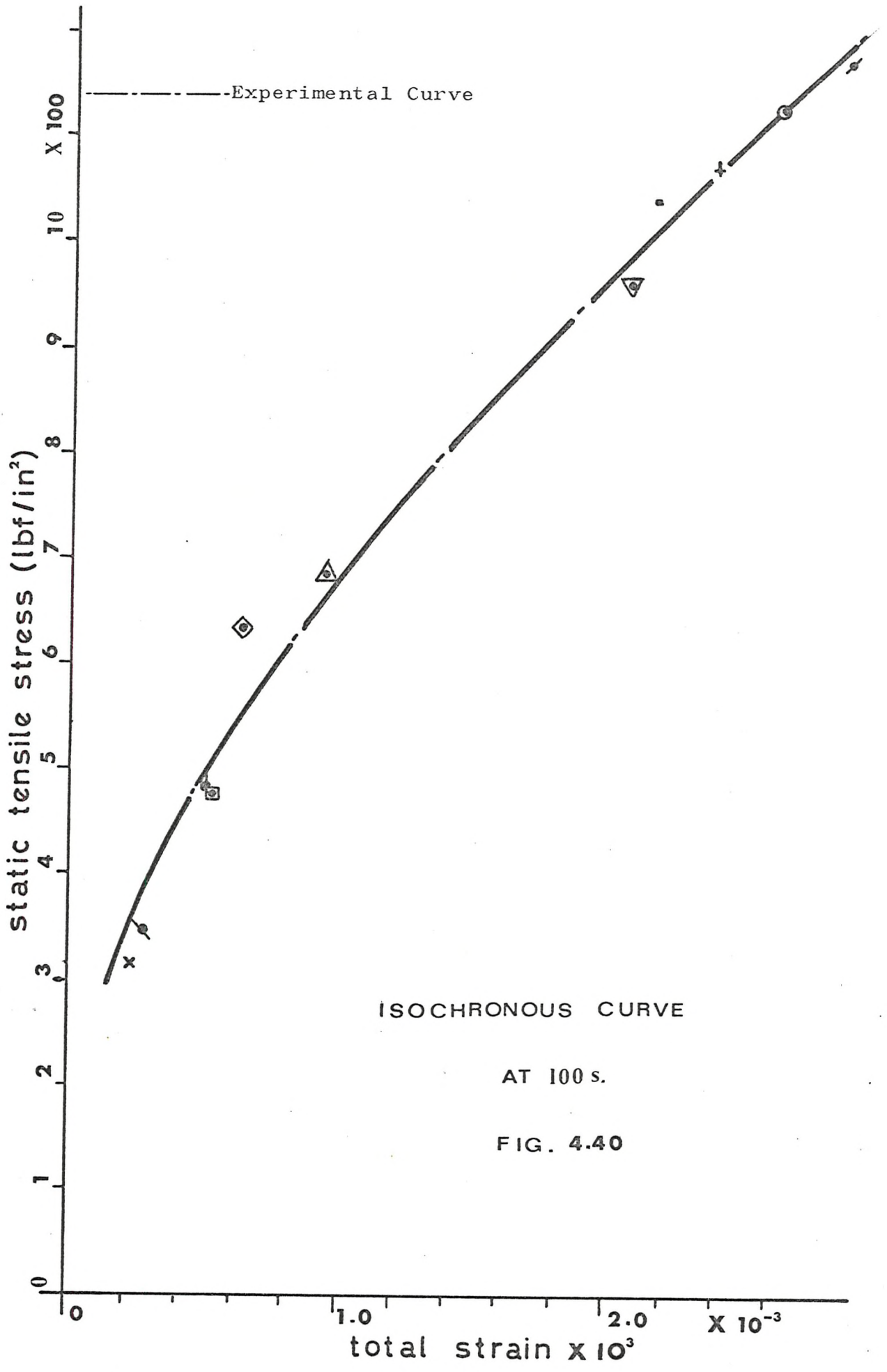

ISOCHRONOUS CURVE

AT 100 s.

FIG. 4.40

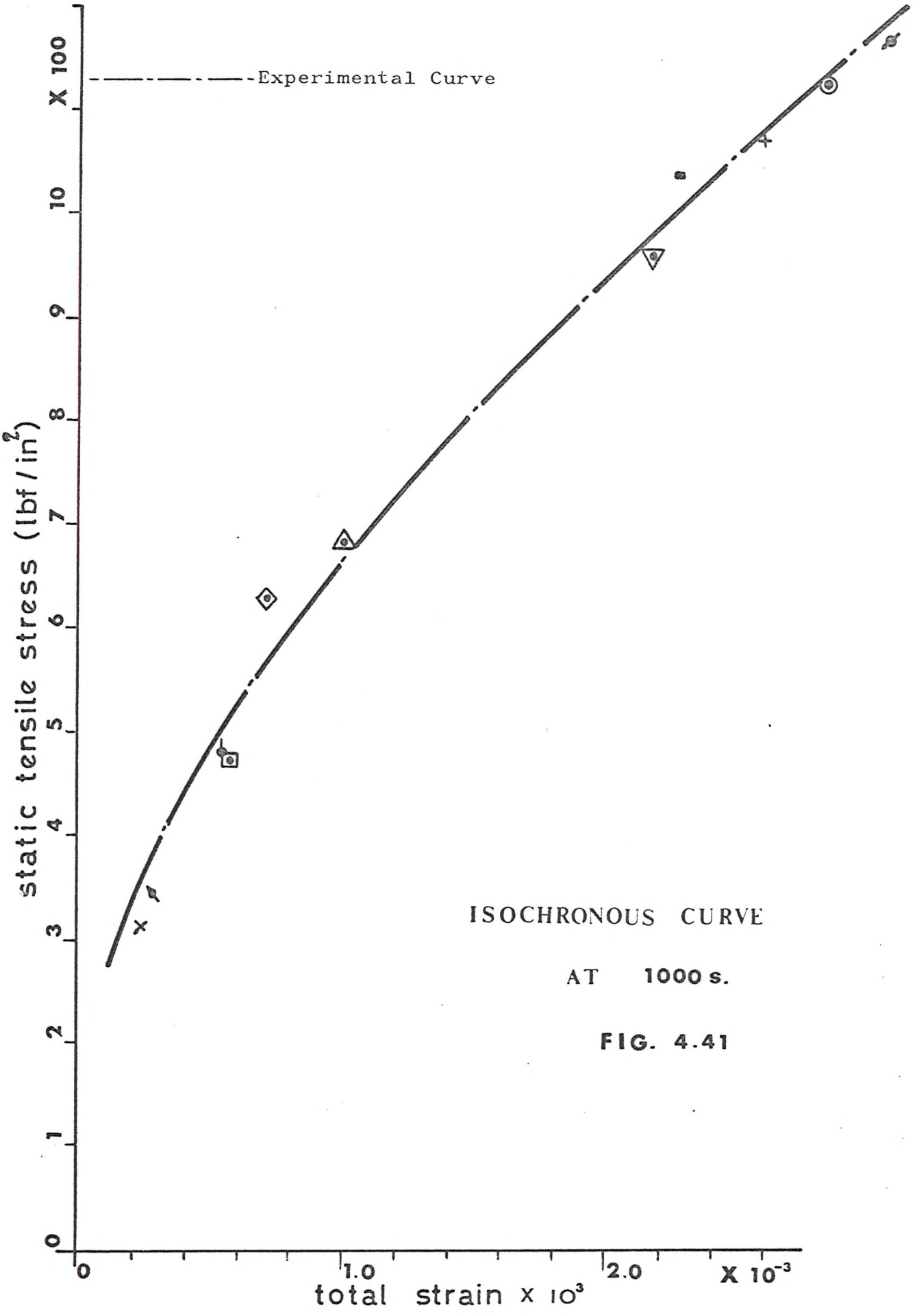

ISOCHRONOUS CURVE

AT 1000 s.

FIG. 4.41

4.7.2 Analysis of Creep Data

The creep curves were reduced to three components of strain: instantaneous strain (ε_o), primary creep strain (ε_1) and secondary creep strain (ε_2). The method by which these components were derived is given in Chapter 3 (Sec. 3.7.3).

A family of straight lines resulted from the plot of log (primary creep compliance, J_1) against the log (time) at various stress levels (Fig. 4.42). There was also this linear relationship in the case of the unreinforced material (Fig. 3.51).

$$\therefore \quad J_{1i} = J_o \, t^{A_i} \qquad \ldots \quad (4.1)$$

$$\text{or} \quad \frac{\varepsilon_{1i}}{\sigma_i} = J_o \, t^{A_i}$$

where J_{1i} is the primary creep compliance at the i^{th} level of stress

J_o the primary creep compliance at 1s (given in Table 4.13)

and A_i the slope of the straight lines at the i^{th} level of stress (given in Table 4.13)

Figure 4.44 shows the variation of the index (A_i) as a function of the applied stress (σ_i), which if interpreted as being linearly related gives

$$A_i = \left\{ \frac{2440 - \sigma_i}{16200} \right\} \quad \ldots \quad (4.2)$$

J_o, when plotted as a function of stress (Fig. 4.45) shows a considerable degree of scatter. If J_o is assumed to be proportional to σ_i then

$$J_o = \left\{ \frac{\sigma_i \times 10^{-6}}{2360} \right\} \quad \ldots \quad (4.3)$$

By combining equations 4.1, 4.2 and 4.3 the primary creep strain (ε_1) is given by

$$\varepsilon_1 = \left[\frac{\sigma_i^2 \times 10^{-6}}{2360} \right]^{\frac{2440 - \sigma_i}{16200}} t \quad \ldots \quad (4.4)$$

The dependence of the minimum creep rate (B_i) upon the applied stress is illustrated in Fig. 4.43 and the linear regression estimate is given as

$$B_i = \left\{ \frac{\sigma_i \times 10^{-12}}{25.26} \right\}$$

$$\therefore \quad \varepsilon_{2i} = \left\{ \frac{\sigma_i \times 10^{-12}}{25.26} \right\} t \quad \ldots \quad (4.5)$$

The total strain is the sum of ε_o, ε_1 and ε_2 and, using equations 4.4 and 4.5 the total strain at any instant in time ($< 33 \times 10^{-6}$ s.) at any level of stress is given by

$$\varepsilon_t = \frac{\sigma_i}{E_o} + t\left\{\frac{\sigma_i^2 \times 10^{-6}}{2360}\right\}\left[\frac{2440 - \sigma_i}{16200}\right] + t\left\{\frac{\sigma_i \times 10^{-12}}{25.26}\right\} \quad \ldots (4.6)$$

Total creep values have been calculated using equation (4.6) and compared with the experimental results (Appendix H, Tables H6.1 to H6.12). These tables show maximum and minimum errors of -24% to +30% measured from the calculated values. Generally errors were much smaller than this.

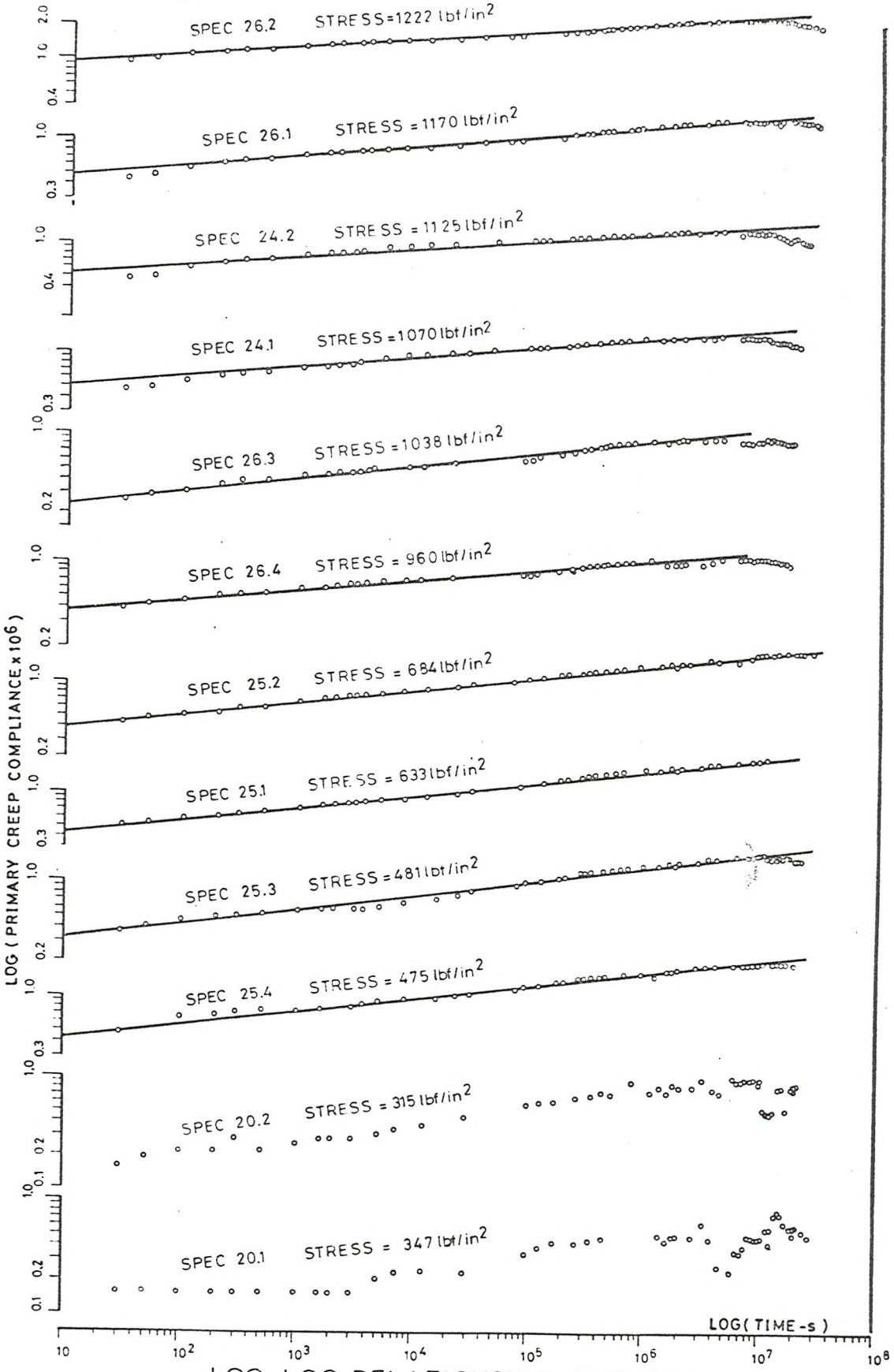

LOG-LOG RELATIONSHIP BETWEEN PRIMARY CREEP COMPLIANCE AND TIME

fig. 4.42

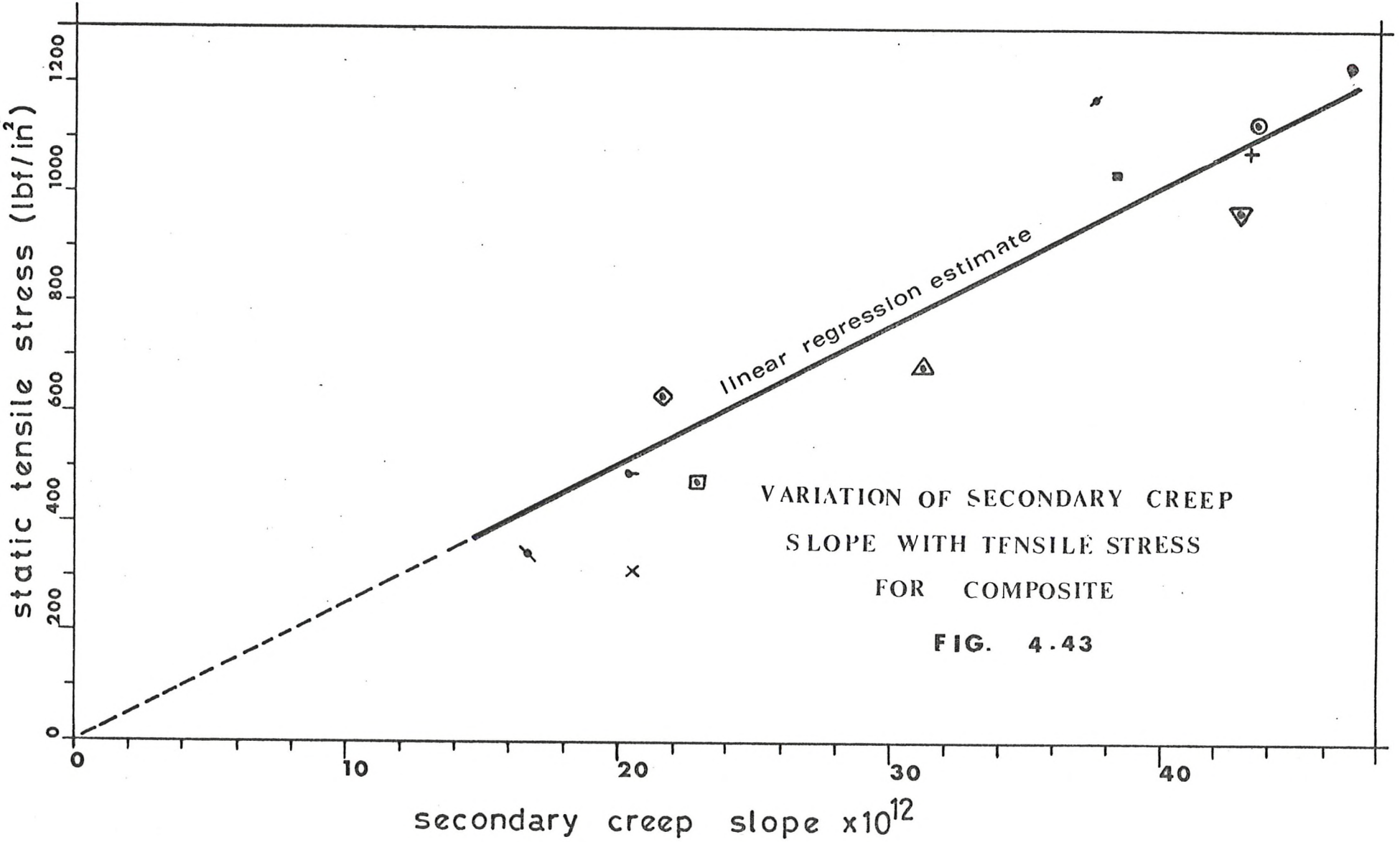

VARIATION OF SECONDARY CREEP SLOPE WITH TENSILE STRESS FOR COMPOSITE

FIG. 4.43

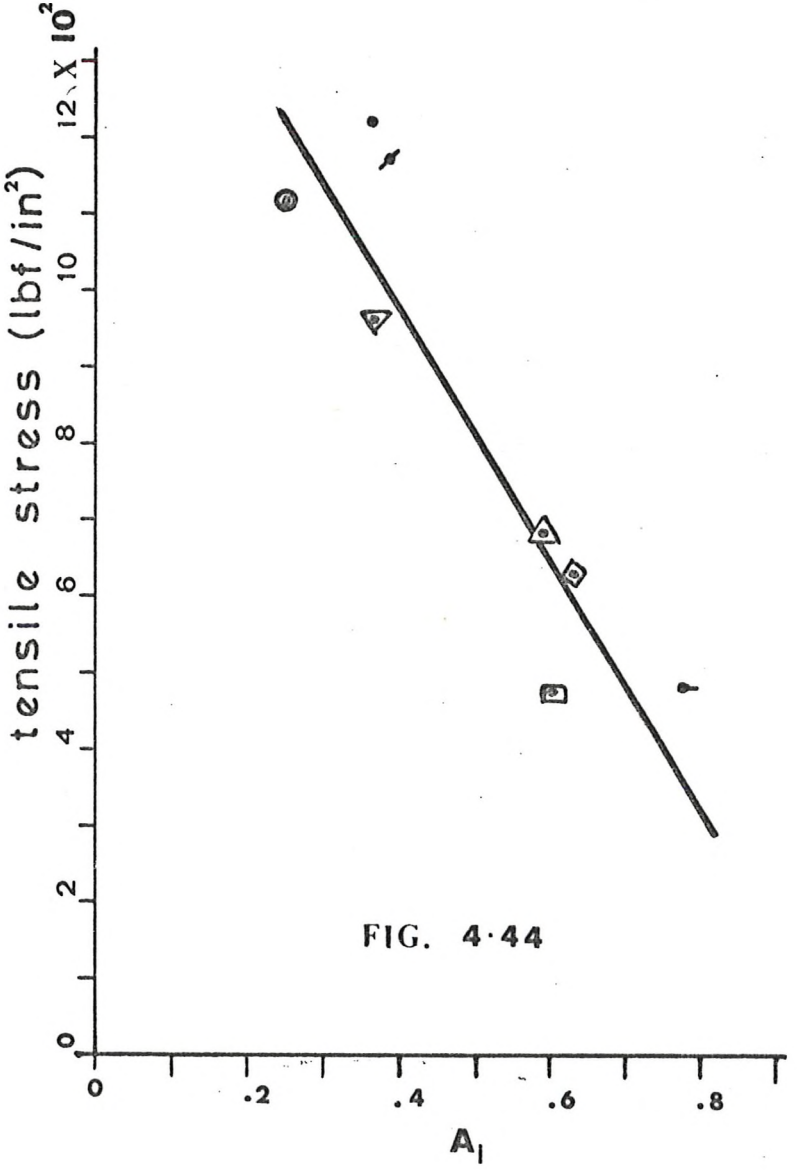

FIG. 4·44

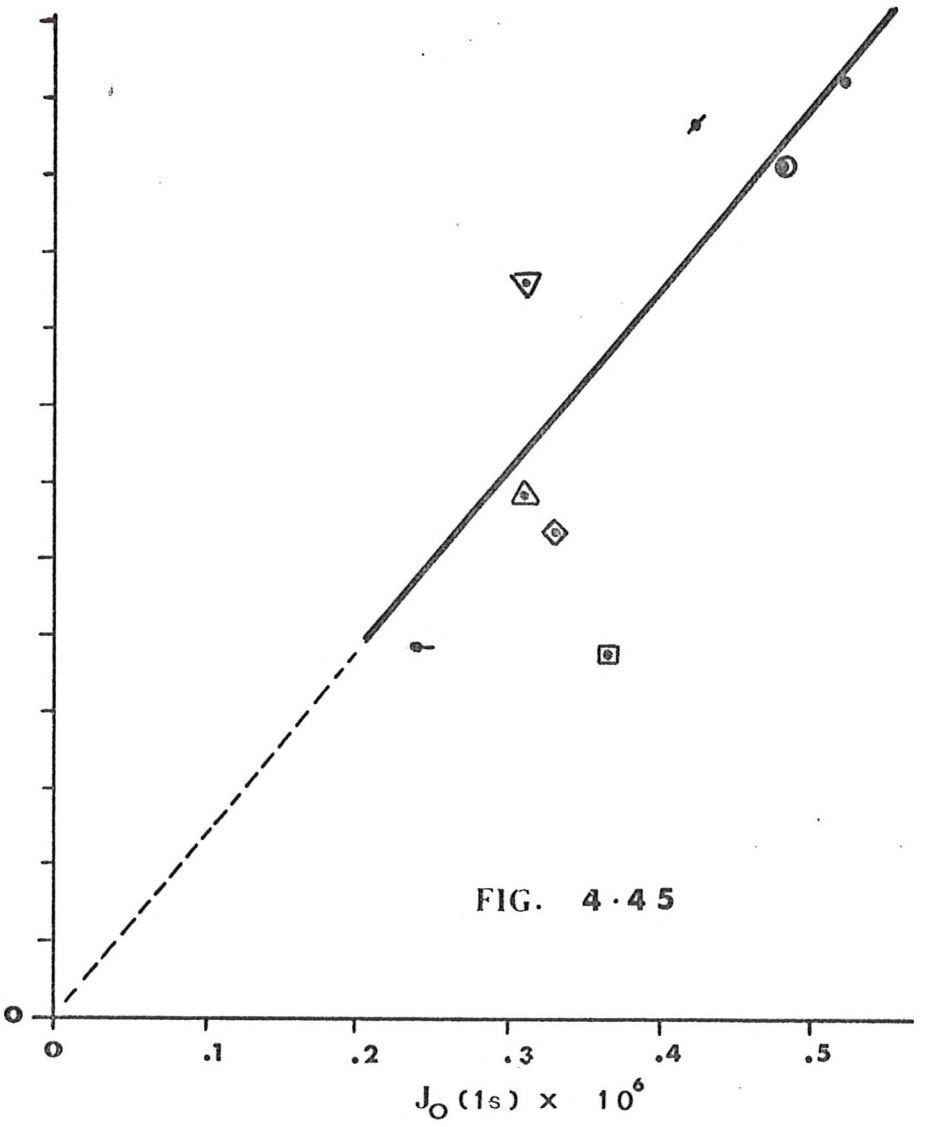

FIG. 4·45

CHAPTER 5

GLASS-REINFORCED/POLYMER-CEMENT

(Various Types of Reinforcement)

5.1 Outline

In order to furnish a broad picture of the glass-reinforced/polymer-cement composite, three laminates were produced. These laminates used as their reinforcement:

a) 2 layers of glass cloth - Y229 (Sheet 21)
b) 2 layers of continuous filament mat (Sheet 22)
c) 1 layer of woven roving (Sheet 23)

The matrix of each sheet consisted of Portland cement, Primal E330, water and Nopco NZX in the proportions s/c = 0.2, w/c = 0.3 and a/c = 0.002 (ref. page 44).

Fig. 5.1 indicates the position and type of specimen cut from each sheet. It also illustrates the roll direction of each layer of reinforcement.

Preparation of the test piece is described in Appendix C (Sec. C2) and a description of the above glass reinforcements can be found in Appendix B (Sec. B1).

In addition to the laminates a number of rods were manufactured to provide an understanding of the material when using a unidirectional reinforcement. These rods were made with constant glass content, w/c ratio and a/c ratio, but the s/c ratio varied from 0.125 to 0.25. They were all tested at a constant crosshead speed of 0.005 in/min.

sheet 21

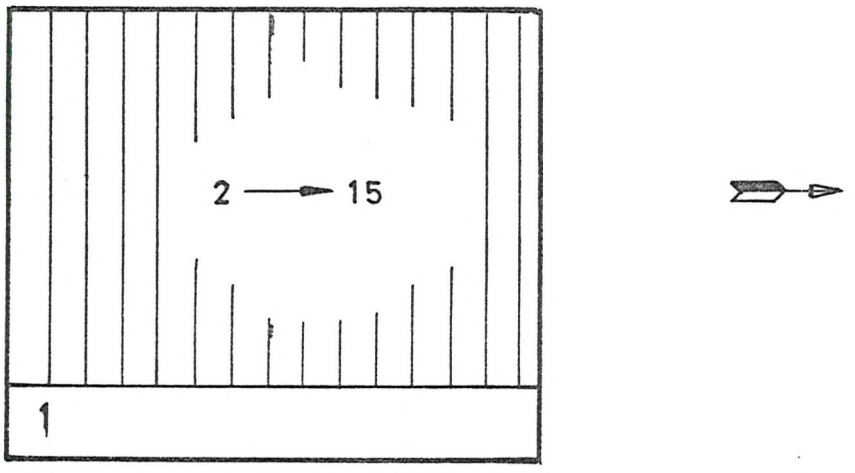

sheet 22

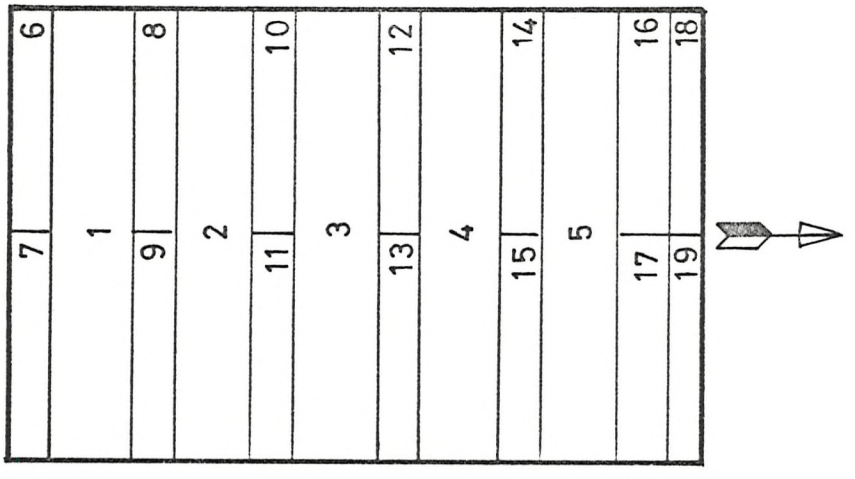

sheet 23

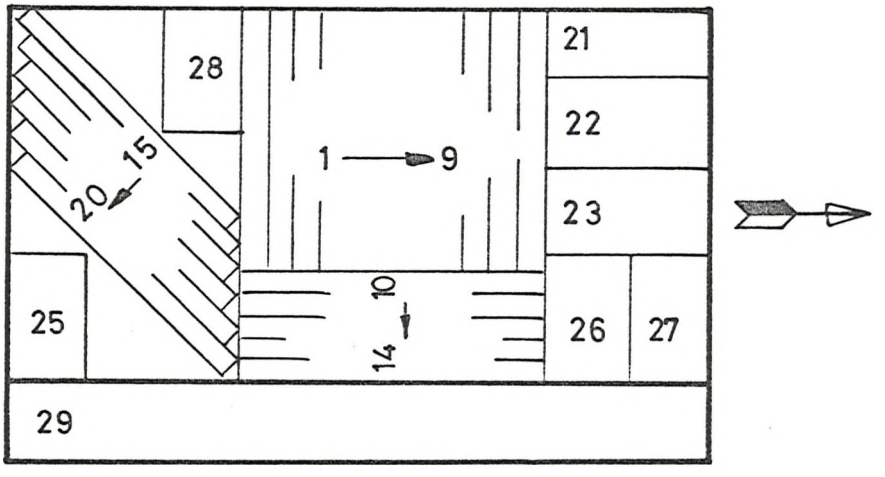

arrows indicate roll direction
of reinforcement

CUTTING PLAN OF POLYMER CEMENT BOARDS
REINFORCED BY: GLASS CLOTH, C.F.M. & W.R.

FIG 5.1

5.2 Production of Unidirectional Reinforced Rods

The object of manufacturing glass-reinforced/polymer-cement rods was to provide specimens with an even distribution of unidirectional fibres which could be tested under conditions of uniaxial loading. Fig. 5.2 shows the equipment used and mode of production of the rods. In all cases the polymer-cement rods were reinforced by two 60-end, E-glass rovings giving a total of 120 ends, (Appendix B, Sec. B1) having a weight of 0.11874 g/inch.

The rods were moulded in glass tubes which each had an internal diameter of approximately 6 mm. Both ends of the glass tube were belled to prevent the glass fibres from being severed during the drawing operation; also to allow the fibres and cement to be drawn through the glass tube without excessive tensile force being applied to the fibres. All the moulding tubes were coated internally with mould oil.

Fresh cement paste was prepared (Chapter 3, Sec. 3.2) and placed in a cement bath (Fig. 5.2). A length of 60-end glass roving was doubled and attached to the drawing wire. This wire was passed through the centre of the glass tube then the

fibres and the end of the tube were completely immersed in the cement paste. Gentle agitation of glass fibres within the paste ensured that a good impregnation was achieved but great care was taken not to damage the fibres. The bath, paste and fibres were vibrated to release any trapped air.

A quantity of fresh paste only was drawn up the glass tube. This prevented the fibres from being exposed to the atmosphere during the whole drawing operation, thus minimising air entrainment.

When the foregoing operations were completed the moulded rods were kept for 24 hours in the glass moulds. At the end of this period the rods were demoulded and stored vertically in a rack at a constant temperature of 22^{o}C and relative humidity of 40-60%.

It was not possible to prepare rods with a s/c ratio of less than 0.125 at a w/c ratio of 0.3, due to thickening of the paste at very low s/c ratios.

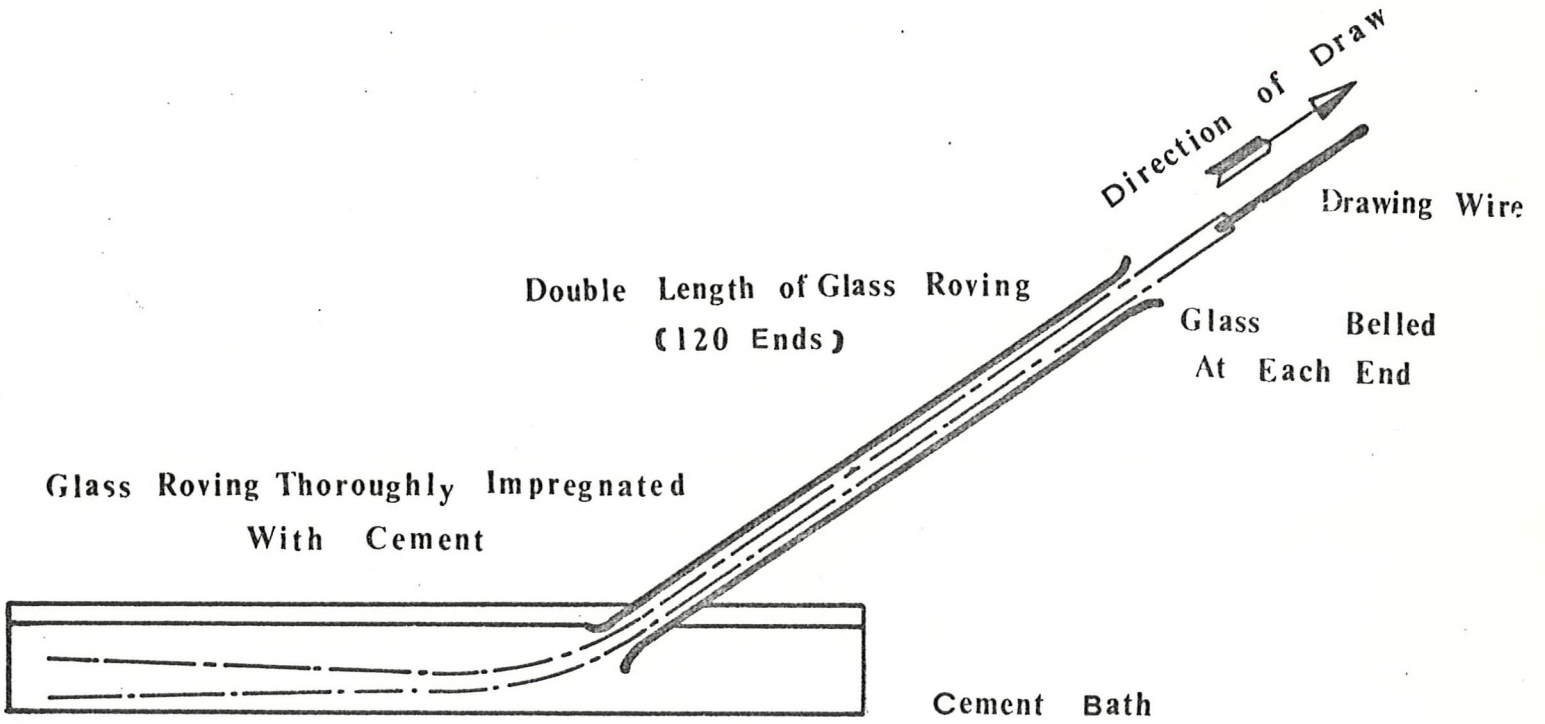

EQUIPMENT FOR THE MANUFACTURE OF GLASS

REINFORCED POLYMER – CEMENT RODS

FIG. 5.2

5.3 Experimental Method for Testing Rod Specimens

The technique employed here varied little from that used for the testing of the specimens of rectangular cross-section. The rods were secured in the Instron testing machine by special chucks. Care was taken not to tighten the chucks too much especially if the grip increased at greater loads. When testing specimens with a low s/c ratio it was necessary to wrap a thin plastic film around the circumference of the specimens to ensure that damage was not brought about by the serrations on the grip.

Tensile strains were detected over a gauge length of 2 inches by the Instron strain gauge extensometer (Appendix C, Sec. C1.2). It was therefore possible to obtain a load-extension record.

All rods were tested at an age of 27 days at a crosshead speed of 0.005 in/min.

5.4 Experimental Results (Rods)

Experimental and calculated results of glass reinforced rods when tested under uniaxial loading conditions are given in Table 5.1.

Figs. 5.3 to 5.9 show the relationship between tensile load and strain for the reinforced rod specimens. These diagrams may be compared directly since the quantity of glass, diameter and length for each specimen is the same. Shown on each figure is the load-strain diagram for the glass alone. This line has been constructed by assuming the elastic modulus of the fibres to be 10^7 lbf/in^2. The area of the 120 ends of E-glass subjected to tensile load is 2.78×10^{-3} in^2 (assuming the specific gravity of glass is 2.53). This would give a glass content by volume of 6.43%.

The range of the initial stiffness of the specimens appears to increase with decreasing s/c ratio. Figs. 5.3 to 5.9 illustrate that a final linear zone is reached. The slope of this linear region appears to decrease with a reduction of s/c ratio.

If the initial elastic modulus of the composite rods E_o (Table 5.1, Col. 5) is due to the contribution of the glass area A_f and the matrix

area A_m, also the relationship between stress and strain is linear, then by the simple law of mixtures

$$E_o(A_f + A_m) = E_f A_f + E_m A_m \quad \ldots (5.1)$$

where E_f and E_m is the initial elastic modulus of the glass and matrix respectively

$$\therefore \quad E_m = \frac{E_o(A_f + A_m) - E_f A_f}{A_m} \quad \ldots (5.2)$$

The values of E_m calculated using equation (5.2) are given in Table 5.1, Col. 6. For comparison, Section 3.3.2 and 3.3.3 show that the maximum initial elastic modulus for the unreinforced matrix was 0.549×10^6 lbf/in^2 (29 days) and 0.618×10^6 lbf/in^2 (88 days): w/c ratio and s/c ratio of matrix was 0.3 and 0.2 respectively tested in tension at a crosshead speed of 0.005 in/min.

Table 5.1, Col. 7, tabulates the product of the assumed elastic modulus for the glass (10^7 lbf/in^2) and the tensile failure strain of the specimens. This gives an estimate of the stress in the glass at failure.

TABLE 5.1

MECHANICAL PROPERTIES OF GLASS REINFORCED POLYMER-CEMENT RODS

Spec. No.	S/C Ratio	Ultimate Stress lbf/in^2	Ultimate Strain x 10^3	Elastic Modulus of Composite E_o lbf/in^2 x 10^{-6}	Estimated Elastic Modulus Matrix E_m x 10^{-6}	Estimated Stress in glass at failure x 10^{-3} lbf/in^2
18.1	0.2	5440.8	6.5000	1.5139	0.8030	65.0
18.2		6515.2	9.2500	1.3607	0.6656	92.5
18.3		6248.8	8.9700	1.4596	0.8619	89.7
18.4		5100.3	7.4000	1.5742	0.8996	74.0
18.5		6519.9	9.6000	1.4658	0.9313	96.0
18.6		4864.7	7.7400	1.2809	0.7903	77.4
18.15	0.25	7458.0	11.2000	1.2475	0.6751	112.0
18.16		6123.2	8.3100	1.3760	0.7983	83.1
18.17		7124.3	10.2200	1.2034	0.5772	102.2
18.18		7015.1	11.1200	0.7849	0.1655	111.2
18.19	0.225	7510.7	11.5800	0.9937	0.4200	115.8
18.20		6231.8	9.4000	1.0666	0.4783	94.0
18.21		5724.6	8.1000	1.1265	0.5233	81.0
18.22		6859.6	10.3000	1.0289	0.4326	103.0

TABLE 5.1 (Continued)

Spec. No.	Ratio	Ultimate Stress lbf/in^2	Ultimate Strain $\times 10^3$	Elastic Modulus of Composite E_o lbf/in^2 $\times 10^{-6}$	Estimated Elastic Modulus Matrix $E_m \times 10^{-6}$	Estimated Stress in glass at failure $\times 10^{-3}$ lbf/in^2
18.23	0.2	7487.4	10.8600	1.2918	0.7199	108.6
18.24		6510.8	9.0900	1.2637	0.6934	90.9
18.25		5879.1	10.0500	1.1884	0.7193	100.5
18.26		6029.7	9.8700	1.2880	0.8337	98.7
18.27	0.175	6032.2	8.9000	1.6659	1.1929	89.0
18.28		7035.9	9.6600	1.5635	1.0864	96.6
18.29		5348.9	8.4800	1.8298	1.3693	84.8
18.30		6975.9	10.1200	1.5711	1.0464	101.2
18.31	0.15	6040.5	8.8300	1.8593	1.4138	88.3
18.32		4581.3	6.4800	1.6570	1.2478	64.8
18.33		6286.6	9.4300	1.6809	1.2089	94.3
18.34		6115.5	9.1600	1.6609	1.2126	91.6
18.36	0.125	4793.6	5.7100	1.7159	1.2792	57.1
18.37		4982.2	8.6100	1.5043	1.1133	86.1
18.38		2833.5	7.0300			70.3

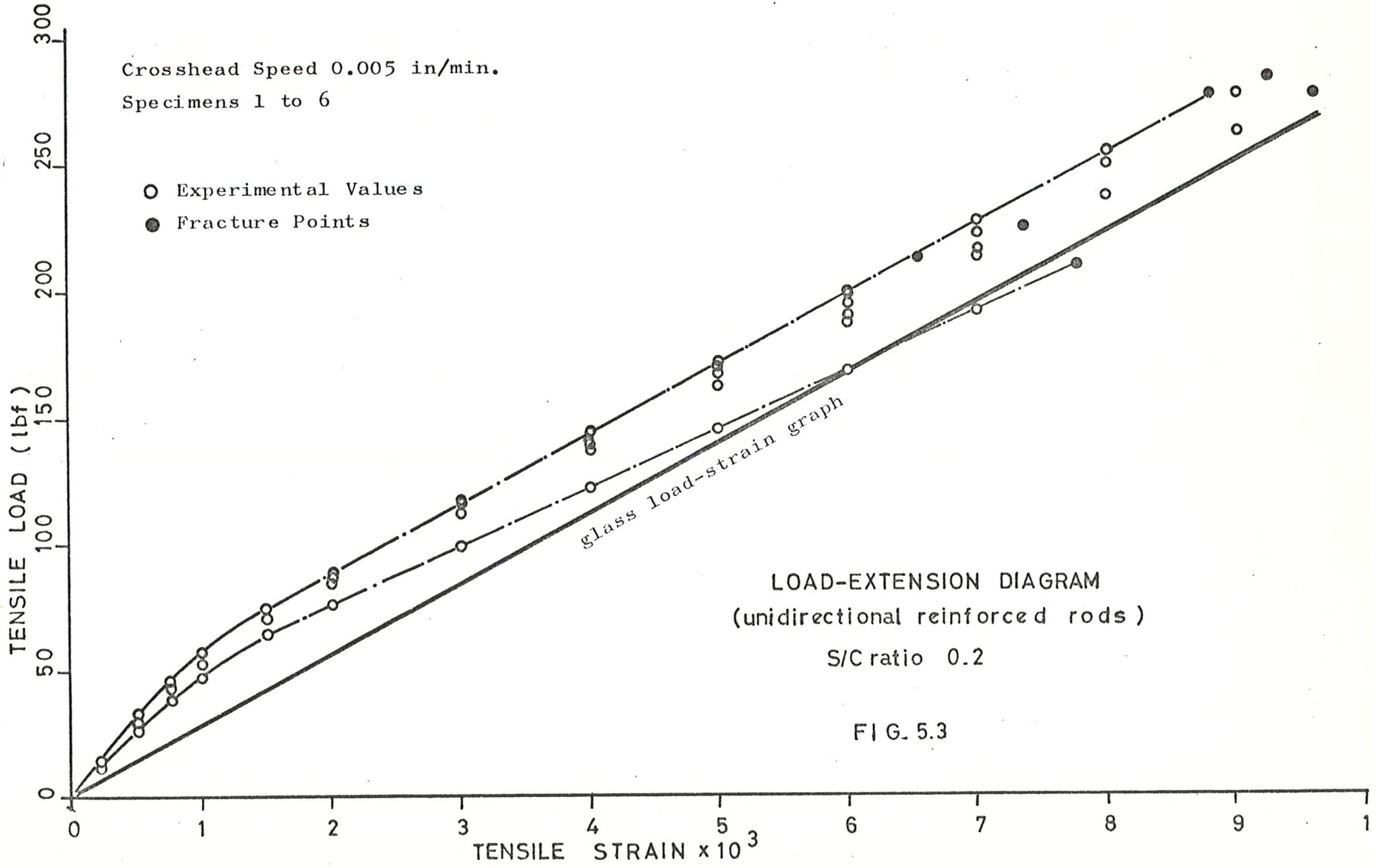

LOAD-EXTENSION DIAGRAM
(unidirectional reinforced rods)
S/C ratio 0.2

FIG. 5.3

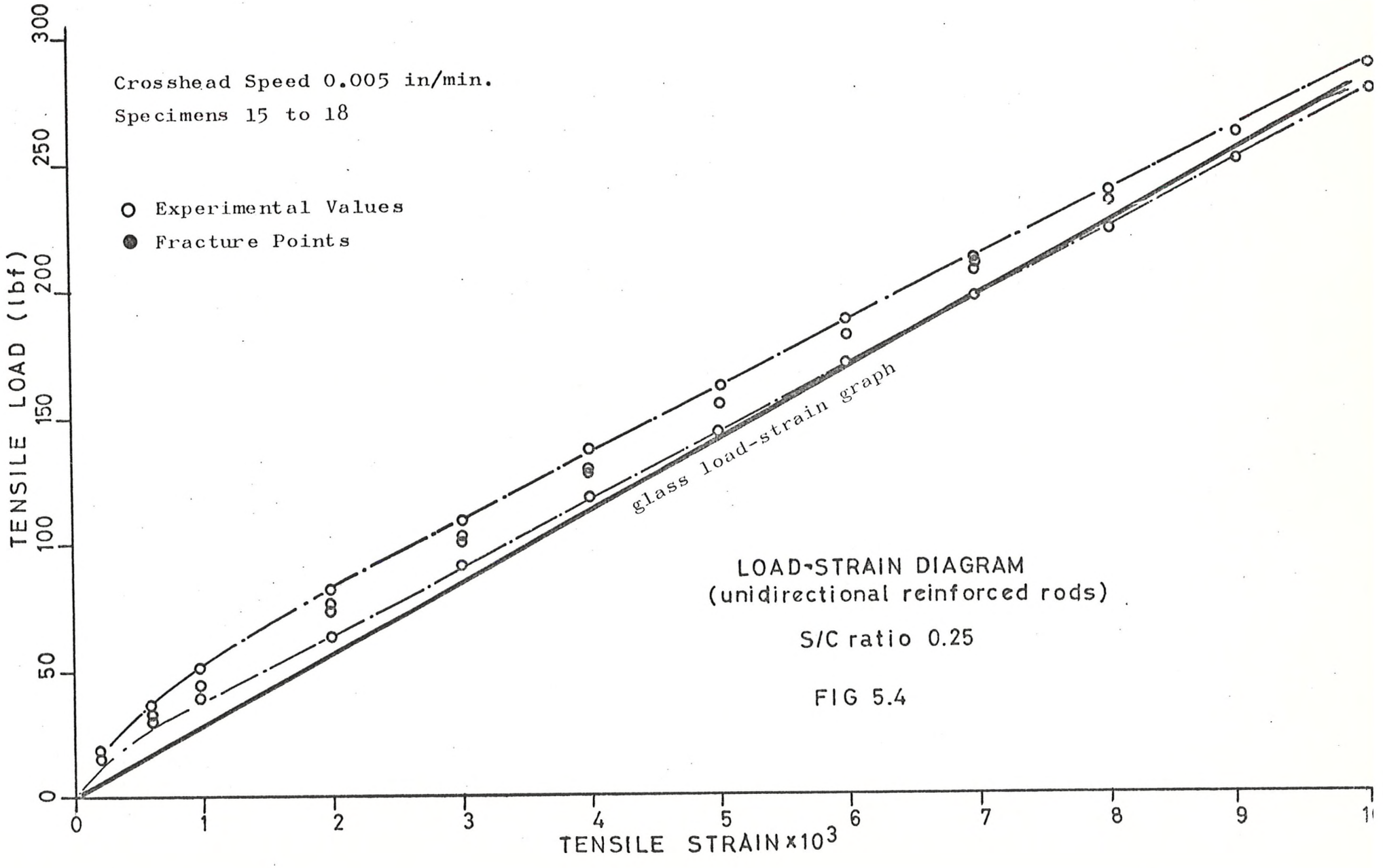

LOAD-STRAIN DIAGRAM
(unidirectional reinforced rods)

S/C ratio 0.25

FIG 5.4

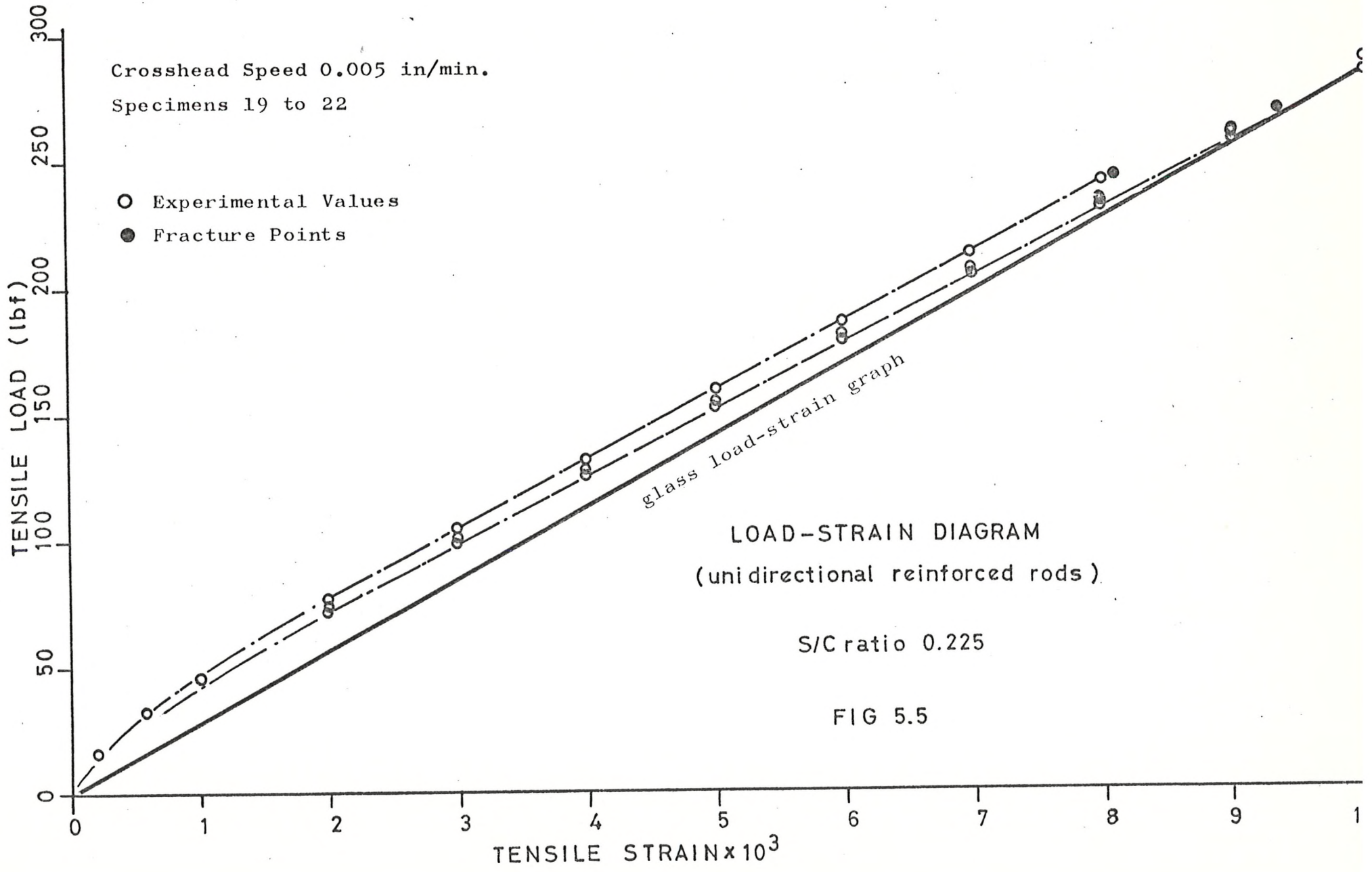
Crosshead Speed 0.005 in/min.
Specimens 19 to 22
Experimental Values
Fracture Points
TENSILE LOAD (lbf)
TENSILE STRAIN x 10^3
glass load-strain graph
LOAD-STRAIN DIAGRAM
(unidirectional reinforced rods)
S/C ratio 0.225
FIG 5.5
0
50
100
150
200
250
300
1
2
3
4
5
6
7
8
9

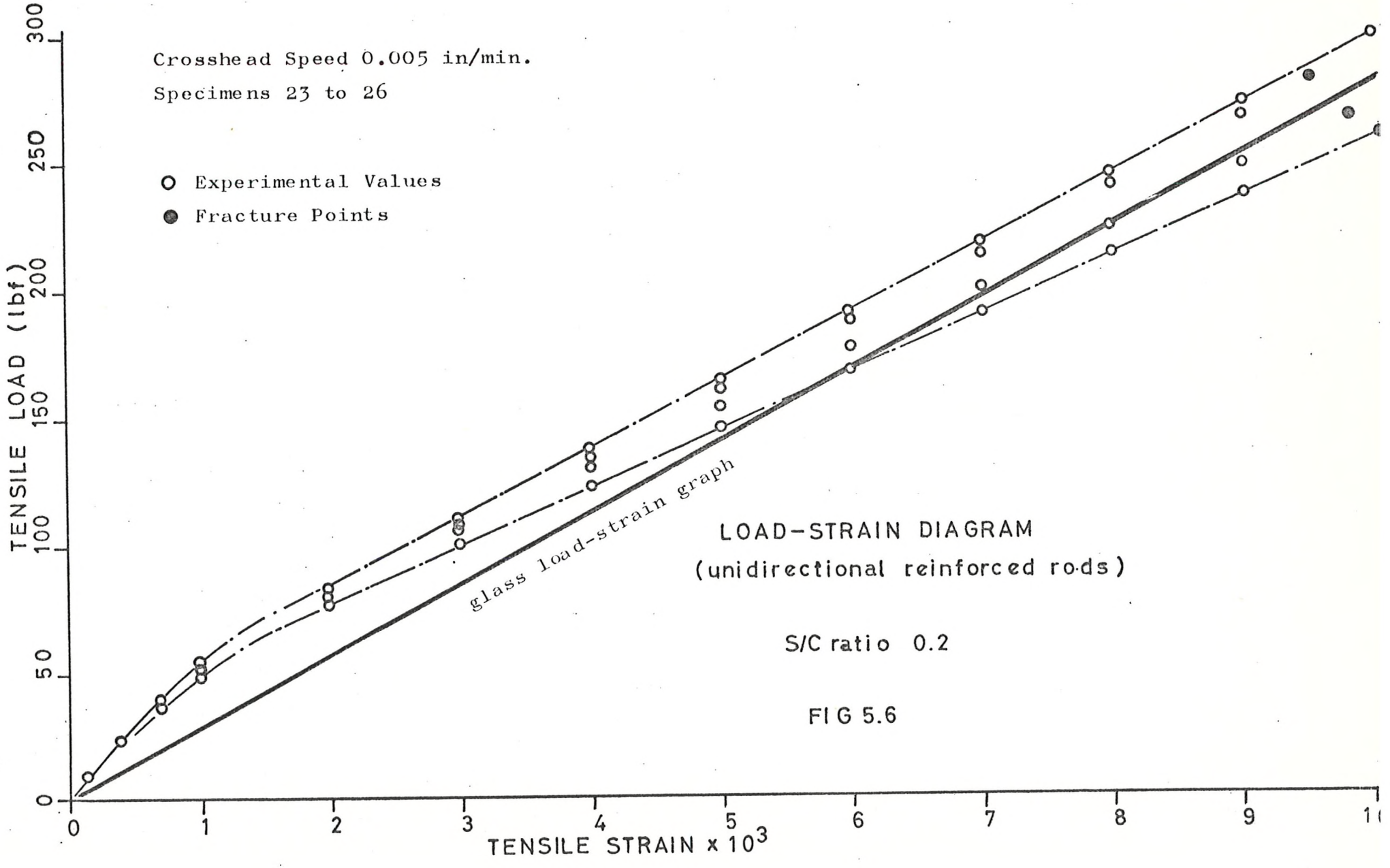

LOAD-STRAIN DIAGRAM
(unidirectional reinforced rods)

S/C ratio 0.2

FIG 5.6

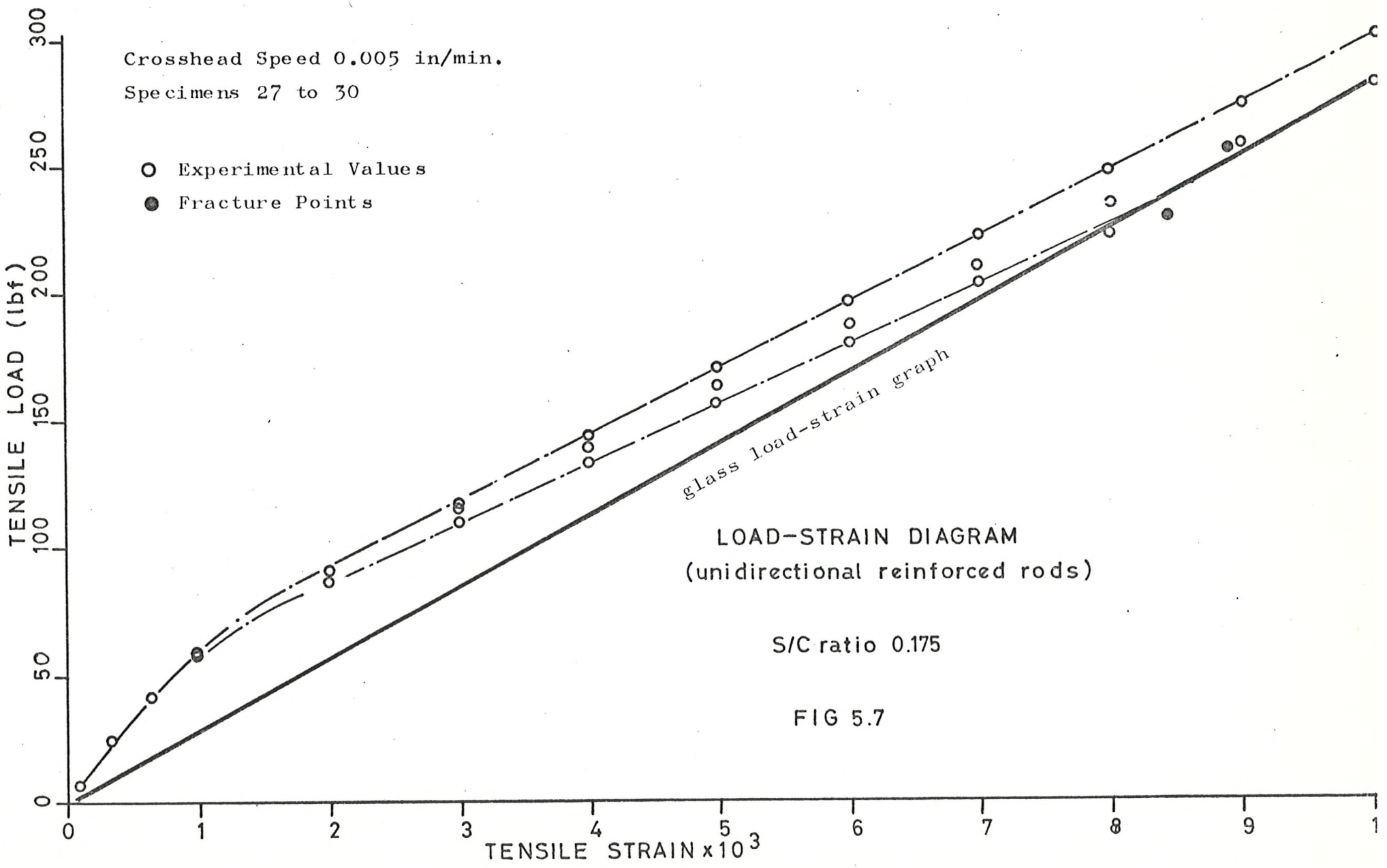

LOAD–STRAIN DIAGRAM
(unidirectional reinforced rods)

S/C ratio 0.175

FIG 5.7

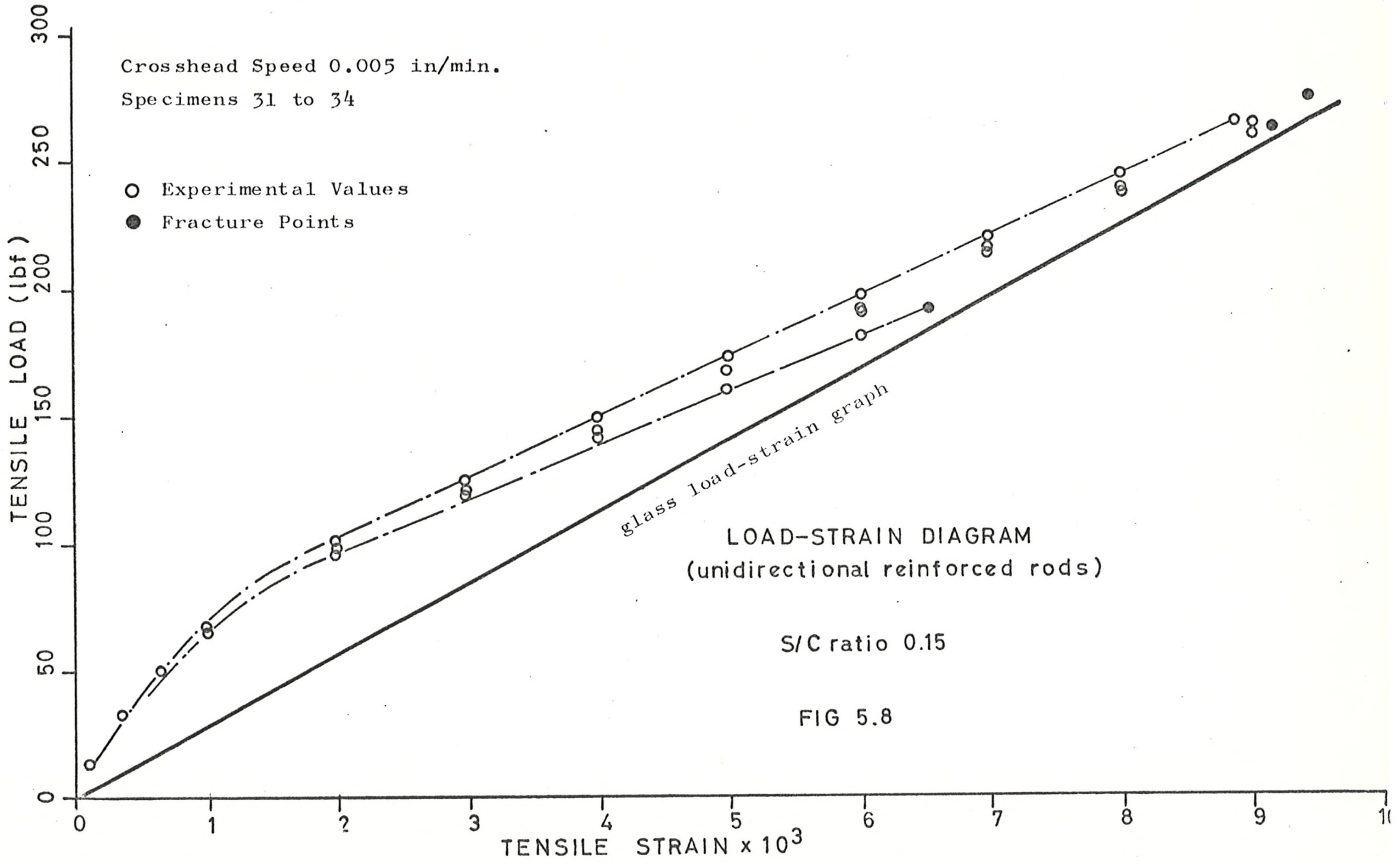

LOAD-STRAIN DIAGRAM
(unidirectional reinforced rods)

S/C ratio 0.15

FIG 5.8

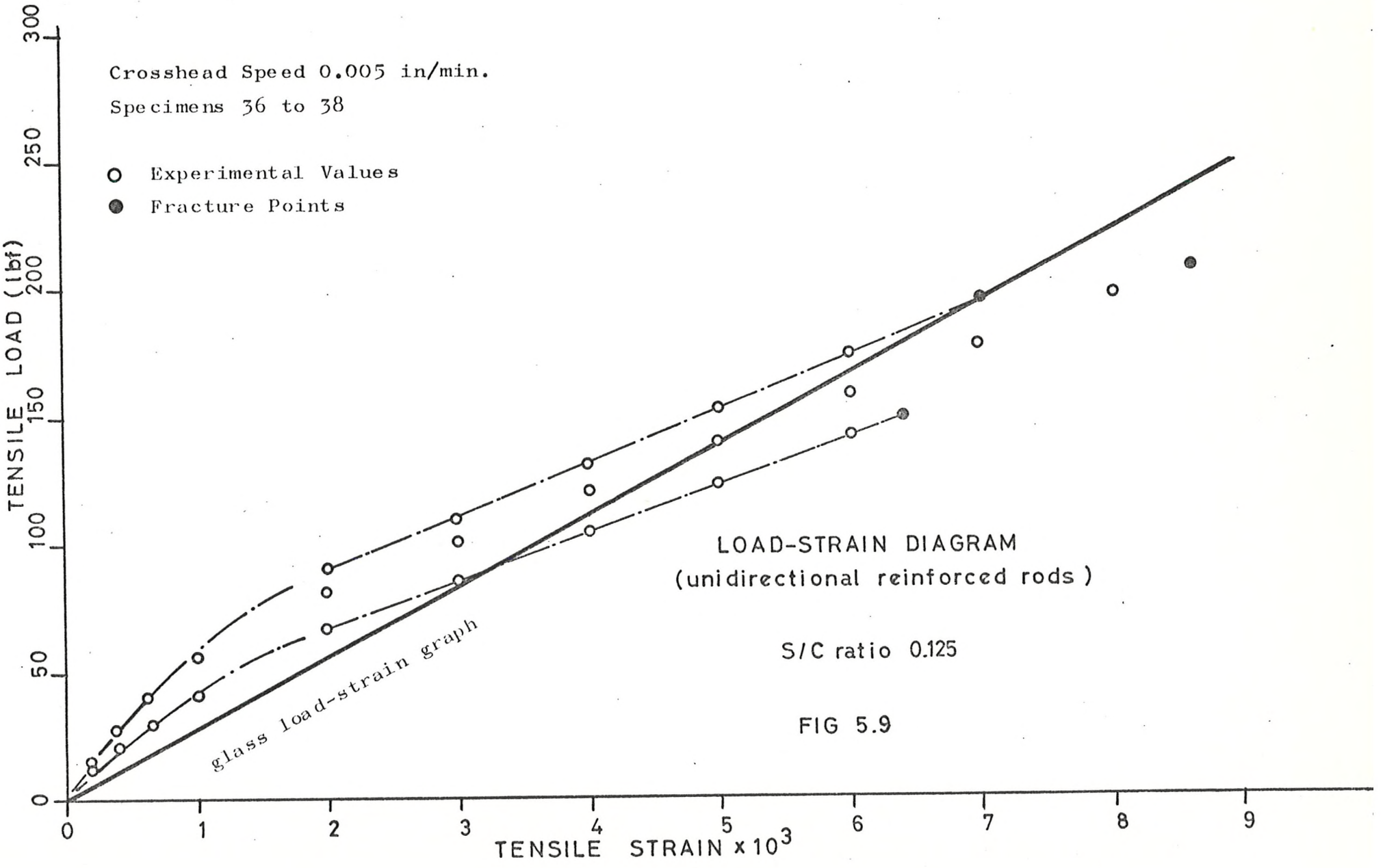
Crosshead Speed 0.005 in/min.
Specimens 36 to 38
Experimental Values
Fracture Points
TENSILE LOAD (lbf)
0
50
100
150
200
250
300
0
1
2
3
4
5
6
7
8
9
TENSILE STRAIN x 10^3
glass load-strain graph
LOAD-STRAIN DIAGRAM
(unidirectional reinforced rods)
S/C ratio 0.125
FIG 5.9

5.5 Tensile Experimental Results (Various Reinforcements)

A summary of the initial elastic modulus and ultimate tensile strengths is given in Tables 5.2 and 5.3, tested at a crosshead speed of 0.005 in/min at an age of 30 days. The reinforcements used were glass cloth, continuous filament mat and woven roving (see Appendix B, Sec. B1). Detailed results may be found in Appendix H, Table H7.

Fig. 5.10 illustrates the stress-strain relationship of specimens when using glass cloth as the reinforcement. The relatively high tensile strengths developed in this material are due mainly to the glass cloth since very little matrix material was used (i.e. very high glass volume content).

Fig. 5.11 illustrates a material where continuous filament mat is the reinforcement. Here it is evident that the initial elastic range is almost non existent leading to a long linear region where moderate strengths are developed. There does not appear to be any significant advantage in using continuous filament mat instead of chopped strand mat.

When using woven roving as the reinforcement Figs. 5.12, 5.13 and 5.14 show the orthotropic-properties of the material. This is demonstrated by comparing Figs. 5.12 and 5.13 where specimens were cut parallel to the warp and weft directions and the tensile properties are approximately the same. Fig. 5.14 shows the significant fall of tensile strength when cutting specimens at 45^{o} to the weft direction where the fibres are not aligned with the applied load.

All specimens showed a high degree of variability.

TABLE 5.2

STRESS AT FRACTURE LBF/IN^2

Specimen Numbers	Mean Stress	Standard Deviation	% Coeff. of Var.	Limits, p = 0.1	
				Upper	Lower
21.2 - 21.6	6776.0	648.02	9.564	7393.2	6158.7
22.6 - 22.12	2532.2	171.69	6.78	2733.9	2330.5
23.1 - 23.5	3419.9	648.73	18.97	4037.8	2801.9
23.10 - 23.14	4310.7	419.02	9.72	4709.8	3911.5
23.15 - 23.19	1694.1	100.3	5.92	1789.7	1598.5

TABLE 5.3

INITIAL ELASTIC MODULUS (LBF/IN^2)

Specimen Numbers	Initial Elastic Modulus E_o x 10^{-6}	Standard Deviation x 10^{-6}	% Coeff of Var.	Limits, p = 0.1 x 10^{-6}	
				Upper	Lower
21.2 - 21.6	0.9792	0.1681	17.17	1.1394	0.8191
22.6 - 22.12	0.4025	1.245	30.93	0.5487	0.2562
23.1 - 23.5	2.4243	1.188	48.98	3.5554	1.2931
23.10 - 23.14	4.309	1.856	43.09	6.0779	2.5407
23.15 - 23.19	1.5192	0.7853	51.69	2.2673	0.7712

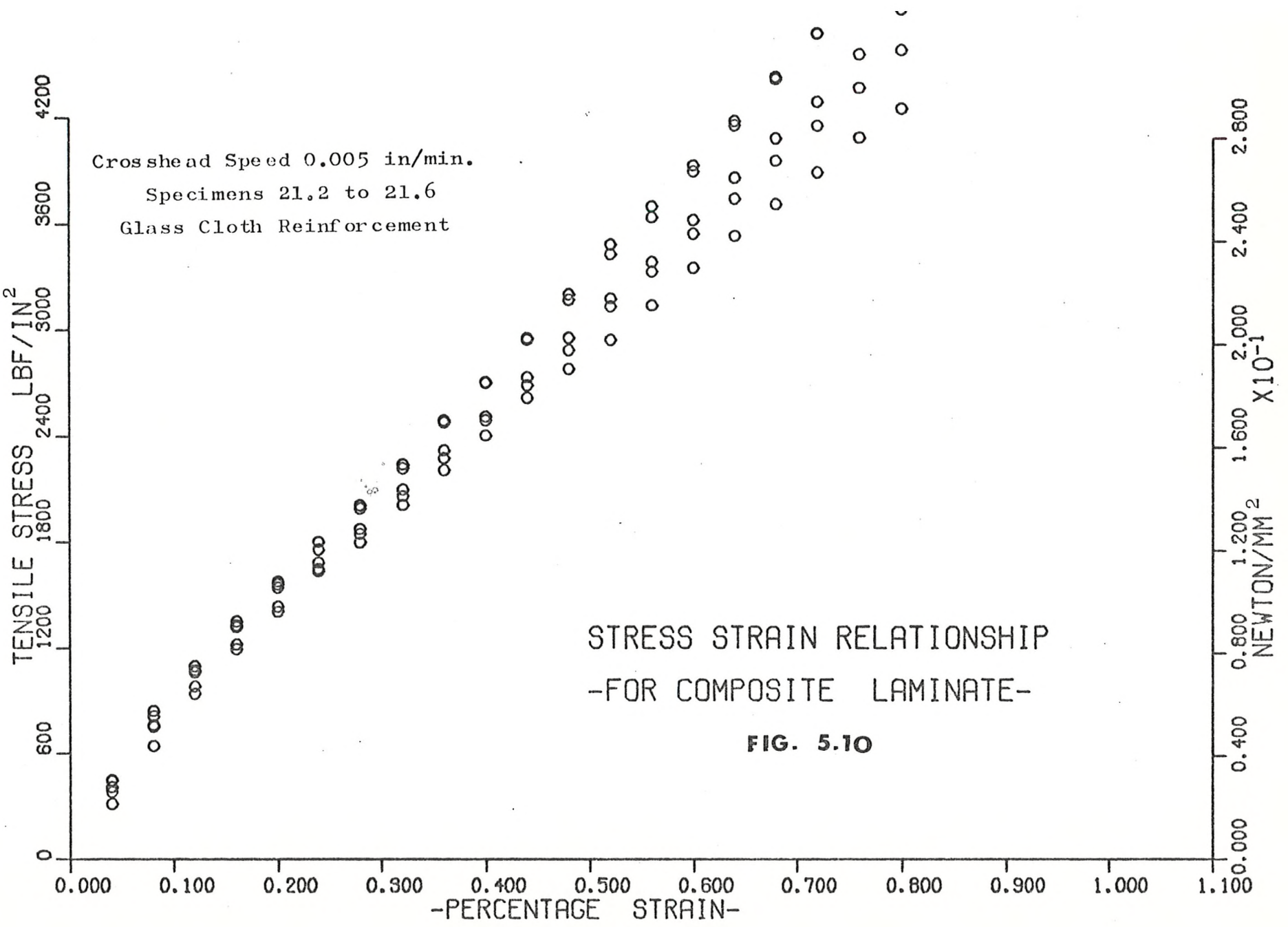
Crosshead Speed 0.005 in/min.
Specimens 21.2 to 21.6
Glass Cloth Reinforcement
TENSILE STRESS LBF/IN^2
0
600
1200
1800
2400
3000
3600
4200
0.000
0.100
0.200
0.300
0.400
0.500
0.600
0.700
0.800
0.900
1.000
1.100
-PERCENTAGE STRAIN-
0.000
0.400
0.800
1.200
1.600
2.000
2.400
2.800
NEWTON/MM^2 X10^{-1}
STRESS STRAIN RELATIONSHIP
-FOR COMPOSITE LAMINATE-

FIG. 5.10

Crosshead Speed 0.005 in/min.

Specimens 22.6, 22.8, 22.10 and 22.12

Continuous Filament Mat Reinforcent.

STRESS STRAIN RELATIONSHIP

-FOR COMPOSITE LAMINATE-

FIG. 5.11

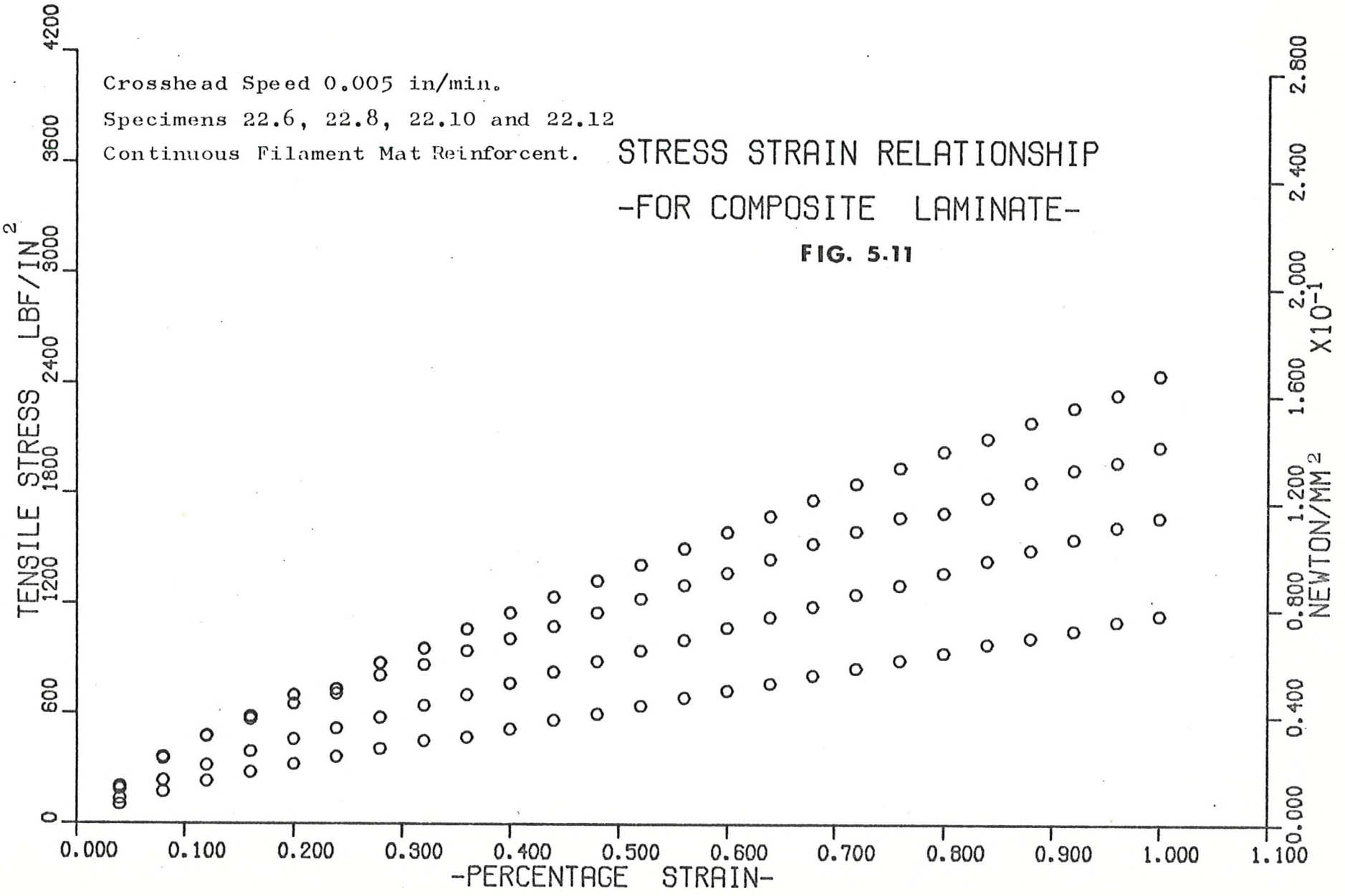

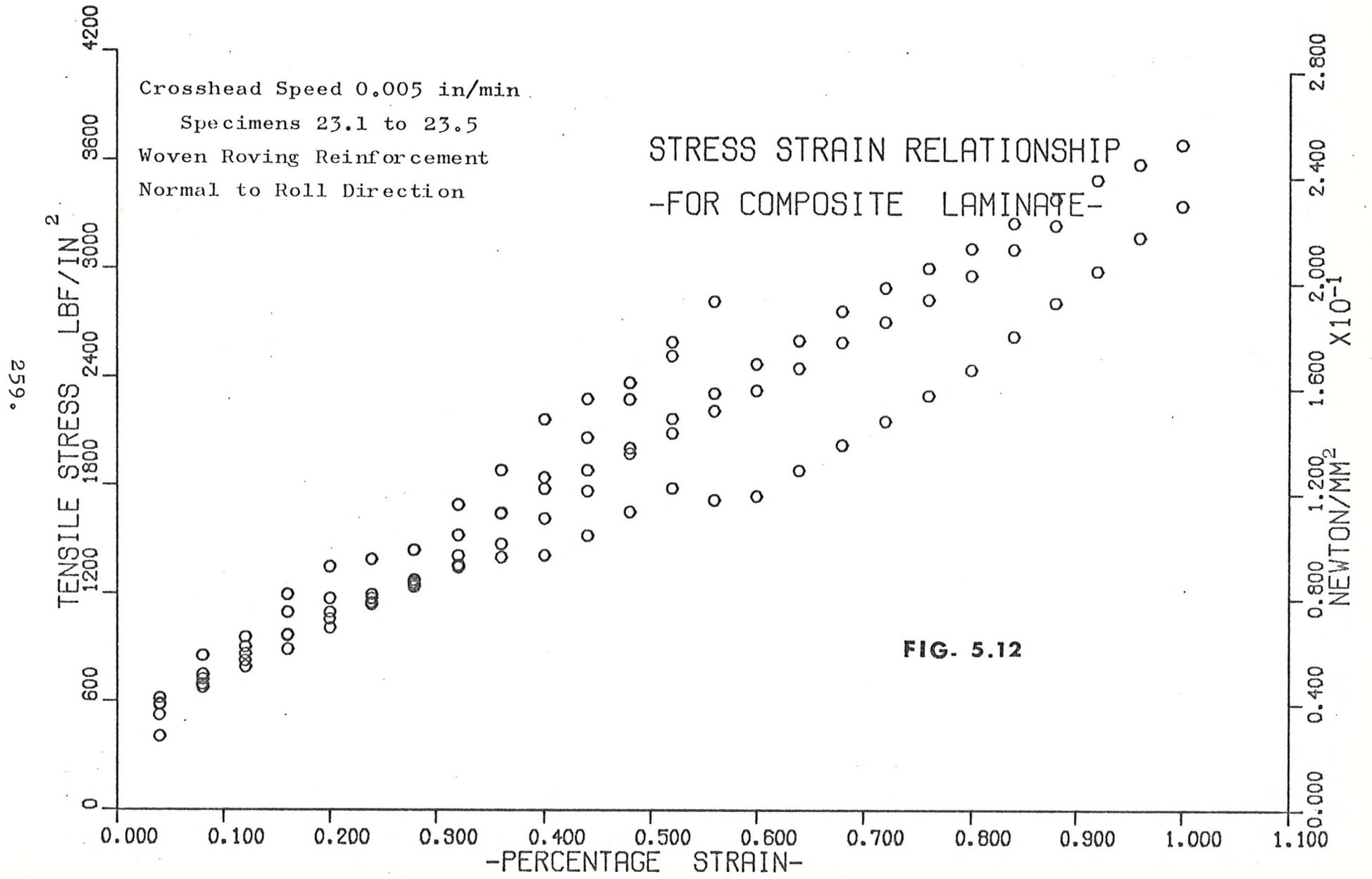
Crosshead Speed 0.005 in/min
Specimens 23.1 to 23.5
Woven Roving Reinforcement
Normal to Roll Direction
STRESS STRAIN RELATIONSHIP
-FOR COMPOSITE LAMINATE-
TENSILE STRESS LBF/IN2
NEWTON/MM2 X10-1
-PERCENTAGE STRAIN-
0
600
1200
1800
2400
3000
3600
4200
0.000
0.400
0.800
1.200
1.600
2.000
2.400
2.800
0.000
0.100
0.200
0.300
0.400
0.500
0.600
0.700
0.800
0.900
1.000
1.100

FIG. 5.12

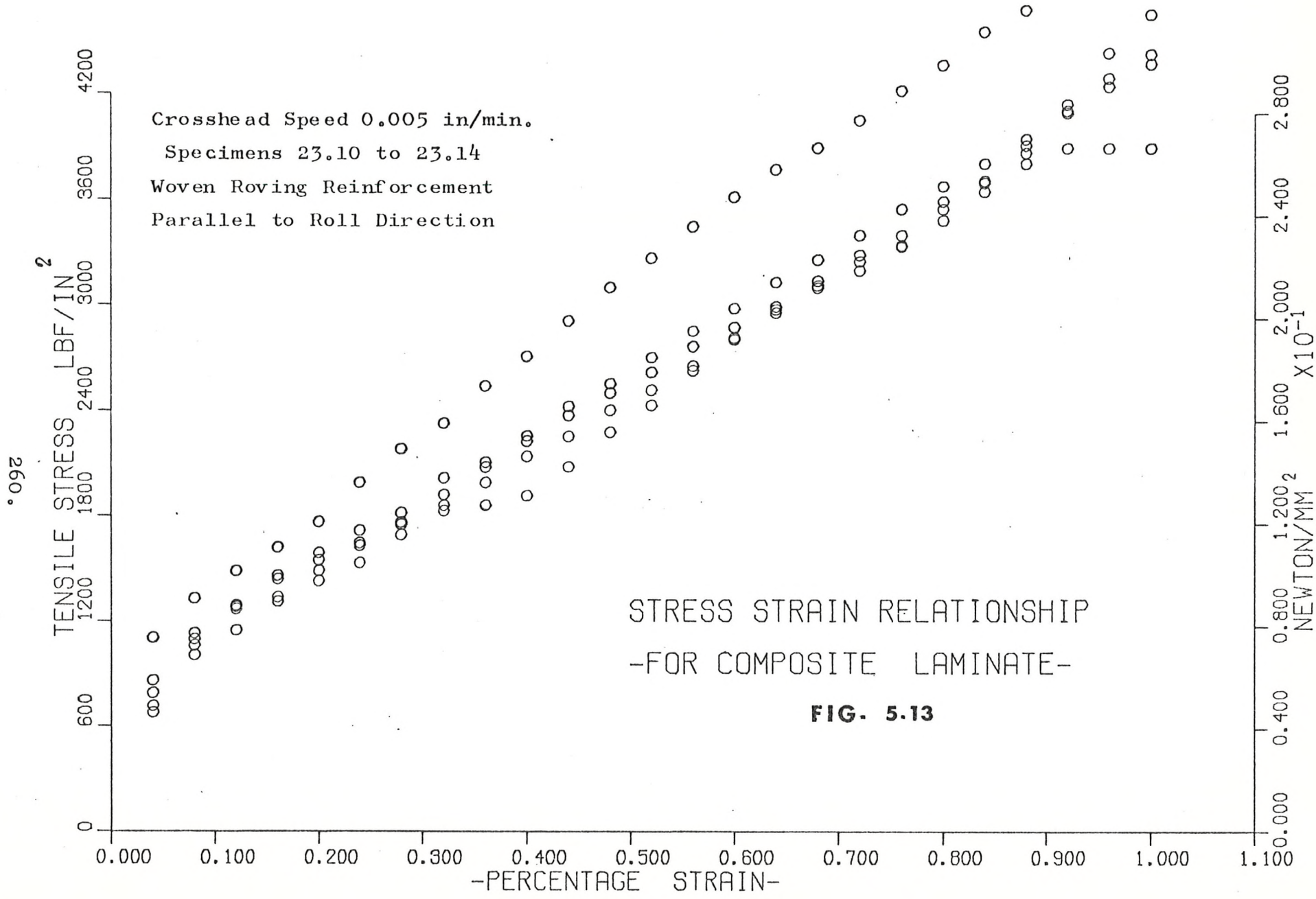

STRESS STRAIN RELATIONSHIP

-FOR COMPOSITE LAMINATE-

FIG. 5.13

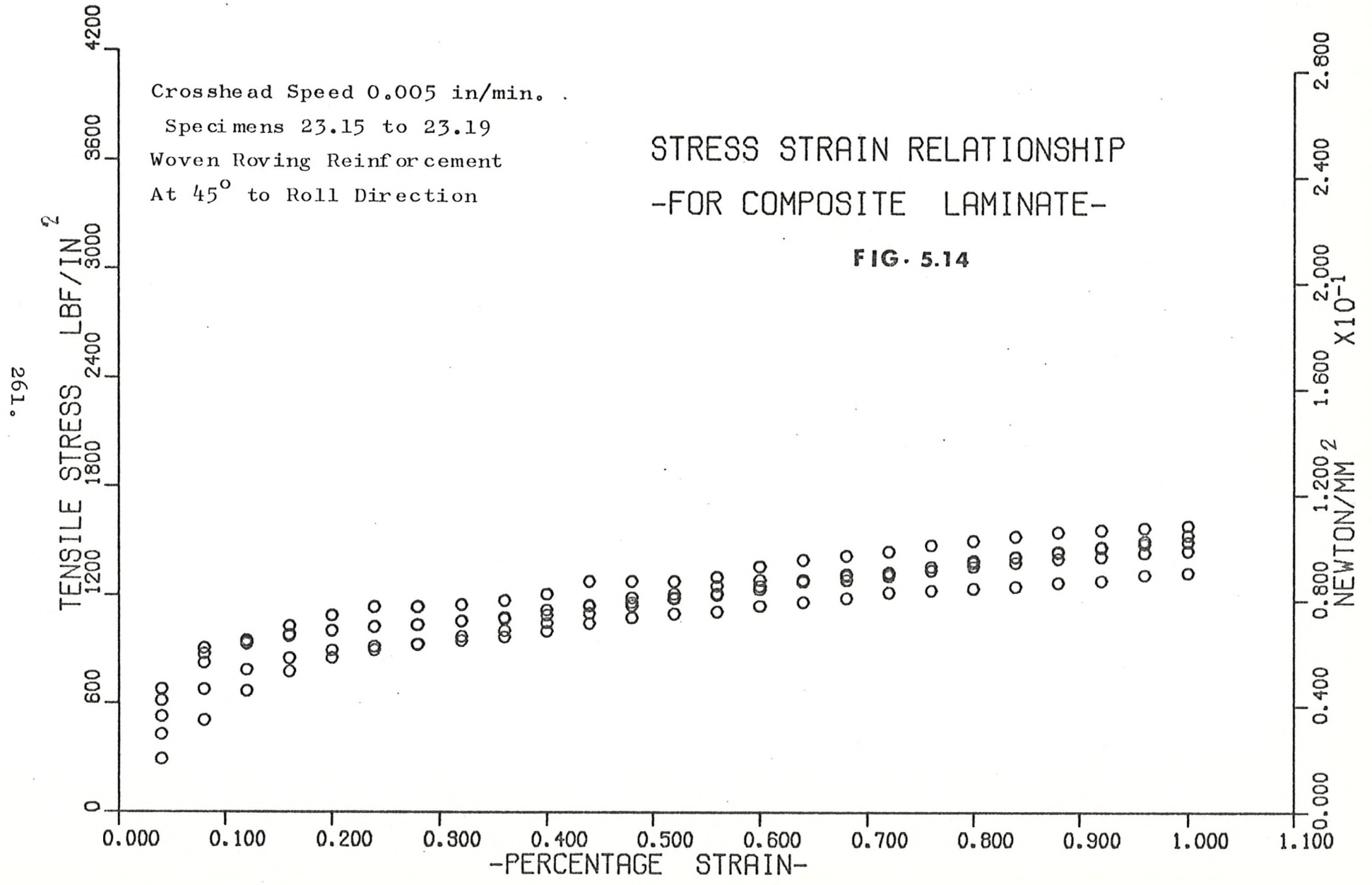
Crosshead Speed 0.005 in/min.
Specimens 23.15 to 23.19
Woven Roving Reinforcement
At 45° to Roll Direction
STRESS STRAIN RELATIONSHIP
-FOR COMPOSITE LAMINATE-
FIG. 5.14
TENSILE STRESS LBF/IN2
0
600
1200
1800
2400
3000
3600
4200
NEWTON/MM2 X10-1
0.000
0.400
0.800
1.200
1.600
2.000
2.400
2.800
0.000
0.100
0.200
0.300
0.400
0.500
0.600
0.700
0.800
0.900
1.000
1.100
-PERCENTAGE STRAIN-

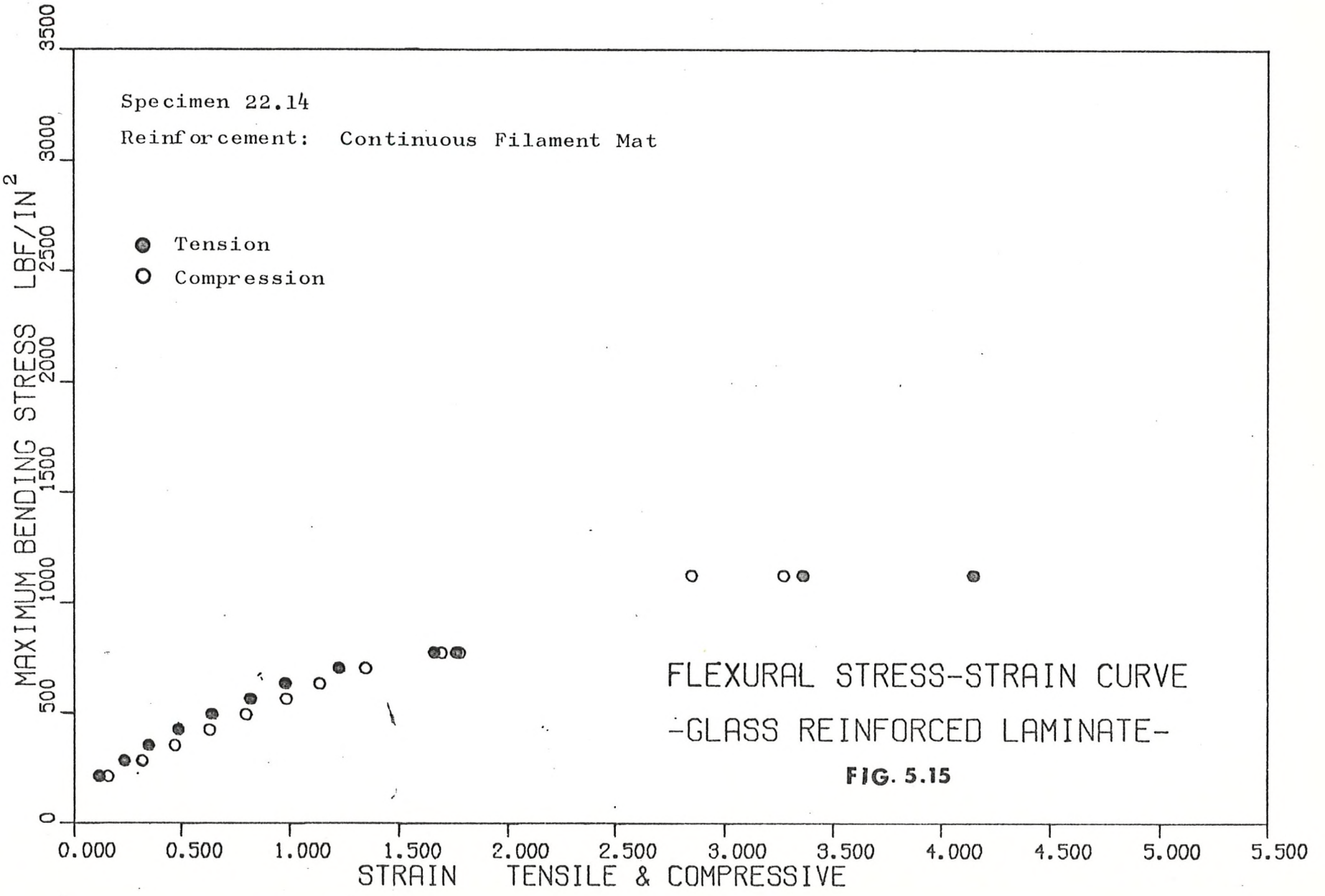

FLEXURAL STRESS-STRAIN CURVE

-GLASS REINFORCED LAMINATE-

FIG. 5.15

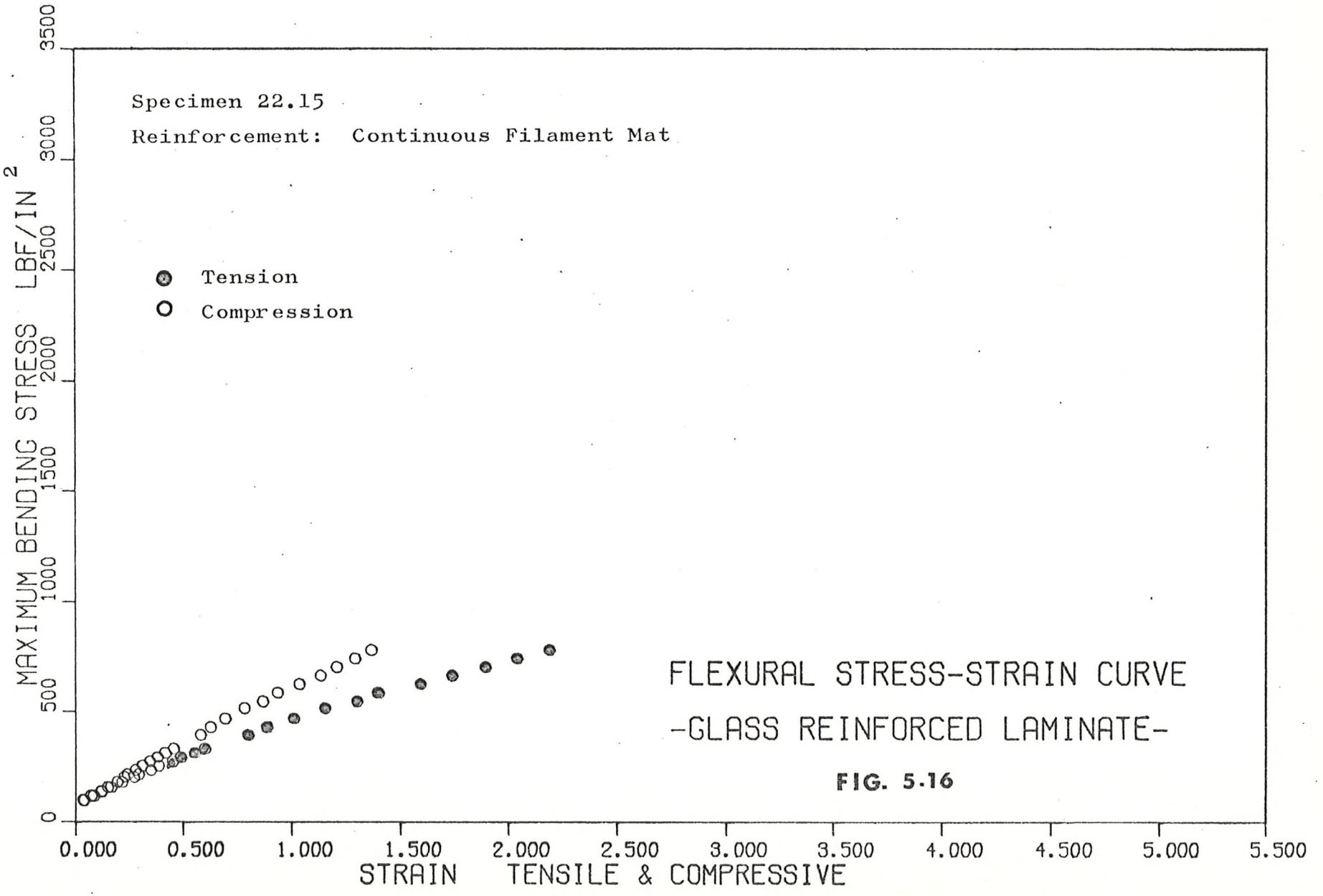

FLEXURAL STRESS-STRAIN CURVE

-GLASS REINFORCED LAMINATE-

FIG. 5.16

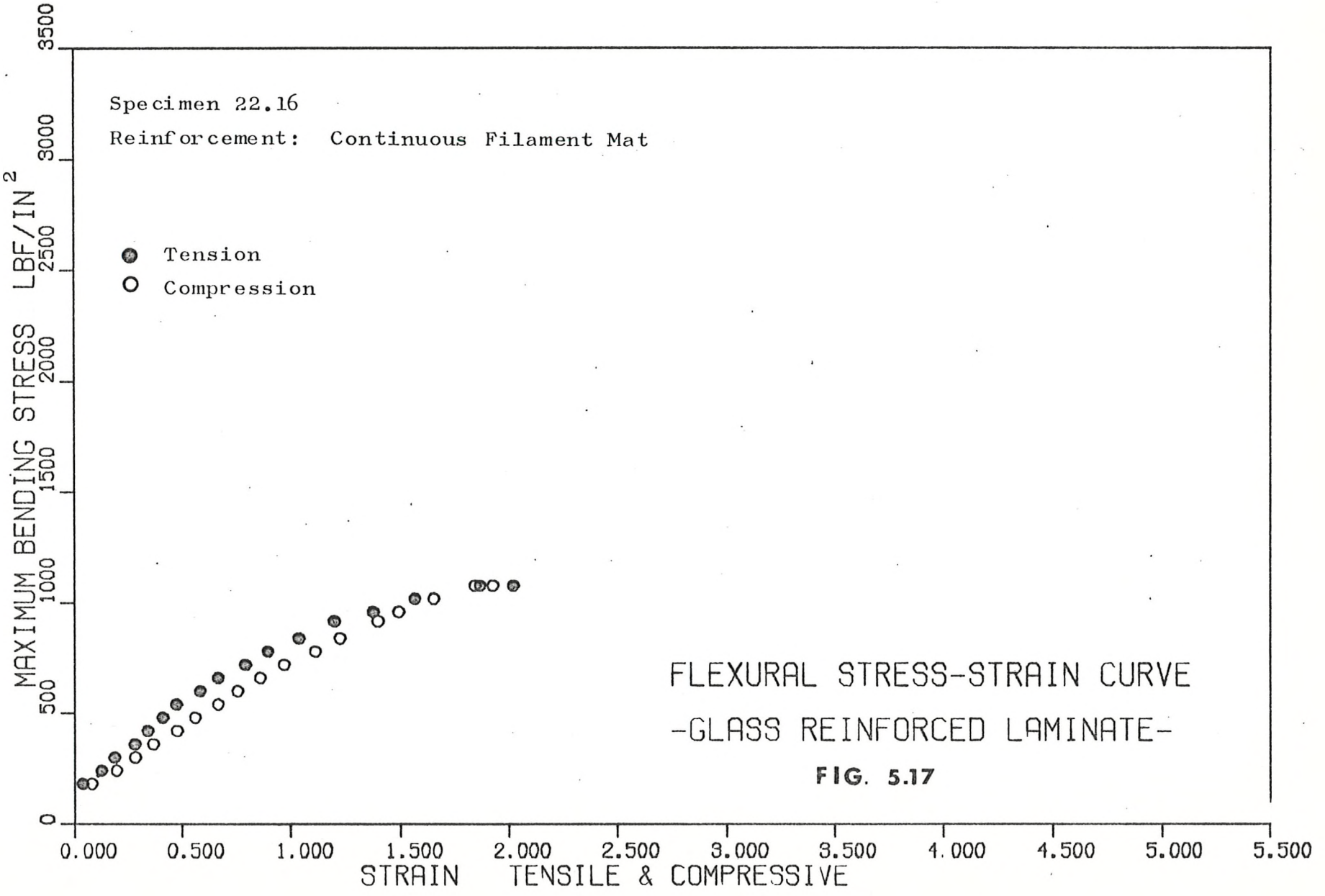

FLEXURAL STRESS-STRAIN CURVE

-GLASS REINFORCED LAMINATE-

FIG. 5.17

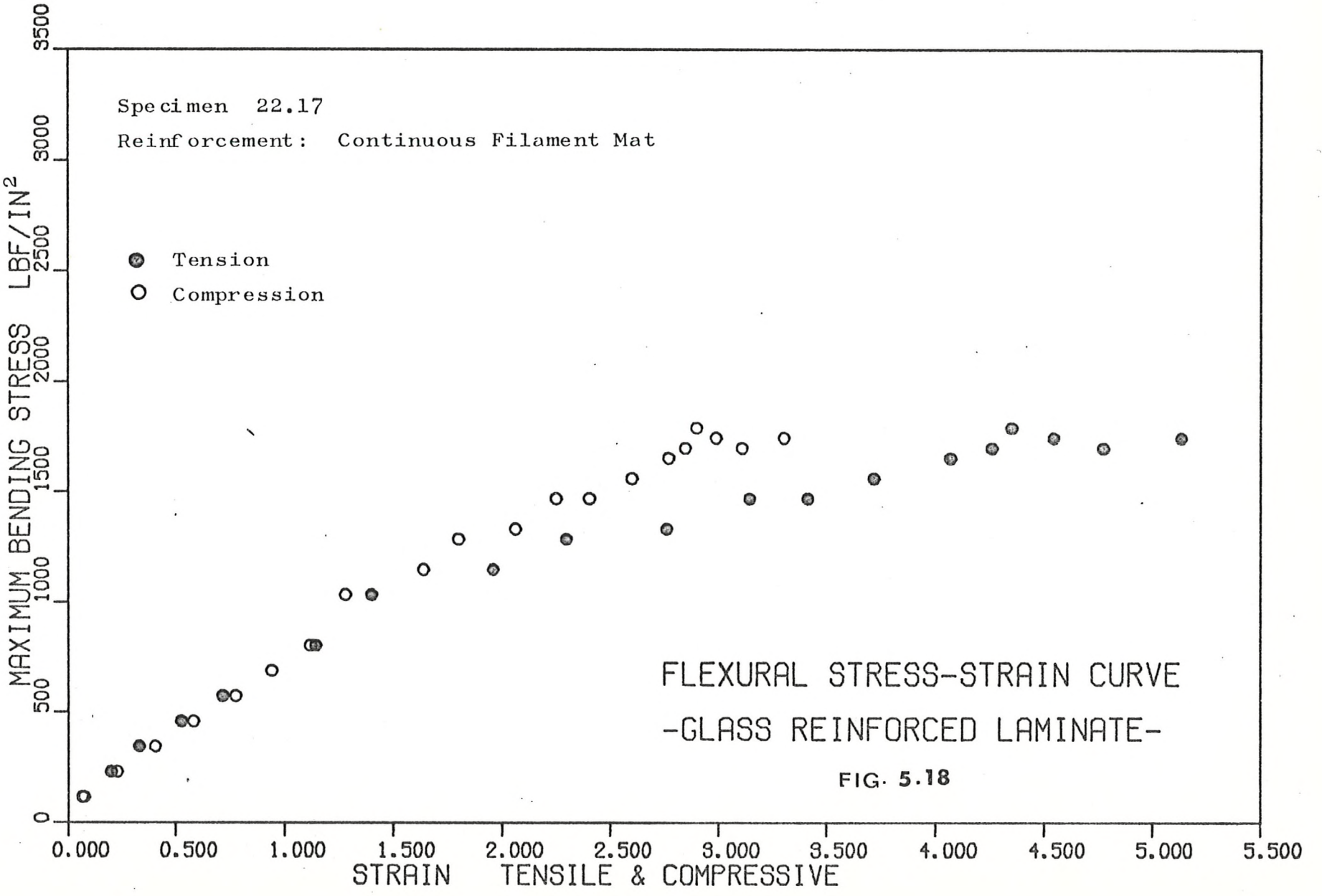

FLEXURAL STRESS-STRAIN CURVE

-GLASS REINFORCED LAMINATE-

FIG. 5.18

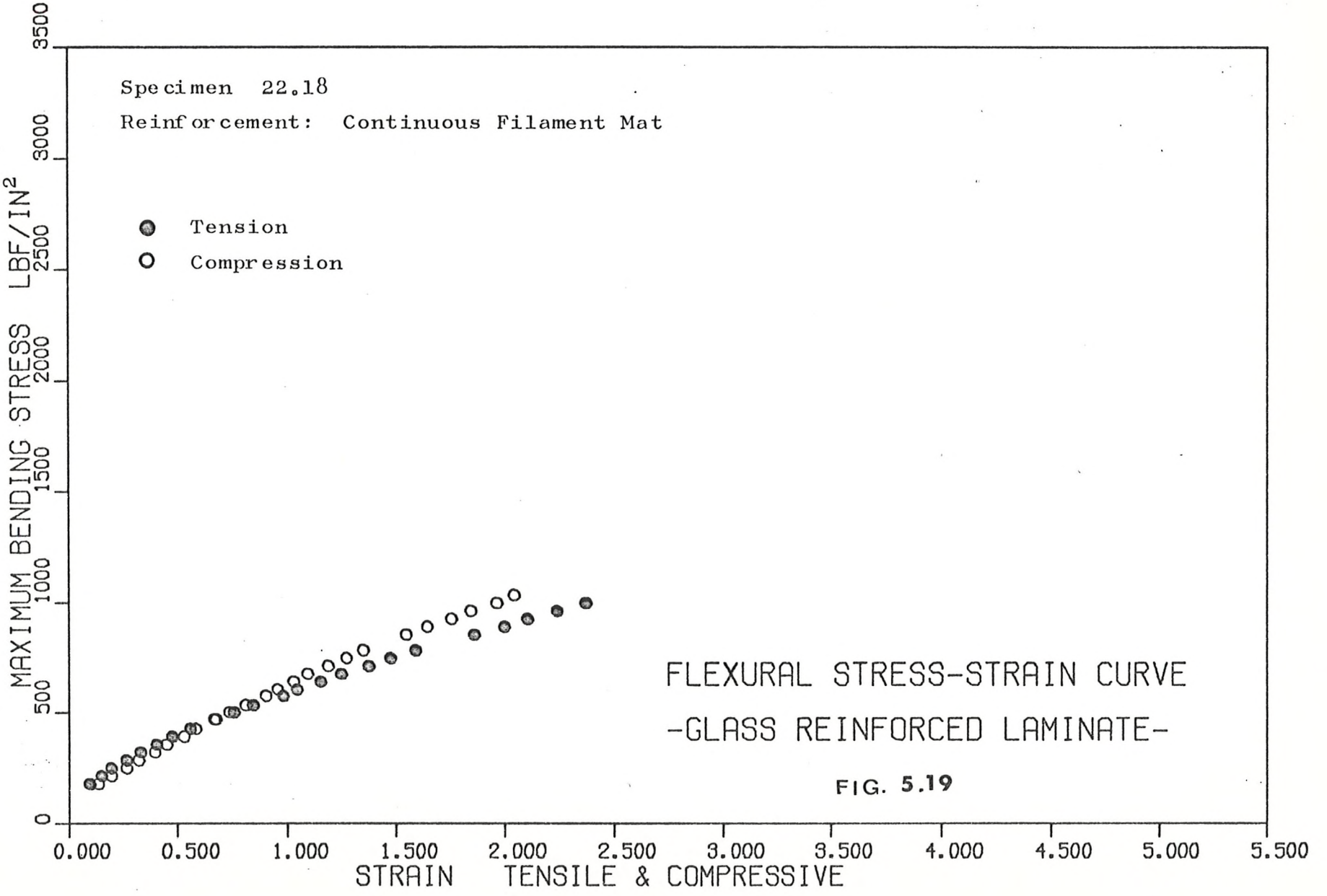

FLEXURAL STRESS-STRAIN CURVE

-GLASS REINFORCED LAMINATE-

FIG. 5.19

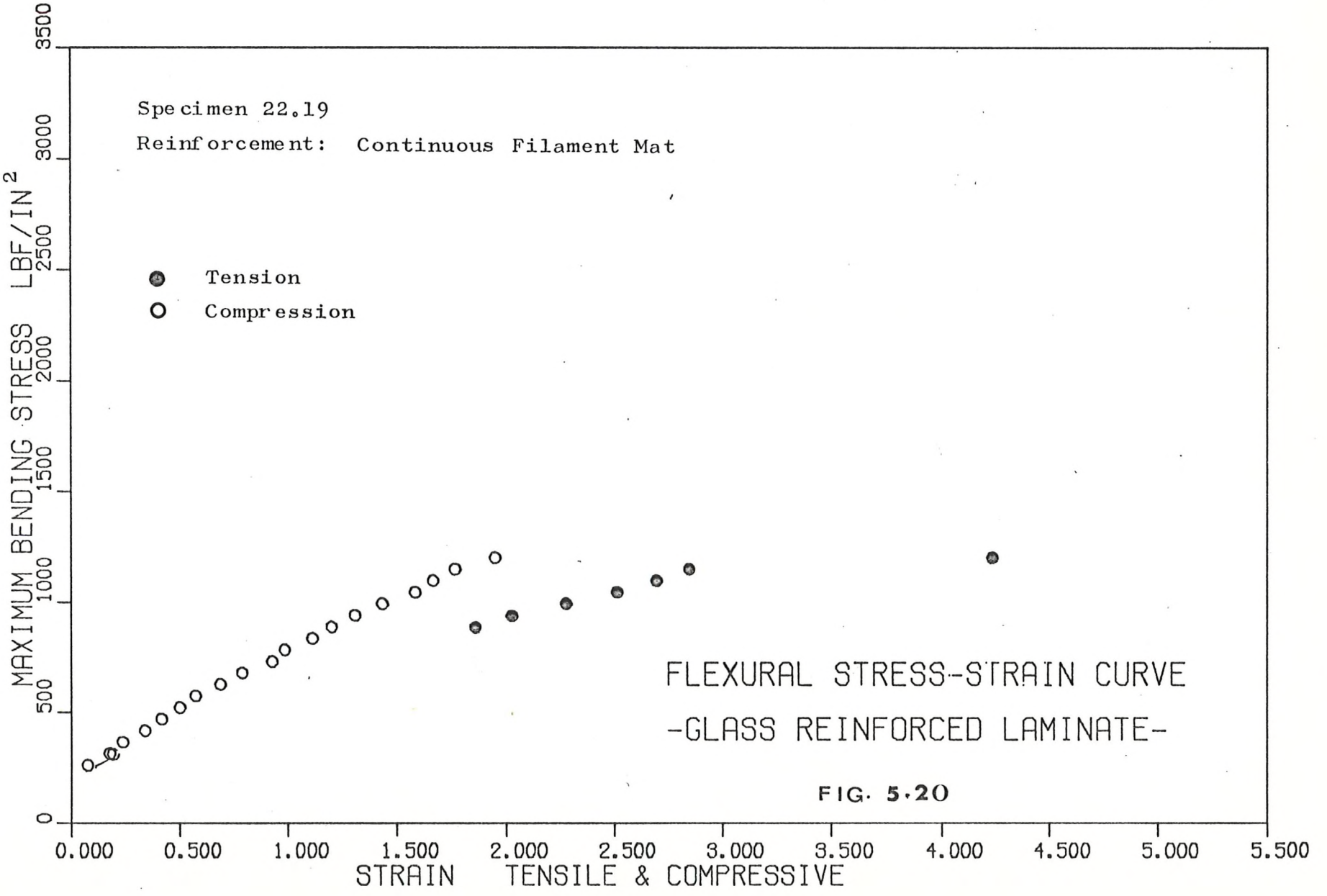
Specimen 22.19
Reinforcement: Continuous Filament Mat
Tension
Compression
MAXIMUM BENDING STRESS LBF/IN 2
0
500
1000
1500
2000
2500
3000
3500
0.000
0.500
1.000
1.500
2.000
2.500
3.000
3.500
4.000
4.500
5.000
5.500
STRAIN TENSILE & COMPRESSIVE
FLEXURAL STRESS-STRAIN CURVE
-GLASS REINFORCED LAMINATE-

FIG. 5.20

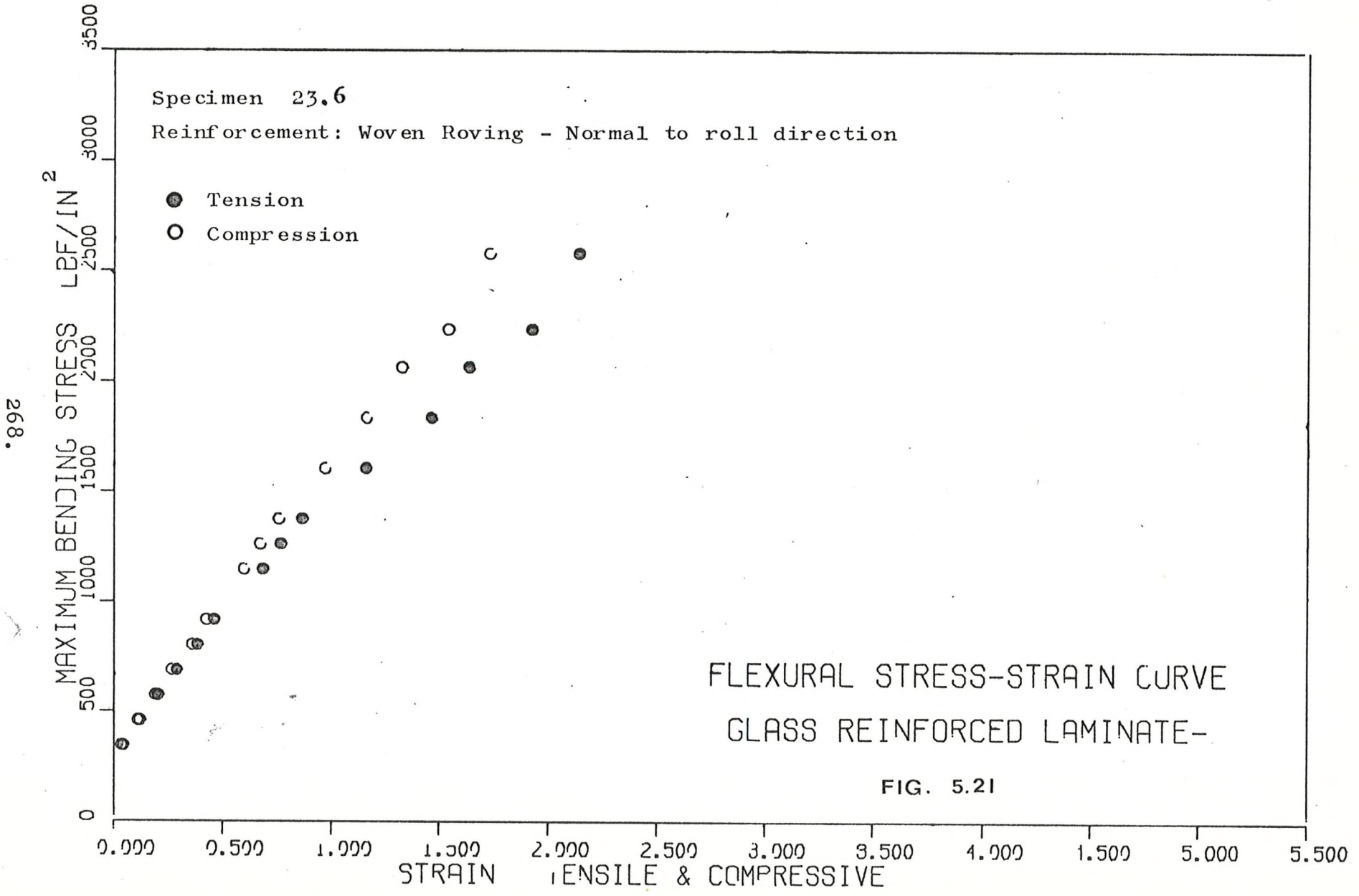
Specimen 23.6
Reinforcement: Woven Roving - Normal to roll direction
Tension
Compression
MAXIMUM BENDING STRESS LBF/IN 2
0
500
1000
1500
2000
2500
3000
3500
0.000
0.500
1.000
1.500
2.000
2.500
3.000
3.500
4.000
4.500
5.000
5.500
STRAIN TENSILE & COMPRESSIVE
FLEXURAL STRESS-STRAIN CURVE
GLASS REINFORCED LAMINATE-
FIG. 5.21

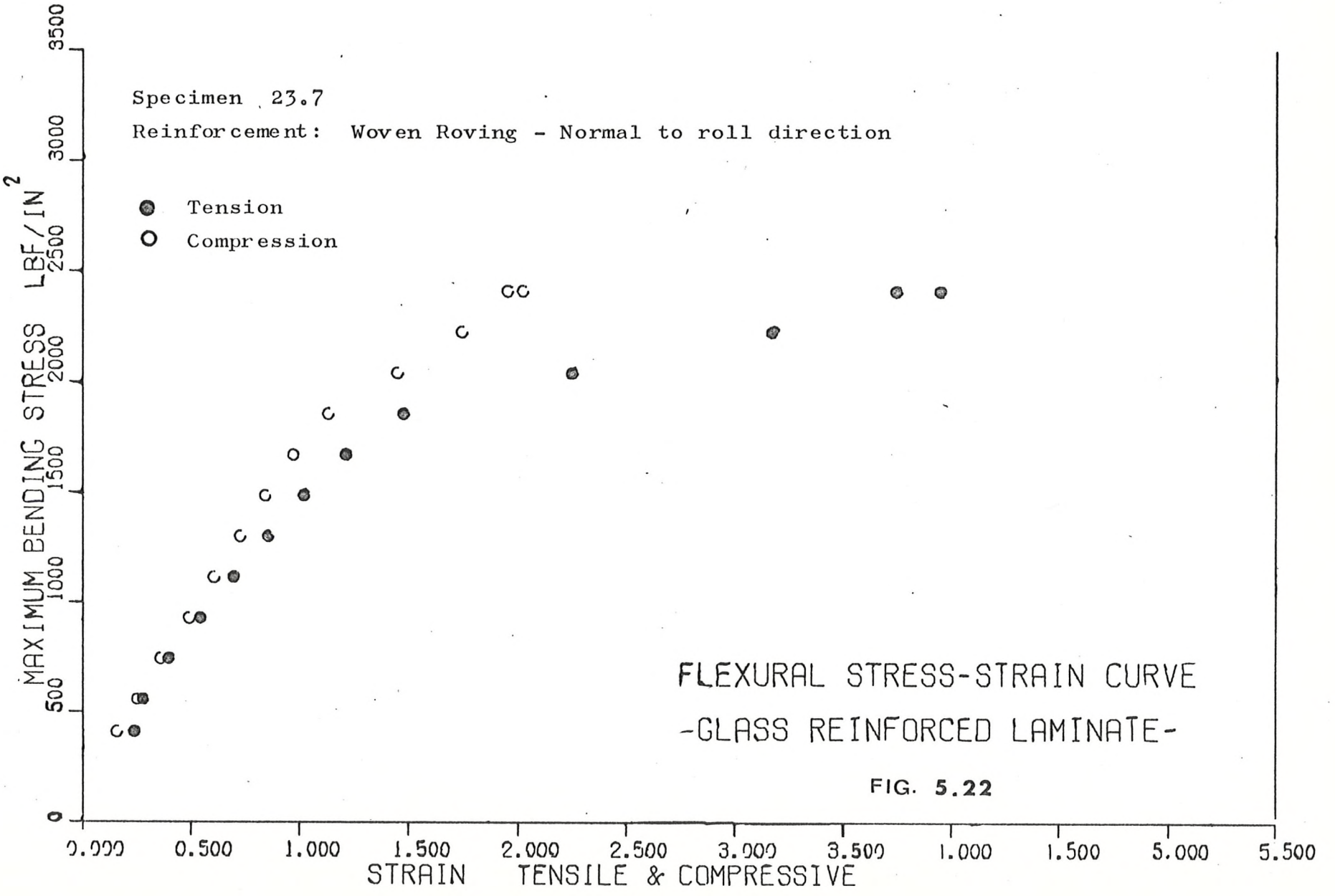
Specimen 23.7
Reinforcement: Woven Roving - Normal to roll direction
Tension
Compression
MAXIMUM BENDING STRESS LBF/IN 2
0
500
1000
1500
2000
2500
3000
3500
0.000
0.500
1.000
1.500
2.000
2.500
3.000
3.500
1.000
1.500
5.000
5.500
STRAIN TENSILE & COMPRESSIVE
FLEXURAL STRESS-STRAIN CURVE
-GLASS REINFORCED LAMINATE-

FIG. 5.22

FLEXURAL STRESS-STRAIN CURVE
-GLASS REINFORCED LAMINATE-
TENSILE & COMPRESSIVE
STRAIN
MAXIMUM BENDING STRESS LBF/IN²
Specimen 23.9
Reinforcement: Woven Roving - Normal to roll direction
Tension
Compression
0.000
0.500
1.000
1.500
2.000
2.500
3.000
3.500
4.000
4.500
5.000
5.500
0
500
1000
1500
2000
2500
3000
3500

FIG. 5.23

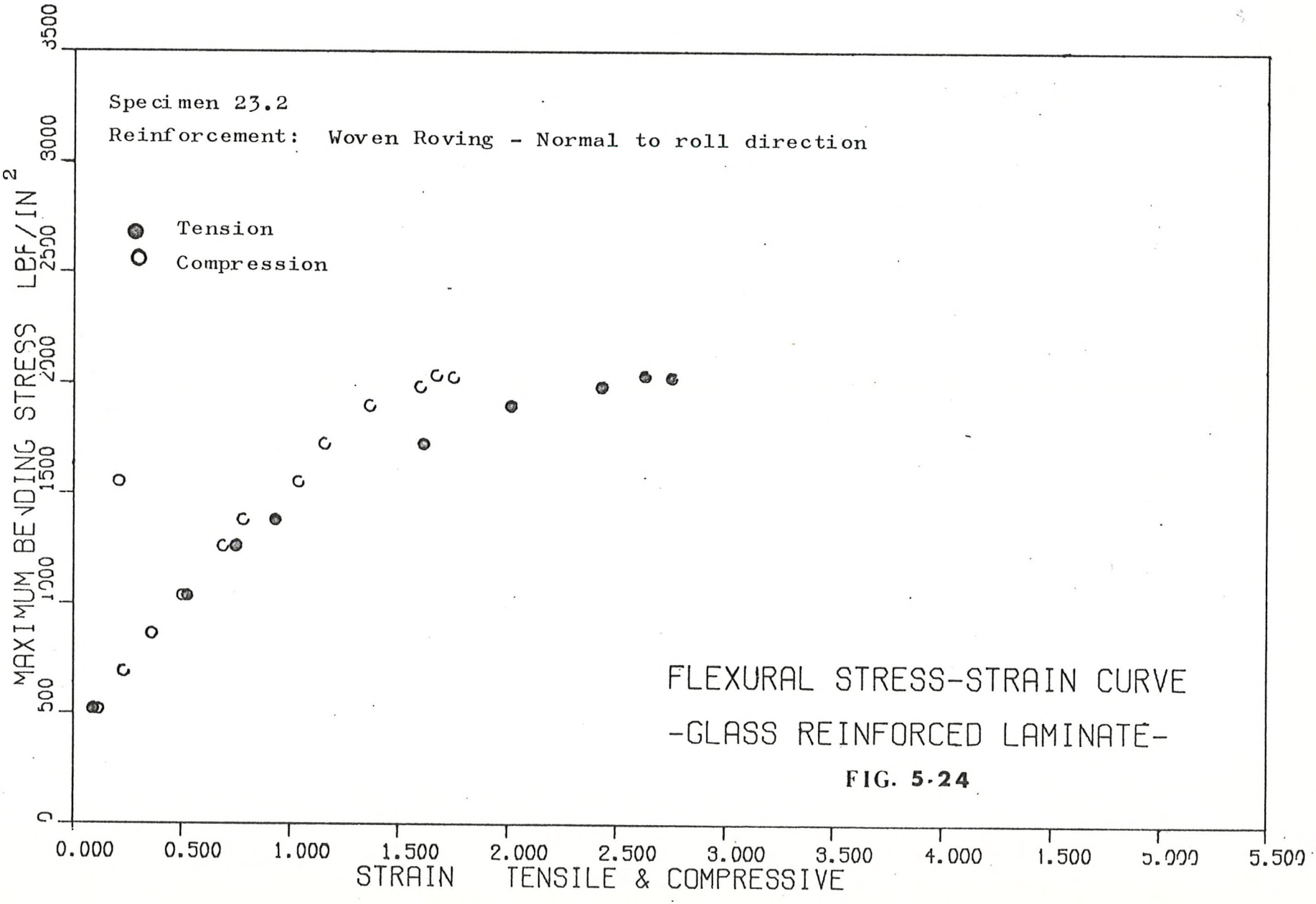

FLEXURAL STRESS-STRAIN CURVE

-GLASS REINFORCED LAMINATE-

FIG. 5-24

ANALYSIS OF RESULTS

CHAPTER 6

6.1 Orthotropic Plate Theory

In the two dimensional case stresses are related to strains by

$$\begin{bmatrix} \varepsilon_{11} \\ \varepsilon_{22} \\ \varepsilon_{12} \end{bmatrix} = \begin{bmatrix} \frac{1}{E_1} & -\frac{\nu_{12}}{E_1} & 0 \\ -\frac{\nu_{21}}{E_2} & \frac{1}{E_2} & 0 \\ 0 & 0 & \frac{1}{G} \end{bmatrix} \cdot \begin{bmatrix} \sigma_{11} \\ \sigma_{22} \\ \sigma_{12} \end{bmatrix}$$

$$\text{or} \quad \underline{\varepsilon} = \left[C\right] \underline{\sigma} \qquad \ldots\ldots\ldots \quad (6.1)$$

where $\underline{\sigma}$ and $\underline{\varepsilon}$ are the stress and strain vectors respectively and $\left[C\right]$ is the Compliance or Flexibility matrix.

By inversion[18] equation (6.1) leads to

$$\begin{bmatrix} \sigma_{11} \\ \sigma_{22} \\ \sigma_{12} \end{bmatrix} = \begin{bmatrix} \frac{E_1}{g} & \frac{\nu_{22} E_1}{g} & 0 \\ \frac{\nu_{11} E_2}{g} & \frac{E_2}{g} & 0 \\ 0 & 0 & G \end{bmatrix} \cdot \begin{bmatrix} \varepsilon_{11} \\ \varepsilon_{22} \\ \varepsilon_{12} \end{bmatrix} \qquad (6.2)$$

where $g = 1 - \nu_{11}\nu_{22}$

$$\text{or} \quad \underline{\sigma} = \left[K\right] \underline{\varepsilon} \qquad \ldots\ldots\ldots \quad (6.3)$$

where $\left[K\right]$ is called the stiffness matrix.

6.2 Rotation of Axes

If the orthotropic plate of Section 6.1 is placed so that the axes are at some angle θ this will give a new rectangular co-ordinate system $1'$ $2'$ (Fig. 6.1a).

It is necessary to express the stresses in the $1'$ $2'$ system in terms of the 1, 2 system therefore a transformation matrix $[T_1]$ is required such that

$$\underline{\sigma'} = [T_1]\,\underline{\sigma} \qquad \ldots\ldots \quad (6.4)$$

The transformation matrix $[T_1]$ can be shown as

$$\begin{bmatrix} \cos^2\theta & \sin^2\theta & 2\sin\theta\cos\theta \\ \sin^2\theta & \cos^2\theta & -2\sin\theta\cos\theta \\ -\sin\theta\cos\theta & \sin\theta\cos\theta & (\cos^2\theta - \sin^2\theta) \end{bmatrix}$$

In a similar way a transformation matrix $[T_2]$ can be found to express strains in the $1'$ $2'$ system, in terms of the 1, 2 system such that

$$\underline{\varepsilon'} = [T_2]\,\underline{\varepsilon} \qquad \ldots\ldots \quad (6.5)$$

where

$$[T_2] = \begin{bmatrix} \cos^2\theta & \sin^2\theta & \sin\theta\cos\theta \\ \sin^2\theta & \cos^2\theta & -\sin\theta\cos\theta \\ -2\sin\theta\cos\theta & 2\sin\theta\cos\theta & (\cos^2\theta - \sin^2\theta) \end{bmatrix}$$

It is now possible to also establish the stiffness matrix

$$\left.\begin{array}{l} \text{Since } \underline{\sigma} = \left[K\right] \underline{\varepsilon} \quad \text{in the 1 , 2 system} \\ \text{then } \underline{\sigma}' = \left[K'\right] \underline{\varepsilon}' \quad \text{in the 1', 2' system} \end{array}\right\}$$

From equations (6.4) and (6.5) and by inversion

$$\underline{\sigma} = \underline{\sigma}' \left[T_1\right]^{-1}$$

$$\text{and } \underline{\varepsilon} = \underline{\varepsilon}' \left[T_2\right]^{-1}$$

By substitution into $\underline{\sigma} = \left[K\right] \underline{\varepsilon}$ yields

$$\underline{\sigma}' \left[T_1\right]^{-1} = \left[K\right] \underline{\varepsilon}' \left[T_2\right]^{-1}$$

$$\text{or } \underline{\sigma}' = \left\{\left[T_1\right] \left[T_2\right]^{-1} \left[K\right]\right\} \underline{\varepsilon}'$$

$$\text{so } \underline{\sigma}' = \left[K'\right] \underline{\varepsilon}' \qquad \ldots\ldots \quad (6.6)$$

Thus giving the stiffness matrix relating stresses and strains parallel to the 1', 2' axes.

$$\text{where } \left[K'\right] = \left[T_1\right] \left[T_2\right]^{-1} \left[K\right] \qquad \ldots\ldots \quad (6.7)$$

It follows by analogy with equation (6.6) that

$$\underline{\sigma} = \left[K'\right] \underline{\varepsilon} \qquad \ldots\ldots$$

6.3 Stiffness Matrices for a Random Fibre Array and An Isotropic Sheet of Matrix

Suppose the thickness of any parallel array of fibres is δt which has a stiffness matrix of $[K']$ (equation 6.7), then the stiffness with respect to the 1, 2 axes in terms of force per unit length will be

$$\underline{\sigma}\,\delta t = [K']\,\underline{\varepsilon}\,\delta t \qquad \ldots\ldots (6.8)$$

A random distribution of fibres in the laminate will consist of a large number of parallel filaments superimposed at different angles θ between 0 and π. If the distribution of these fibres is uniform then the equivalent thickness of the array of fibres aligned between θ and $(\theta + \delta\theta)$ will be t

$$\therefore \delta t = \frac{\delta\theta}{\pi} t$$

Using the relationship given in equation (6.8) gives

$$\underline{\sigma}\,\delta t = [K'_\theta]\,\frac{\delta\theta}{\pi} t\,\underline{\varepsilon} \qquad \ldots\ldots (6.9)$$

where $[K'_\theta]$ is the stiffness matrix for any array of fibres inclined at any angle θ with respect to the 1, 2 axes (See Fig. 6.1a)

Integration of equation (6.9) with respect to the thickness yields the stress vector

$$\underline{\sigma} = \left\{ \frac{1}{\pi} \int_0^{\pi} \left[K'_\theta \right] \, d\theta \right\} \underline{\varepsilon}$$

or $$\underline{\sigma} = \left[K_L \right] \underline{\varepsilon}$$

by the argument of equation (6.6) to (6.7)

then $$\left[K'_\theta \right] = \left[T_1 \right] \left[T_2 \right]^{-1} \left[K \right]$$

so

$$K_L = \frac{1}{\pi} \int_0^{\pi} \left\{ \left[T_1 \right] \left[K \right] \left[T_2 \right]^{-1} \right\} d\theta$$

$$\therefore \pi K_L = \int_0^{\pi} \begin{bmatrix} C^2 & S^2 & 2SC \\ S^2 & C^2 & -2SC \\ -SC & SC & C^2 - S^2 \end{bmatrix} \cdot \begin{bmatrix} K_{11} & K_{12} & K_{13} \\ K_{21} & K_{22} & K_{23} \\ K_{31} & K_{32} & K_{33} \end{bmatrix} \cdot \begin{bmatrix} C^2 & S^2 & -SC \\ S^2 & C^2 & +SC \\ 2SC & -2SC & C^2 - S^2 \end{bmatrix} d\theta$$

where S - Sin θ , C - Cos θ

$$\therefore 8K_L = \begin{bmatrix} (3K_{11} + 2K_{12} + 3K_{22} + 4K_{33}) & (K_{11} + 6K_{12} + K_{22} - 4K_{33}) & (o) \\ (K_{11} + 6K_{12} + K_{22} + 4K_{33}) & (3K_{11} + 2K_{12} + 3K_{22} + 4K_{33}) & (o) \\ (o) & (o) & (K_{11} - 2K_{12} + K_{22} + 4K_{33}) \end{bmatrix}$$

..... (6.10)

In the case of a glass mat, consisting of a random array of glass fibres, K = elastic modulus for the glass (E_f) and all the other K's are zero. Assuming Poisson's ratio for the fibres = $\frac{1}{3}$ then

$$K_\iota = \frac{E_f}{8} \begin{bmatrix} 3 & 1 & 0 \\ 1 & 3 & 0 \\ 0 & 0 & 1 \end{bmatrix} \quad \ldots\ldots \quad (6.11)$$

For an isotropic sheet of cement

$$K_\iota = \frac{E_m}{g_m} \begin{bmatrix} 1 & \nu_m & 0 \\ \nu_m & 1 & 0 \\ 0 & 0 & \frac{(1-\nu_m)}{2} \end{bmatrix} \quad \ldots. \quad (6.12)$$

where E_m = Elastic modulus of matrix

ν_m - Poisson's ratio of matrix

$g_m = (1 - \nu_m^2)$

By analogy with equation (6.2)

$$\nu_{22} = \frac{k_{12}}{k_{11}}$$

and $E_1 = k_{11} \times g$

where $g = (1 - \nu_{22})$

6.4 Elastic Structural Models

Allen suggests the use of two simple models which will represent the structure and elastic properties of a composite which is reinforced by a random array of elastic fibres.

6.4.1 Structural Model 1. Fig. 6.1 (b)

This consists of an isotropic layer of cement of thickness t_m and a sheet of randomly distributed glass fibres having an equivalent glass thickness of t_f which would behave in an isotropic manner.

The stiffness matrix for the model is derived by superimposing the stiffness matrix for the cement sheet and glass mat. Thus using equations (6.10) and (6.11):

$$K\,(\text{model}) = K\,(\text{cement sheet}) + K\,(\text{glass mat})$$

$$= \frac{\phi E_f}{8}\begin{bmatrix} 3 & 1 & 0 \\ 0 & 3 & 0 \\ 0 & 0 & 1 \end{bmatrix} + \frac{(1-\phi)E_m}{g_m}\begin{bmatrix} 1 & \nu_m & 0 \\ \nu_m & 1 & 0 \\ 0 & 0 & \frac{(1-\nu_m)}{2} \end{bmatrix}$$

$$= \begin{bmatrix} k_{11} & k_{12} & k_{13} \\ k_{21} & k_{22} & k_{23} \\ k_{31} & k_{32} & k_{33} \end{bmatrix} \quad \ldots\ldots \quad (6.13)$$

From equation (6.13), prediction of the elastic constants for the model is possible.

6.4.2 Structural Model 2. Fig. 6.1 (c)

The model consists of alternate rectangular section rods of glass and cement superimposed upon one another in such a manner to produce a composite reinforced by a random distribution of fibres, dispersed uniformly through the thickness of the composite. The bond between the matrix rods and glass rods is assumed to be good so that stress is carried by the rods in all directions.

Equation (6.10) describes the stiffness matrix for the composite described above. Allen has shown the elements of this array $[K]$ to be

$$K_{11} = \frac{E_f}{g_f}\left\{\frac{1 + \phi(\phi - 1)\left[\lambda g_f + \frac{g_f}{\lambda} - 2(1 - \nu_f \nu_m)\right]}{\lambda(\phi - 1) + \phi}\right\}$$

where

$$\lambda = \frac{E_f g_f}{E_m g_m}$$

$$K_{12} = K_{21} = \frac{E_f}{g_f}\,\frac{\nu_m(\phi - 1) + \nu_f\phi}{\lambda(\phi - 1) + \phi}$$

$$K_{22} = \frac{E_f}{g_f}\,\frac{1}{\lambda(\phi - 1) + \phi}$$

and

$$K_{33} = \frac{1}{\frac{\phi - 1}{G_m} + \frac{\phi}{G_f}}$$

(a)

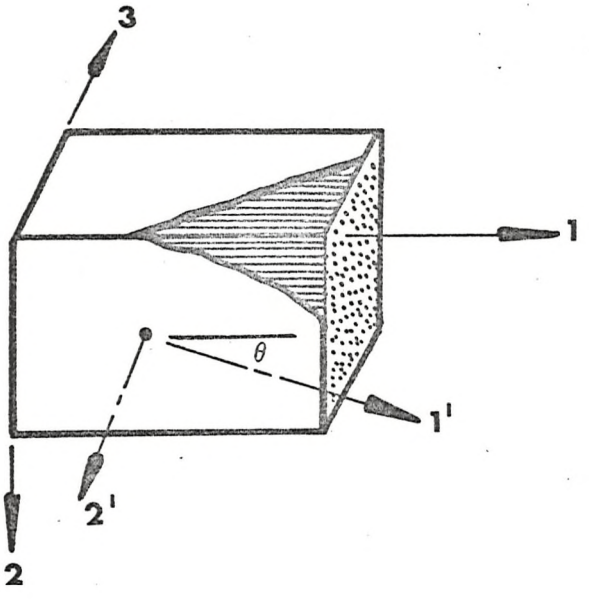

fundamental structure

(b)

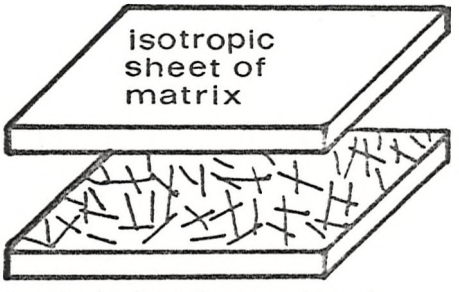

MODEL 1

(c)

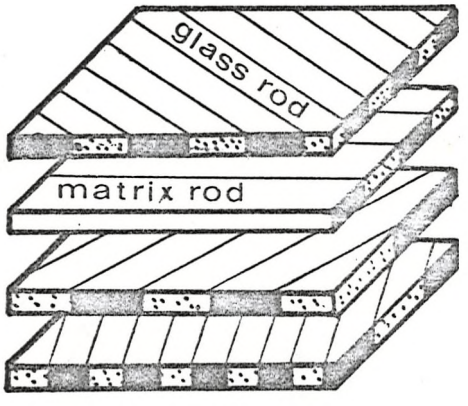

MODEL 2

STRUCTURAL MODELS

FIG 6.1

6.5 Comparison of Predicted and Experimental Results

The prediction of the elastic properties of a glass reinforced matrix using Allen's models 1 and 2 is illustrated in Figs. 6.2, 6.3, 6.4 and 6.5.

Figs. 6.2 and 6.3 show the variation of the initial elastic modulus for a composite having a glass content by volume ($\emptyset$) of 0 to 14%. Four cases are shown for models 1 and 2, assuming the composite matrix to have a constant elastic modulus of 0.3, 0.4, 0.5 and 0.6 x 10^6 lbf/in^2 with a Poisson's ratio (ν_m) of 0.25. In all cases the elastic modulus of the fibres (E_f) is assumed to be 10^7 lbf/in^2 with a Poisson's ratio (ν_f) of 0.33. Superimposed on Figs. 6.2 and 6.3 are the experimental results for the tensile initial elastic modulus of thin laminates of polymer-cement (s/c ratio 0.2, w/c ratio 0.3) reinforced by two layers of chopped strand mat, tested at a crosshead speed of 0.005 in/min. The experimental points, which are drawn from throughout the study, show quite clearly a high degree of scatter and illustrate that the simple model 1 may be used to predict the elastic properties of the laminates equally as well as the more complex model 2 (Table 6.1).

Variations of Poisson's ratio brought about by alterations of glass content by volume and matrix elastic modulus, are shown in Figs. 6.4 and 6.5. These curves assume the use of models 1 and 2 with $E_f = 10^7$ lbf/in^2 and $\nu_f = 0.33$.

Model 1 predicts a lower value than Model 2 for the initial elastic modulus of the composite, at a particular matrix elastic modulus and glass content by volume. Model 1 predicts higher Poisson ratio values than Model 2 for the same parameters.

Spec. No.	Initial Composite Elastic Modulus (E_o) $lbf/in^2 \times 10^{-6}$	% Glass Content by Volume Ø	Predicted Modulus of Matrix (E_m $lbf/in^2 \times 10^{-6}$)	
			MODEL 1	MODEL 2
12.3	0.6265	8.94	0.361	0.32
12.11	0.6247	9.09	0.354	0.31
12.14	0.4752	8.96	0.193	0.16
12.19	0.6976	8.96	0.438	0.36
12.20	0.6078	8.98	0.34	0.30
12.23	0.7085	8.91	0.457	0.395
12.5	0.5488	8.87	0.278	0.24
24.4	0.5985	11.03	0.295	0.21
24.5	0.5517	11.06	0.206	0.16
24.6	0.5850	11.89	0.215	0.17
25.6	0.8966	7.63	0.696	0.63
25.7	0.9290	10.35	0.652	0.565
26.5	0.625	10.61	0.334	0.255
26.6	0.6746	10.62	0.359	0.305
26.7	0.8199	11.1	0.484	0.435
11.3	0.617	6.44	0.43	0.39
11.5	0.7713	6.66	0.59	0.54
11.21	0.6732	7.28	0.465	0.425
11.24	0.767	7.31	0.564	0.51
11.25	0.866	7.38	0.67	0.61
11.28	0.730	7.34	0.524	0.475

TABLE 6.1

PREDICTED EFFECTIVE ELASTIC MODULUS FOR COMPOSITE MATRIX USING MODELS 1 AND 2

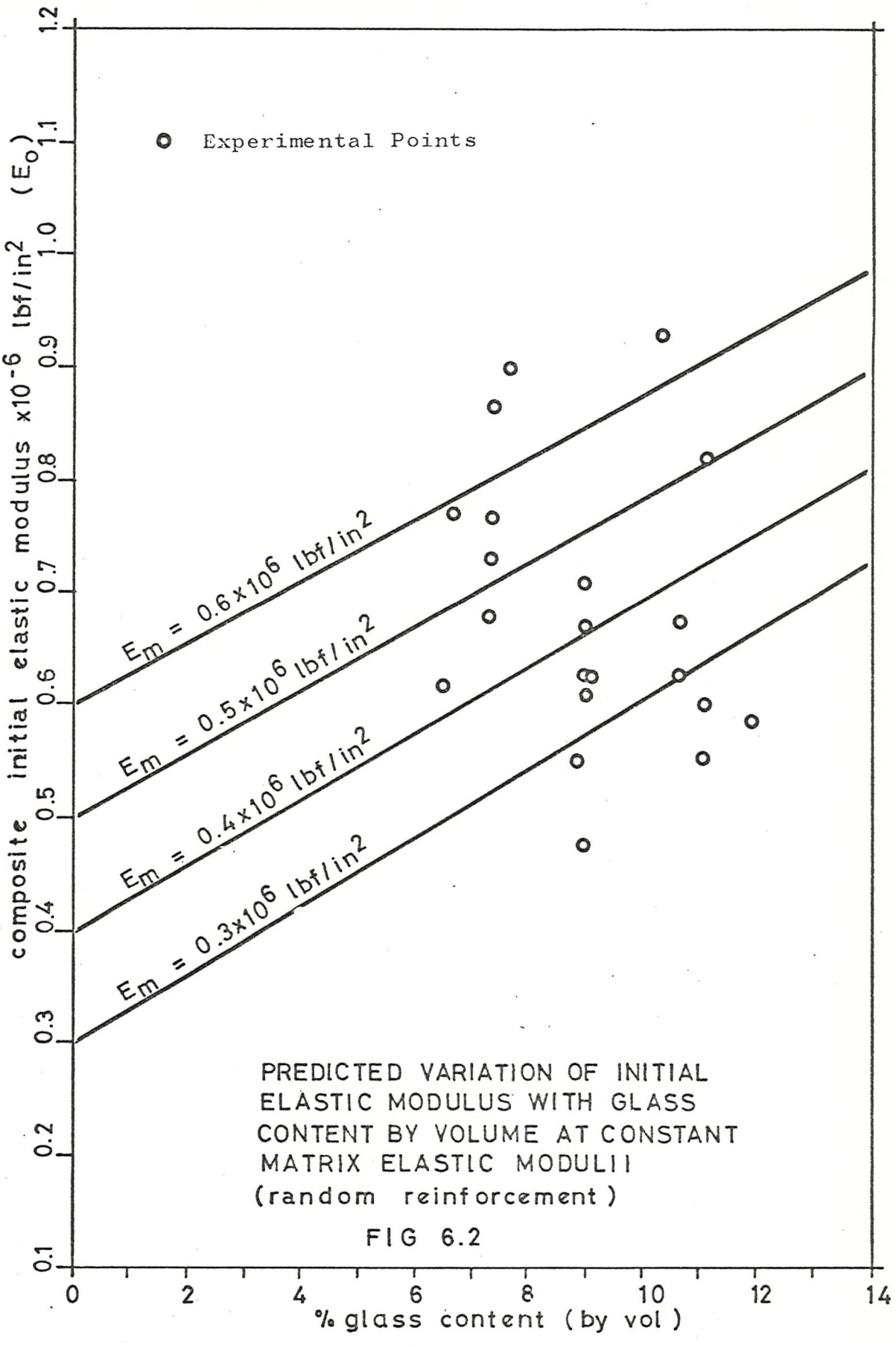

PREDICTED VARIATION OF INITIAL ELASTIC MODULUS WITH GLASS CONTENT BY VOLUME AT CONSTANT MATRIX ELASTIC MODULII (random reinforcement)

FIG 6.2

MODEL 2

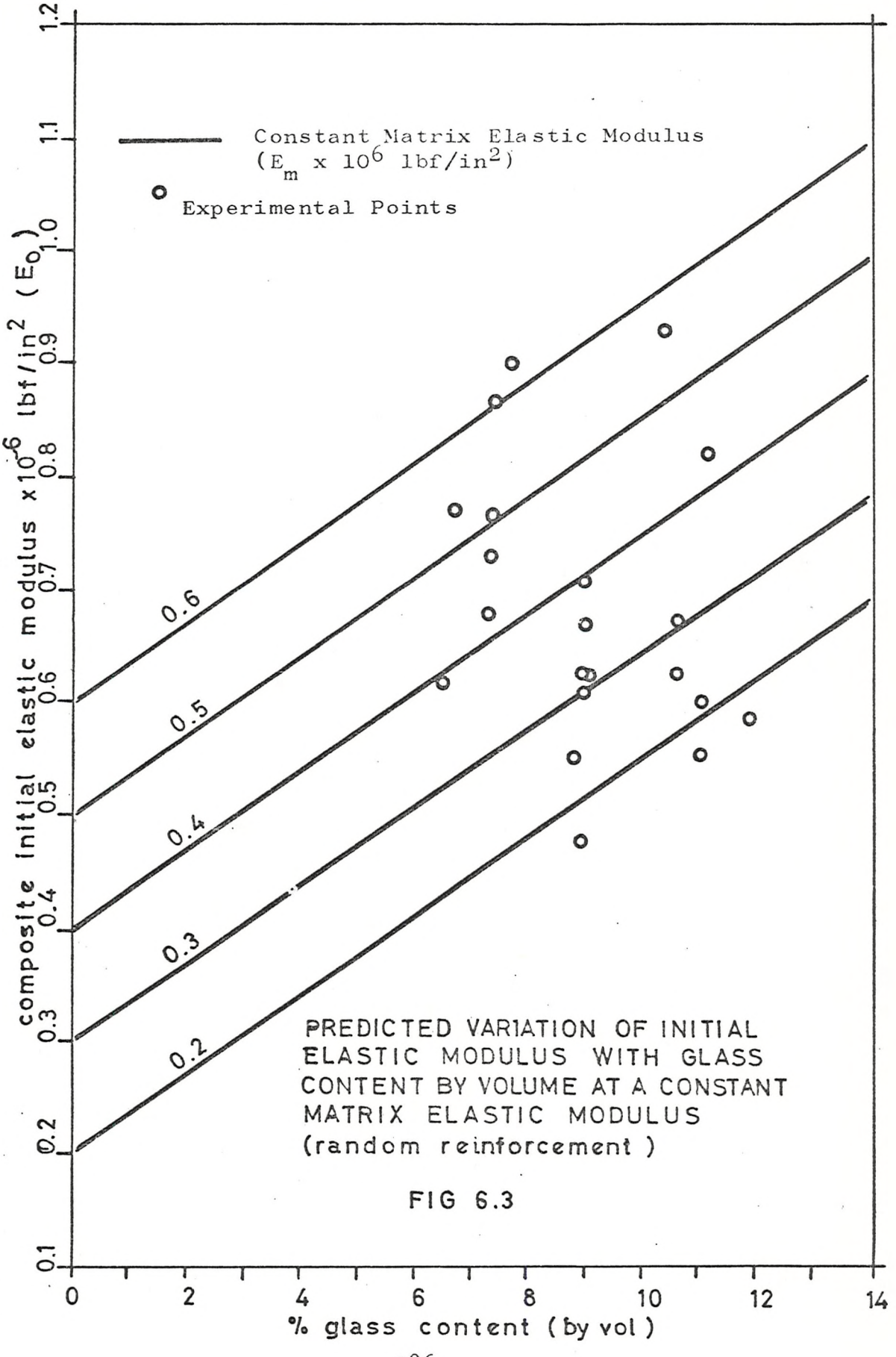

PREDICTED VARIATION OF INITIAL ELASTIC MODULUS WITH GLASS CONTENT BY VOLUME AT A CONSTANT MATRIX ELASTIC MODULUS (random reinforcement)

FIG 6.3

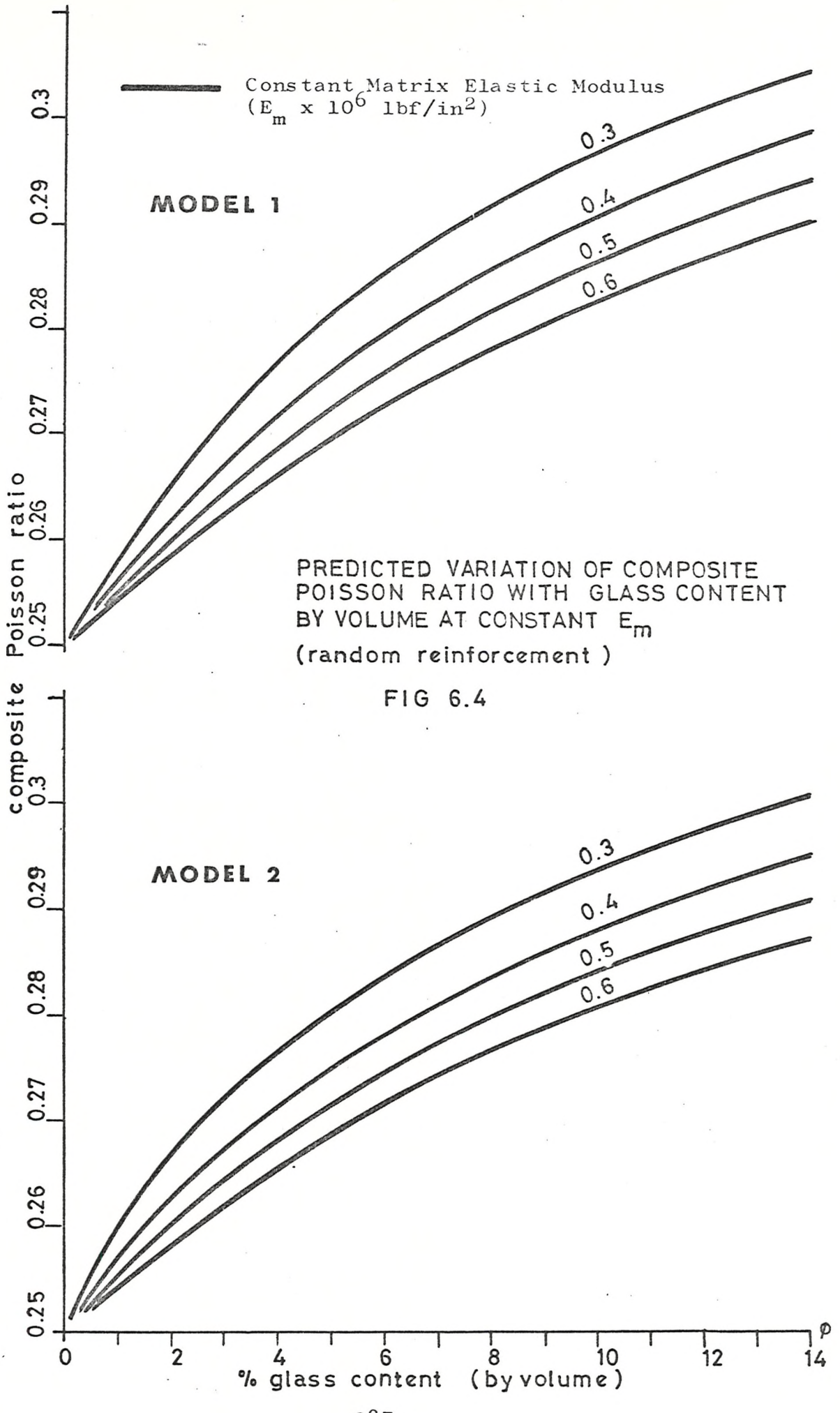

PREDICTED VARIATION OF COMPOSITE POISSON RATIO WITH GLASS CONTENT BY VOLUME AT CONSTANT E_m
(random reinforcement)

FIG 6.4

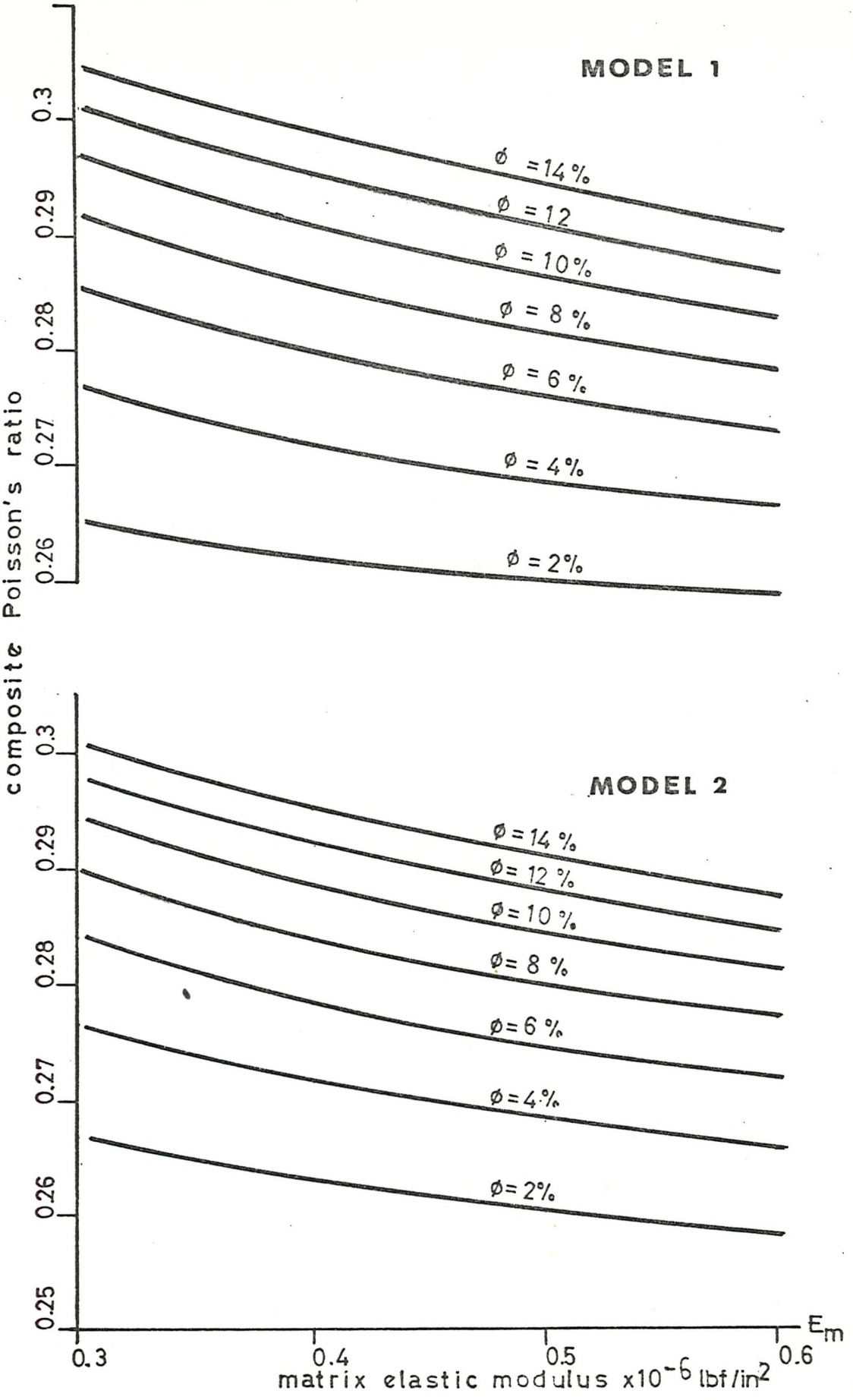

PREDICTED VARIATION OF COMPOSITE POISSON RATIO WITH MATRIX ELASTIC MODULUS (constant % glass content by volume — random reinforcement)

FIG 6.5

6.6 Superposition of the Glass and Matrix Stress-Strain Diagrams

The secant modulus against strain graphs for the thin laminates of polymer-cement reinforced by chopped strand mat (Sec. 4.4.1, Figs. 4.14 to 4.21) show that the secant modulus at failure is slightly less than $\eta E_f \phi$, where η is an efficiency factor = $\frac{1}{3}$. Table 6.2 shows a comparison between $\eta E_f \phi$ and the final secant modulus of these laminates when tested at various crosshead speeds. The series of tests of Sec. 5.4 shows the final secant modulus to be close to $E_f \phi$ where $\eta = 1$ for unidirectional fibres. Fig. 6.6a illustrates the idealised relationship between secant modulus and strain. It also indicates an elastic range if it exists.

It is suggested here that the stress strain diagram for this non-linear material may be constructed by considering the separate properties of the glass and matrix by employing the principle of superposition.

Fig. 6.6 (b) shows the stress-strain diagram for a hypothetical matrix reinforced by a chopped strand mat. This composite has a glass volume of ϕ, but the matrix has no stiffness and does not contribute towards the strength of the composite.

Fig. 6.6 (c) illustrates a typical stress-strain diagram for the polymer-cement matrix reinforced by a chopped strand mat. This composite has a glass content by volume of $\emptyset$. Also shown in this figure is the expected stress-strain relationship for a composite which has a brittle matrix. Assuming that the strain in the matrix equals the strain in the fibres which are aligned with the applied load and that the interface bond between fibre and matrix is good, then it should be possible to subtract Fig. 6.6 (b) from Fig. 6.6 (c) to produce Fig. 6.6 (d).

Fig. 6.6 (d) gives the calculated stress-strain diagram for the matrix by the above described subtraction of Figs. 6.6 (b) and 6.6 (c). At strains greater than the fracture strain of the unreinforced material, (Sec. 3.3.3, Table 3.6), the load is gradually transferred to the glass as the number of cracks in the matrix increases. If the matrix were brittle then, at low strains, large crack formations will grow resulting in a rapid transfer of load to the glass, possibly giving premature failure of some of the glass fibres. This is supported by Allen [5] and work done by the author.

Each specimen reinforced by C.S.M. and tested at various crosshead speeds (Sec. 4.4) was analysed

in the manner just described. The expected stress-strain scatter diagrams for the matrix are given in Figs. 6.7 to 6.14 which were plotted by the computer, programme G44E. The empirical curves of Fig. 3.22 are superimposed on each diagram which also provides a comparison between the stress-strain diagrams of Figs. 3.15 to 3.19 and the calculated values shown on Figs. 6.7 to 6.14. It was seen that the estimated fracture strain shown on Figs. 6.7 to 6.14 was slightly less than the fracture strain of the reinforced material. This may be due to the reinforcement acting as stress raisers, especially whilst the specimen is under test. Maximum stresses in Figs. 6.7, 6.9, 6.10 and 6.12 do not accurately compare with Figs. 3.15 to 3.19 but may be regarded as reasonable evidence to support the suggestion of superposition principles.

SUPERPOSITION OF STRESS-STRAIN GRAPHS

FIG 6.6

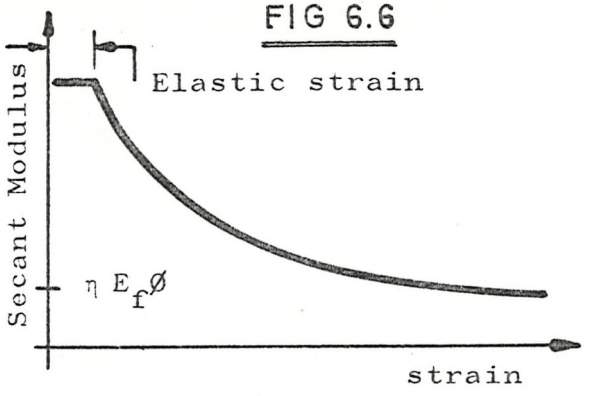

(a)

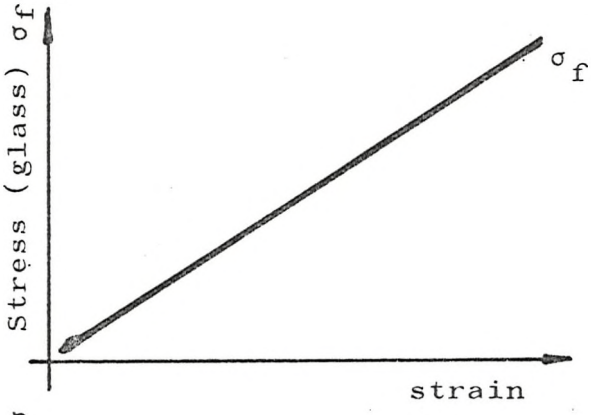

(b)

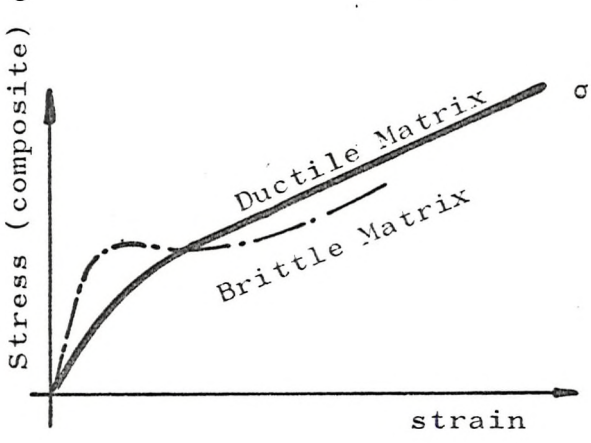

(c)

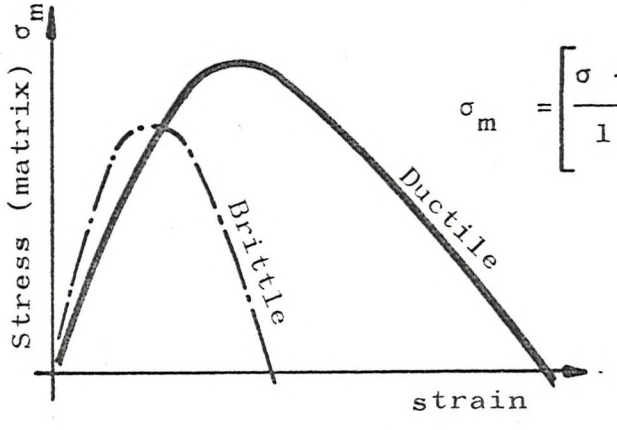

(d)

TABLE 6.2

COMPARISON OF EXPERIMENTAL SECANT MODULUS WITH CALCULATED GLASS ELASTIC MODULUS - RANDOM REINFORCEMENT

Cross-head Speed in/min	Spec. No.	% Glass Content By Vol. (Ø)	Secant Modulus E_s lbf/in^2 x 10^{-6}	$\eta E_f Ø$ E_f lbf/in^2 x 10^{-6}
0.005	13.1	9.09	0.2337	0.303
	13.2	9.39	0.1335	0.313
	13.3	9.56	0.2046	0.319
	13.4	9.34	0.2266	0.314
	13.5	9.28	0.2113	0.309
	13.6	9.51	0.2171	0.317
	13.7	9.87	0.1908	0.319
0.01	13.8	10.1	0.2744	0.337
	13.9	10.36	0.2752	0.345
	13.10	10.48	0.2638	0.349
0.02	13.11	10.13	0.2398	0.338
	13.12	9.6	0.2126	0.320
	13.13	8.99	0.2560	0.299
0.05	13.14	8.33	0.1959	0.278
	13.15	8.66	0.2157	0.289
	13.16	8.92	0.1966	0.297
0.1	13.17	8.83	0.2392	0.294
	13.18	8.81	0.1934	0.293
	13.19	9.21	0.3131	0.307
0.2	13.20	9.76	0.2221	0.325
	13.21	9.86	0.3100	0.329
	13.22	9.85	0.3149	0.325
0.5	13.23	9.70	0.2419	0.323
	13.24	9.50	0.2509	0.317
	13.25	9.18	0.2615	0.306
1.0	13.27	9.05	0.1741	0.302
	13.28	9.06	0.1939	0.302

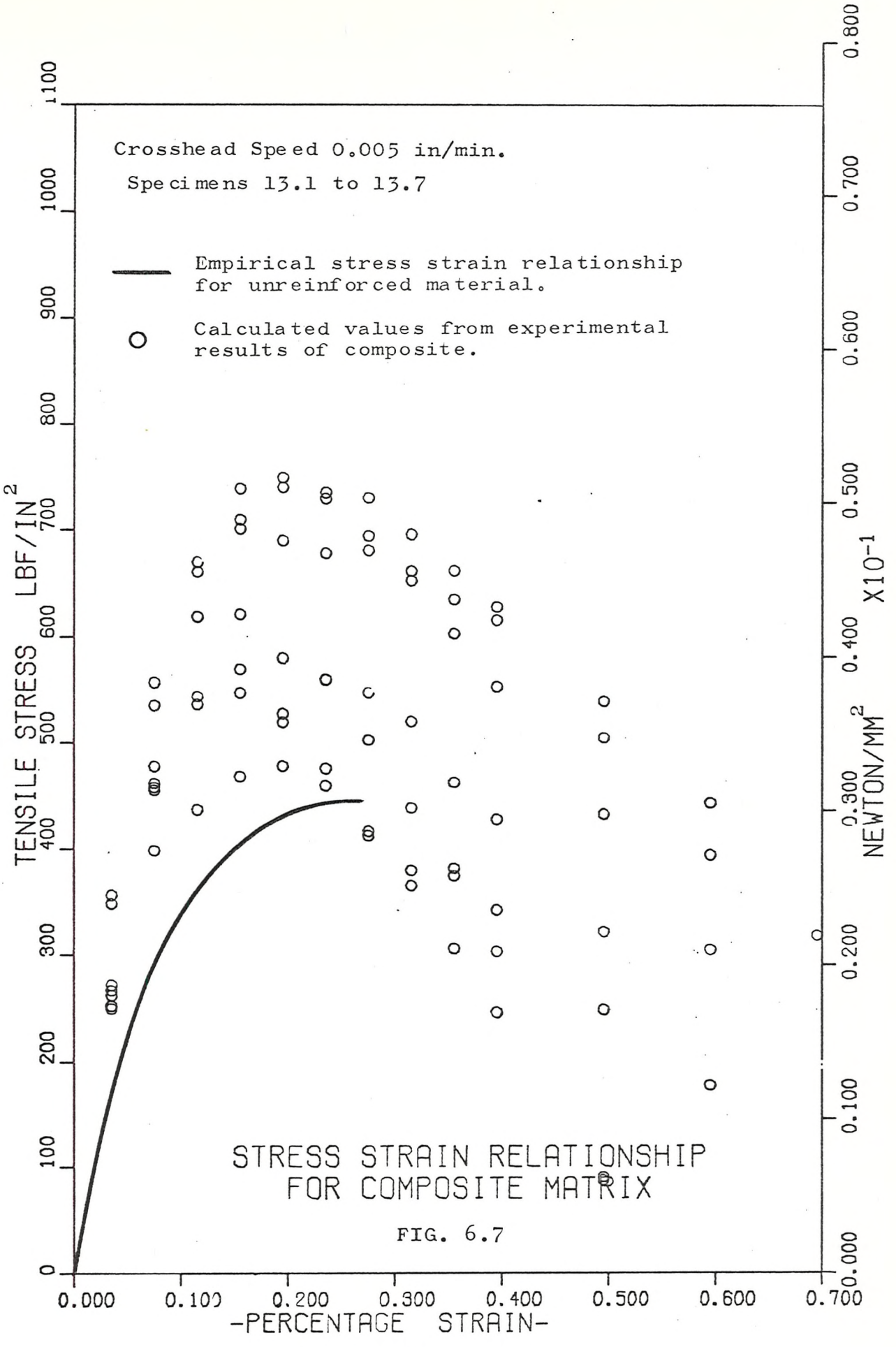

STRESS STRAIN RELATIONSHIP FOR COMPOSITE MATRIX

FIG. 6.7

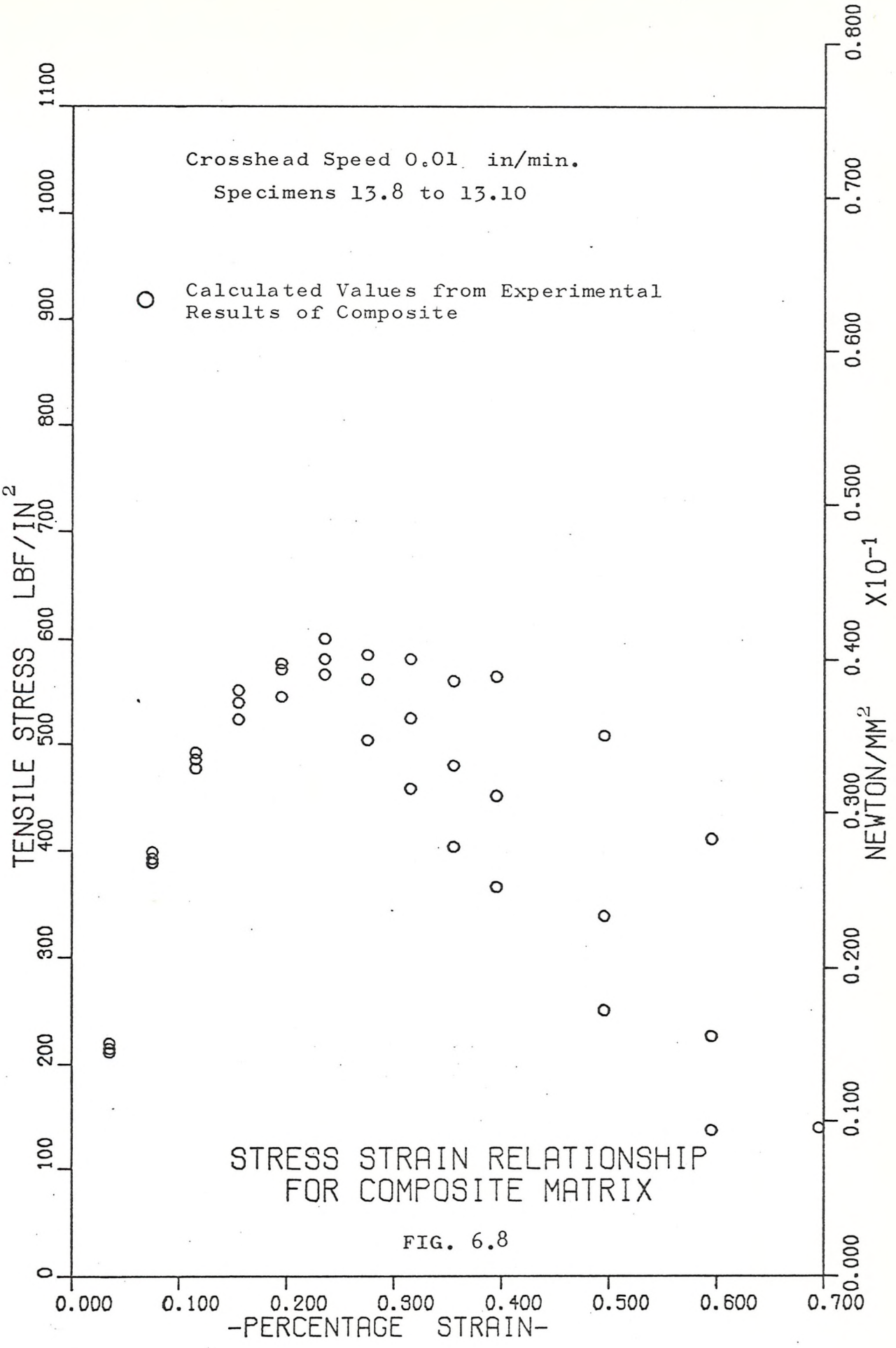

STRESS STRAIN RELATIONSHIP FOR COMPOSITE MATRIX

FIG. 6.8

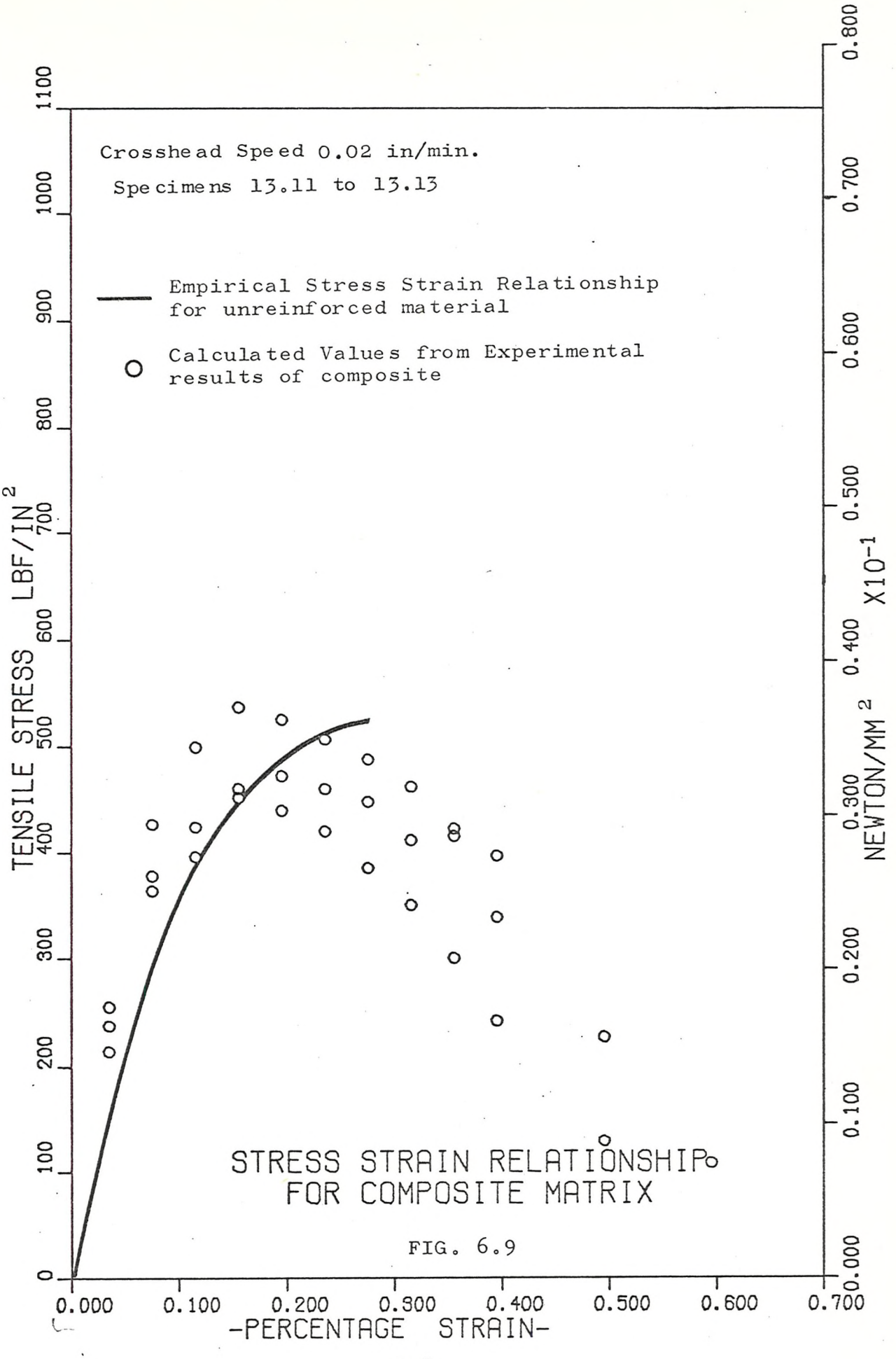

STRESS STRAIN RELATIONSHIP FOR COMPOSITE MATRIX

FIG. 6.9

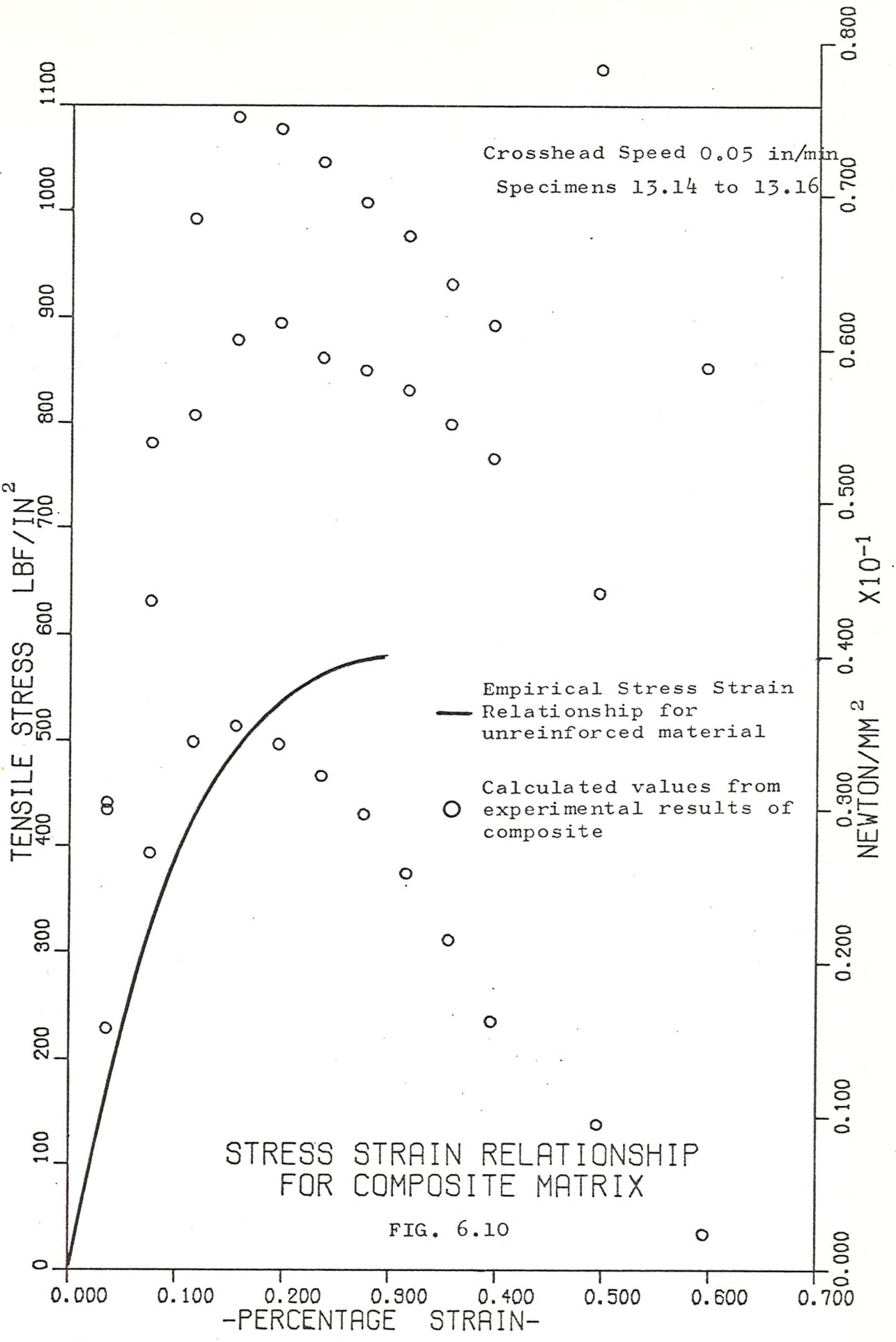

STRESS STRAIN RELATIONSHIP FOR COMPOSITE MATRIX

FIG. 6.10

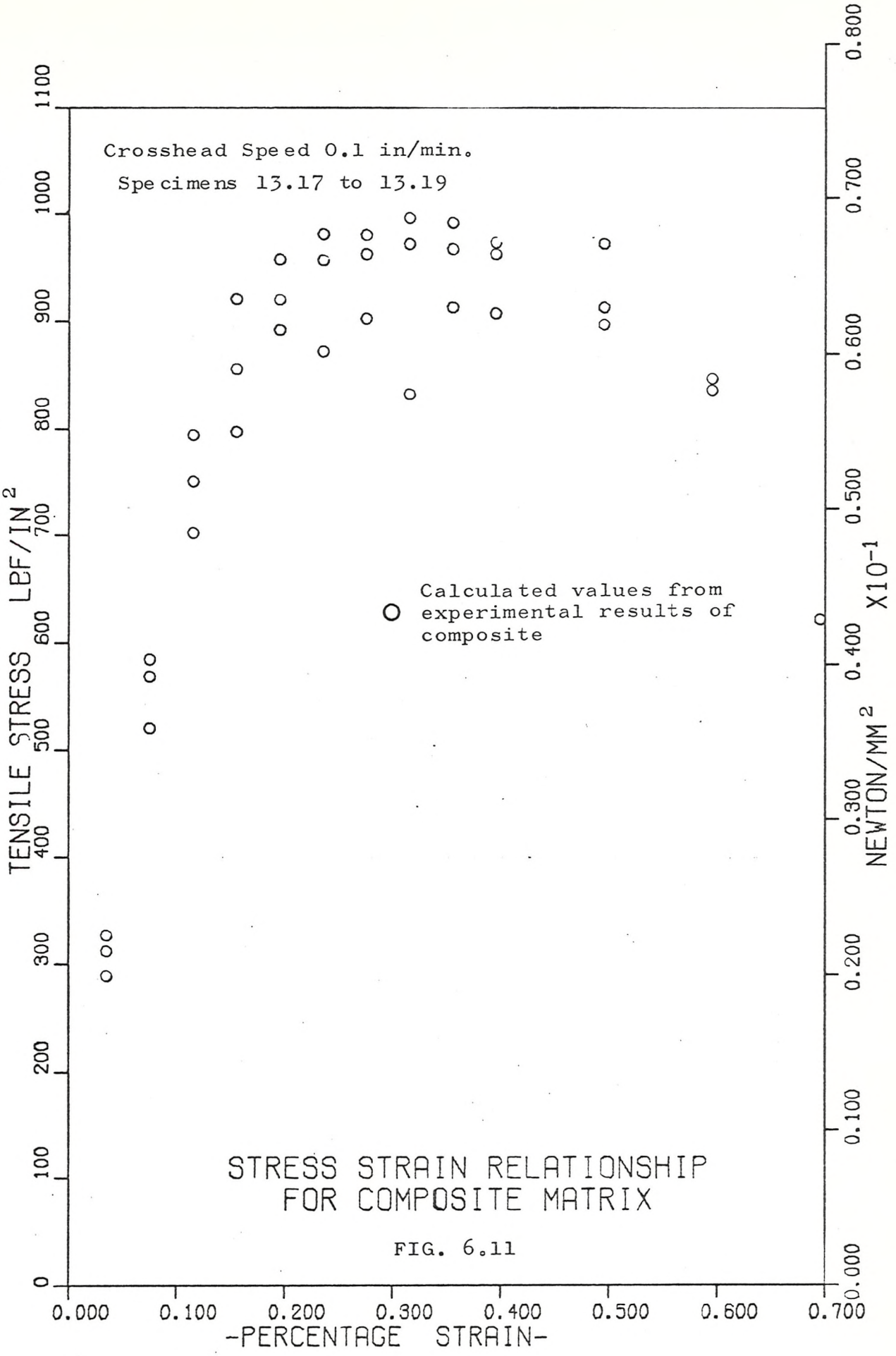

STRESS STRAIN RELATIONSHIP FOR COMPOSITE MATRIX

FIG. 6.11

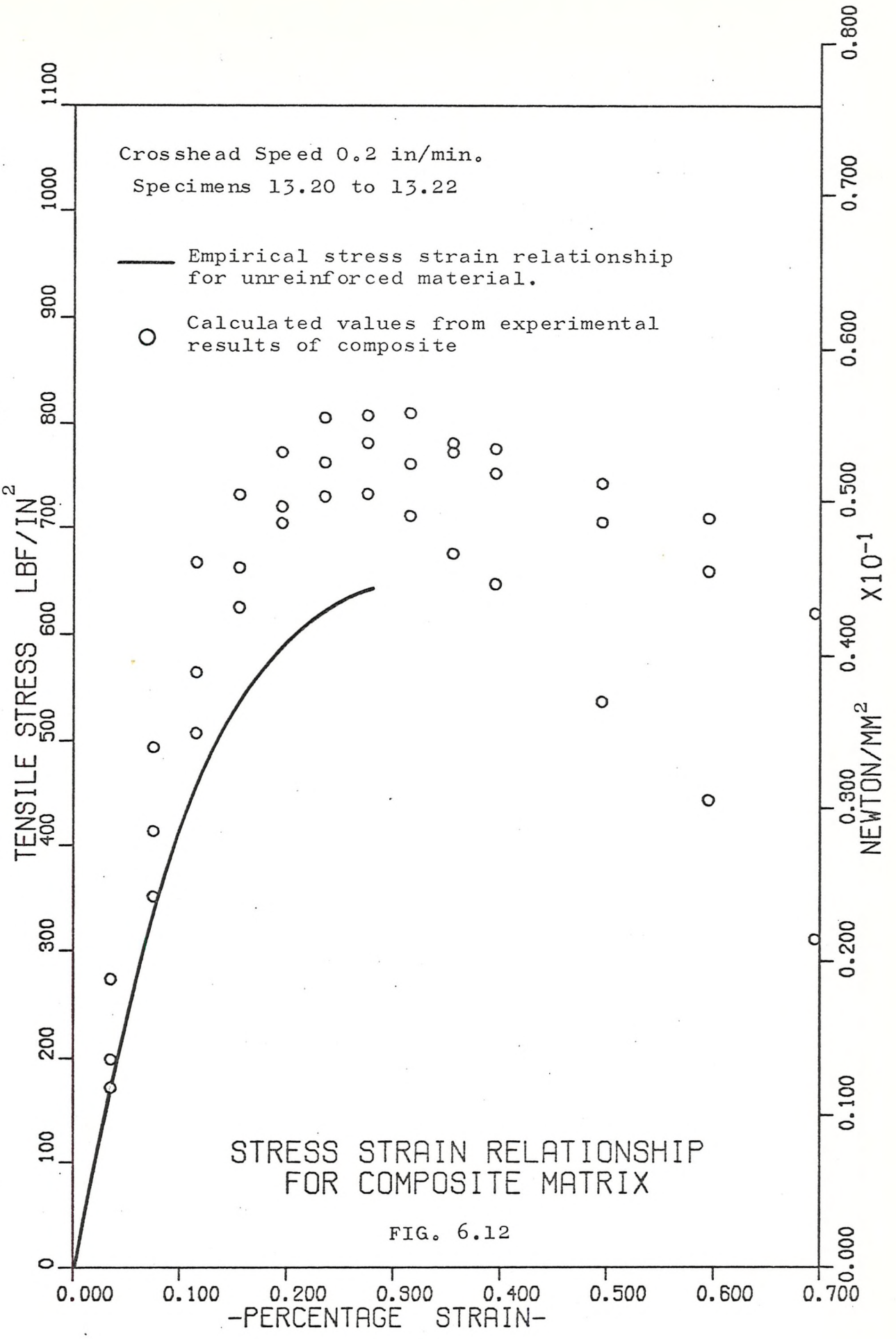
Crosshead Speed 0.2 in/min.
Specimens 13.20 to 13.22
Empirical stress strain relationship for unreinforced material.
Calculated values from experimental results of composite
TENSILE STRESS LBF/IN^2
NEWTON/MM^2 X10^{-1}
-PERCENTAGE STRAIN-
0 100 200 300 400 500 600 700 800 900 1000 1100
0.000 0.100 0.200 0.300 0.400 0.500 0.600 0.700 0.800
0.000 0.100 0.200 0.300 0.400 0.500 0.600 0.700
STRESS STRAIN RELATIONSHIP
FOR COMPOSITE MATRIX

FIG. 6.12

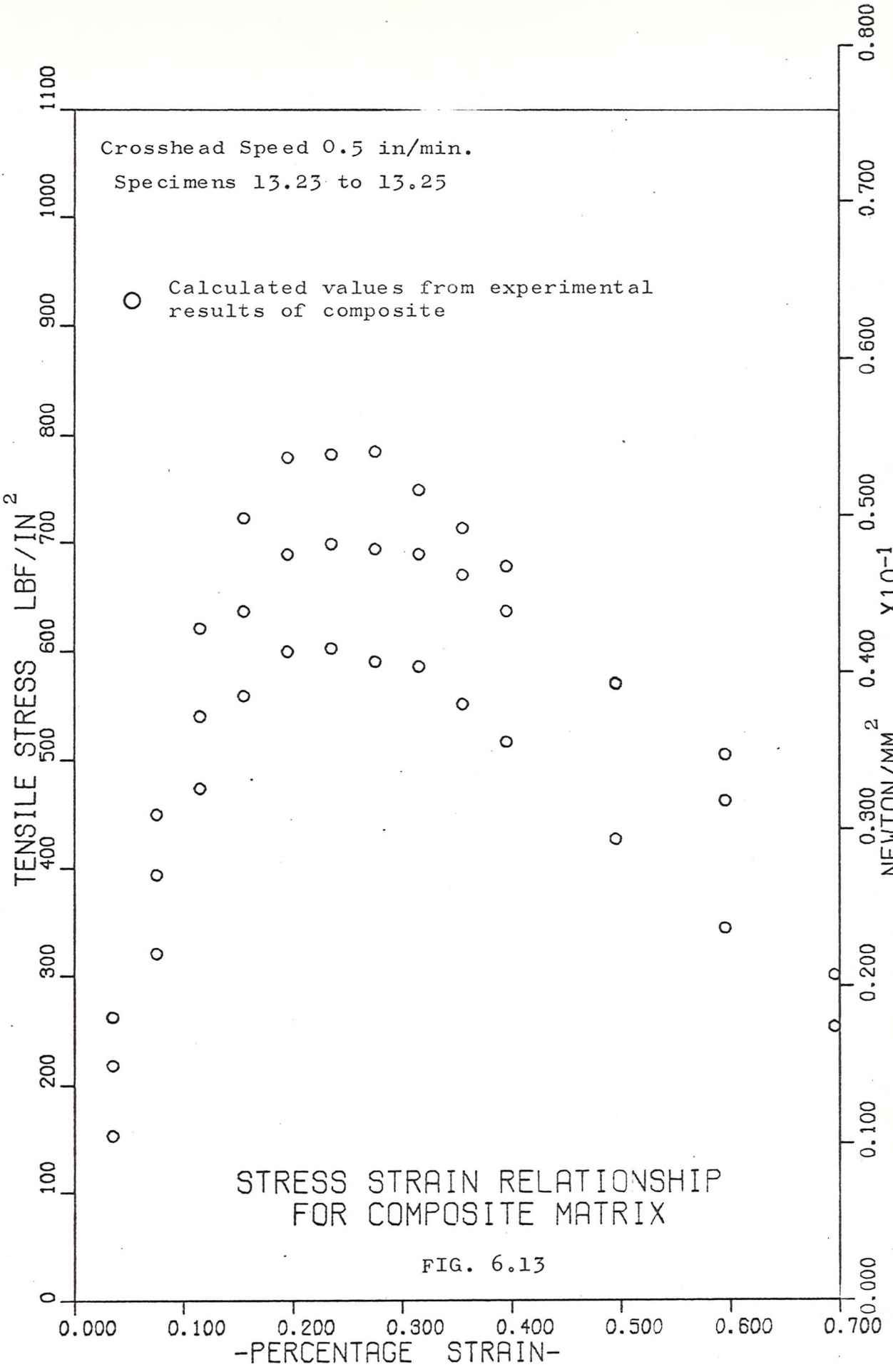

STRESS STRAIN RELATIONSHIP FOR COMPOSITE MATRIX

FIG. 6.13

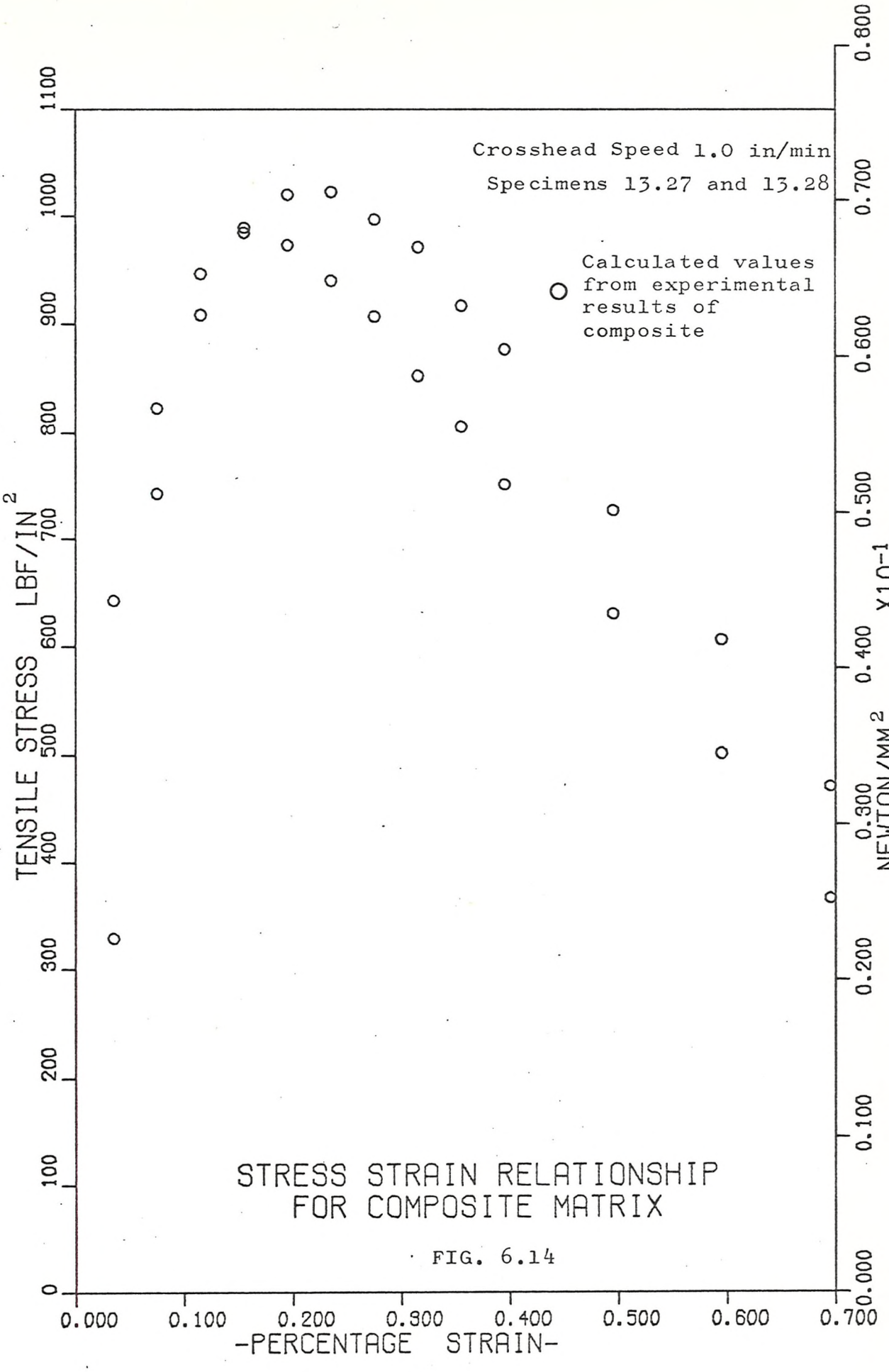

STRESS STRAIN RELATIONSHIP FOR COMPOSITE MATRIX

FIG. 6.14

CHAPTER 7

CLOSURE

7.1 Heuristic Reasoning

7.1.1 Admixtures

There is an increasing interest in the use of admixtures in inorganic cement systems as a means of delaying crack propogation. At present there is not a great deal of detailed information about the mechanical properties of these systems.

If admixtures are employed for ordinary Portland cement the tensile cracking strain of the hardened paste is increased, depending upon the admixture used. Admixtures also influence the workability, setting time and void content of the fresh paste.

7.1.2 Matrix

The matrix used in this investigation may be classified as a viscoelastic material. However, there may be an initial linear relationship between stress and strain. During tensile tests there were suggestions that microscopic cracks occur in the matrix at a strain which corresponds to the fracture strain of ordinary Portland cement. Therefore

initially the matrix may rely upon the normal bonding mechanisms of the cement particles. When these bonds are broken the polymer would be available for sustaining stress. There is not sufficient evidence to support this hypothesis since detailed tests were not conducted in this region of the stress-strain diagram.

Creep curves at various stress levels may be reduced to three components of strain: Elastic, Primary and Secondary, as a means of deriving the creep laws in the range of time 0 to 33×10^6 s. Recordings at greater times indicated zero creep. Creep analysis is sensitive to shrinkage and changes of environmental humidity. This could be resolved by coating the test specimen with a light extensible impervious material. The accuracy with which the instantaneous strain is detected is also an important factor. The apparatus used for the long term creep study in this investigation appears to have been adequate, but would be suspect if it were necessary to record smaller creep strains.

It is thought that the increase of strength with age is brought about by the continuing hydration process of the cement particles. When tensile

specimens are tested under varying rates of strain there is evidence to support a mathematical relationship between stress, strain and short times (at one age, temperature and humidity). It is not clear why the compressive strength is not greatly affected by age.

Measurements of Poisson's ratio were not particularly successful in view of the very small strains being detected. This led to the use of the most sensitive range of the Boulton-Paul meter, raising doubt about the stability of the apparatus in this range.

7.1.3 The Composite

The manufacturing technique for the production of glass-reinforced inorganic cementitious materials presents many difficulties. These problems are aggravated by the fact that a requirement of high strength cement is a low water/cement ratio. In its fresh state this cement would be difficult to work and the manufacturing process made impossible. The alternative is to manufacture components with a high water/cement ratio and then draw off as much water as possible. Another alternative is to use a cement-admixture system which increases the workability at low water/cement ratios. The disadvantage is

decreased stiffness and increased cost. The Primal-Portland cement-glass system was found to combine quite well using the hand layup technique which produced uniform laminates with a very good surface finish.

Stress strain recordings of the thin reinforced laminates used in this study indicated that the matrix allowed a reasonable transfer of load to the glass fibres. There is no evidence that the presence of fibres increases the initial fracture strain of the matrix. There may be in fact a reduction of the strain at which initial damage occurs since the transverse fibres act as stress raisers and promote early crack propogation.

Effects upon the stress-strain diagram brought about by variations of applied strain rate are obscure. This is mainly due to the high variability of the laminates. It would therefore be advisable to manufacture closely controlled test pieces if a definite conclusion is to be reached.

Superposition of the stress-strain diagrams for the glass and matrix gives a reasonable representation of the stress strain diagram of the composite at various rates of strain. Superposition would only be possible within the range of strain of

the matrix. This is so because it appears that the matrix of the composite may be capable of supporting load beyond the expected fracture strain of the matrix alone. This depends upon the type of reinforcement.

When examining the fracture area of the specimen there is no evidence of fibre pullout, implying an efficient bond between the matrix and glass.

Considering the high variability of the laminates, the long term creep laws are acceptable. All creep specimens showed a constant rate of creep for time 10^7 s. and zero creep rate for time 20×10^6 s. When using C.S.M. as the reinforcement it is shown quite clearly that the discontinuous fibres are not arranged in a completely random manner. Laminates using other types of reinforcement such as woven roving and cloth, illustrates clearly the way in which the directional properties of the laminate may be controlled.

7.2 Conclusions

7.2.1 Matrix

1) Primal-Portland cement systems are affected by environment. Soaking in water results in a substantial decrease of tensile strength; this is recovered and increased by drying of the specimen. (No strength is less than the strength of ordinary Portland cement).

2) Tensile strength increases with age. The rate of increase is small at ages greater than 30 days. Compressive strengths do not show a marked increase with age.

3) Tensile strength is influenced by the rate of applied strain, so also is compressive strength.

4) The material is time dependent. The dependence of primary creep compliance with time varies with level of stress. The isochronous curves do not display a linear relationship. No relationship is established between primary creep compliance and stress level (at ls.).

5) Shrinkage rate is small. This is influenced by change of environment.

6) Non destructive tests indicate the polymer to be a dispersion of starlets in a matrix of cement.

7.2.2 Composite

1) The method of manufacture of thin laminates of glass reinforced polymer-cement is quite satisfactory. It could be developed to produce a closer control upon the variability of the test piece.

2) The influence of applied strain rate is not marked.

3) Long term creep tests show a relationship between time, stress level, primary and secondary creep. The isochronous curves display a non-linear relationship between stress and strain.

4) The principle of superposition can be used to establish the stress-strain diagram of the composite at various rates of strain.

5) Structural models may be used to predict the initial elastic properties of the composite.

CITED LITERATURE

1. ALI, M.A., GRIMER, F.J.,
   Mechanical Properties of Glass Fibre Reinforced Gypsum ,
   B.R.S. Current Paper EN66/68, August.

2. ALLEN, H.G.,
   The Fabrication Properties of Glass Reinforced Cements,
   Composites, Sept. 1969, pp. 19-24.

3. ALLEN, H.G.,
   Private Communication.

4. ALLEN, H.G.,
   The Strength and Stiffness of Two Glass-Fibre Reinforced Cement Laminates,
   Composite Materials, April 1971.

5. ALLEN, H.G.,
   Review of Progress of a Research Project Sponsored by C.I.R.I.A. in the period October 1967 to August 1968.

6. ALLEN, H. G. and CHANNER, R.S.,
   Use of Additives to Increase the Tensile Cracking Strain of Portland Cement Pastes in Glass-Fibre Reinforced Laminates,
   C.I.R.I.A. Report.

7. ARRIDGE, R.G.C.,
   Orientation Effects in Fibre Reinforced Composites Where the Modulus of the Fibres Is No More Than An Order of Magnitude Greater Than That of the Matrix,
   Proc. S.P.I. 18th Annual Conference,
   Sec. 4A, Feb. 1963.

8. BARTEE, E.M.,
   Statistical Method in Engineering,
   Charles E. Merrill Books Inc.

9. BARTOS, P.,
   Private Communication

10. BELL, J.E.,

The Effect of Glass Fibre Geometry on Composite Material Strength, A.R.S.J., 31, 1961.

11. BIRYUKOVICH, K.L., Yu. L., and D.L.,

Glass Fibre Reinforced Cement, (Steklotsement, Russian), Budivel'Nik, Kiev - 1964, Translated from the Russian by C.E.R.A.

12. BRITISH STANDARD 12 : 1958,

Portland Cement (Ordinary and Rapid-Hardening).

13. BRITISH STANDARD 915 : 1947,

High Alumina Cement.

14. BUTLER, D.B.,

The Finer Grinding of Portland Cement and the Comparative Value of the Coarser Particles. Proceedings of the Institute of Civil Engineering, 1898, 132, 343.

15. COUTINHO, A.S.,

The Influence of the Type of Cement on Its Cracking Tendency. Rilem Symposium, December 1959, Bulletin No. 5.

16. COX, H.L.,

The Elasticity and Strength of Paper and Other Fibrous Materials. Brit. Journal App. Physics, 3 March 1952, pp. 72-79.

17. CUTLER, N.A.,

Premixed Polyester Moulding Compounds in Europe. British Plastics, August 1959.

18. GERE, J.M. and WEAVER, W.,

Matrix Algebra for Engineers, Van. Nostrand.

19. GILKEY, H.J. and MURPHY, G.,

The Percentage Stress-Strain Diagram as an Index to the Comparative Behaviour of Materials Under Load,
Iowa State College Bulletin No. 159,
Vol. XLI. No. 48, April 1943.

20. GRIFFITH, A.A.,

Phil. Transaction Roy. Soc.
221 (A), 163. (1920).

21. GRIMER, F.J., ALI, M.A.,

The Strengths of Cements Reinforced With Glass Fibres.
B.R.S. Current Paper EN37/68 July.

22. HELMUTH, R.A., TURK, D.H.,

The Reversible and Irreversible Drying Shrinkage of Hardened Portland Cement and Tricalcium Silicate Pastes.
Journal of the P.C.A. Research and Development Laboratories, Bull. No. 215.

23. HELMUTH, R.A., TURK, D.H.,

Elastic Moduli of Hardened Portland Cement and Tricalcium Silicate Pastes: Effect of Porosity.
Research and Development Laboratories of the P.C.A., Bull. No. 210.

24. HIRSCH, T.J.,

Modulus of Elasticity of Concrete Affected by Elastic Modulus of Cement Paste Matrix and Aggregate.
A.C.I. Journal, Proceedings V59, No. 3,
March 1962, pp. 427-452.

25. HOLISTER and THOMAS,

Fibre Reinforced Materials.
Elsevier.

26. HSU, T.T.C., SLATE, F.O.,

Tensile Bond Strength Between Aggregate and Cement Paste or Mortar.
Journal of the A.C.I. April 1963.
Title No. 60-25, pp. 465-486.

27. KRENCHEL, H.,

Fibre Reinforcement.
Akademisk Forlag Copenhagen, 1964.

28. LEA, F.M., and DESCH, C.H.,

The Chemistry of Cement and Concrete.
E. Arnold Limited.

29. LEADERMAN, H.,

Elastic and Creep Properties of Filamentous Materials and Other High Polymers.
The Textile Foundation, Washington D.C. 1944.

30. LINDLEY, D.V., and MILLER, J.C.P.,

Cambridge Statistical Tables.
Cambridge University Press.

31. LOEWENSTEIN, K.L.,

Glass Systems in Composite Materials.
L. Holliday (Editor). p. 151.

32. MAJUMDAR, A.J., RYDER, J.F.,

Glass Fibre Reinforcement of Cement Products,
B.R.S. Paper CP67/68.
Glass Technology, Vol. 9, No. 3, June 1968.

33. MIDGLEY, H.G.,

Electron Microscopy of Set Portland Cement.
Symp. Southampton, 1969.

34. NEVILLE, A.M.,

Properties of Concrete.
Pitman and Sons Limited.

35. PAO, Y-H., and MARIN, J.,

An Analytical Theory of the Creep Deformation of Materials.
J. Appl. Mech. 20, 245, 1953.

36. POWERS, T.C., and BROWNYARD, T.L.,

Studies of the Physical Properties of Hardened Portland Cement Paste.
Vol. 43, 101, 249, 469, 549, 669, 845, 933.
(1946-1947).

37. POWERS, T.C.,

The Bleeding of Portland Cement and Concrete. Research Lab. Portland Cement Assoc. Bull. 2, 1939 (p. 135).

38. POWERS, T.C.,

Physical Properties of Cement Paste and Concrete. Proceedings of the Fourth International Symposium on the Chemistry of Cement 1960. Paper V-1.

39. RAY, W.S.,

An Introduction to Experimental Design. The Macmillan Co.

40. ROBSON, T.D.,

High-Alumina Cement and Concretes. John Wiley and Son Inc.

41. SASMAL, B.G.,

Private Communication.

42. SENATSKII, N.N.,

Dough-Moulding Compositions Based on Polyester Resins.

43. SHAFFER, B.W.,

Stress-Strain Relations of Reinforced Plastics Parallel and Normal to their Internal Filaments. A.I.A.A. Journal, Vol. 2, No. 2, 1964.

APPENDIX A

A1. STATISTICAL THEORY

A1.1 The NORMAL or GAUSSIAN Distribution

Assuming that an infinite number of tests are conducted and the histogram for these discrete variables is plotted, a continuous frequency function f(x) results, where x is the continuous random variable. The frequency function f(x) as shown graphically in Figure A1 should then satisfy the following:

$$f(x) \geq 0$$

$$\int_{-\infty}^{+\infty} f(x)dx = 1$$

and

$$\int_{a}^{b} f(x)dx = P\{E\}$$

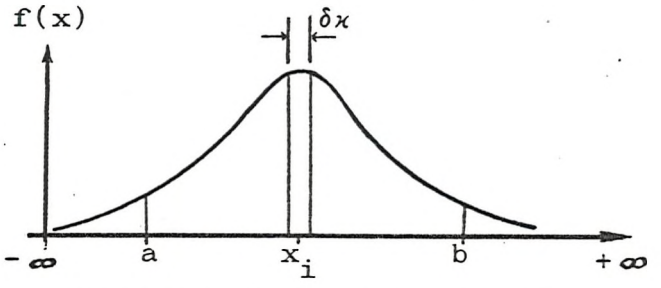

DISTRIBUTION OF THE PROBABILITY DENSITY FUNCTION
FIG. A1

where $P\{E\}$ is the probability that an event E will occur and $E = (a < x < b)$.

The normal distribution of the continuous random variable may be defined as:

$$f(x) = c\, e^{-\frac{1}{2}\left(\frac{x-a}{b}\right)^2} \qquad \ldots (A1)$$

where the parameter 'c' must be such to make the total area of the distribution equal to one.

A1.2 Moments of the Normal Distribution

In order to evaluate the statistical moment for a continuous distribution lying between the finite intervals (a, b), let this interval δx_i be divided into n sub intervals and x_i = i^{th} sub interval and the midpoint (Figure A1).

The k^{th} moment of f(x) is the limit of this sum as the width of the sub interval approaches zero, and the k^{th} moment about the origin of a continuous distribution with frequency function f(x) and denoted by μ_k is:

$$\int_{-\infty}^{+\infty} x^k f(x)dx \qquad \ldots (A2)$$

The first moment of the theoretical distribution (μ_1) about the distribution mean (μ) is zero and the second moment which is known as the population variance and denoted σ^2 giving the population standard deviation from the mean is σ.

Now by employing the Generating function g(x) (A1) may be shown to be:

$$f(x) = \left[\frac{1}{\sigma\sqrt{(2\pi)}}\right] e^{-\frac{1}{2}\left(\frac{x-\mu}{\sigma}\right)^2}$$

and if we let $Z = \left(\frac{x-\mu}{\sigma}\right)$ called the standardised normal variable, then:

$$f(x) = \frac{1}{\sigma\sqrt{(2\pi)}} e^{-\frac{1}{2}Z^2} \qquad \ldots (A3)$$

giving a mean value of zero and a standard deviation of one. So the two parameters completely specify the normal distribution. Here the size of the sample 'n' is infinite.

A1.3 Random Sampling

It is obvious that during experimentation the sample size cannot be infinite, therefore the true first and second moments cannot be obtained and have to be estimated. If a finite number of responses is selected they will be represented by an unknown distribution since the precise distribution cannot be exactly determined. A measurement of the distribution can be made by drawing a sample from it. Generally the precision of the sample is a function of its size 'n' and as 'n' increases the precision with which the sample measures the true distribution will also increase.

The two requirements of a random sample are:

1) All x_{kn} responses are independent.
2) The frequency function of the random variable 'x' shall remain constant from response to response,

   i.e. $f(x) = f(x_{kn})$

   where n - sample size

   k - number of trials

It is therefore necessary to introduce sample moments. The sample k^{th} moment about the origin for a RANDOM sample of size 'n', taken from a

frequency function of a continuous or discrete variable x is given by:

$$m'_k = \frac{1}{n} \sum_{i=1}^{n} x_i^k$$

Therefore when k = 1, the 1st sample moment about the origin, which is known as the sample mean and denoted by $\bar{x}$, is given by:

$$\bar{x} = \frac{1}{n} \sum_{i=1}^{n} x_i \qquad \ldots (A4)$$

and the k^{th} sample moment about the mean is

$$m_k = \frac{1}{n} \sum_{i=1}^{n} (x_i - \bar{x})^k$$

Therefore the sample second moment about the mean called the sample variance and denoted s^2 is

$$s^2 = \frac{1}{n} \sum_{i=1}^{n} (x_i - \bar{x})^2 \qquad \ldots (A5)$$

If we consider the case where x_i is the response in a sample of size n, with a mean $(\bar{x})$, and the theoretical mean is μ, and for a large sample $(n \longrightarrow \infty)$ the population variance σ^2

$$= \frac{1}{n-1} \sum_{i=1}^{n} (x_i - \bar{x})^2$$

This means that $\frac{1}{n-1}\sum_{i=1}^{n}(x_i - \bar{x})^2$ is an estimate of σ^2 and is usually denoted by $\hat{s}^2$

$$\therefore \quad \hat{s}^2 = \frac{1}{n-1}\left[\sum_{i=1}^{n}(x_i - \bar{x})^2\right] \quad \ldots \quad (A6)$$

or

$$\hat{s}^2 = \frac{1}{(n-1)}\left[\sum_{i=1}^{n} x_i^2 - \bar{x}\sum_{i=1}^{n} x_i\right]$$

$$\ldots \quad (A7)$$

The term (n-1) is called the degrees of freedom and denoted ν which is the number of independent contrasts obtained from the responses.

If 'n' is large then s is an unbiased estimate of σ, but if n is small, as in the case of the experimentation used in this investigation, then s is a biased estimate of σ, and the distribution of a random variable x_i is described by the Student's-t distribution instead of the normal distribution where t is given by:

$$\frac{\bar{y} - \mu}{\hat{s}/\sqrt{(n)}}$$

$\bar{y}$ - arithmetic mean of a sample drawn from variable y

μ - mean of the theoretical distribution

$\hat{s}$ - estimate of σ

n - total number of trials or responses in a sample

A2. ANALYSIS AND INTERPRETATION OF EXPERIMENTS

(One Independent Variable)

When a random sample is drawn from a given random variable without any reference to the sublevels of the variable it is said that the levels of the variable are NOT PREDETERMINED.

It is more usual to classify the levels of the variable into PREDETERMINED sublevels, or the variables may be inherently predetermined into sublevels.

The predetermined characteristic of the independent variable is an important criterion in the analysis and interpretation of experimental results.

A2.1 Linear Regression

Here the case of not predetermined levels of the variable will be considered. A computer programme (G44D) has been provided in Appendix E.

The amount of variation in the dependent variable that is due to the variance of the independent variable is known as regression of the dependent variable upon the independent variable. If the dependence is linear then the regression is said to be linear.

It can be shown that, if a condition of minimum error is to exist, the linear relationship between

two variables is given by:

$$y_i' = b_o + b_1 x_i \qquad \ldots (A8)$$

where y_i' the regression estimate of y_i

b_o the best estimate at the intercept of the y axis and is given by

$$b_o = \bar{y} - b_1 \bar{x} \qquad \ldots (A9)$$

and b_1 slope of the linear regression and is

$$\frac{\left(\sum_{i=1}^{n} x_i y_i\right) - n\bar{x}\bar{y}}{\left(\sum_{i=1}^{n} x_i^2\right) - n\bar{x}^2} \qquad \ldots (A10)$$

b_1 is the estimated regression coefficient of y on x.

From equation (A9) it can be seen that $\bar{y}$ is always on the regression line so the deviation of y_i (e_i) from the estimated regression line may be expressed as: Its difference between its deviation from the mean of y_i and the deviation of the regression value y_i'

VARIATION ABOUT THE REGRESSION is the sums of squares of errors with (n-2) degrees of freedom

$$\sum_{i=1}^{n} e_i^2 \qquad \ldots (A11)$$

TOTAL VARIATION is the sums of squares of y responses about their mean with (n-1) degrees of freedom

$$\sum_{i=1}^{n} (y_i - \bar{y})^2 \qquad \ldots (A12)$$

VARIATION DUE TO REGRESSION has 1 degree of freedom

$$\sum_{i=1}^{n} (y_i - \bar{y})^2 \qquad \ldots (A13)$$

Thus variation:

TOTAL = ABOUT REGRESSION + DUE TO REGRESSION

The unbiased estimate of the true variance

$$\hat{s} = \frac{\sum_{i=1}^{n}(y_i - \bar{y})^2}{(n - 1)}$$

OR $$\frac{\text{Sums of Squares of } y}{\text{Degrees of freedom}}$$

which is the MEAN SQUARE VALUE.

It can be shown that if two sums of squares, say SS_1 and SS_2 have independent χ^2 distributions with ν_1 and ν_2 degrees of freedom then

$$F = \frac{SS_1/\nu_1}{SS_2/\nu_2}$$

$$= \frac{MS_1}{MS_2} \qquad \ldots \text{(A14)}$$

This follows the F distribution and as in the case of the normal or Students-t distribution, tables of areas can be found in statistical tables. The hypothesis (H_o : y is dependent on x) is tested for an assumed level of α.

A2.2 Truth Frequency Theory

This theory discusses a class of assumptions and the proposition that an event will happen a certain number of times under given conditions.

Before the experiment is run it is necessary to decide what level of significance is to be used. This level of significance is the risk that the investigator is willing to take by rejecting the null hypothesis when it is actually true. This is called an error of the first kind and denoted α and in the case of this investigation was kept at 10%.

Statistical tables provided the values of t for a probability of 0.1 for particular degrees of freedom.

When probability is considered to be a truth frequency, the method of inductive reasoning employed is that of CONFIDENCE INTERVALS. Intervals are calculated for a mean value $\bar{x}$ and the limits constitute a tolerance outside of which x would not be expected to fall with a risk of α.

In the case of the Student 't' distribution this limit given about the mean value is

$$\bar{x} \pm t \frac{\hat{s}}{\sqrt{(n)}} \qquad \ldots (A15)$$

A2.3 Two Way Analysis of Variance

A computer programme (G44C) has been provided in Appendix E.

The work described here may be applied to any number of independent variables at predetermined levels.

Table A1 shows the responses a_{jk} as a result of the x_n levels of a variable x combined with the y_m levels of the variable y. This table has been arranged in matrix form which will give the required statistics, so that it will lend itself to interpretation as follows:

Total Sum of Squares (TSS) where nm = number of degrees of freedom

$$= \sum_{k=1}^{n} \sum_{j=1}^{m} a_{jk}^{2} - \frac{1}{mn}\left(\sum\sum a_{jk}\right)^{2}$$

Column Sums of Squares (SSC) with (n-1) degrees of freedom

$$= \sum_{k=1}^{n} \left(\sum_{j=1}^{m} a_{jk}\right)^{2}$$

Row Sums of Squares (SSR) with (m-1) degrees of freedom

$$= \sum_{j=1}^{m} \left(\sum_{k=1}^{n} a_{jk} \right)^2$$

Error Sums of Squares (ESS) with (n-1)(m-1) degrees of freedom

ESS = TSS - SSC - SSR

Thus the mean square value can be evaluated by dividing the sums of squares by its corresponding degrees of freedom.

The row and column effects may be tested by calculating the 'F' number for each and comparing it with the critical 'F' number obtained from statistical tables for a given α value as shown before

where F (calculated)

$$= \frac{\text{M.S. (Rows)}}{\text{M.S. (Errors)}}$$ for row effects

and $$= \frac{\text{M.S. (Cols)}}{\text{M.S. (Errors)}}$$ for column effects

Standard deviation for columns and rows may be evaluated in the normal manner, thus extending the work to produce confidence limits if required.

RESPONSES OF VARIABLES AT DIFFERENT EXPERIMENTAL LEVELS

TABLE A1

Number of Columns = n

Number of Rows = m

	x_1	x_2	x_3 ---------- x_k ---------- x_n
y_1	a_{11}	a_{12}	a_{13} ---------- a_{1k} ---------- a_{1n}
y_2	a_{21}	a_{22}	a_{23} ---------- a_{2k} ---------- a_{2n}
y_3	a_{31}	a_{32}	a_{33} ---------- a_{3k} ---------- a_{3n}
⋮	⋮	⋮	⋮
y_j	a_{j1}	a_{j2}	a_{j3} ---------- a_{jk} ---------- a_{jn}
⋮	⋮	⋮	⋮
y_m	a_{m1}	a_{m2}	a_{m3} ---------- a_{mk} ---------- a_{mn}

A3. RANDOMISATION OF EXPERIMENTS

The results of an experiment can easily be invalidated due to bias which is caused by any unmeasured, unknown or undesirable influence upon the variation of the responses and may lead to erroneous conclusions with respect to a particular set of data. If these influences follow a particular pattern then it is referred to as bias.

This bias may be caused by small fluctuations in temperature, humidity, void content, etc, and also possibly by the variations in the procedure of the experiment itself.

Thus an attempt was made to remove some of this bias by carefully planned experimental programmes, and those variables which were difficult to control such as variation of density from sheet to sheet, or the design of the experimental equipment, were reduced by randomisation of the sample selection.

An experiment is said to be randomised when the order in which the responses are taken, has been predetermined in such a way that the responses have equal probability of occurring.

Two way analysis of variance may be used as a test of randomness to test the hypothesis that row

and column effects are zero. This may be summarised in an ANOVA table showing the comparison of computed and critical F numbers for a risk of α.

The techniques of randomisation may be found in many texts, two of which are BARTREE[8], RAY[39].

APPENDIX B

B1. THE REINFORCEMENT

The glass is made from the molten state and is poured through approximately 204 small holes in the bottom of a platinum furnace. As the molten glass rods fall they solidify to form microscopically fine FILAMENTS (about 10 micron diameter). They are then passed through a size and bundled together to form a STRAND. A coating on the fibres not only protects them but may act as a chemical bonding agent between the glass and the matrix material (31). Its presence in this respect when placed with cement has not been shown to be an advantage. These strands can now be used in the production of a ROVING which is simply the collecting together of a number of strands. The rovings may be manufactured so that they can contain from 1 to 120 strands. In this state the strands are usually referred to as ENDS. Strands may also be twisted together to form a YARN and, in turn, the yarns are used to produce a GLASS CLOTH and a fabric called WOVEN ROVING. These fabrics can be purchased with a great variety of weights and choice of weave (Plate B1).

Glass fibre mats are manufactured by chopping the strands into short lengths ranging from between one and two inches. These short lengths are laid at random and held together with a resin binder. These are called CHOPPED STRAND MATS (C.S.M.).

In a similar manner CONTINUOUS FILAMENT MATS (C.F.M.) are made by laying very long lengths of strands and binding together as previously described. In view of the long lengths of filaments it is not necessary to use a high binder content, thus the mat is softer in character than C.S.M.

Glass fibres are used as a reinforcing material since they are cheap to produce compared with other fibres such as CARBON, ALUMINIUM, etc, and glass in its fibre form has a moderately high elastic modulus and strength. A comparison of some fibres is shown in Table B1.

There is a great difference between the properties of glass in its bulk form and glass in fibre form. Glass in its bulk form is a hard brittle material and not very strong (of the order of 10^4 lbf/in^2 tensile strength), whereas the theoretical tensile strength of glass fibres has been estimated to be in the region of 0.5×10^6 lbf/in^2. This strength depends upon the fibre diameter and mode of production.

For fibre diameters of less than 10 microns the tensile strength increases as the diameter decreases. This vast difference in strength is due to inherent flaws in the glass which act as stress raisers, as shown by Griffith [20]. Fibres are used in two extreme forms:

a) chopped fibres which are considered to be finite in length.

b) continuous filaments which are classified as infinite in length, but finite in length if surface flaws, caused during manufacture, fabrication or handling, are present.

The specific gravity of glass fibres is usually quoted as lying between 2.50 and 2.65. It has been shown here at Southampton, using a very long single strand E glass, that the specific gravity was 2.53 and values ranging between 10.5 and 11.3 x 10^6 lbf/in^2 were obtained for the tensile modulus.

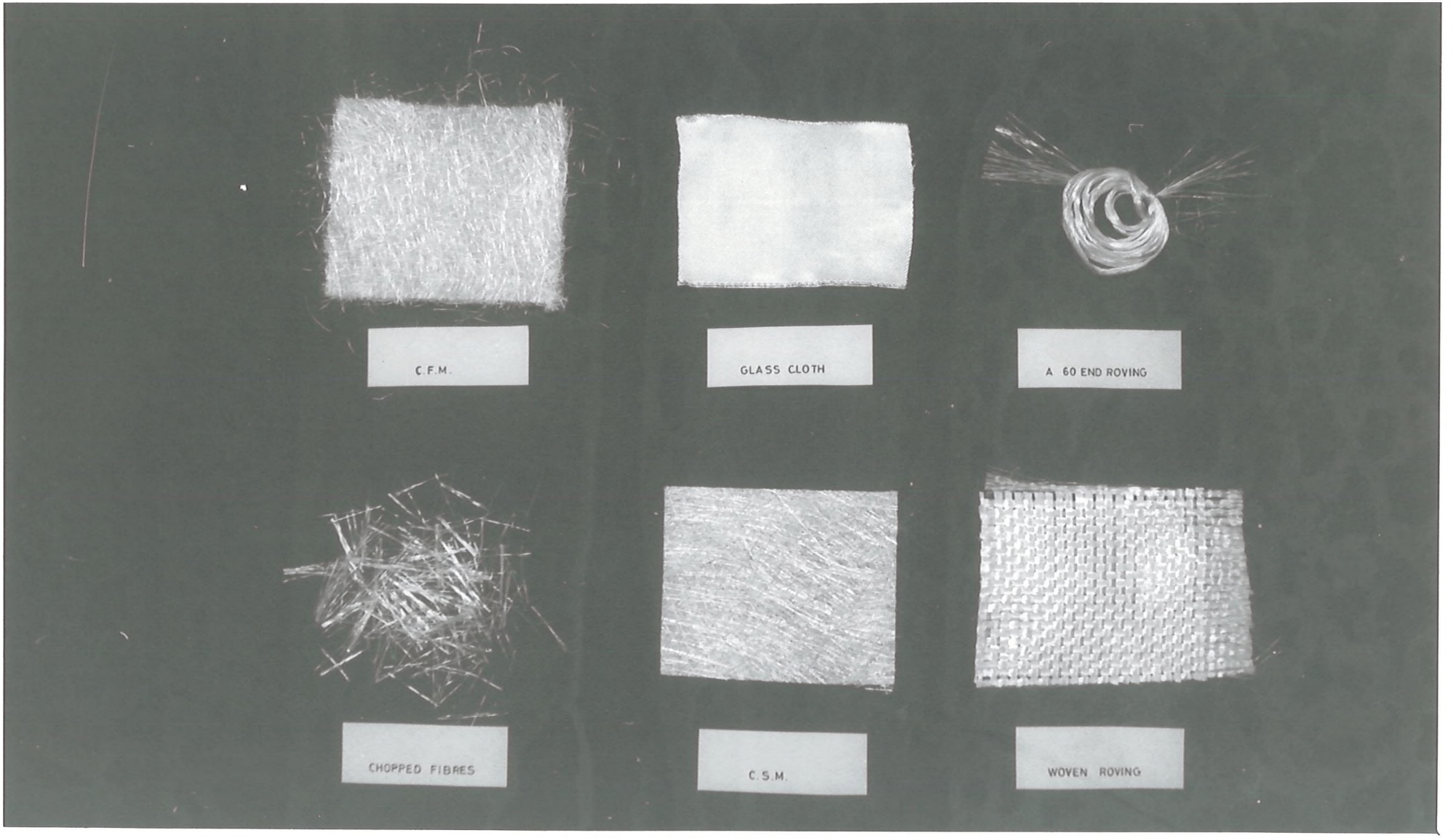

VARIOUS GLASS REINFORCEMENTS
Plate B1

TABLE B1

THE PROPERTIES OF FIBRES

	Tensile Strength (σm) $lbf/in^2 \times 10^{-6}$	Young's Modulus (E) $lbf/in^2 \times 10^{-6}$	Specific Gravity (g)	$\sigma m/g$ $lbf/in^2 \times 10^{-5}$	E/g $lbf/in^2 \times 10^{-6}$
Asbestos (crocidolite)	0.85	27.0	2.5	3.4	11.0
Mica	0.45	46.0	2.7	2.7	17.0
Etched Soda Glass	0.4 mean	9.8	2.5	1.6	3.9
	0.5 max	9.8	2.5	2.0	3.9
Drawn Silica	0.86 mean	10.5	2.5	3.5	4.2
Glass in air	1.5 max	10.5	2.5	6.0	4.2
Glass in vacuo	1.2 mean	10.5	2.5	4.8	4.2
Glass at 77°C	2.0 mean	10.5	2.5	8.0	4.2
Boron Glass	0.35	64.0	2.3	1.5	27.0
High Tenacity Nylon 66	0.12	0.7	1.1	1.0	0.6
Solution Spun Nylon 4	0.27		1.14	2.4	

Holister and Thomas (25)

B2. HIGH ALUMINA CEMENT (H.A.C.)

Robson[40] in his book describes the manufacture of high alumina cement in some detail and it is an important study for those wishing to understand the fundamental concept of the chemistry and mechanisms of high alumina cement.

Only some of the particular aspects of this cement are detailed here since these are particularly related to the mechanical properties of the material which was studied.

The specific gravity of various high alumina cements vary from just under 3.0 to about 3.25. The fineness of grinding affects the time of initial set and therefore the strengths at early ages.[14] The finer the grinding the earlier will be the age at which initial set occurs, although the effect of ultimate strength is not marked. 45% to 60% by weight of high alumina cement consists of particles with a diameter of less than 30 microns.

The soundness of H.A.C. can be confirmed by the use of the LE CHATELIER test, although the expansion is always absent or negligible, thus rendering some doubt as to the usefulness of the result. British Standard Specification for high alumina cement (B.S. 915) requires that the maximum

expansion in the Le Chatelier test should be 1 mm. which is much less than the 10 mm. for ordinary Portland cement.

The setting times of H.A.C. are determined by needle penetration tests on neat cement pats under controlled conditions of temperature and humidity. Using a standard water to cement ratio of 0.22, and Vicat test, B.S. 915 specifies that the initial set time should be between 2 and 6 hours after gauging, with final set occurring not more than two hours after the initial set time. The development of strength of H.A.C. is very rapid once the final set has been reached.

H.A.C. in general does not show an initial evolution of heat. Heat liberation usually occurs about 2/4 hours after gauging, but once having started it is very rapid and its temperature is at a maximum about 8 to 10 hours after placing so that special precautions have to be taken within the first 24 hours to ensure that there is sufficient moisture present to allow complete hydration of the cement.

Dynamic Elastic Modulus values for H.A.C. mortars are given in the region of (5 to 7) x 10^6 lbf/in^2 depending upon water/cement ratio and age.

B3. PORTLAND CEMENT (P.C.)

A great volume of information has been produced by many workers on the study of the physical and mechanical properties of cement paste. This is illustrated by Powers and Brownyard [36].

The quality of cement varies widely. It is therefore necessary to state its characteristics by means of easily defined physical properties. Powers showed that the preparation of fresh cement paste is an important criterion in the characteristics of cement pastes. It is important to closely control the mode of production.

Table B2 shows the requirements of British Standard and amply describes the method of obtaining these parameters. Further implications are shown in Lea and Desch [28] which is a classic book for those interested in the field of materials made with Portland cement.

The mechanical properties of hardened cement paste have been shown to depend upon many factors, the most important of which are:

1) water to cement ratio: high w/c ratio results in low strength and high deformation.
2) curing condition.
3) age: at early ages the tensile

and compressive strengths increase rapidly until about 30 days when the rate of increase of strength is very small.

4) the manner in which the particular test is conducted.

B3.1 Fineness

Cement may be ground to a very fine state of division. It has been shown that the particle size affects the mechanical properties of the hardened paste. In the case of mortars a finely ground cement coats the surface of the inert material more completely than course ground cement. There will also be a greater surface exposure in proportion to its mass, thus giving a better reaction with water resulting in improved cohesion between the inert particles leading to increased tensile strengths. Fineness also affects the initial setting time (14).

B3.2 Porosity

This is a basic property of cement paste, although its definition is not agreed. Powers suggests as a definition of porosity: the ratio of the pore spaces which can be occupied by water that is evaporable at a constant low external humidity, at a given temperature, to solid. This excludes the presence of entrained air bubbles

and the like, which are regarded as cavities rather than integral parts of the paste.

The elastic modulus is greatly affected by pores produced by entrainment of air in cement paste as well as capillary pores as shown by Hirsch[24]. Helmuth and Turk[23] manufactured specimen free from air voids. Graphs were plotted to show a strong dependence of elastic modulus on a function of the capillary porosity (ε_c) and total porosity (ε_t). Poisson's ratio appeared to be independent of the porosity at a constant value of 0.268.

B3.3 Shrinkage

Cement paste has a porosity of about 30 to 40% by volume and a network of extremely fine pores. This leads to water evaporation from these spaces which causes volume changes of the cement paste.

If cement paste is subjected to wetting and drying under carbon-dioxide-free conditions then reversible and irreversible shrinkage may be observed. Helmuth and Turk[22] have attempted to correlate these shrinkages with porosity for cement pastes. Coutinho[15] has studied the cracking tendencies of various cements and mortars under free and restrained shrinkage.

TABLE B2

REQUIREMENT OF PROPERTIES FOR ORDINARY PORTLAND CEMENT (B.S. 12 1958)

Compressive Strength (Mortar)	Not less than	15.17 N/mm^2 (2200 lbf/in^2) at 3 days
	Not less than	22.44 N/mm^2 (3400 lbf/in^2) at 7 days
* Tensile Strength (Mortar)	Not less than	2.07 N/mm^2 (300 lbf/in^2) at 1 day
Setting Times	Not less than	45 minutes ... Initial Set
	Not more than	10 hours ... Final Set
Soundness	Not more than	10 mm expansion
Specific Surface	Not less than	0.225 m^2/g
Density	At 0.475 porosity	

* Using rapid hardening Portland cement

B3.4 Stress-Strain Relationship for Portland Cement Paste

Tensile and compressive strengths are dependent upon w/c ratio. Krenchel[27] (p. 58) quotes strains at the ultimate stress to be 3 to 4 x 10^{-3} (compressive) and 0.4 to 0.6 x 10^{-3} (tensile). He also states that the tensile and compressive stress-strain diagrams are linear up to approximately 50 to 60% of the ultimate stress and the deviation of the stress strain curve from the initial slope is slight. According to Krenchel the elastic modulus in tension and compression is similar, ranging from 6.4 x 10^6 lbf/in^2 (w/c = 0.16) to 2.27 x 10^6 lbf/in^2 (w/c = 0.4).

Gilkey and Murphy[19] (p. 26) give compressive strains in the range 4 x 10^{-3} (w/c = 0.13) to 4.8 x 10^{-3} (w/c ratio = 0.53) at an age of 28 days. Hsu and Slate[26] also illustrate similar characteristics quoting strengths of neat cement paste at an age of 30 days, at a w/c ratio of 0.256, as 573 lbf/in^2 (tensile) 12800 lbf/in^2 (compressive), and at a w/c ratio of 0.36 as 523 lbf/in^2 (tensile), 9570 lbf/in^2 (compressive).

In flexural tests on neat cement beams having a w/c ratio of 0.32 stored at 16°C and R.H. 95% a

linear relationship between load and deflection up to failure has been shown. Maximum tensile strains were given as 0.35×10^{-3} (10 months) and 0.415×10^{-3} (1 month) with corresponding elastic modulii of 5.7 to 4.66×10^{6} lbf/in^2 and flexural stresses of 1995 to 1929 lbf/in^2.

APPENDIX C

C1. THE INSTRON TESTING MACHINE

The fundamental measuring instrument used during the investigation was a Universal Instron Testing Machine as shown in Plate C1 and circuit diagram Figure C1.

The machine incorporates a highly sensitive electronic weighing system with load cells that use strain gauges for detecting and recording tensile and compressive loads.

A moving crosshead is operated by two vertical drive screws and a positional servo-mechanism for unique accuracy and flexibility of control over the crosshead motion.

Tension cells (Plate C2 top left) are fitted to the upper crosshead. Grips (Figure C2) are attached to the central spindle by means of a flexible bayonet-type coupling.

A compression cell (Plate C2 top right) is placed inside a separate support carriage and positioned beneath the moving crosshead.

When a load is applied to the load cell it causes a proportional change in the resistance of the strain gauge. These gauges are arranged in a bridge circuit and excited by a stabilised oscillator.

The resultant signal is amplified, rectified to D.C. and fed into a nul-balance high speed recorder. The amplifier also incorporates a device for balancing the load cell.

An X - Y chart recorder is provided and is driven synchronously with respect to the crosshead movement. The servo system allows a maximum chart speed of 10 in/s. Maximum following errors at the chart are less than 0.02 in. exclusive of any extensometer error. The system exhibits good stability and zero drift. The amount of chart movement possible is limited by the characteristics of the extensometer.

In all cases an electrical signal from the extensometer sensing element is compared against a signal from a similar follow-up balancing unit which drives the chart. Any imbalance between these two signals is amplified to operate the servo drive motor which simultaneously drives the chart and the follow up unit through a gear train until the system is rebalanced. Thus the chart motion is an accurate reproduction of the extensometer. The accuracy of the overall load weighing system is $\pm$ 0.5%.

A change of gearing arrangement in the mechanical drive assembly offers a 40 to 1 spread in magnification ratios with respect to the extensometer movement.

The X - Y graph plotter was used in conjunction with two of its extensometer drive systems.

C1.1 Baldwin Microformer

Basically this is a variable differential transformer with a movable core which varies the magnetic coupling between the primary winding and two balanced secondary windings. These secondary windings are connected in phase opposition so that the output voltage from the microformer will vary linearly with the position of the core. 0.05 in of extensometer displacement will produce 7.5 in of chart movement (150:1 magnification).

C1.2 Strain Gauge Extensometer (Plate C2 bottom)

The strain gauge extensometer operates from a 120 ohm strain gauge bridge and, in view of the low signal level, requires the use of a strain gauge preamplifier. This provides the necessary amplification and control circuits for the operation of the X - Y chart plot system. The sensitivity of the amplifier is such that approximately 0.3 mv/v output from the strain gauge bridge will produce 10 inch of chart motion. This means a magnification at the chart of 500 times the extensometer movement.

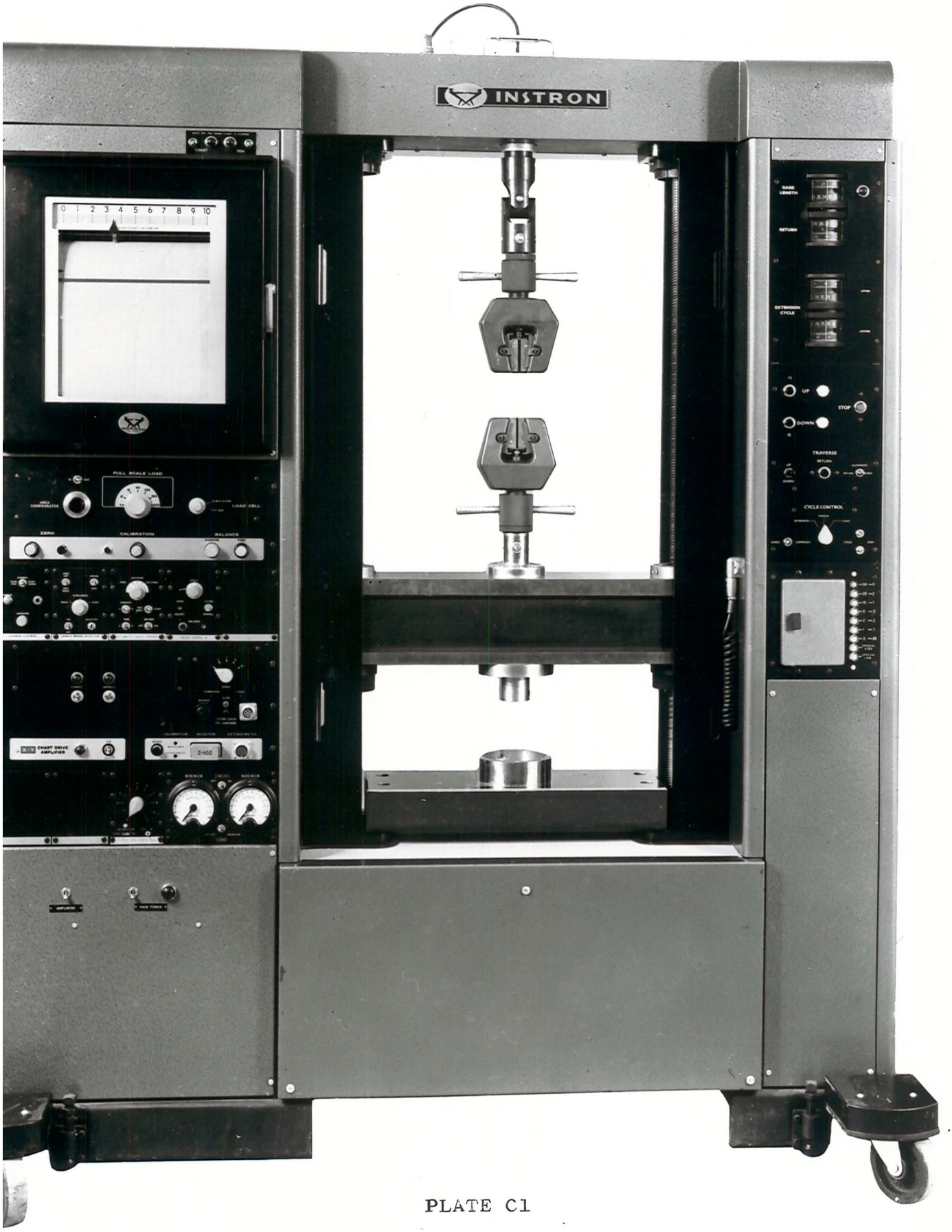
INSTRON
0 1 2 3 4 5 6 7 8 9 10
FULL SCALE LOAD
ZERO
CALIBRATION
BALANCE
CHART DRIVE AMPLIFIER
Z-102
MINIMUM
MAXIMUM
GAGE LENGTH
RETURN
EXTENSION CYCLE
UP
DOWN
STOP
TRAVERSE
CYCLE CONTROL

PLATE C1

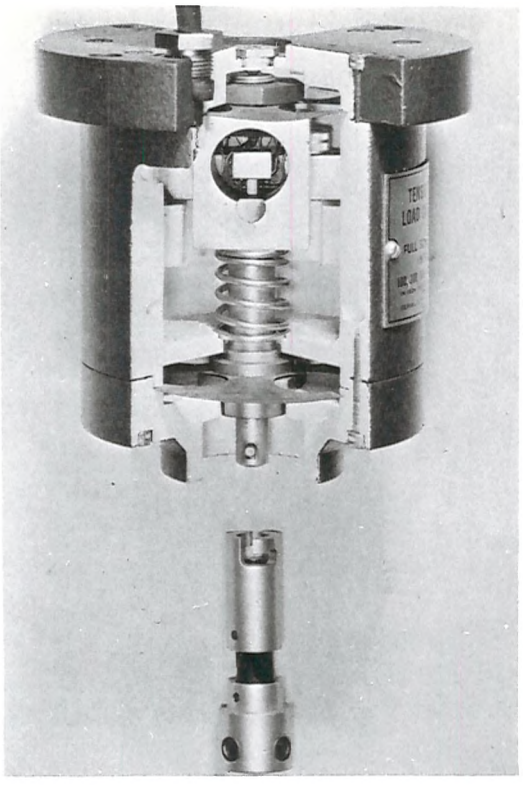

TENSION LOAD CELL

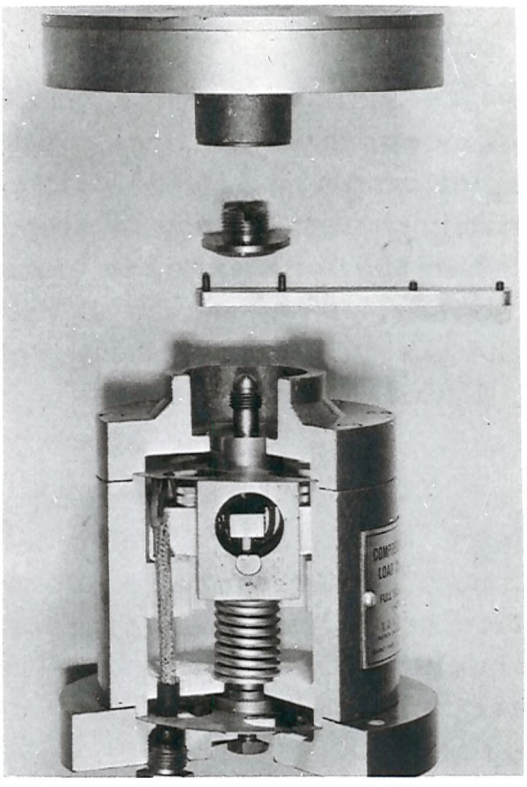

COMPRESSION LOAD CELL

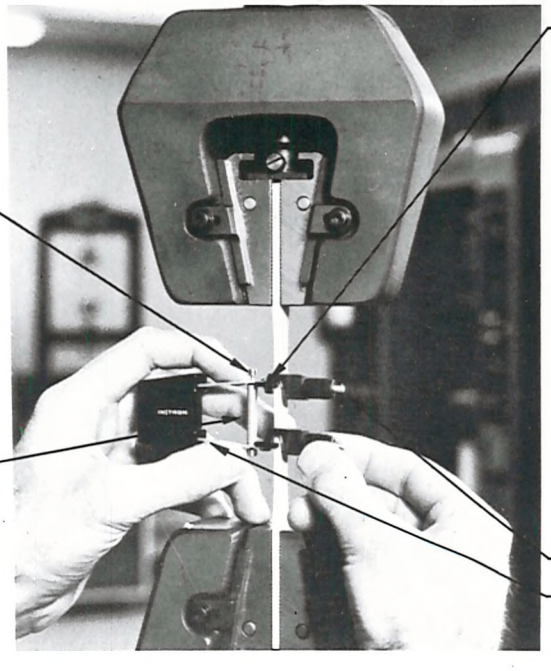

Be sure the knife edge seats properly in the specimen "V" seat with the clamp centered.

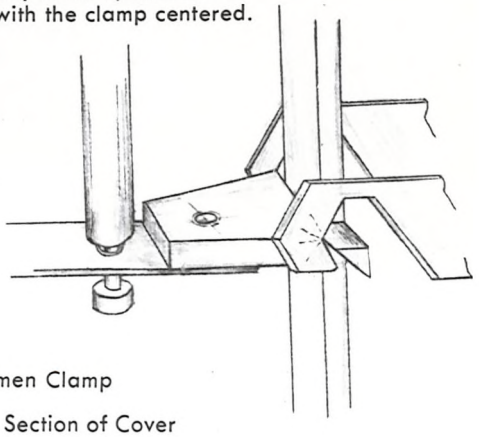

PLATE C2

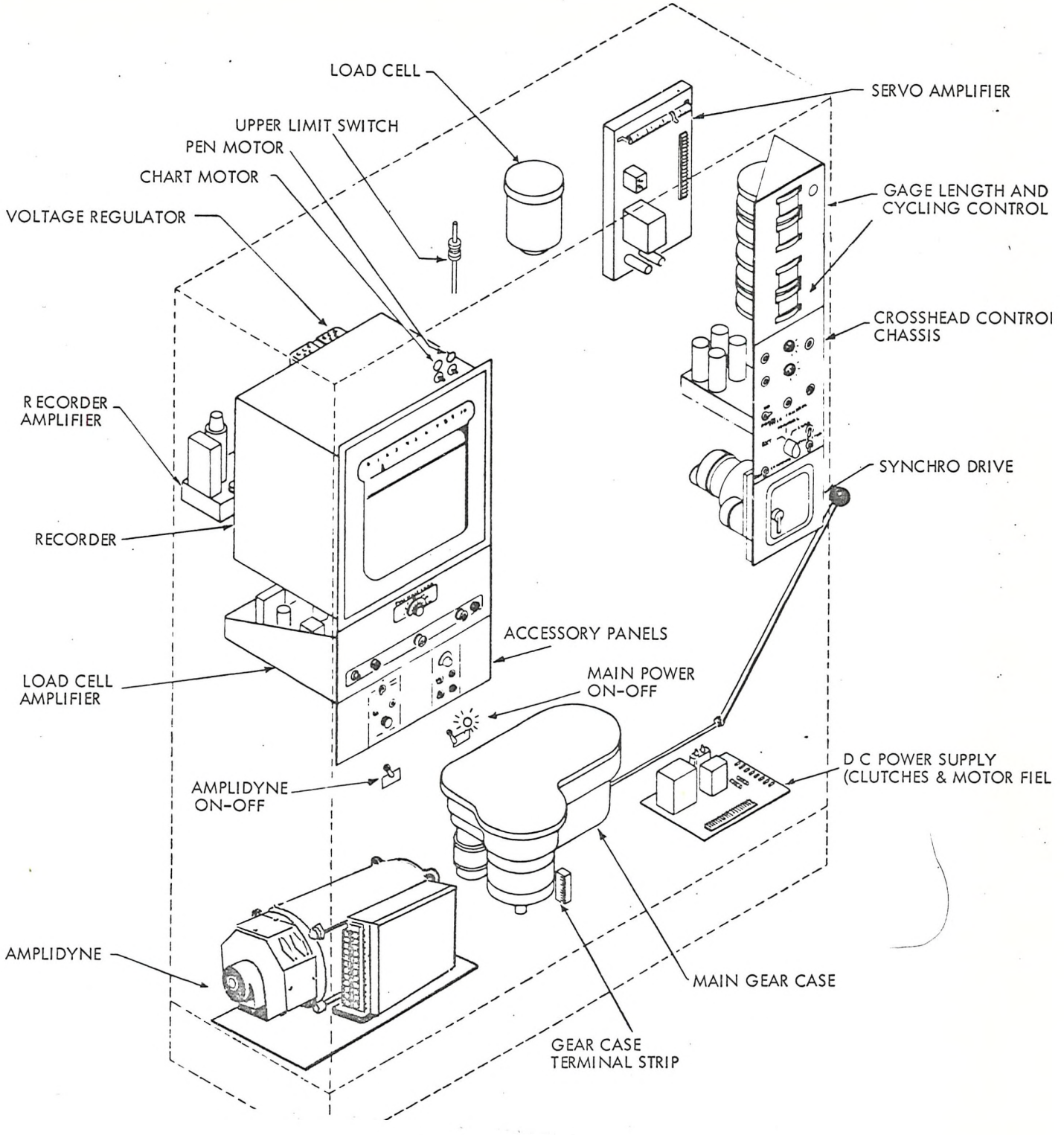

DIAGRAMMATIC ARRANGEMENT OF INSTRON TESTING MACHINE

FIG. C1

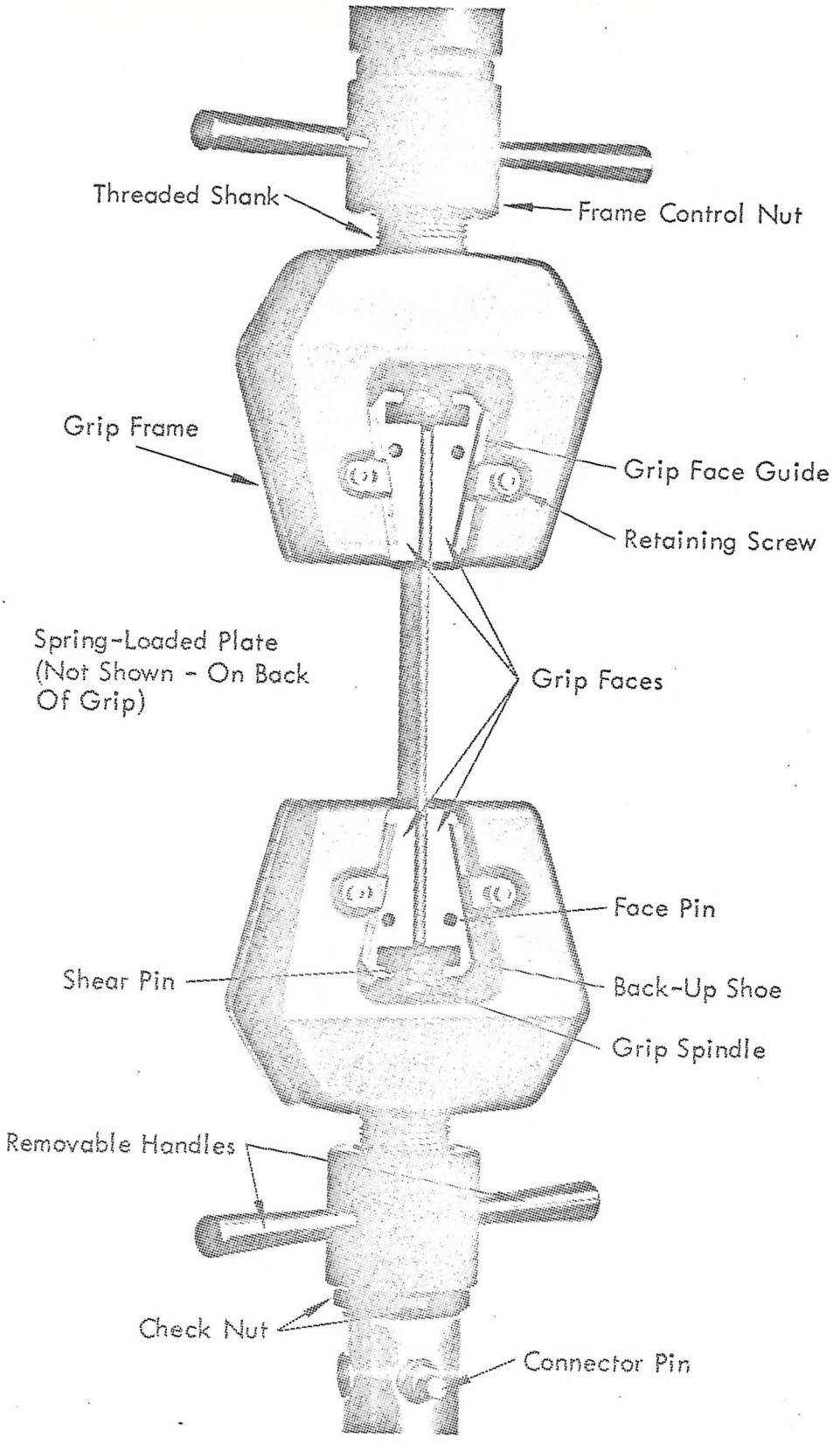

GRIPS FOR TENSILE SPECIMEN

FIG. C2

C2. SHAPING AND PREPARING THE TEST PIECE

All specimens throughout the project were shaped in a careful manner to ensure a minimum of specimen damage and a maximum degree of dimensional accuracy. To this end steel templates were used and these were machined to provide the test sample size and shape.

Every test piece was marked out oversize on the reinforced and unreinforced sheets of cement as shown on the appropriate figures throughout the thesis. Station numbers were marked on the proposed specimen at 1 inch intervals along its length in every case, giving 11 stations for tensile specimens and 5 for compression specimens. This allowed the widths and thicknesses to be recorded at these reference points and also to provide a reference number for the exact position at which specimen fracture occurred. The specimens were also marked with identity numbers at this stage.

The sheets were then cut to approximately the test piece size by using a steel-cutting band saw. Great care was taken here since damage to the test piece could quite easily result, particularly in the case of the unreinforced boards. It only remained now for the test piece to be cut to correct shape and degree of accuracy required by the investigation. This

was done by employing the use of a specially constructed piece of apparatus developed by Allen[3] as shown in Figure C3, which consisted of an electric drill mounted in such a way that a diamond impregnated routing tool in the drill chuck protrudes through a flat steel table. The apparatus is placed in a box with a perspex top and a vacuum, caused by an air suction pump, draws away flying glass fibres and dust which otherwise would constitute a health risk. The oversize specimens were clamped between the two steel templates whose dimensions and shape are shown in Figure C4. A cylindrical bush is fitted around the routing tool which acts as a guard and accurate guide but, to allow for this, the templates were designed undersize. All specimen dimensions were within a tolerance $\pm$ 0.002 in.

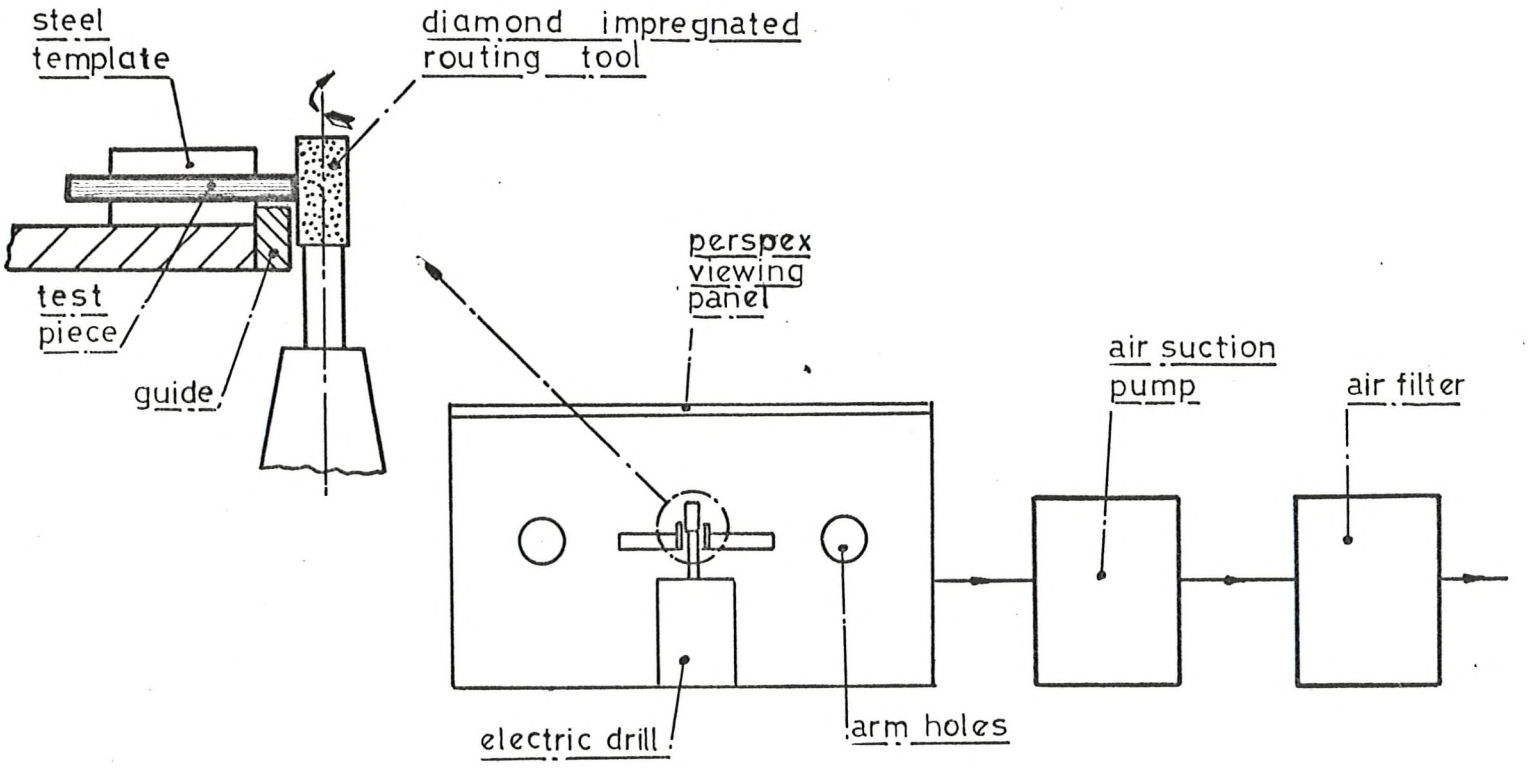

DIAGRAM SHOWING SHAPING OF TEST PIECE
FIGURE C.3

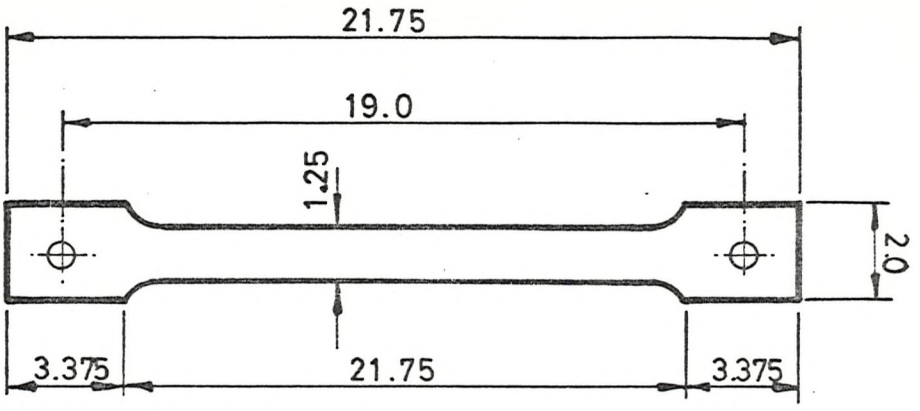

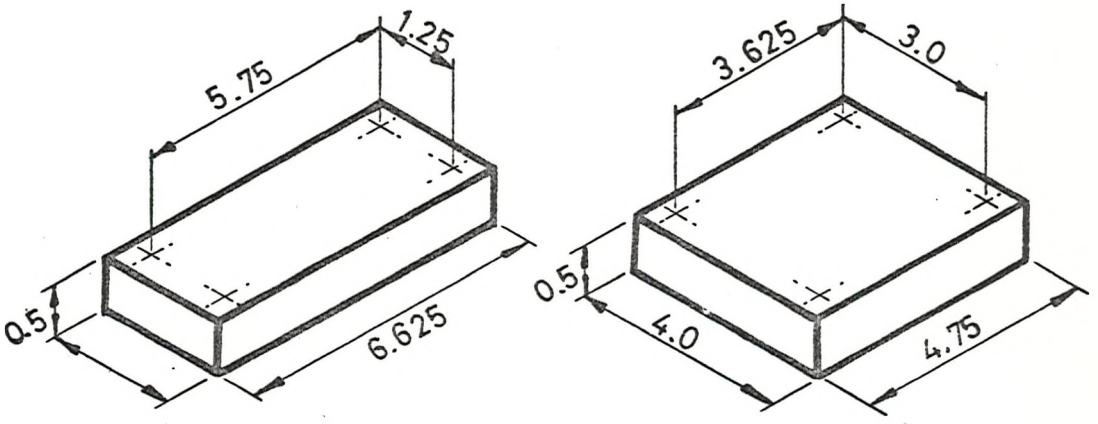

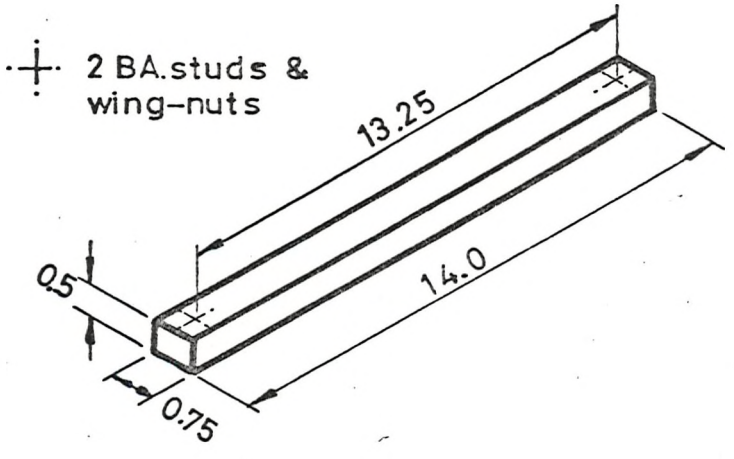

specimen size, larger than template by 0.125
All dimensions in inches (not to scale)

STEEL TEMPLATES FOR SHAPING SPECIMENS

(2 off each)

FIG.C4

APPENDIX D

D1. FILAMENT WINDING

This is a technique which is used widely in the fibre reinforced plastics field. Filament-wound structures show high values for specific strength, and on a strength for weight basis, filament-wound components are capable of giving higher performances than any other structural material.

This improvement in physical properties is made possible by the accurate alignment of the reinforcing fibres in the line of the maximum applied force. Thus it is possible to obtain maximum utilisation of the reinforcement. It is also important to note that these structures may be mechanised and thus put on a mass production basis resulting in reduced costs.

Basic Equipment Functions

In delivering the roving or yarn from their spools on to the component being wound, three basic operations must be performed:

Tension: The yarn or rovings must be delivered to the mandrel under controlled tension. Random tension variation must be kept to a minimum. The distribution of tension from strand to strand and from end to end must be uniform and it is necessary that the overall

tension level should be adjustable.

Impregnation: In using a wet winding system, the roving or yarn leaves the spool in its dry condition and is thoroughly impregnated with cement as it passes through the delivery system. There should be no voids or dry spots. On the other hand no excess of cement should remain on the glass. The amount of cement deposited on the glass should be constant, but the ratio of glass to cement weights should be adjustable.

Guidance: The individual rovings or yarns must be formed into a ribbon which is flat and smooth. The strand spacing within the ribbon should be uniform and the total ribbon width should be constant. This ribbon must be guided on to the mandrel surface in such a manner that it remains uniform regardless of the winding pattern geometry.

When considering the winding of filaments using cement as a filler it was necessary to pass the filaments through a cement mix which had a high water/cement ratio. The excess water would be drawn off after or during production. To this end a mandrel (Plate D1) was manufactured. The flat surfaces on which the finished sheets were formed consisted of

two perforated brass sheets. The other two sides were of clear perspex allowing observation of the distribution of suction over the inside of the sheet. A pressure, lower than atmospheric pressure, was achieved by drawing off the air through a hollow shaft which was the centre spindle. This was designed to allow the mandrel to rotate without the air seal being disturbed. The air was drawn through a baffle box thus ensuring that water was not drawn into the suction pump, at the same time enabling the water to be collected so that the water/cement ratio of the cement in the hardened material could be estimated.

The problems arising from this technique were numerous and the major points are listed below:

I) In order to impregnate the rovings a cement slurry was required and, therefore, the adhesion of the cement to the coated glass was poor. The result was a single roving of glass fibre with either very little or an excess cement adhesion.

II) Since the coating of the glass with cement was uneven a roller was required at the mandrel which tended to disturb the alignment of the fibres. There was

considerable adhesion of the cement to the roller which tended to lift the fibres, sometimes resulting in their damage.

III) Tensioning of the fibres and their alignment was difficult. When a second pass was made, i.e. to obtain two layers of continuous filaments, the result generally was a spreading of the lower layer and touching of fibres which would give a poor laminate.

IV) Suction was seen to be uneven over the plane of the laminate which meant that the water/cement ratio of the binding matrix would vary from place to place.

A number of these problems have been considered by Allen[3] and the technique of manufacturing filament wound laminates has been improved.

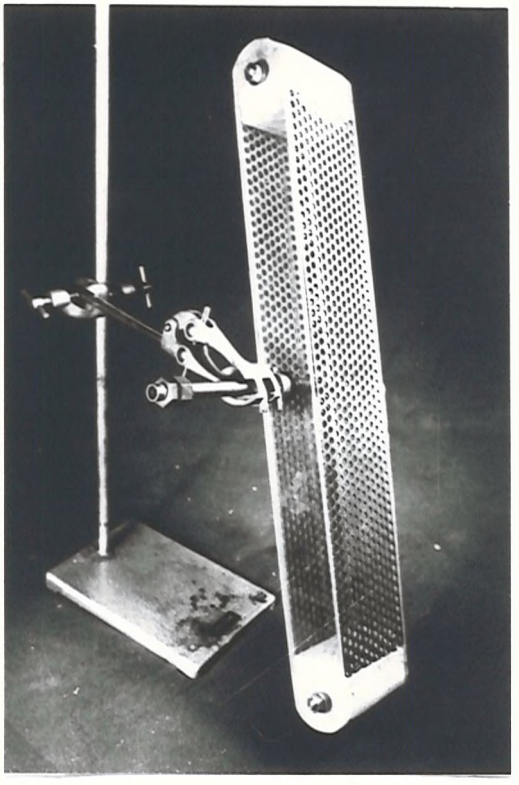

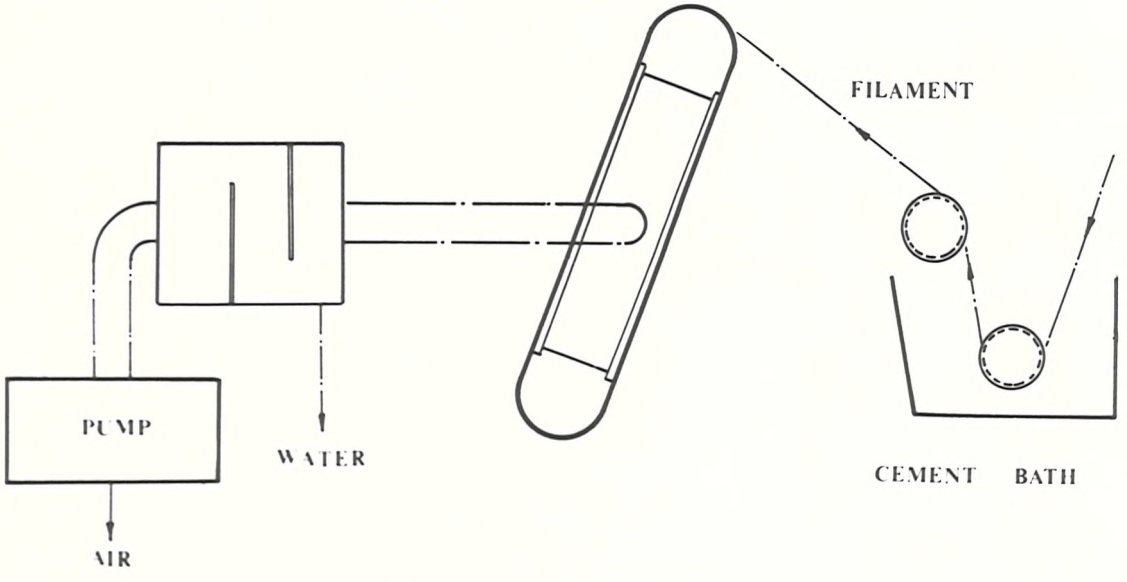

FILAMENT WINDING RIG
PLATE D1

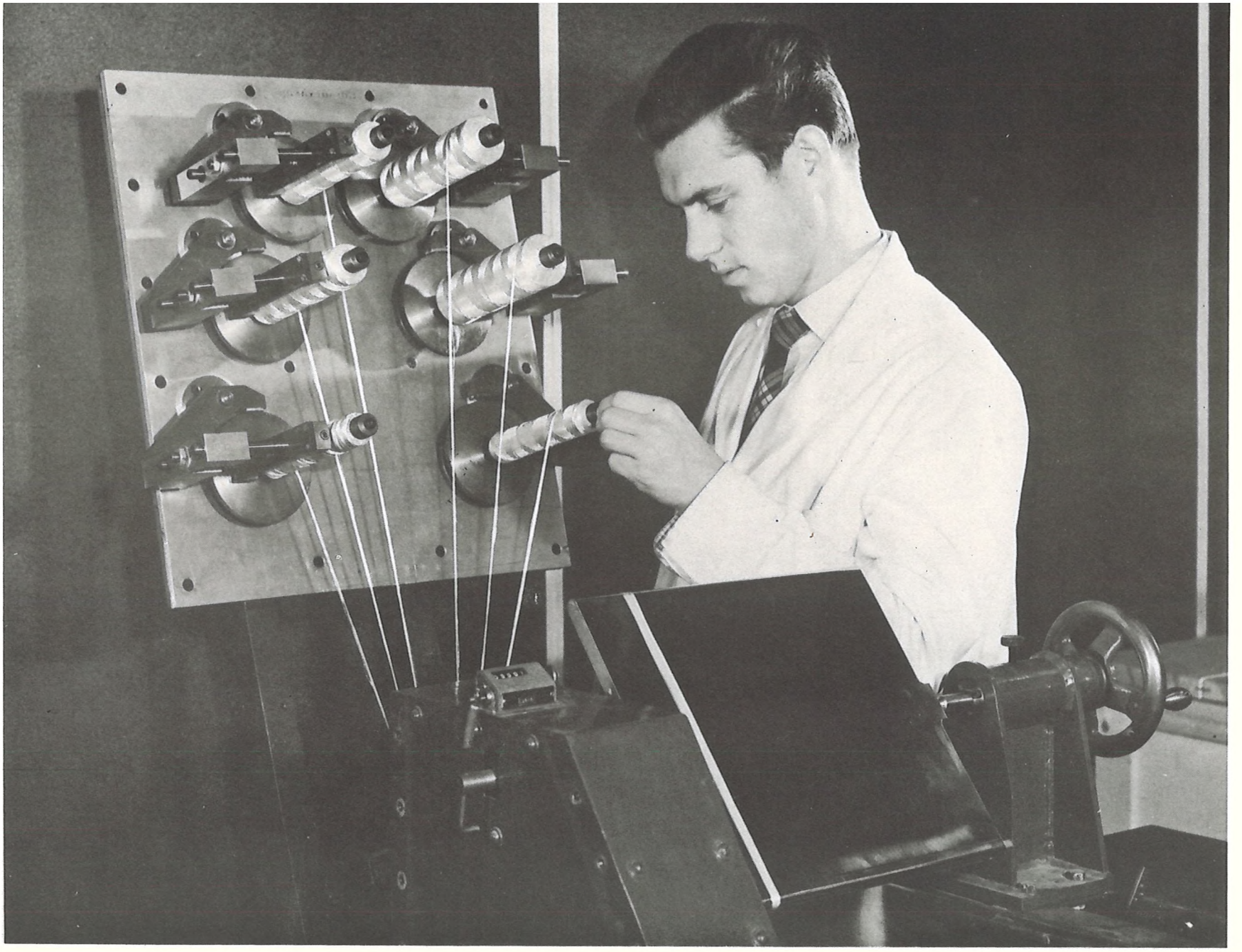

Plate D2 FLAT LAMINATE MACHINE

D2. THE SPRAY TECHNIQUE

This method is simply the mixing of a cement slurry (i.e. a cement mix with a high water/cement ratio, say about 0.5) and chopped glass rovings about 2 inches long. These could be shortened by increasing the number of blades in the cutting drum of the glass chopper. Both glass rovings and cement slurry are drawn into a compressed air stream prior to moulding (Figure D1).

The glass rovings, which are unwound from a spool or cheese **1** are drawn into the glass chopper **2** which is driven by air supplied by the compressor **3**. The quantity of glass passing through the chopper is a function of the rotational speed of chopping blades and this can be measured by a tachometer placed at the rotating shaft. It will also depend upon the number of cheeses being used. This rotational speed can in turn be controlled by the quantity of air admitted to the chopper via the control valve **4**. The rovings used have a low size content and are specially manufactured for this type of work in the plastics industry.

A slurry is prepared by first placing in a drum a measured amount of high alumina cement, to which the appropriate quantity of water is added. This is

mixed for three minutes. The slurry is then placed in the hopper **5** which is integral with the cement delivery pump **6**. The cement is then sucked from this hopper into the electrically driven delivery pump which pushes the slurry through a 2 inch diameter pipe to the spray gun **7**. Since the pump runs at a constant speed the quantity of cement to be delivered can be regulated by a valve **8** which passes some of the cement back to the hopper. At the spray gun the cement is drawn into the compressed air jet. It is at this stage that the chopped glass fibres and the cement slurry mix are directed towards the mould **9** as shown in Figure D1.

The mould may be of any desired shape but must have a vacuum space behind the moulded surface to draw off the excess water from the cement slurry. The water/cement ratio of the hardened cement matrix would be in the order 0.25 to 0.3, and this ratio may be estimated by weighing the quantity of water collected in the water trap **10** for a given interval of time. A low water/cement ratio is a requirement of optimum strength and will give a material with a higher degree of stiffness.

The Building Research Station at Watford have developed this technique and found that the design of moulds of this suction type is not without problems

but they have nevertheless been successful. During the development stage of this project a number of problems were encountered and if this line were pursued much time, patience and finance would have been entailed. Some of these problems are detailed below.

Apart from the great problem of designing a suction mould, the simplest of which is a mould for the manufacture of flat uniform sheets, it was found that the final material would not lend itself to theoretical analysis without the use of very sophisticated statistics. The rate at which the slurry/glass spray was moved longitudinally and transversely not only controls the thickness of the material but also its density and the glass volume ratio. This would mean that the spraying apparatus would have to be mounted upon rails, thus allowing complete control over this movement. The suction at the back of the mould could not be ensured as being constant and uniform all over the surface of the mould if there was a variation of laminate thickness or air leakage due to faulty mould design or manufacture. This would result in a variation of the water/cement ratio of the hardened material which in itself would be difficult to estimate accurately.

The following variables would have to be closely controlled before any attempt could be made to investigate the mechanical properties of the hardened material and thus try to correlate with theoretical predictions.

1) Rate of flow of cement.
2) Air flow to the cement nozzle.
3) Angular velocity of glass chopper.
4) Height of the spray device from the mould.
5) Transverse speed of nozzle.
6) Longitudinal speed of nozzle.
7) The suction at the back of the mould.

It was most important to ensure that all the equipment was carefully cleaned since the cement could harden within the pump and delivery pipes, thus resulting in damage to the equipment.

The sheets have to be removed from their mould 24 hours after manufacture. During this time they are covered with water soaked hessian sacking, since the rate of heat evolution during this period is high and, due to high humidity of its surrounds, complete hydration is allowed to take place.

Plate D3 shows the manufacture of glass fibre reinforced sheets by the above-described manner. This photograph was supplied by the Building Research Station where the work is in progress.

THE MANUFACTURE OF FLAT REINFORCED SHEETS BY SPRAY TECHNIQUE

PLATE D3

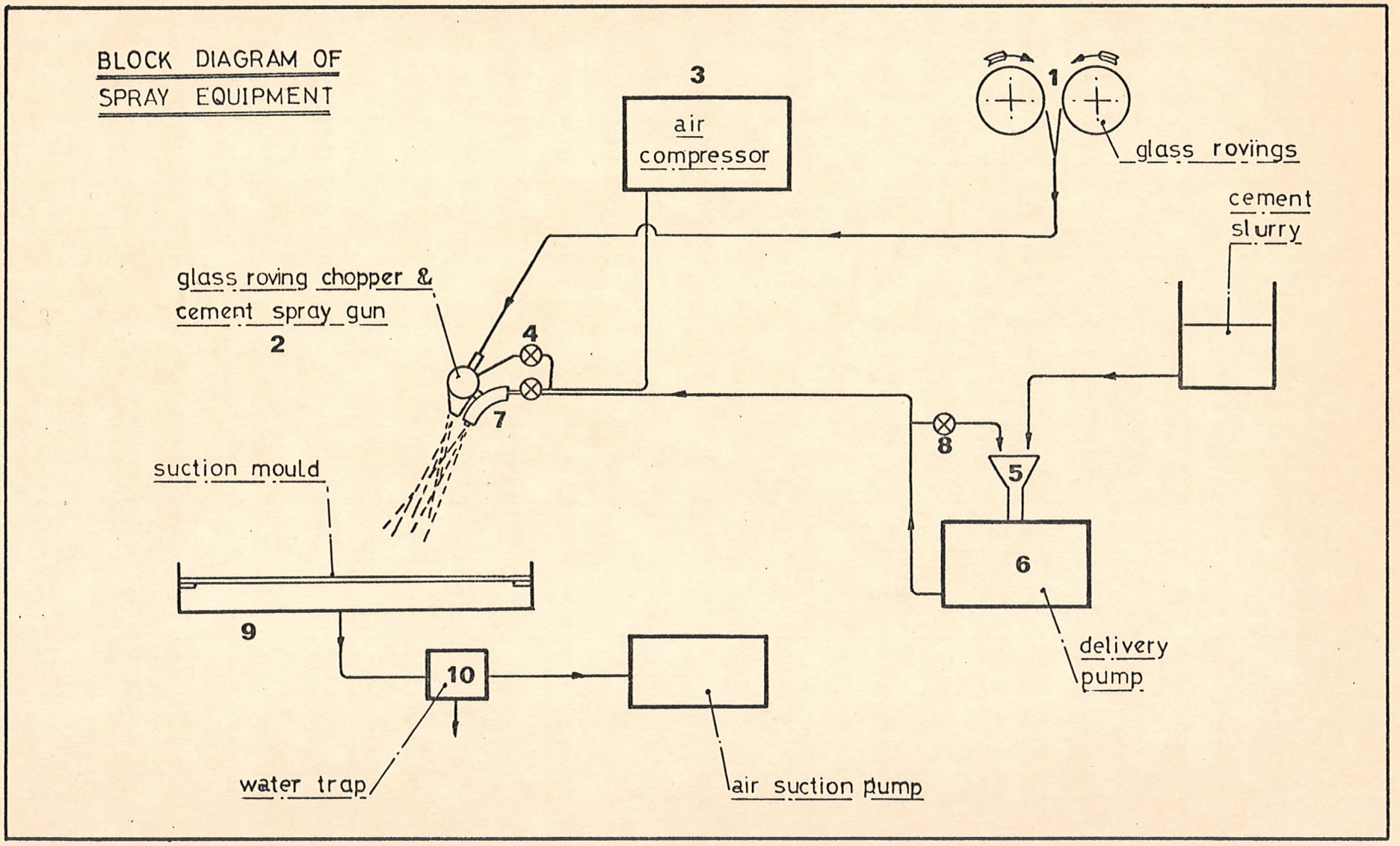
BLOCK DIAGRAM OF
SPRAY EQUIPMENT
3
air
compressor
1
glass rovings
cement
slurry
glass roving chopper &
cement spray gun
2
4
7
8
5
6
suction mould
9
10
delivery
pump
water trap
air suction pump

FIG. D1

D3. THE HAND LAYUP METHOD

The most convenient way of obtaining a laminate is to lay the individual constituents into a mould. Such was the case of the reinforcement of H.A.C. with chopped strand mat where a release oil was first applied to a sheet of perspex, followed by a thin layer of cement paste (applied with a brush), then a layer of chopped strand mat. The mat was then rolled by hand to force the cement up into the interstices and release any trapped air. This process was repeated until three layers of C.S.M. were laid. Finally a layer of cement was placed, the excess skimmed off with another sheet of perspex and a small pressure then applied to the sandwich. It was quite noticeable that bleeding of the cement occurred and that the water was being pressed from the laminates, thus forming rivers and pits at the surface. It followed that, during the curing process, this water evaporated leaving an uneven surface, whilst the moulded surface was mirror-like. Many attempts were made to improve this situation but not with complete success.

The laminate remained in this condition for twenty four hours before demoulding so there was very little evaporation during this period. After demoulding, the sheets were totally submerged in water for the final cure period.

It was noticed that the final hardened sheet approximated closer to a sandwich construction than a homogeneous material. The glass layers across the area which is perpendicular to the plane of the mat were not uniformly distributed. The compaction and impregnation of the cement paste was also found to be poor. These sheets which were approximately 15" x 9" each, were cut into 1 inch wide strips and prepared in the manner described in Sec. C2 to provide tensile specimens with dimensions and glass contents as shown in Table D1.

The specimens, numbered 0.1 to 0.7, were tested in tension using the Instron Universal Testing Machine (Sec. C1), with a crosshead speed of 0.5 in/min. In order to evaluate the initial elastic modulus the Instron Extensometer (Sec. C1.2) was used, but was removed at the earliest opportunity since it was thought that the extensometer may sustain damage when the specimen failed. Because of this the elastic modulus values quoted for specimen 0.1 to 0.7 for the upper portion of the stress/strain graph are not accurate since the chart was being driven at a constant speed and not by an extensometer signal during this stage of the

test. This means then that error will occur in the calculation of these values since the stiffness of the machine had not been calibrated.

The general character of the stress/strain graph can be seen in Figure D2 which also indicates the notation used. The stress/strain diagram for high alumina cement reinforced by a random array of glass fibres, in the form of chopped strand mat, has two distinct zones. The first is a direct linear relationship between stress and strain up to the limit of proportionality (e) where the matrix remains uncracked. This is followed by a knee in the curve where cracks are forming in the cement matrix and more load is being transferred to the reinforcement. A further linear relationship exists in the upper portion of the stress/strain curve.

To obtain a greater understanding of the material a repeated loading test was used where the load was applied to the specimen to a point beyond the elastic limit (e) at a constant rate of crosshead speed (0.02 in/min). The load was then released at the same rate as loading. This was repeated as illustrated in Figure D3 where it is obvious that the initial elastic modulus of each loading curve decreases with increased cycle indicating that there is a breakdown of the material. It also shows that the limit of

proportionality is raised with every cycle but the upper slope of the stress/strain curve is the same in every case, being that of the upper slope shown on Figure D2.

The quantity of glass present in the composite was estimated by considering the weight of the mat per unit area (as quoted by the manufacturer). This was taken as a percentage of the total weight of the specimen but, since this quantity measured in terms of volume is a more important parameter, it was necessary to transform values of percentage glass content by weight to percentage glass content by volume.

TABLE D1

MECHANICAL PROPERTIES OF SPECIMENS 0.1 TO 0.7

Spec. No.	Age (Days)	w/c Ratio	Mean Area (in^2)	% Glass Content by Volume (Ø)	Elastic Modulus of Composite $lbf/in^2 \times 10^{-6}$	STRESS	
						σ_i lbf/in^2	σ_u lbf/in^2
0.1	16	0.45	0.225	4.53	1.100	912	2290
0.2	16	0.45	0.217	4.67	-	-	2230
0.3	16	0.45	0.213	4.30	0.586	986	1760
0.4	8	0.40	0.170	6.28	0.852	1205	2800
0.5	7	0.35	0.185	5.56	0.774	1325	2565
0.6	7	0.35	0.184	5.40	0.960	1320	2270
0.7	7	0.35	0.166	6.44	0.980	1325	2790

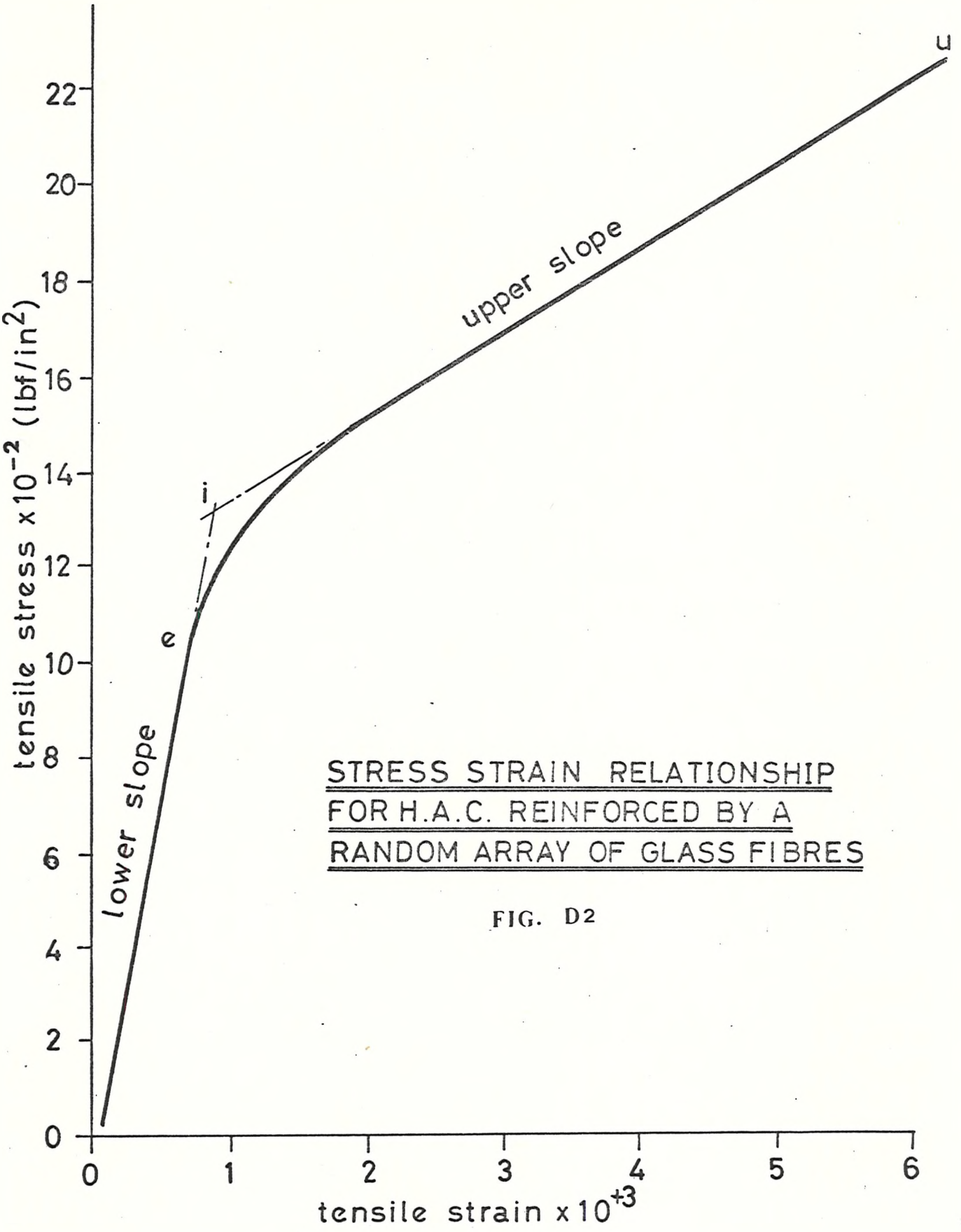

STRESS STRAIN RELATIONSHIP FOR H.A.C. REINFORCED BY A RANDOM ARRAY OF GLASS FIBRES

FIG. D2

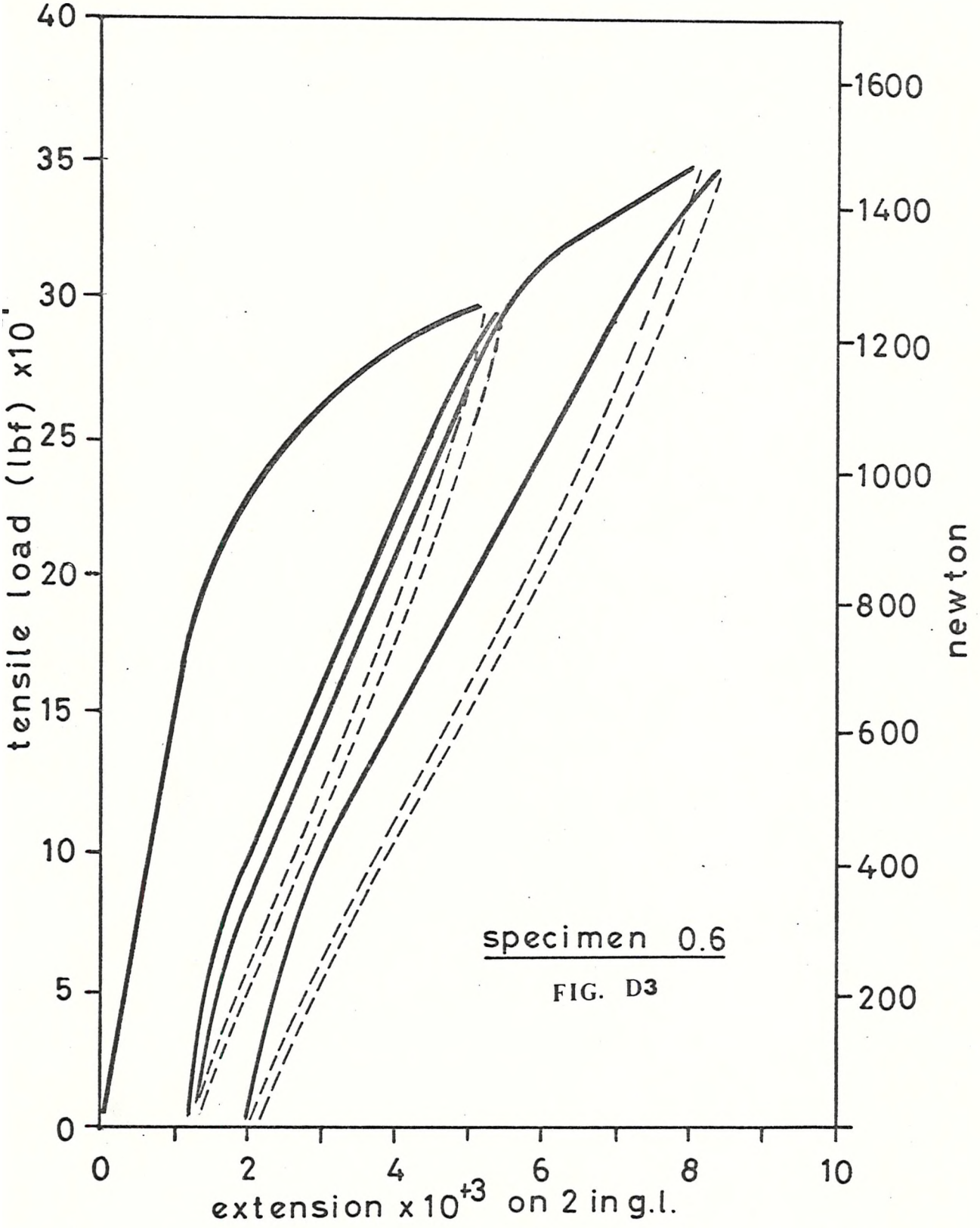

FIG. D3

LOAD/ EXT GRAPH — REPEATED LOADING

D4. TECHNIQUES INVOLVING PRESSURE

D4.1 Hand Layup

Plate D5 shows a mould in which individual specimens (0.8 to 0.24) were manufactured. This involved the placing of alternate layers of cement and glass mat within the mould and afterwards applying a pressure of approximately 2800 lbf/in^2 to the specimen via the piston illustrated (Plate D5). Since the piston was a loose fit, excess cement and trapped air were squeezed from the specimen until the desired thickness was obtained. The pressure was maintained for a period of two hours as early release caused air to be drawn back into the specimen. The specimen remained in the mould for a total time of 24 hours when it was removed and immediately placed in wet hessian, thereby maintaining a moist atmosphere for the final cure period.

Specimens 0.8 to 0.12 were reinforced with three layers of C.S.M. which has a nominal weight of 1.5 ozf/ft^2. The load/strain curves for these specimens are shown on Figure D4. Specimens 0.13 to 0.24 (Fig. D5) were reinforced with C.F.M. and due to the low binder content, manufacture was difficult but possibly cement impregnation was improved since the mat separated and allowed the cement to penetrate. The top and bottom faces of each specimen had a layer of overlay tissue to improve the surface finish.

Specimens 0.8 to 0.23 were tested for specific gravity and void content by selecting 1 inch long samples from each test piece which were placed in a moist atmosphere to ensure initial saturated conditions.

The volume of each sample was determined by weighing in and out of distilled water. This difference of weight gives the graviametric weight of each sample and is equal to the displaced volume. The samples were then dried and placed in a DESSICATOR for 24 hours, giving the dry weight of the specimen. It was assumed that the difference between the wet and dry weights gave an indication of the voids in the composite. The values for specific gravity and void content of the composite so derived are shown in Table D3.

It can be seen that the gross cross-sectional area of the test piece consists of at least cement, glass and voids which means that the volume occupied by the cement is less than $(1 - \emptyset)$ by an amount equal to the void content.

TABLE D2

TENSILE STRESSES AND STRAINS FOR LAMINATES OF HIGH ALUMINA CEMENT REINFORCED BY CHOPPED STRAND MAT AND CONTINUOUS FILAMENT MAT

Spec. No.	Mean Area (in^2)	Tensile Strains x 10^3			Tensile Stresses			E_{fm} x 10^{-6} lbf/in^2
		ε_e	ε_i	ε_u	σ_e lbf/in^2	σ_i lbf/in^2	σ_u lbf/in^2	
0.8	0.232	0.17	0.20	2.0	989.5	1376.7	1733.8	6.1435
0.9	0.290	0.16	0.30	3.9	620.0	1336.6	1464.0	4.9192
0.10	0.226	0.10	0.18	1.2	220.7	1324.1	1743.4	8.0152
0.11	0.238	0.10	0.18	4.1	714.6	1084.5	2227.9	6.0028
0.12	0.273	0.10	0.11	5.8	365.8	1152.3	2304.3	8.1500
0.13	0.199	0.20	0.35	6.52	854.3	1849.3	2361.9	5.0254
0.14	0.250	0.13	0.26	5.30	639.5	1339.0	2078.5	5.3200
0.15	0.246	0.18	0.30	2.88	527.7	1075.7	1420.7	3.5314
0.16	0.221	0.25	0.36	2.40	948.1	1413.1	1724.7	3.7654
0.17	0.244	0.27	0.39	4.28	821.0	1334.1	1621.5	3.4236
0.18	0.282		0.12	1.32	354.8	957.9	1206.2	5.9069
0.19	0.265	0.03		0.45			1653.4	
0.20	0.287	0.10		0.40	556.6		1113.2	
0.21	0.216		0.30	0.60		1085.5	1293.3	3.8524
0.22	0.216			0.60		619.6	786.1	
0.23	0.317		0.10	1.30	599.6	915.1	1167.6	6.9400

Maximum Age: 21 DAYS

Specimen 0.24 : Damaged

TABLE D3

ESTIMATED SPECIFIC GRAVITY AND VOID CONTENT OF G.R. LAMINATES OF H.A.C.

Specimen Number	Specific Gravity of Wet Specimen (A)	Specific Gravity of Dry Specimen (B)	Void Content Based on (A) %	Void Content Based on (B) %
0.8	2.1210	1.9256	9.215	10.155
0.9	2.4420	2.2720	6.978	7.502
0.10	2.3170	2.0760	10.517	11.753
0.11	2.2700	2.0250	10.805	12.114
0.12	2.2180	1.9830	10.632	11.897
0.13	2.2190	1.9480	12.183	13.873
0.14	2.2420	2.0350	9.241	10.182
0.15	2.2440	2.0030	10.736	12.027
0.16	2.0793	1.8510	10.975	12.328
0.17	2.2950	2.0990	8.521	8.469
0.18	2.2600	2.0130	10.921	12.260
0.19	2.0580	1.8470	10.244	11.439
0.20	2.2740	2.0400	5.960	6.338
0.21	2.2050	1.9780	10.314	11.500
0.22	2.2280	1.9300	13.402	15.476
0.23	2.1680	1.9640	9.414	10.393

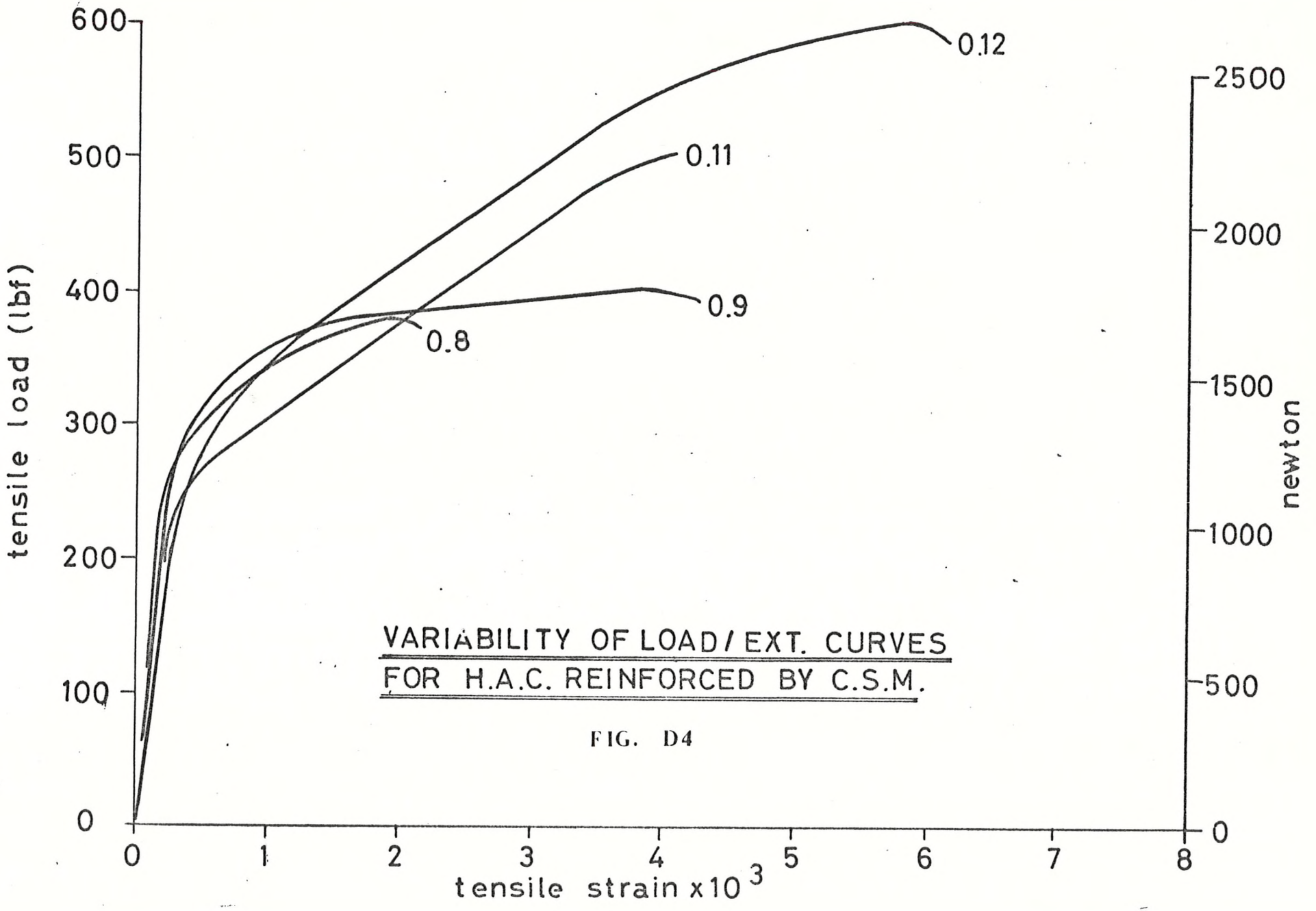

VARIABILITY OF LOAD / EXT. CURVES FOR H.A.C. REINFORCED BY C.S.M.

FIG. D4

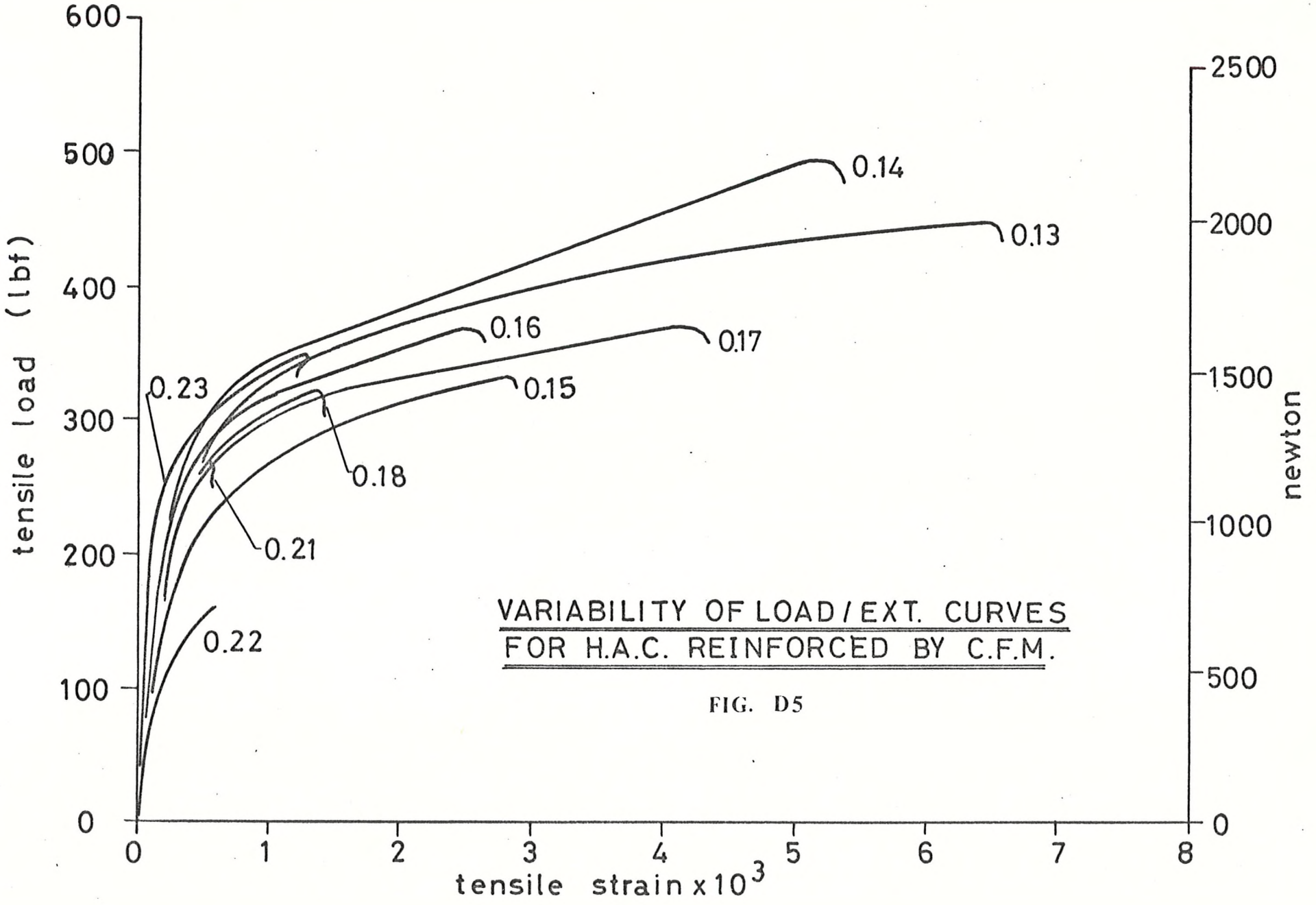
600
500
400
300
200
100
0
tensile load (lbf)
2500
2000
1500
1000
500
0
newton
0.14
0.13
0.16
0.17
0.23
0.15
0.18
0.21
0.22
0 1 2 3 4 5 6 7 8
tensile strain x 10^3
VARIABILITY OF LOAD / EXT. CURVES
FOR H.A.C. REINFORCED BY C.F.M.

FIG. D5

D4.2 Suction Moulding

When combining the hand layup method with the spray technique (described in Sections D3, D2) together with the application of pressure to the laminate, another manufacturing technique evolves - suction moulding. The moulds used were a smaller version of those shown in Figure D1 and were lined with wet porous paper to keep the laminate intact. The laminates are laid up in this suction mould using a high water/cement ratio in the cement binder. After completion the air suction pump is switched on, thus causing a vacuum to be generated at the back face of the laminate which draws off the excess water through the porous paper and perforated sheet. Unfortunately, whilst drawing off the water, air is also drawn through the laminate which produces a poor surface finish and increases the void content of the laminate. Likewise, by placing a sheet of perspex on the top surface, then applying suction, again air voids are formed in the spaces the water occupied prior to being drawn off.

Attempts were also made to laminate with a continuous suction present but this made the cement and glass difficult to work in view of the low water/cement ratio of the fresh cement paste. Pressure was then applied to the laminate in order to obtain

greater compaction of the cement, improve the surface finish and reduce its void content.

The specimens upon demoulding were the correct shape and dimension for testing and were placed in a high humidity environment during the cure period. After this period they were tested in tension when the Instron extensometer was clamped to the test piece at the centre of its length and not removed until after fracture. Tensile strains so obtained can be seen in Table D2 and the tensile stress/strain curves showed the same characteristics as those illustrated in Figure D2.

Table D2 shows a comparison between the stress and strain at e, i and u. Cracking of the cement is suspected at i which is at a strain of approximately 0.1×10^{-3}. Accompanying this progressive cracking of the matrix is a marked reduction of the elastic modulus. This is emphasised because the contribution of the random distribution of glass fibres to the stiffness of the composite is small, especially at low glass volume contents ($\emptyset$). When this cracking takes place load is transferred to the glass subjecting it to an elevated stress, thus fracture of some of the fibres may occur.

D4.3 Dough Moulding

Since considerable work has been done on the premixing of chopped glass fibres and polyester resin and the technique is adequately described by Senatskii [42] and Cutler [17] attempts were made to follow similar suggestions and apply them to the mixing of cement and chopped glass fibres.

To this end a quantity of dry H.A. cement powder and chopped glass fibres (aboutl/4 inch in length) was placed in a tumbler (Plate D 4). This was then rotated so that the cement particles were thoroughly mixed with the chopped fibres. The correct quantity of water was added in small increments between each rotation. This procedure was continued until the full quantity of water had been added. It was found necessary to obtain a final composition which had a greater water/cement ratio of the matrix than was required. The mass of chopped fibres and cement slurry was removed and placed in the mould as shown in Plate D5 compressed until a required thickness was obtained - at the same time removing the excess water - and giving the required low water/ cement ratio.

All specimens were demoulded and placed in water for the remaining cure period and upon testing were found to be very weak and difficult to test, thus no further work was carried out.

Demoulding of the laminate was not difficult, although removal of the porous paper from the moulded sheet was not completely possible. The bottom surface of the laminate took the appearance of the perforated sheet.

Curing took place in a humidity chamber. This simply was a box, with one end open, through which a water mist was injected. A sheet of polythene was hung at the other end which restricted the flow of the water mist.

Several exploratory tensile tests were carried out on specimen manufactured in this way which showed the same characteristics as seen in Figs. D4 and D5 with no obvious improvement or deterioration of mechanical properties.

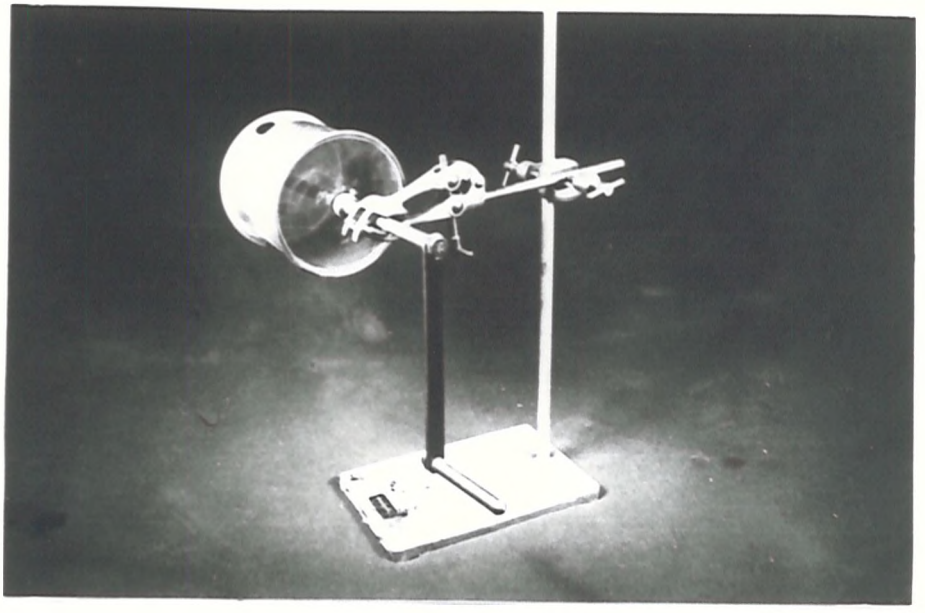

DOUGH MOULDING TUMBLER
PLATE D4

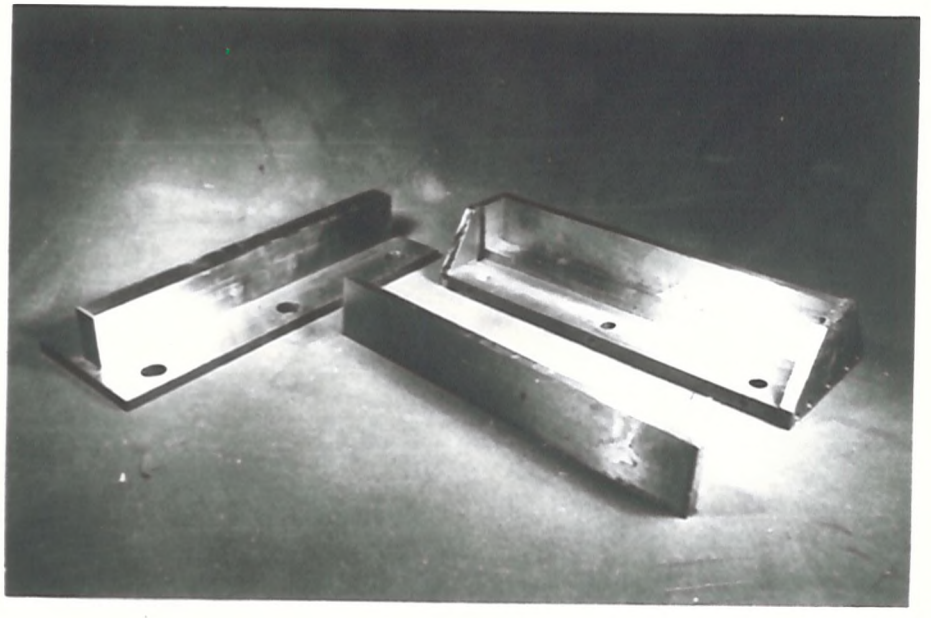

SINGLE TENSILE SPECIMEN
PLATE D5